T. Kohyama
J. Canadell
D.S. Ojima
L.F. Pitelka
(Eds.)

Forest Ecosystems and Environments

Scaling Up from Shoot Module to Watershed

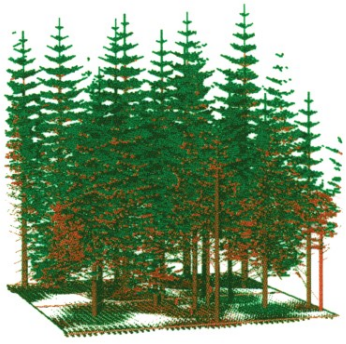

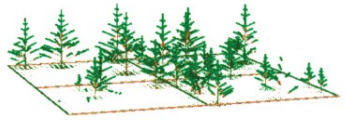

Springer

T. Kohyama, J. Canadell, D.S. Ojima, L.F. Pitelka (Eds.)

Forest Ecosystems and Environments

Scaling Up from Shoot Module to Watershed

Reprinted from *Ecological Research* Vol. 20 (3) 2005

T. Kohyama, J. Canadell, D.S. Ojima, L.F. Pitelka (Eds.)

Forest Ecosystems and Environments

Scaling Up from Shoot Module to Watershed

Reprinted from *Ecological Research* Vol. 20 (3) 2005

With 94 Figures, Including 2 in Color

Springer

Takashi Kohyama, Dr.
Graduate School of Environmental Earth Science, Hokkaido University, Sapporo 060-0810, Japan

Josep Canadell, Dr.
Global Carbon Project, Earth Observation Centre, CSIRO Division of Atmospheric Research, GPO Box 3023, Canberra, ACT 2601, Australia

Dennis S. Ojima, Dr.
Natural Resource Ecology Laboratory, NESB, B229, Colorado State University, Fort Collins, CO 80523-1499, USA

Louis F. Pitelka, Dr.
Appalachian Laboratory, University of Maryland Center for Environmental Science, 301 Braddock Road, Frostburg, MD 21532-2307, USA

Library of Congress Control Number: 2005928608

ISBN 4-431-26074-9 Springer-Verlag Tokyo Berlin Heidelberg New York

Printed on acid-free paper

Springer is a part of Springer Science+Business Media
springeronline.com

Printed in Japan

Typesetting: Scientific Publishing Services Ltd., India
Printing and binding: Hicom, Japan

Ecol Res (2005) 20: 241–242
DOI 10.1007/s11284-005-0040-2

PREFACE

Takashi Kohyama · Josep Canadell · Dennis S. Ojima
Louis F. Pitelka

Forest ecosystems and environments: scaling up from shoot module to watershed

Published online: 31 March 2005

Terrestrial ecosystems are experiencing rapid changes of their structure and function as a result of an ever growing pressure by human demands on natural resources. Over the past decades, forcing by direct and indirect human activities has reached a point that is now rivaling the natural forcing that has shaped the Earth system over millennia. This unprecedented phenomenon has attracted a major investment by the scientific community to detect the impacts, attribute the changes to processes, and explore future trajectories. This scientific information is fundamental to creating the knowledge base that will inform policy development and will allow human societies to mitigate and adapt to these rapid changes.

With the goal of developing a novel research agenda in support to the above objectives, the ''Global Change and Terrestrial Ecosystems'' core project (GCTE, Walker et al. 1999; Canadell et al. 2005) was created in 1991 under the auspices of the International Geosphere-Biosphere Programme (IGBP). By contrast with other components of the Earth system, terrestrial ecosystems are constructed with short-lived and long-lived organic compounds with varied diffusivity, resulting in pronounced spatial and temporal heterogeneity. Up scaling and integrating to global scales of such heterogeneous ecosystems in relation to global environmental change has been described and forecasted through the GCTE research agenda.

Other aspects of heterogeneity come from hierarchical and compositionally diversified features of terrestrial ecosystems. Plants create a vegetation framework with organismic hierarchy, from cell physiology to whole individual-level regulation, and biological components at each trophic level characterized by biodiversity related to compositional functional differentiation. Therefore, GCTE has promoted the integration and the study of feedbacks between processes driven by plant and ecosystem physiology, population and community dynamics, and biogeochemistry.

The ''Global Change Impacts on Terrestrial Ecosystems in Monsoon Asia'' project (TEMA) (1995–2003) was the Japanese contribution to the GCTE global effort. Coastal East and Southeast Asia, as the target region of TEMA, are characterized by wet growing seasons influenced by monsoon climates, and species-rich forest ecosystems develop along a latitudinal gradient from equatorial to boreal zone, and an altitudinal gradient from lowland up to the forest limit (Ohsawa 1995). The TEMA aimed to predict the effects of environmental change on the distribution and structure of forest ecosystems in the target region (Hirose et al. 1998). Core parts of TEMA were designed to integrate forest ecosystem processes from leaf physiology to micro-meteorological budgets, and to predict long-term changes of vegetation composition and architecture through demographic processes. The TEMA paid particular attention to watershed processes, where forest metabolism affects ecosystem properties and biogeochemical budgets of freshwater ecosystems. This is particularly important because rivers, wetlands and lakes are experiencing direct and indirect effects of environmental change. The unique challenge of TEMA research was the attempt to integrate various scales of

T. Kohyama (✉)
Graduate School of Environmental Earth Science,
Hokkaido University,
Sapporo 060-0810, Japan
E-mail: Kohyama@ees.hokudai.ac.jp

J. Canadell
Global Carbon Project, Earth Observation Centre,
CSIRO Division of Atmospheric Research,
GPO Box 3023, Canberra, ACT 2601,
Australia

D. S. Ojima
Natural Resource Ecology Laboratory,
NESB, B229, Colorado State University, Fort Collins,
CO 80523-1499, USA

L. F. Pitelka
Appalachian Laboratory,
University of Maryland Center for Environmental Science,
301 Braddock Road,
Frostburg, MD 21532-2307, USA

heterogeneous ecological processes from fine-scale ecophysiology to watershed ecosystems.

This special issue outlines a synthetic view achieved by TEMA, building from an initial synthesis (Hirose and Walker 1996), a mid-term special issue (Nakashizuka et al. 1999) and numerous research papers. The first section of this issue ''Integration of ecophysiological processes to stand dynamics'' deals with the process-based scaling-up from leaf physiology to population, and to landscape ecosystem production, applying experimental, modeling and monitoring approaches. The second section ''Latitudinal/altitudinal transects of East Asia'' presents case studies and region-wide meta-analysis of forests along latitudinal and altitudinal gradients, followed by a tree demographic process-based modeling approach to geographic forest zonation. The third section ''Monitoring and modeling atmosphere-forest-soil processes'' presents carbon budgets for scales ranging from stand to small watershed of various types of Japanese temperate forests. The last section, ''Forest–lake interface in watershed ecosystems'' presents catchment-scale biogeochemical budgets and regulation, stream water diagnosis of forest soil status, and carbon budgets and methane dynamics of lake ecosystems. The four sections collectively represent the scaling up concept that has driven the intellectual and research development of TEMA over this past decade, a research that ultimately needs to yield integrated and system-level knowledge base for a better understanding of ecosystem functioning (i.e. ecosystem goods and services) upon which the well being of societies relies. Beside this issue, overall TEMA achievements are summarized in Kohyama et al. (2005).

The GCTE project ended in 2003, and the succeeding international projects such as Global Land Project (GLP), Global Carbon Project (GCP), and Monsoon Asia Integrated Regional Studies (MAIRS) are already in place or in different stages of development. The concepts promoted by TEMA will contribute to, and be extended through these projects.

We acknowledge that the planning and the implementation of GCTE-TEMA was possible thanks to the support by many scientists, and particularly by Nobuhiko Handa, Yoh Iwasa, Hiroya Kawanabe, Kihachiro Kikuzawa, Yosuke Matsumoto, Yasushi Morikawa, the late Shigeru Nakano, Tohru Nakashizuka, Masahiko Ohsawa, Yasuyuki Oshima, Will Steffen, Noriyuki Tanaka, Ichiro Terashima, Eitaro Wada, and Brian Walker.

References

Canadell J, Pataki D, Pitelka L (eds) (2005) Terrestrial ecosystems in a changing world. The IGBP Series. Springer, Berlin Heidelberg New York

Hirose T, Walker B (eds) (1996) Global change and terrestrial ecosystems in monsoon Asia. Vegetatio 121:1–191

Hirose T, Kohyama T, Oshima Y (1998) GCTE activities in Japan. Glob Environ Res 1:19–24

Kohyama T, Urabe J, Hikosaka K, Shibata H, Yoshioka T, Konohira E, Murase J, Wada E (2005) Terrestrial ecosystems in monsoon Asia: scaling up from shoot module to watershed. In: Canadell J, Pataki D, Pitelka L (eds) Terrestrial ecosystems in a changing world. The IGBP Series. Springer, Berlin Heidelberg New York

Nakashizuka T, Kohyama T, Whitmore TC, Ashton PS (eds) (1999) Tree diversity and dynamics of western Pacific and eastern Asian forests. J Veg Sci 10:763–860

Ohsawa M (1995) Latitudinal composition of altitudinal changes in forest structure, leaf-type, and species richness in humid monsoon Asia. Vegetatio 121:3–10

Walker B, Steffen W, Canadell J, Ingram J (1999) The terrestrial biosphere and global change: implications for natural and managed ecosystems. Cambridge University Press, Cambridge

CONTENTS

Section 4 Forest–lake interface in watershed systems

REVIEWERS

T Hara
K Hikosaka
T Hiura
T Hiyama
S Kaneko
K Kikuzawa
K Kitayama
K Kobayashi
Y Kosugi
T Masaki
Y Matsuura
J Murase
S Nakano
T Nakashizuka
N Ohte
H Sato
K Sato
H Shibata
A Sugimoto
H Tanaka
A Takenaka
K Umeki
T Yoshioka

Section 1
Integration of ecophysiological processes to stand dynamics

Ecol Res (2005) 20: 243–253
DOI 10.1007/s11284-005-0041-1

ORIGINAL ARTICLE

Kouki Hikosaka · Yusuke Onoda · Toshihiko Kinugasa
Hisae Nagashima · Niels P. R. Anten · Tadaki Hirose

Plant responses to elevated CO_2 concentration at different scales: leaf, whole plant, canopy, and population

Received: 15 September 2004 / Accepted: 28 December 2004 / Published online: 1 March 2005

Abstract Elevated CO_2 enhances photosynthesis and growth of plants, but the enhancement is strongly influenced by the availability of nitrogen. In this article, we summarise our studies on plant responses to elevated CO_2. The photosynthetic capacity of leaves depends not only on leaf nitrogen content but also on nitrogen partitioning within a leaf. In *Polygonum cuspidatum*, nitrogen partitioning among the photosynthetic components was not influenced by elevated CO_2 but changed between seasons. Since the alteration in nitrogen partitioning resulted in different CO_2-dependence of photosynthetic rates, enhancement of photosynthesis by elevated CO_2 was greater in autumn than in summer. Leaf mass per unit area (LMA) increases in plants grown at elevated CO_2. This increase was considered to have resulted from the accumulation of carbohydrates not used for plant growth. With a sensitive analysis of a growth model, however, we suggested that the increase in LMA is advantageous for growth at elevated CO_2 by compensating for the reduction in leaf nitrogen concentration per unit mass. Enhancement of reproductive yield by elevated CO_2 is often smaller than that expected from vegetative growth. In *Xanthium canadense*, elevated CO_2 did not increase seed production, though the vegetative growth increased by 53%. As nitrogen concentration of seeds remained constant at different CO_2 levels, we suggest that the availability of nitrogen limited seed production at elevated CO_2 levels. We found that leaf area development of plant canopy was strongly constrained by the availability of nitrogen rather than by CO_2. In a rice field cultivated at free-air CO_2 enrichment, the leaf area index (LAI) increased with an increase in nitrogen availability but did not change with CO_2 elevation. We determined optimal LAI to maximise canopy photosynthesis and demonstrated that enhancement of canopy photosynthesis by elevated CO_2 was larger at high than at low nitrogen availability. We also studied competitive asymmetry among individuals in an even-aged, monospecific stand at elevated CO_2. Light acquisition (acquired light per unit aboveground mass) and utilisation (photosynthesis per unit acquired light) were calculated for each individual in the stand. Elevated CO_2 enhanced photosynthesis and growth of tall dominants, which reduced the light availability for shorter subordinates and consequently increased size inequality in the stand.

Keywords Allocation · Carbon fixation · Competition · Nitrogen availability · Nitrogen use · Scaling up

K. Hikosaka (✉) · Y. Onoda · T. Kinugasa
H. Nagashima · N. P. R. Anten · T. Hirose
Graduate School of Life Sciences,
Tohoku University, Aoba, Sendai 980-8578, Japan
E-mail: hikosaka@mail.tains.tohoku.ac.jp
Tel.: +81-22-2177735
Fax: +81-22-2176699

Present address: N. P. R. Anten
Department of Plant Ecology, Utrecht University,
P.O. Box 800.84, 3508 TB, Utrecht, The Netherlands

Introduction

During the last 200 years, atmospheric CO_2 concentration has increased from a pre-industrial level of 280 μmol mol^{-1} to 370 μmol mol^{-1} (in 2004). It is still increasing at a rate of 1.5 μmol mol^{-1} per year and may reach 700 μmol mol^{-1} at the end of this century (IPCC 2001). Because CO_2 is a substrate for photosynthesis, an increase in atmospheric CO_2 concentration stimulates photosynthetic rates in C_3 plants (Kimball 1983; Cure and Acock 1986; Bazzaz 1990; Poorter 1993; Sage 1994; Curtis 1996; Ward and Strain 1999). However, the effect of elevated CO_2 on growth and reproduction is often much weaker than that predicted by the photosynthetic response. It also differs considerably between species and between plants grown under different conditions

(Bazzaz 1990; Arp 1991; McConnaughay et al. 1993; Sage 1994; Farnsworth and Bazzaz 1995; Makino and Mae 1999; Ward and Strain 1999; Jablonski et al. 2002). Nutrient availability has been considered one of the key factors for the variation in plant responses to elevated CO_2 (e.g. Ziska et al. 1996; Lutze and Gifford 1998; Kim et al. 2001; Stitt and Krapp 1999; Kimball et al. 2002).

Nitrogen is one of the most important mineral nutrients that limit plant growth in many natural and managed ecosystems (Aerts and Chapin 2000). Since a large fraction of leaf nitrogen is in the photosynthetic apparatus, a strong correlation holds between photosynthetic capacity and nitrogen content of leaves (Evans 1989; Hikosaka 2004). Higher photosynthetic rates at high CO_2 concentrations may lead to an imbalance of carbon and nitrogen in the plant body because carbon acquisition is stimulated relative to nitrogen uptake at elevated CO_2. Accumulated carbohydrates sometimes cause a feedback limitation of photosynthesis (Peterson et al. 1999; Medlyn et al. 1999; Stitt and Krapp 1999).

Plants respond to the availability of limited resources by altering their physiological and morphological characteristics to ameliorate the resource imbalance. At low nutrient availability, for example, plants allocate more biomass to roots, which compensates for low nutrient uptake rates per unit root mass (Brouwer 1962). This contributes to balancing carbon and nitrogen uptake and to the maximisation of relative growth rates (Hirose 1987, 1988; Hilbert 1990). CO_2 responses of plants may also involve adaptive acclimation, which potentially increases plant growth and reproduction at elevated CO_2 levels. Optimality models may be useful to assess the adaptability of plant responses (Anten et al. 2000).

In the GCTE-TEMA program, we studied plant responses to elevated CO_2 at different scales: leaf, whole-plant, canopy, and population. Nitrogen was considered as a key factor to analyse the variation in the CO_2 responses. In this article, we summarise our findings.

Leaf

The photosynthetic rate of a leaf is determined by the amount of leaf nitrogen and its partitioning between photosynthetic and non-photosynthetic proteins, and among the various photosynthetic components (Hikosaka 2004). We studied nitrogen use in leaves grown at elevated CO_2 both theoretically and experimentally.

Nitrogen partitioning in the photosynthetic apparatus in leaves grown at elevated CO_2 concentrations: importance of seasonal acclimation

Light-saturated rates of photosynthesis are limited either by RuBPCase (ribulose-1,5-bisphosphate carboxylase/oxygenase) activity or by the RuBP regeneration process (Farquhar et al. 1980). The former tends to limit photosynthesis at lower CO_2 concentrations while the latter does so at higher CO_2 concentrations. The capacity of the two processes is considered to co-limit at around the current CO_2 concentration (Wullschleger 1993). Therefore, under future higher CO_2 concentrations, it is possible that only the RuBP regeneration process will limit photosynthesis. Both RuBP carboxylation and RuBP regeneration processes need a substantial amount of nitrogen to maintain high photosynthetic capacity (Evans and Seemann 1989; Hikosaka 1997). To use nitrogen efficiently, nitrogen should be reallocated from non-limiting to limiting processes (Evans 1989; Hikosaka and Terashima 1995). It has been suggested that nitrogen reallocation from RuBP carboxylation to the RuBP regeneration processes would increase photosynthetic nitrogen use efficiency at elevated CO_2 (Sage 1994; Webber et al. 1994; Medlyn 1996). Using a theoretical model of nitrogen partitioning in the photosynthetic apparatus, Hikosaka and Hirose (1998) suggested that nitrogen reallocation to RuBP regeneration in the doubled CO_2 level would increase photosynthesis by 20%. This prediction was supported by an experimental study using a transgenic rice plant with a reduced amount of RuBPCase (Makino et al. 1997, 2000). When compared at the same nitrogen content, the transgenic rice had greater amounts of proteins in the RuBP regeneration process and higher photosynthetic rates than the wild type at high CO_2 concentrations. In normal plants, however, nitrogen allocation between RuBP carboxylation and regeneration processes does not seem to be influenced by CO_2 concentrations at which plants are grown (Medlyn et al. 1999).

Recent studies, however, have found that growth temperature affects the balance between RuBPCase and the RuBP regeneration process. Hikosaka et al. (1999) demonstrated that *Quercus myrsinaefolia* leaves grown at a low temperature had a higher ratio of RuBP regeneration capacity (expressed as the maximum electron transport rate, J_{max}) to carboxylation capacity (V_{cmax}) than those grown at a high temperature, and consequently that photosynthesis was more sensitive to CO_2 in plants acclimated to low temperature. A similar trend was found by Wilson et al. (2000), who reported that autumn leaves had a higher ratio of J_{max}/V_{cmax} than summer leaves in several deciduous tree species from temperate forests. These results suggest that seasonal changes in temperature alter the balance between RuBP carboxylation and RuBP regeneration, which will affect the extent of CO_2 stimulation of photosynthesis.

We tested the hypothesis that seasonal changes in air temperature affect the balance and modulate the CO_2 response of photosynthesis (Onoda et al. 2005). V_{cmax} and J_{max} were determined in summer and autumn for leaves of *Polygonum cuspidatum* grown at two CO_2 concentrations. The elevated CO_2 concentration reduced both V_{cmax} and J_{max} without changing the J_{max}/V_{cmax} ratio. Seasonal environment, on the other hand, altered the ratio such that the J_{max}/V_{cmax} ratio was higher in autumn than summer leaves. This alteration made the

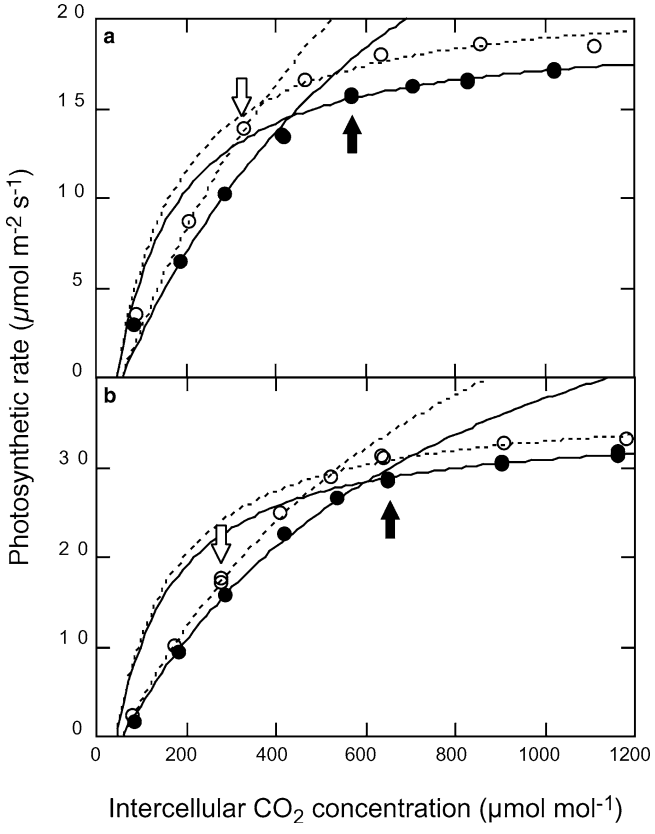

Fig. 1 Photosynthetic rate versus intercellular CO_2 concentration of *Polygonum cuspidatum* grown either at ambient CO_2 (370 μmol mol^{-1}, *open symbols*) or at elevated CO_2 (700 μmol mol^{-1}, *closed symbols*) in August (**a**) and October (**b**). The model of Farquhar et al. (1980) was fitted to the observations. *Arrows* indicate the photosynthetic rate at growth CO_2 concentration

photosynthetic rate more dependent on CO_2 concentration in autumn leaves (Fig. 1). Therefore, when photosynthetic rates were compared at growth CO_2 concentration, the stimulation in photosynthetic rate was larger in autumn than summer leaves. Across the two seasons and the two CO_2 concentrations, V_{cmax} was strongly correlated with RuBPCase and J_{max} with cytochrome *f* content. These results suggest that seasonal changes in climate influence the relative amount of photosynthetic proteins, which in turn affects the CO_2 response of photosynthesis.

Whole plant

Photosynthates acquired by leaves are used for the production of leaves, stems, roots, and reproductive organs. Increase in allocation to the leaf would be beneficial for photosynthesis, but may reduce other functions such as nutrient uptake and reproduction. We studied changes in biomass allocation with CO_2 elevation with respect to the balance between enhanced photosynthesis and other functions.

Maximisation of relative growth rate at elevated CO_2 concentrations

Plants respond to an alteration of nitrogen availability by changing their root/shoot (R/S) ratio. Brouwer (1962) and Davidson (1969) proposed the "functional equilibrium" hypothesis; i.e. the R/S ratio changes to maintain the activity ratio between the shoot and root. According to this hypothesis, any environmental changes that increase root activity would decrease the R/S ratio and any environmental changes that increase shoot activity would increase the R/S ratio. As elevated CO_2 increases photosynthetic activity of the leaf, the functional equilibrium predicts an increase in the R/S ratio and a reduction in leaf mass ratio (LMR, the fraction of plant mass in the leaf) in plants growing at elevated CO_2. However, LMR in actual plants does not necessarily respond to elevated CO_2 as expected (Stulen and den Hertog 1993; Luo et al. 1999). While some studies showed a reduction in LMR at elevated CO_2 as expected (e.g. Larigauderie et al. 1988; Wilson 1988), others showed that LMR did not change with CO_2 elevation (e.g. Pettersson et al. 1993; Curtis and Wang 1998).

Many studies have shown that leaf mass per unit area (LMA) consistently increases under elevated CO_2 (Poorter et al. 1996; Yin 2002). LMR and LMA are important parameters to describe plant growth. Relative growth rate (RGR, growth rate per unit plant mass) is factorised into three components: RGR = NAR × LMR/LMA, where NAR is net assimilation rate (growth rate per unit leaf area). This equation indicates that an increase in LMA reduces RGR. Increase in LMA at elevated CO_2 has been ascribed to accumulation of non-structural carbohydrates as a result of a source-sink imbalance (Poorter et al. 1997). However, Luo et al. (1994) suggested a possible advantage of increasing LMA under elevated CO_2, because it would contribute to increasing leaf nitrogen content per unit area (N_{area}): $N_{area} = N_{mass} \times LMA$, where N_{mass} is leaf nitrogen concentration per unit mass. The decrease in N_{mass} as a result of elevated CO_2 may be compensated for by an increase in LMA to maintain a high N_{area} (Luo et al. 1994; Peterson et al. 1999). However, the effect of increased LMA on whole-plant growth has not been studied (but see Hirose 1987). Hilbert et al. (1991) studied the optimal biomass allocation under elevated CO_2, but did not consider the effect of LMA.

To test the hypothesis that an increase in LMA at elevated CO_2 benefits plant growth by maintaining a high N_{area}, we raised *P. cuspidatum* at ambient and elevated CO_2 concentrations with three levels of nitrogen availability (Ishizaki et al. 2003). Elevated CO_2 significantly increased LMA but the effect on LMR was small. The increased LMA compensated for the lowered N_{mass}, leading to similar N_{area} between ambient and elevated CO_2 conditions. The effect of change in LMA on RGR was investigated by means of a sensitivity analysis: LMA

values observed at ambient and elevated CO_2 were substituted into a steady-state growth model to calculate RGR. In this model, NAR was assumed to be a function of N_{area}. Allocation of more biomass to roots increased N_{mass} via increased nitrogen uptake, but decreased leaf mass. An increase in LMA increased N_{area} but decreased leaf area. At ambient CO_2, substitution of a high LMA (observed at elevated CO_2) did not increase RGR, compared with RGR for a low LMA (observed at ambient CO_2), whereas at elevated CO_2 the RGR values calculated for the high LMA were always higher than those calculated for the low LMA. The optimal combination of LMR and LMA to maximise RGR was determined for different CO_2 and nitrogen availabilities (Fig. 2). The optimal LMR was nearly constant, while the optimal LMA increased with CO_2 elevation, and decreased at higher nitrogen availabilities. These results suggest that the increase in LMA contributes to growth enhancement under elevated CO_2. The changes in LMR of actual plants may be a compensation for the limited plasticity of LMA.

Reproductive growth at elevated CO_2

Although vegetative growth is enhanced by elevated CO_2, it is not always reflected by an increase in reproductive yield (final mass of the reproductive part). From more than 150 reports on the effect of elevated CO_2 on the reproductive yield of both crop and wild species, Jablonski et al. (2002) found a mean relative yield increase of 12% in fruits and 25% in seeds. These responses were smaller than the response of total plant mass (31%). In some cases, elevated CO_2 even reduced reproductive yield, though vegetative mass was increased (Larigauderie et al. 1988; Fajer et al. 1991; Farnsworth and Bazzaz 1995). Thus, the increase in reproductive yield is not parallel to that in plant growth, and the enhancement of vegetative growth is not a reliable predictor of enhancement of reproductive yield (Ackerly and Bazzaz 1995).

The difference in responses to elevated CO_2 between vegetative growth and reproductive yield should be explained by factors involved in the process of reproductive growth. Reproductive growth is determined not only by biomass production but also by biomass allocation to the reproductive part. We analysed reproductive growth under elevated CO_2 using a simple growth model (Kinugasa et al. 2003). Reproductive mass was expressed as the product of (1) the duration of the reproductive period, (2) the rate of biomass acquisition in the reproductive period, and (3) the fraction of acquired biomass allocated to the reproductive part (Sugiyama and Hirose 1991; Shitaka and Hirose 1998). We raised *Xanthium canadense*, an annual, under ambient and elevated CO_2 concentrations with two nitrogen availabilities. Elevated CO_2 increased reproductive yield at high nitrogen availability, but this increase was caused by increased capsule mass without a significant increase in seed production (Fig. 3). The

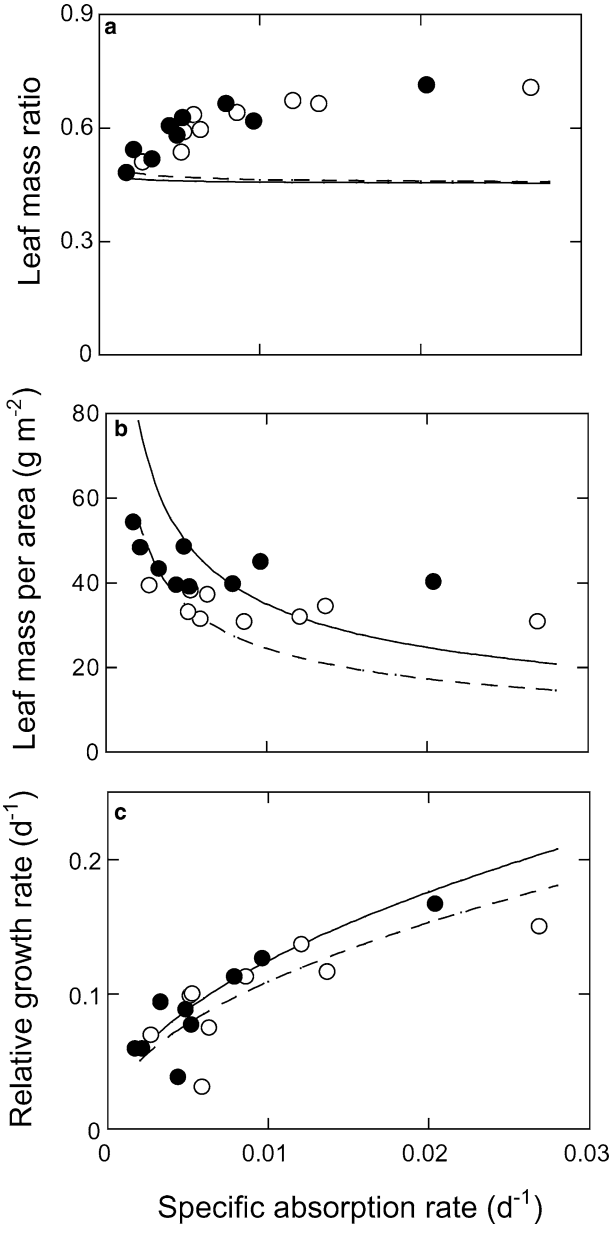

Fig. 2 The optimal leaf mass ratio (**a**) and leaf mass per unit area (**b**) that maximise the relative growth rate (**c**), plotted against specific absorption rate of nitrogen per unit root mass. *Lines* are the theoretical optimum calculated from the model for 370 (*dashed*) and 700 (*solid*) μmol mol^{-1} CO_2 and symbols are data observed for *P. cuspidatum* grown at 370 (*open*) and 700 (*closed*) μmol mol^{-1} CO_2. Redrawn from Ishizaki et al. (2003)

increase in total reproductive mass was due mainly to an increase in the rate of biomass acquisition in the reproductive period, with a delay in leaf senescence. This positive effect was partly offset by a reduction in biomass allocation to the reproductive part at elevated CO_2. The duration of the reproductive period was not affected by elevated CO_2.

Seed production was strongly constrained by the availability of nitrogen for seed growth. The nitrogen concentration in seeds was very high in *X. canadense*

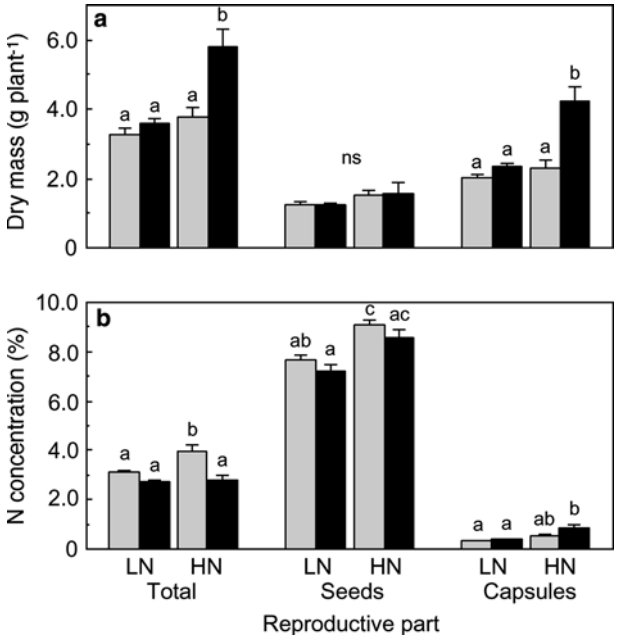

Fig. 3 Dry mass (**a**) and N concentration (**b**) of the reproductive part (total, seeds, and capsules) of *Xanthium canadense*. Different *letters* above columns indicate a significant difference between treatments ($P < 0.05$, Tukey–Kramer method). *White bars* 360 μmol mol^{-1}, *black bars* 700 μmol mol^{-1} CO_2. *LN* and *HN* represent low and high nitrogen availability (12 and 24 mM N), respectively. Redrawn from Kinugasa et al. (2003)

and did not decrease at elevated CO_2 (Fig. 3). On the other hand, capsule production seems to be less constrained by nitrogen availability. Capsules had very low nitrogen concentration and elevated CO_2 increased capsule mass at high nitrogen availability. Interestingly Kimball et al. (2002) reported that the boll (seed + lint) yield of cotton was increased 40% by elevated CO_2 while the lint fiber portion of the yield increased even more, by about 54%. In soybean, elevated CO_2 increased the pod wall mass more than seed yield (Allen et al. 1988). It seems that elevated CO_2 leads to a greater increase in the mass of a reproductive structure with a low nitrogen concentration than a structure with a high nitrogen concentration. This may be one of the reasons for a large variation in CO_2 response of reproductive yield.

Canopy

Leaf canopy is a unit of photosynthesis at the ecosystem level. It is a collection of leaves that are exposed to a large gradient of light availability and have different photosynthetic characteristics depending on their microclimate. An important question is whether enhancement of canopy photosynthesis at elevated CO_2 is solely ascribed to enhanced leaf photosynthetic rate or also involves alteration in canopy structure.

Effect of elevated CO_2 on canopy photosynthesis: does leaf area index respond to growth CO_2?

Reviewing studies on canopy photosynthesis, Drake and Leadly (1991) showed that elevated CO_2 increased canopy photosynthesis in almost all cases. The extent to which canopy photosynthesis increases, however, depends on species and on the availability of other resources (Bazzaz 1990; Arp 1991; McConnaughay et al. 1993). The rate of canopy photosynthesis is affected not only by photosynthetic rates in leaves but also by leaf area index (LAI, leaf area per unit ground area) in the canopy. There are disagreements about the effect of elevated CO_2 on leaf area development: LAI increased with elevated CO_2 in the canopy of perennial ryegrass (Nijs et al. 1988), soybean (Campbell et al. 1990), and rice (Rowland-Bamford et al. 1991), while it remained the same in artificial tropical forest ecosystems (Körner and Arnone 1992) and experimental stands of annuals (Hirose et al. 1996).

Leaf area development is strongly determined by nitrogen availability (Anten et al. 1995). Hirose et al. (1996) found a strong correlation between LAI and aboveground plant nitrogen, regardless of growth CO_2 levels in annual stands, suggesting that an increase in LAI at elevated CO_2 will occur only if plants simultaneously take up more nitrogen, through increased root growth and/or through increased root activity. However, Harz-Rubin and DeLucia (2001) found that vegetation stands under elevated CO_2 had greater LAI even when compared at the same nitrogen uptake. Kim et al. (2001) also found LAI for a given nitrogen uptake to be greater for plants under elevated CO_2, but only when nitrogen uptake itself was high, and not when it was low.

Although an increase in LAI enhances canopy photosynthesis due to increased light interception, when nitrogen in the canopy is limited an increase in LAI reduces leaf nitrogen per unit leaf area, leading to a decline in the photosynthetic capacity of leaves. There exists an optimal LAI at which the canopy photosynthetic rate for a given canopy nitrogen is maximised (Anten et al. 1995; Hirose et al. 1997). It has been shown that predicted LAI values are strongly correlated with measured LAIs (Anten et al. 2000). Anten et al. (2004) applied the concept of optimal LAI to stands of rice grown under free air CO_2 enrichment (FACE). In this experiment, LAI increased with increasing nitrogen availability but was not affected by elevated CO_2. Elevated CO_2 did not affect total plant nitrogen in the stand, but slightly reduced leaf nitrogen per unit ground area due to reduced allocation of nitrogen to leaves. These results indicate that elevated CO_2 increases LAI when compared at the same leaf nitrogen levels, which is consistent with the model prediction (Fig. 4a, b). However, the increase in LAI by elevated CO_2 was only 6–8%, both in the experiment and the prediction, suggesting that nitrogen availability is the most important factor for leaf development even under elevated CO_2.

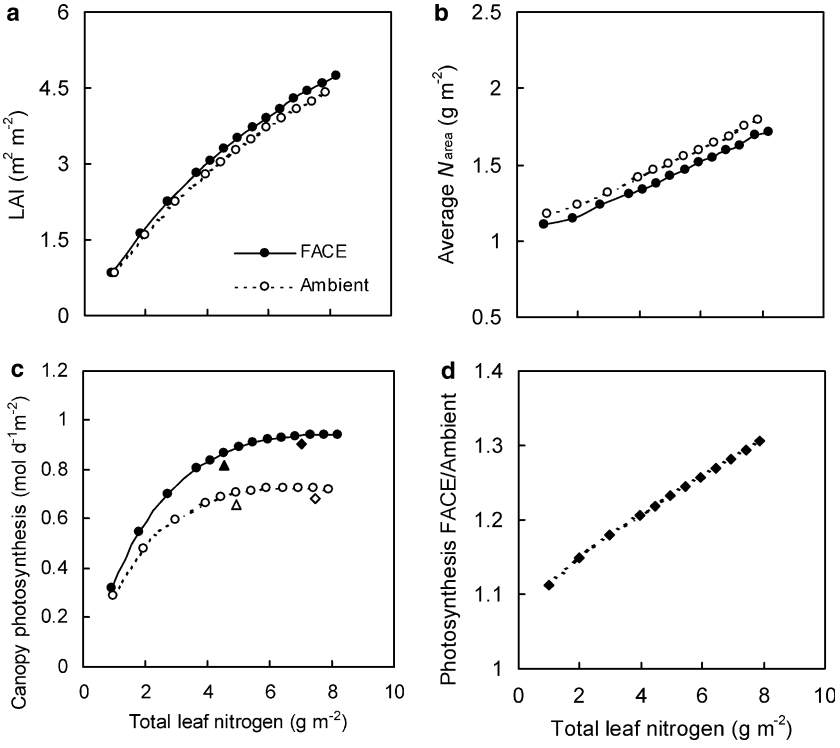

Fig. 4 The predicted relationship between leaf area index (LAI),canopy photosynthesis and leaf nitrogen in rice stands grown at FACE (free air CO_2 enrichment, ambient plus 200 μmol mol^{-1} CO_2) and ambient conditions. **a** Optimal LAI for maximum carbon gain as a function of total amount of leaf nitrogen in the canopy (N_{canopy}), **b** associated optimal average leaf nitrogen content (optimal $N_{area} = N_{canopy}$/ optimal LAI), and **c** net daily canopy carbon gain. Canopy photosynthesis at actual N_{canopy} is also given in **c**: *open symbols* ambient CO_2; *closed symbols* FACE; *triangles* standard nitrogen (9 g N m^{-2}); *diamonds* high nitrogen (15 g N m^{-2}). **d** Ratio of canopy photosynthesis in elevated CO_2 to that in ambient CO_2 (FACE: ambient). Redrawn from Anten et al. (2004)

Anten et al. (2004) further analysed the canopy photosynthetic rates in the rice stands. There are clear indications that the positive effect of elevated CO_2 on canopy carbon gain increases with nitrogen availability (Fig. 4c, d). So far, this interactive effect of CO_2 and nitrogen has been attributed to two mechanisms. First, inhibition of leaf photosynthesis by carbohydrate accumulation at elevated CO_2 tends to be stronger under low than under high nitrogen availability (Rogers et al. 1996). Second, nitrogen uptake increases under elevated CO_2 only when nitrogen availability is high, and not when it is low (Stitt and Krapp 1999). Anten et al. (2004) proposed a mechanism of an interactive effect of nitrogen and CO_2 that is independent of the above two factors. When nitrogen availability is low, the canopy is relatively open and most leaves receive relatively high light. Under these conditions, the effect of elevated CO_2 on canopy photosynthesis will be predominantly through its effect on the light-saturated rate of photosynthesis in the leaves. But as nitrogen availability increases, the canopy becomes denser and lower leaves become increasingly shaded. Under these conditions the enhanced quantum yield under elevated CO_2 will have an increasingly positive effect on canopy photosynthesis (see Fig. 5e in Anten et al. 2004).

Population

Plant population consists of individuals varying in size. Competition for light has been suggested as an important factor for the development of size inequality (Weiner 1990). Using even-aged, monospecific stands of an annual herb, we studied the effect of elevated CO_2 on competition between individuals and the mechanism of development of size inequality.

Effects of elevated CO_2 on size distribution of individuals in a monospecific stand

Competition among individuals in plant populations are categorised with respect to symmetry in competition: symmetric and asymmetric competition (Weiner 1990). Symmetric competition indicates that individuals in a stand acquire resources in proportion to their size, while in asymmetric competition large individuals acquire more than proportional amounts of resources. It has been suggested that competition for light is asymmetric (Ford and Diggle 1981; Weiner 1986; Jurik 1991; Nagashima 1999; Hikosaka et al. 1999), while that for nutrients is more symmetric (Weiner et al. 1997; Hikosaka and Hirose 2001). The mode of competition is critical to the development of size inequality in the stand. Size inequality is assessed with the coefficient of variation (CV) (Weiner 1990). Symmetric competition, where plant growth is proportional to the size, does not alter size inequality, while asymmetric competition increases size inequality in the stand.

Since diffusion of CO_2 within plant stands is very fast, competition for CO_2 is unlikely to occur among individuals (Jones 1992). Even though elevated CO_2 benefits all individuals in the stand, the enhancement of growth by elevated CO_2 may indirectly alter the mode of competi-

tion (Wayne and Bazzaz 1997). There are two alternative hypotheses in this respect. One is that elevated CO_2 makes the competition more asymmetric and increases size inequality in the stand. It occurs when enhanced growth of larger individuals suppresses light acquisition of smaller individuals. The other is that elevated CO_2 decreases the degree of asymmetry in competition and, consequently, size inequality. This is because the end-product inhibition of photosynthesis due to elevated CO_2 (Stitt and Krapp 1999) may be stronger in larger plants exposed to high light, and because the reduction of the light compensation point of photosynthesis at elevated CO_2 will benefit the smaller shaded individuals more than the larger ones (Osborne et al. 1997).

To test these hypotheses, we established even-aged monospecific stands of an annual, *Chenopodium album*, at ambient and double CO_2 levels, with high and low nutrient availabilities in open-top chambers (Nagashima et al. 2003). The growth of individual plants was monitored non-destructively every week until flowering. Elevated CO_2 significantly enhanced plant growth at high nutrient levels, but did not at low nutrient levels. The size inequality represented by CV tended to increase at elevated CO_2. Size structure of the stands was analysed by the cumulative frequency distribution of plant size (Fig. 5). At early stages of plant growth, CO_2 elevation benefited all individuals and shifted the whole size distribution of the stand to large size classes. At later stages, dominant individuals were still larger at elevated than at ambient CO_2, but the difference in small subordinate individuals between the two CO_2 levels became smaller. Although these tendencies were found at both nutrient availabilities, the difference in size distribution between CO_2 levels was larger at high nutrients. The CO_2 elevation did not significantly enhance the growth rate as a function of plant size except for the high nutrient stand at the earliest stage, indicating that the higher biomass at elevated CO_2 at later stages in the high nutrient stand was caused by the larger size of individuals at the earliest stage. Thus, elevated CO_2 seems to increase size inequality in vegetation stands and this effect becomes stronger at high nitrogen availability.

Effects of elevated CO_2 on light competition: an individual-based analysis of light acquisition and utilisation

We then investigated the physiological factors that underlie the effects of elevated CO_2 on the competitive interactions between plants. As mentioned above, difference in size structure results from different size-dependent growth rates of individuals in the stand. In a dense stand, large, dominant individuals have an advantage in capturing light because they place their leaves in the highest, most illuminated parts of the canopy. Small, subordinate individuals, on the other hand, may have an advantage because they need less investment of biomass in support tissues to maintain leaves at lower positions (Givnish 1982). As a result, they can allocate relatively more biomass to leaf area growth, and this can mitigate the negative effects of shading (Anten and Hirose 1998). To indicate the efficiency of biomass-use to capture light, Hirose and

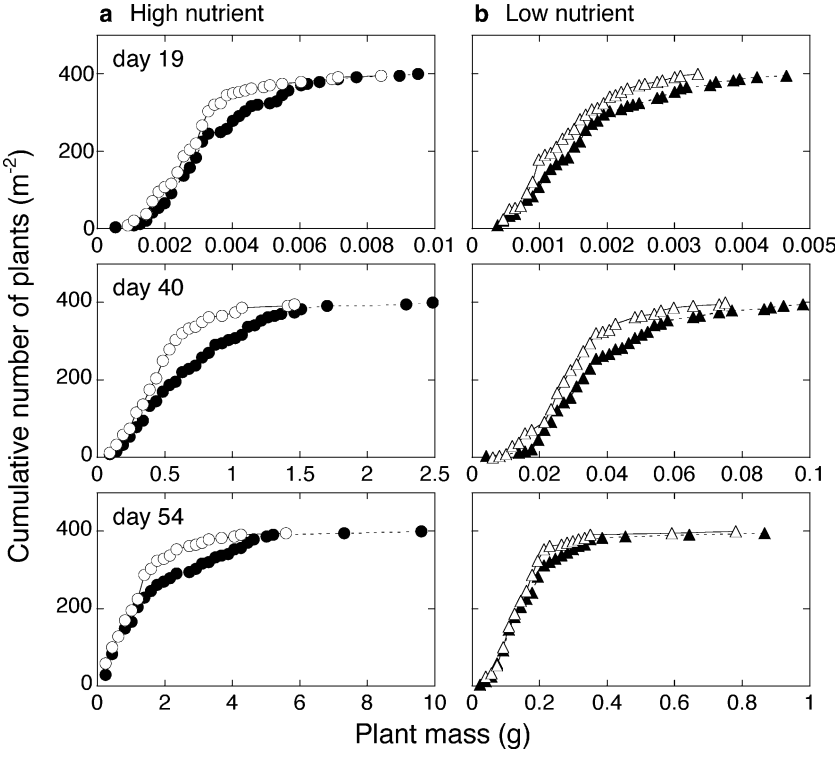

Fig. 5 Comparisons of cumulative frequency distributions of biomass in the even-aged stand of *Chenopodium album* between ambient (360 μmol mol^{-1}, *open symbols*) and elevated (700 μmol mol^{-1}, *closed symbols*) CO_2 concentrations, at high (**a**) and low (**b**) nutrient levels (3.6 and 0.36 g N m^{-2} $week^{-1}$, respectively). These results are shown for 19, 40, and 54 days after emergence. Redrawn from Nagashima et al. (2003)

Werger (1995) introduced the parameter Φ_{mass}, defined as photon flux captured per unit above-ground mass. They suggested that Φ_{mass} might not differ between dominant and subordinate species in multispecies systems. However, plant growth is determined not only by the amount of acquired resources, but also by the efficiency of resource use (growth per unit amount of resource acquired). Hikosaka et al. (1999) defined light-use efficiency of photosynthesis (LUE) as photosynthesis per unit photon interception, and described the photosynthesis of individuals as the product of Φ_{mass} and LUE: $RPR = \Phi_{mass} \times LUE$, where RPR is the relative photosynthetic rate (photosynthetic rate per unit above-ground mass). Provided that plant growth is proportional to leaf photosynthesis, RPR is closely related to the relative growth rate (RGR). With a modification of the canopy photosynthesis model of Hirose and Werger (1987), Hikosaka et al. (1999) estimated the photosynthetic rate of individuals in a natural, monospecific stand of an annual, *X. canadense*. They found that Φ_{mass} was higher in larger individuals, while LUE was highest in intermediate individuals. As a consequence, RPR was high in intermediate and larger individuals, and lowest in smaller individuals.

The model described above was then applied to monospecific stands growing at ambient and at elevated CO_2 (Hikosaka et al. 2003). As in the previous study (Nagashima et al. 2003), we established even-aged stands of an annual, *C. album*, at two CO_2 levels in open-top chambers with sufficient nutrient supply. The whole-plant photosynthesis of every individual in the stand was calculated from (1) the distribution of light

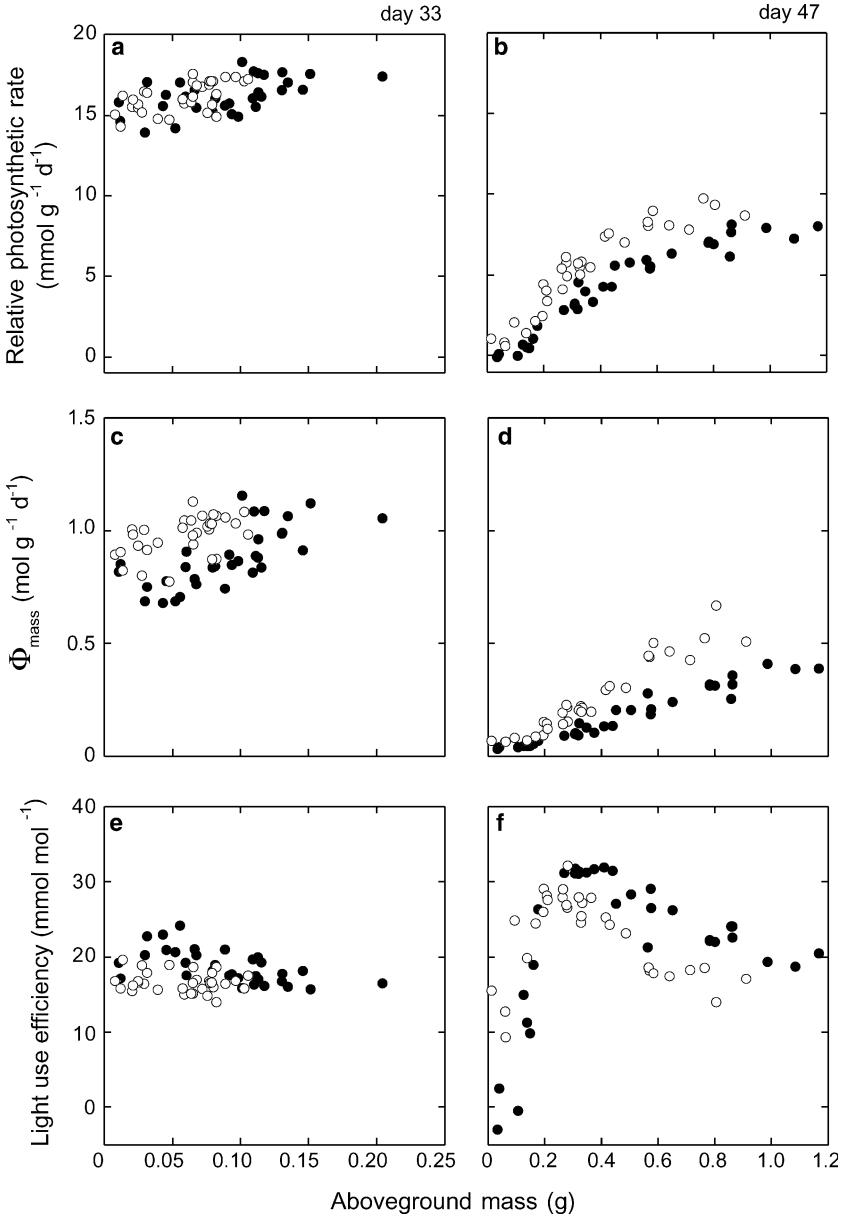

Fig. 6 Relative photosynthetic rates (RPR, whole-plant photosynthetic rate per unit above-ground mass; **a**, **b**), Φ_{mass} (photon flux captured per unit above-ground mass; **c**, **d**), and light use efficiency (LUE, photosynthesis per unit captured photon; **e**, **f**), as a function of above-ground dry mass at 33 (**a**, **c**, **e**) and 47 (**b**, **d**, **f**) days after emergence. $RPR = \Phi_{mass} \times LUE$. *Open circles* ambient; *closed circles* elevated CO_2 (360 μmol mol^{-1} and 700 μmol mol^{-1}, respectively). Redrawn from Hikosaka et al. (2003)

and leaf nitrogen, and (2) the relationships between photosynthetic parameters and leaf nitrogen content per area. Elevated CO_2 increased light-saturated rates of photosynthesis by 10–15% and the initial slope of the light-response curve by 11%, but had no effect on dark respiration. The relative rate of photosynthesis (RPR, the rate of photosynthesis per unit above-ground mass) was analysed as the product of light capture (Φ_{mass}, the photon flux captured per unit above-ground mass) and light-use efficiency (LUE, plant photosynthesis per unit photon capture) (Fig. 6). At an early stage of stand development (33 days after germination), RPR was nearly constant and no difference was found between ambient and elevated CO_2. However, CO_2 elevation influenced the components of RPR differently. Elevated CO_2 reduced Φ_{mass}, which offset the increase in LUE. Later (47 days), RPR was positively correlated with plant mass at both CO_2 concentrations. When compared at an equal plant mass, RPR was lower at elevated CO_2, which was caused by a reduction in Φ_{mass} despite some compensation by higher LUE. We conclude that elevated CO_2 increases size inequality of a stand through enhanced photosynthesis and growth of dominants, which reduce the light availability for subordinates and consequently increase size inequality in the stand.

Conclusion

Elevated CO_2 enhances photosynthetic rates. The enhanced photosynthesis, however, does not directly lead to increased plant growth and reproduction. As nitrogen uptake is not stimulated as much as carbon uptake, CO_2 elevation alters the C/N balance in the plant body. Plants respond to elevated CO_2 by changing biomass allocation to mitigate the altered C/N balance. Increase in LMA compensates for lowered leaf nitrogen concentration per unit mass to maintain a certain level of leaf nitrogen per unit area. In plants with protein-rich seed, reproductive growth is limited by nitrogen rather than by carbon. Elevated CO_2 does not increase reproductive yield as much as vegetative growth. Proportionate allocation of biomass to reproduction decreases when reproductive growth is limited by nitrogen rather than by carbon. Effects of elevated CO_2 at canopy and population levels are manifested through interactions between light and nitrogen availability, and also through interactions among individuals. In a leaf canopy, leaf area increases with CO_2 elevation when nitrogen uptake is simultaneously increased. If dominant plants increase their leaf area, they will reduce light availability in the lower layers of the canopy and thus the growth of plants there, which makes competition among individuals more asymmetric. Interaction among individuals makes responses to elevated CO_2 fairly sensitive to nitrogen availability in the soil. Integrating these responses would be indispensable for understanding functioning of plants in a high-CO_2 world.

Acknowledgements We would like to dedicate this paper to Mr. Ken-Ichi Sato to commemorate his contribution to the Experimental Garden of Tohoku University. This study was supported in part by the Japanese Ministry of Education, Culture, Science, Sports and Technology.

References

Ackerly DD, Bazzaz FA (1995) Plant growth and reproduction along CO_2 gradients: non-linear responses and implications for community change. Global Change Biol 1:199–207

Aerts R, Chapin FS III (2000) The mineral nutrition of wild plants revisited: a re-evaluation of processes and patterns. Adv Ecol Res 30:1–67

Allen LHJ, Vu JCV, Valle RR, Boote KJ, Jones PH (1988) Nonstructural carbohydrates and nitrogen of soybean grown under carbon dioxide enrichment. Crop Sci 28:84–94

Anten NPR, Hirose T (1998) Biomass allocation and light partitioning among dominant and subordinate individuals in *X canadense* stands. Ann Bot 82:665–673

Anten NPR, Schieving F, Medina E, Werger MJA, Schuffelen P (1995) Optimal leaf area indices in C_3 and C_4 mono- and dicotyledonous species at low and high nitrogen availability. Physiol Plant 95:541–550

Anten NPR, Hikosaka K, Hirose T (2000) Nitrogen utilization and the photosynthetic system. In: Marshal B, Roberts J (eds) Leaf development and canopy growth. Sheffield Academic Press, Sheffield, pp 171–203

Anten NPR, Hirose T, Onoda Y, Kinugasa T, Kim HY, Okada M, Kobayashi K (2004) Elevated CO_2 and nitrogen availability have interactive effects on canopy carbon gain in rice. New Phytol 161:459–472

Arp WJ (1991) Effects of source-sink relations on photosynthetic acclimation to elevated CO_2. Plant Cell Environ 14:869–875

Bazzaz FA (1990) The response of natural ecosystems to the rising global CO_2 levels. Annu Rev Ecol Syst 21:167–196

Brouwer R (1962) Nutritive influences on the distribution of dry matter in the plant. Neth J Agri Sci 10:399–408

Campbell WJ, Allen LH Jr, Bowes G (1990) Response of soybean canopy photosynthesis to CO2 concentration, light, and temperature. J Exp Bot 41:427–433

Cure JD, Acock B (1986) Crop responses to carbon dioxide doubling: a literature survey. Agric For Meteor 38:127–145

Curtis PS (1996) A meta-analysis of leaf gas exchange and nitrogen in trees grown under elevated carbon dioxide. Plant Cell Environ 19:127–137

Curtis PS, Wang X (1998) A meta-analysis of elevated CO_2 effects on woody plant mass, form, and physiology. Oecologia 113:299–313

Davidson RL (1969) Effect of root/leaf temperature differentials on root/shoot ratios in some pasture grasses and clover. Ann Bot 33:561–569

Drake BG, Leadly PW (1991) Canopy photosynthesis of crops and native plant communities exposed to long-term elevated CO_2. Plant Cell Environ 14:853–860

Evans JR (1989) Photosynthesis and nitrogen relationships in leaves of C_3 plants. Oecologia 78:9–19

Evans JR, Seemann JR (1989) The allocation of protein nitrogen in the photosynthetic apparatus: costs, consequences and control. In: Briggs WR (ed) Photosynthesis. Alan R Liss, New York, pp 183–205

Fajer ED, Bowers MD, Bazzaz FA (1991) Performance and allocation patterns of the perennial herb *P* lantago lanceolata in response to simulated herb ivory and elevated carbon dioxide environments. Oecologia 87:37–42

Farnsworth EJ, Bazzaz FA (1995) Inter- and intra-generic differences in growth, reproduction, and fitness of nine herbaceous annual species grown in elevated CO_2 environments. Oecologia 104:454–466

Farquhar GD, von Caemmerer S, Berry JA (1980) A biochemical model of photosynthetic CO_2 assimilation in leaves of C_3 species. Planta 149:78–90

Ford ED, Diggle PJ (1981) Competition for light in a plant monoculture modelled as a spatial stochastic process. Ann Bot 48:481–500

Givnish TJ (1982) On the adaptive significance of leaf height in forest herbs. Am Nat 120:353–381

Harz-Rubin JS, DeLucia EH (2001) Canopy development of a model herbaceous community exposed to elevated CO_2 and soil nutrients. Physiol Plant 113:258–266

Hikosaka K (1997) Modelling optimal temperature acclimation of the photosynthetic apparatus in C3 plants with respect to nitrogen use. Ann Bot 80:721–730

Hikosaka K (2004) Interspecific difference in the photosynthesis-nitrogen relationship: patterns, physiological causes, and ecological importance. J Plant Res 117:481–494

Hikosaka K, Hirose T (1998) Leaf and canopy photosynthesis of C_3 plants at elevated CO_2 in relation to optimal partitioning of nitrogen among photosynthetic components: theoretical prediction. Ecol Model 106:247–259

Hikosaka K, Hirose T (2001) Nitrogen uptake and use of competing individuals in a *Xanthium canadense* stand. Oecologia 126:174–181

Hikosaka K, Terashima I (1995) A model of the acclimation of photosynthesis in the leaves of C_3 plants to sun and shade with respect to nitrogen use. Plant Cell Environ 18:605–618

Hikosaka K, Murakami A, Hirose T (1999) Balancing carboxylation and regeneration of ribulose-1,5-bisphosphate in leaf photosynthesis: temperature acclimation of an evergreen tree, *Quercus myrsinaefolia*. Plant Cell Environ 22:841–849

Hikosaka K, Sudoh S, Hirose T (1999) Light acquisition and use by individuals competing in a dense stand of an annual herb, *Xanthium canadense*. Oecologia 118:388–396

Hikosaka K, Yamano T, Nagashima H, Hirose T (2003) Light-acquisition and use of individuals as influenced by elevated CO_2 in even-aged monospecific stands of *Chenopodium album*. Funct Ecol 17:786–795

Hilbert DW (1990) Optimization of plant root: shoot ratios and internal nitrogen concentration. Ann Bot 66:91–99

Hilbert DW, Larigauderie A, Reynolds JF (1991) The influence of carbon dioxide and daily photon-flux density on optimal leaf nitrogen concentration and root: shoot ratio. Ann Bot 68:365–376

Hirose T (1987) A vegetative plant growth model: adaptive significance of phenotypic plasticity in matter partitioning. Funct Ecol 1:195–202

Hirose T (1988) Nitrogen availability, optimal shoot/root ratios and plant growth. In: Werger MJA, can der Aart PJM, During HJ, Verhoven JTA (eds) Plant form and vegetation structure. SPB Academic Publishing, The Hague, pp 135–145

Hirose T, Werger MJA (1987) Maximizing daily canopy photosynthesis with respect to the leaf nitrogen allocation pattern in the canopy. Oecologia 72:520–526

Hirose T, Werger MJA (1995) Canopy structure and photon flux partitioning among species in a herbaceous plant community. Ecology 76:466–474

Hirose T, Ackerly DD, Traw MB, Bazzaz FA (1996) Effects of CO_2 elevation on canopy development in the stands of two co-occurring annuals. Oecologia 108:215–223

Hirose T, Ackerly DD, Traw MB, Ramseier D, Bazzaz FA (1997) CO_2 elevation, canopy photosynthesis and optimal leaf area index. Ecology 78:2339–2350

IPCC (2001) Climate change 2001: the scientific basis. In: Houghton JT, Ding Y, Griggs DJ, et al. (eds) Contribution of working group I to the 3rd assessment report of the intergovernmental panel on climate change. Cambridge University Press, Cambridge

Ishizaki S, Hikosaka K, Hirose T (2003) The increase in leaf mass per area benefits plant growth at elevated CO_2 concentration. Ann Bot 91:905–914

Jablonski LM, Wang XZ, Curtis PS (2002) Plant reproduction under elevated CO_2 conditions: a meta-analysis of reports on 79 crop and wild species. New Phytol 156:9–26

Jones HG (1992) Plants and microclimate, 2nd edn. Cambridge University Press, Cambridge

Jurik TW (1991) Population distribution of plant size and light environment of giant ragweed (*Ambrosia trifida* L). Oecologia 87:539–550

Kim HY, Lieffering M, Miura S, Kobayashi K, Okada M (2001) Growth and nitrogen uptake of CO_2-enriched rice under field conditions. New Phytol 150:223–229

Kimball BA (1983) Carbon dioxide and agricultural yield: an assemblage and analysis of 430 prior observations. Agron J 75:779–789

Kimball B, Kobayashi K, Bindi M (2002) Responses of agricultural crops to free-air CO_2 enrichment. Adv Agro 77:293–368

Kinugasa T, Hikosaka K, Hirose T (2003) Reproductive allocation of an annual, *Xanthium canadense*, at an elevated carbon dioxide concentration. Oecologia 137:1–9

Larigauderie A, Hilbert DW, Oechel WC (1988) Effect of carbon dioxide enrichment and nitrogen availability on resource acquisition and resource allocation in a grass *Bromus-mollis*. Oecologia 77:544–549

Luo Y, Field CB, Mooney HA (1994) Predicting responses of photosynthesis and root fraction to elevated $[CO_2]_a$: interactions among carbon, nitrogen, and growth. Plant Cell Environ 17:1195–1204

Luo Y, Reynolds J, Wang Y, Wolfes D (1999) A search for predictive understanding of plant responses to elevated $[CO_2]$. Global Change Biol 5:143–156

Lutze JL, Gifford RM (1998) Acquisition and allocation of carbon and nitrogen by *Danthonia richardsonii* in response to restricted nitrogen supply and CO_2 enrichment. Plant Cell Environ 21:1133–1141

Makino A, Mae T (1999) Photosynthesis and plant growth at elevated levels of CO_2. Plant Cell Physiol 40:999–1006

Makino A, Shimada T, Takumi S, Kaneko K, Matsuoka M, Shimamoto K, Nakano H, Miyao-Tokutomi M, Mae T, Yamamoto N (1997) Does decrease in ribulose-1,5-bisphosphate carboxylase by antisense *rbc*S lead to a higher nitrogen-use efficiency of photosynthesis under conditions of saturating CO_2 and light in rice plants? Plant Physiol 114:483–491

Makino A, Harada M, Kaneko K, Mae T, Shimada T, Yamamoto N (2000) Whole-plant growth and N allocation in transgenic rice plants with decreased content of ribulose-1,5-bisphosphate carboxylase under different CO_2 partial pressures. Aust J Plant Physiol 27:1–12

McConnaughay KDM, Berntson GM, Bazzaz FA (1993) Limitations to CO_2-induced growth enhancement in pot studies. Oecologia 94:550–557

Medlyn BE (1996) The optimal allocation of nitrogen within the C_3 photosynthetic system at elevated CO_2. Aust J Plant Physiol 23:593–603

Medlyn BE, Badeck FW, De Pury DGG, Barton CVM, Broadmeadow M, Ceulemans R, De Angelis P, Forstreuter M, Jach ME, Kellomaki S, Laitat E, Marek M, Philippot S, Rey A, Strassemeyer J, Laitinen K, Liozon R, Portier B, Roberntz P, Wang K, Jarvis PG (1999) Effects of elevated $[CO_2]$ on photosynthesis in European forest species: a meta-analysis of model parameters. Plant Cell Environ 22:1475–1495

Nagashima H (1999) The processes of height-rank determination among individuals and neighborhood effects in *Chenopodium album* L stands. Ann Bot 83:501–507

Nagashima H, Yamano T, Hikosaka K, Hirose T (2003) Effects of elevated CO_2 on the size structure of even-aged monospecific stands of annual, *Chenopodium album*. Global Change Biol 9:619–629

Nijs I, Impens I, Behaeghe T (1988) Effects of rising atmospheric carbon dioxide concentration on gas exchange and growth of perennial ryegrass. Photosynthetica 22:44–50

Onoda Y, Hikosaka K, Hirose T (2005) Seasonal change in the balance between capacities of RuBP carboxylation and RuBP regeneration affects CO_2 response of photosynthesis in *Polygonum cuspidatum*. J Exp Bot 56:755–763

Osborne CP, Drake BG, LaRoche J, Long SP (1997) Does long-term elevation of CO_2 concentration increase photosynthesis in forest floor vegetation? Indian strawberry in a Maryland forest. Plant Physiol 114:337–344

Peterson AG, Ball JT, Luo Y, Field CB, Curtis PS, Griffin KL, Gunderson CA, Norby RJ, Tissue DT, Forstreuter M, Rey A, Vogel CS, CMEAL participants (1999) Quantifying the response of photosynthesis to changes in leaf nitrogen content and leaf mass per area in plants grown under atmospheric CO_2 enrichment. Plant Cell Environ 22:1109–1119

Pettersson R, McDonald AJS, Stadenberg I (1993) Responses of small birch plants (*Betula pendula* Roth) to elevated CO_2 and nitrogen supply. Plant Cell Environ 16:1115–1121

Poorter H (1993) Interspecific variation in the growth response of plants to an elevated ambient CO_2 concentration. Vegetatio 104/105:77–97

Poorter H, Roumet C, Campbell BD (1996) Interspecific variation in the growth response of plants to elevated CO_2: a search for functional types. In: Körner C, Bazzaz FA (eds) Carbon dioxide, populations, and communities. Academic Press, San Diego, pp 375–412

Poorter H, van Berkel Y, Baxter B, den Hertog J, Dijkstra P, Gifford RM, Griffin KL, Roumet C, Roy J, Wong SC (1997) The effect of elevated CO_2 on the chemical composition and construction costs of leaves of 27 C_3 species. Plant Cell Environ 20:474–482

Rogers GS, Milham PJ, Gillings M, Conroy JP (1996) Sink strength may be the key to growth and nitrogen responses in N-deficient wheat at elevated CO_2. Aust J Plant Physiol 23:253–264

Rowland-Bamford AJ, Baker JT, Allen Jr LH, Bowes G (1991) Acclimation of rice to changing atmospheric carbon dioxide concentration. Plant Cell Environ 14:577–583

Sage RF (1994) Acclimation of photosynthesis to increasing atmospheric CO_2: the gas exchange perspective. Photosynth Res 39:351–368

Shitaka Y, Hirose T (1998) Effects of shift in flowering time on the reproductive output of *Xanthium canadense* in a seasonal environment. Oecologia 114:361–367

Stitt M, Krapp A (1999) The interaction between elevated carbon dioxide and nitrogen nutrition: the physiological and molecular background. Plant Cell Environ 22:583–621

Stulen I, den Hertog J (1993) Root growth and functioning under atmospheric CO_2 enrichment. Vegetatio 104/105:99–115

Sugiyama H, Hirose T (1991) Growth schedule of *Xanthium canadense*: does it optimize the timing of reproduction? Oecologia 88:55–60

Ward JK, Strain BR (1999) Elevated CO_2 studies: past, present and future. Tree Physiol 19:211–220

Wayne PM, Bazzaz FA (1997) Light acquisition and growth by competing individuals in CO_2-enriched atmospheres: consequences for size structure in regenerating birch stands. J Ecol 85:29–42

Webber AN, Nie GY, Long SP (1994) Acclimation of photosynthetic proteins to rising atmospheric CO_2. Photosynth Res 39:413–425

Weiner J (1986) How competition for light and nutrients affects size variability in Ipomoea tricolor populations. Ecology 67:1425–1427

Weiner J (1990) Asymmetric competition in plant populations. Trends Ecol Evol 5:360–364

Weiner J, Wright DB, Castro S (1997) Symmetry of below ground competition between *Kochia scoparia* individuals. Oikos 79: 85–91

Wilson JB (1988) A review of evidence on the control of shoot:root ratio in relation to models. Ann Bot 61:433–449

Wilson KB, Baldocchi DD, Hanson PJ (2000) Quantifying stomatal and non-stomatal limitations to carbon assimilation resulting from leaf aging and drought in mature deciduous tree species. Tree Physiol 20:787–797

Wullschleger SD (1993) Biochemical limitations to carbon assimilation in C_3 plants: a retrospective analysis of the A/C_i curves from 109 species. J Exp Bot 44:907–920

Yin X (2002) Response of leaf nitrogen concentration and specific leaf area to atmospheric CO_2 enrichment: a retrospective synthesis across 62 species. Global Change Biol 8:631–642

Ziska LH, Weerakoon W, Namuco OS, Pamplona R (1996) The influence of nitrogen on the elevated CO_2 response in field-grown rice. Aust J Plant Physiol 23:45–52

Ecol Res (2005) 20: 255–269
DOI 10.1007/s11284-005-0057-6

ORIGINAL ARTICLE

Takuya Kubo · Takashi Kohyama

Abies population dynamics simulated using a functional–structural tree model

Received: 4 October 2004 / Accepted: 3 February 2005 / Published online: 21 April 2005

Abstract A functional–structural model, PipeTree, based on *Abies* population data has been developed to reveal the interactions among processes at physiological, individual and population scales. Using field measurements obtained in a comprehensive series of research studies on subalpine *Abies* forest stands on Mt. Shimagare during the 1950s to 1980s, we designed the structural components and physiological process models for PipeTree. The results of the PipeTree simulation support the feasibility of using a functional–structural tree model to evaluate ecosystem performance at the stand level. PipeTree generates patterns similar to those in real subalpine forests, such as diameter–height relationships and time changes in basal area. After demonstrating the validity of the dynamics of a PipeTree population, we applied a sensitivity analysis under a productivity-enhanced environment in which the maximum photosynthetic rate (P_{max}) of PipeTree foliage was increased by 50% (caused, for example, by CO_2 enrichment). The results of P_{max} enhancement simulation show that the 50% increase in P_{max} doubles the net primary production (NPP) in the PipeTree stand. These results suggest the importance of canopy structure in evaluating the function of terrestrial ecosystems.

Keywords Functional–structural model · Pipe model · Resource allocation · Water conductance · *Abies veitchii*

T. Kubo (✉) · T. Kohyama
Graduate School of Environmental Earth Science,
Hokkaido University, Sapporo 060-0810, Japan
E-mail: kubo@ees.hokudai.ac.jp
Fax: +81-11-7064954

T. Kubo · T. Kohyama
Frontier Research Center for Global Change,
Japan Agency for Marine-Earth Science and Technology,
3173-25 Showamachi, Kanazawa-ku, Yokohama,
Kanagawa 236-0001, Japan

Introduction

Mathematical modeling of plant and plant populations to study the relationships between function and structure has a long history. Though the basic philosophy behind the methodology remains the same as in the pioneering work by Monsi and Saeki (1953), which proposed the possibility of mathematically modeling the interaction between plants and the light environment, the implementation of plant models has been undergoing changes over the half century.

One of the first attempts to evaluate plant function in three-dimensional space was done by Oikawa and Saeki (1977) in a straightforward extension of the Monsi-Saeki model. After Takenaka (1994) introduced a branching structure of shoots into plant production models, the spatial configuration of foliage was sufficient to evaluate vegetation function. Takenaka's framework also allowed plant structure to be modified according to local physiological activities, such as a pruning-up process by which shoots shaded by others are eliminated due to the lack of available resources. Recently, plant models of this family, with explicit spatial structure and physiological details, have been called "functional–structural models" (FSM; Sievänen et al. 2000). One of the successful FSMs is LIGNUM (e.g. Sievänen et al. 1997; Perttunen et al. 1998), which was designed as a generic tree simulator. LIGNUM is used to reproduce realistic shoot-branching architecture under some physiological and morphological constraints rather than to evaluate vegetation productivity at scales larger than the individual.

To respond to demands in the era of global change, scientists have developed "big-leaf" models with no details of vegetation canopy, which are much simpler than the Monsi-Saeki model. As Raulier et al. (1999) (who improved the simplified model by introducing multilayer structure) pointed out, big-leaf models are widely used for two major reasons: ease in parameterizing leaf-level photosynthetic measurements and improved tractability

in mathematics. In the world of big-leaf models, a single big leaf is enough to evaluate the ecosystem function of a forest.

The above suggests an apparent segregation between the very simplified class of models for global change and ''virtual plant'' models (Roux et al. 2001) with spatial details. This is not always true because some global change models incorporating spatial structure have arisen in recent years. As the importance of vegetation structure such as spatial configuration of foliage has become accepted, one-dimensional or size-structured plant production models have been developed (Raulier et al. 1999; Ito and Oikawa 2002; Sitch et al. 2003).

One-dimensional models efficiently describe the vertical profile of vegetation, but it is also true that models averaging horizontal heterogeneity of sessile-organism populations generate biased results. In order to adjust for this bias, an approximation method with stand-age distribution (Kohyama 1993; Hurtt et al. 1998; Bugmann 2001; Moorecroft et al. 2001) has been developed. The approximation that takes into account stand age effectively represents the spatial correlation between the upper and lower layers of stand, while the result depends on a parameter of the height, which divides a forest vertically into canopy and understory. To minimize such vagueness in calculations, a direct method including explicit vegetation structure is the most persuasive way of investigation in spite of the huge amount of calculation needed.

In the present study, we address a feasibility study of using a tree FSM as a tool to connect physiological and ecological processes with an explicitly spatially structured model. Firstly, we calibrate our process models and parameters such that the tree model simulates real trees observed in research plots. This is for the scaling-up from shoot to whole individual level. The next step is the examination, by scaling-up from tree to population, of whether density-dependent responses such as morphological changes in the tree canopy and self-thinning can be derived from the interaction among the simulated trees. Finally, the changes in ecosystem functional responses are inferred by a sensitivity analysis for the simulated forest stand.

Field measurements and outline of PipeTree

In order to integrate physiological and ecological processes within a forest stand with three-dimensional structure, PipeTree was developed as a dynamic functional–structural model (Sieväen et al. 2000; Roux et al. 2001). The model is specialized to simulate a particular conifer, *Abies veitchii* Lindl., based on the classical and intensive research series on the subalpine forest on Mt. Shimagare during 1950s and 1980s (e.g. Kuroiwa 1960; Kimura et al. 1960; Kohyama 1980; Kohyama and Fujita 1981; Kohyama et al. 1990). The comprehensive set of investigations ranging from physiological data to community dynamics meets our objective for constructing a detailed model that can reveal the interactions among biological processes at different levels.

From the first report on wave regeneration of *Abies* on Mt. Shimagare (Oshima et al. 1958), various types of ecological research have been carried out around the research forest. As the number of the Shimagare papers is too large to introduce here, we focused on the references which have mainly contributed to the development of PipeTree. Kohyama and Fujita (1981) and Kohyama et al. (1990) revealed the forest structure at the small-stand level in which *Abies veitchii* and *Abies mariesii* Mast. build approximately even-aged and even-canopy-height communities. These papers are the major references for population structure and time change in the PipeTree stand. The information at shoot level was obtained from Kohyama (1980), which shows the details of the shoot habits of *Abies* saplings. The data on physiological processes and biomass production of *Abies* are based on Kuroiwa (1960) and Kimura et al. (1960), respectively.

These references suggest that the observation data of crowded *Abies* stands on Mt. Shimagare offer some advantages over others for modeling. As the species diversity of the forest is very low, we can focus on the most dominant tree species for our modeling. Although the fraction of *Abies mariesii* in *Abies* stand is not negligible, we chose the most dominant species, *Abies veitchii* (hereinafter, just *Abies*) as our modeling target in the study.

The data of the subalpine wave-regenerated forest have two major convenient characteristics for our modeling: the tree age of the forest is almost coherent within a stand, and the individual trees have a simplified branching architecture. As Kohyama and Fujita (1981) set several plots along the stages of the wave regeneration and detected the stand age for each plot, the time-change data of stand structure are available. As mentioned in Kohyama (1980), the branching rules describing the architectural structure of *Abies* are rigid and easy to describe.

Taking advantage of the characteristics of field measurements for the development of PipeTree, we also kept the PipeTree design general by partitioning the computer program modules for each biological function. PipeTree is an *Abies* tree simulator with continuous three-dimensional space and discrete timestep (1-year) change. PipeTree is named after the ''pipe model'' (Shinozaki et al. 1964a, b), because one of the morphological constraints of PipeTree is the conservation law of cross-sectional area of sapwood of stem as described in the section ''Above-ground components.'' The details of PipeTree are described in the following sections, but it is impossible to explain all of the information in the source code because of space limitations. The source code, which is written mainly in C++, can be downloaded at http://hosho.ees.hokudai.ac.jp/kubo/pipetree/v2004/. This gives a more detailed (or perfect) reference for the model.

Structural components of PipeTree

PipeTree consists of above- and below-ground components. Each part can be divided into unit modules which virtually meet the four requirements for an idealized elementary unit (IEU) proposed by Sievänen et al. (2000). The requirements are morphological repetition in trees, local environment dependency, interaction with adjacent units and that the size of the unit be small enough that the local environment around it can be assumed to be homogeneous. We attempted to define the components in PipeTree according to the requirements of an IEU because this was suitable for our modeling objective, i.e. tree development without any "global" control such as an allometric relationship between tree height and basal trunk diameter.

In order to describe the structure of PipeTree, we must introduce the terms "class" and "object." The PipeTree components are called classes. These include the PipeTree class for trees, Stem class for shoots, Root class for below-ground parts, and so on. An instance of a class is called an object. For example, a stem is an object of the Stem class, a tree is an object of PipeTree. As shown here, the first letter of the class name is upper case, while that of the object name is lower case. An operator "." is introduced to refer to the properties of PipeTree objects. For example, tree.height (cm), tree.D10 (cm) and tree.age (year) represent tree height, trunk diameter at 10% of the height and age ($\in\{0, 1, 2, \ldots\}$) of the tree, respectively.

Above-ground components

The structure of the above-ground part of PipeTree is modular. The elementary module object is called a stem and has a cylindrical shape defined by stem.length (cm) and stem.diameter (cm). Figure 1a shows a Stem class object of stem.age = 0 at tree.age = 0. Because this special stem is the origin of all above-ground parts, an alias notation, stem0, is used to express the origin of all Stem objects.

The cross-sectional area of stem, stem.area, is divided into two regions: area of "alive pipes," stem.A_a, and "dead pipes", stem.A_d, in terms of the pipe model (Shinozaki et al. 1964a, b). Alive pipes transport water in trees, dead pipes lack this function. The area of sapwood and heartwood corresponds approximately to stem.A_a and stem.A_d, respectively. Additionally, the "surface area" of the stem, stem.A_s (cm^2), is defined as its curved surface (excluding base area) $\text{stem}.A_s = \text{stem.length} \times 2\sqrt{\pi \times \text{stem.area}}$

At every simulation time step, new Stem objects are generated using stems of stem.age = 1 where stem.age is a variable of stem which is set at zero at new stem emergence and increased by one at every time step. Let us introduce notations stemM and stemD for mother and daughter Stem objects, respectively.

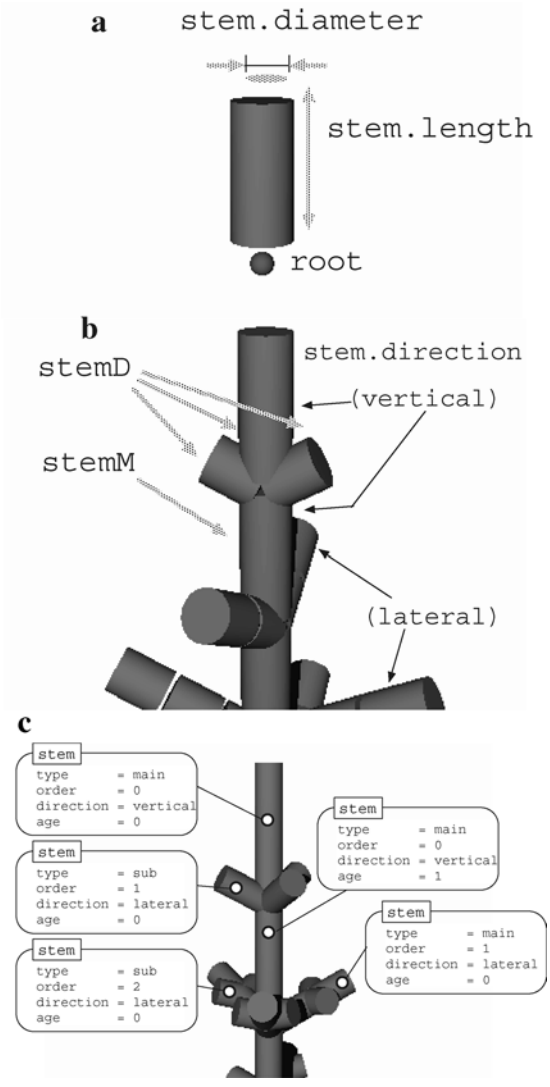

Fig. 1a–c Schemata of Stem objects with needle foliage (represented as a *cylinder*). **a** Stem of stem.age = 0. This is the origin, stem0, of all Stem objects of a PipeTree. At this age, the PipeTree consists of a single stem with needle foliage (represented as *cylinder*) with the attached root object (represented as a *ball*). The size of a stem is characterized by its length (*stem.length*) and diameter (*stem.diameter*). **b** Top of a PipeTree at tree.age = 10. The relationship between mother stem (*stemM*) and her three daughter (*stemD*) objects is shown. The notation *vertical* and *lateral* indicates stem.direction. **c** Structural properties of stem of tree.age = 16; stem.type is axis type $\in\{$main, sub$\}$; stem.order is branch order $\in\{0, 1, 2, \ldots\}$; stem.direction is the direction of shoot elongation in $\in\{$vertical, lateral$\}$; stem.age is stem age in years $\in\{0, 1, 2, \ldots\}$. Note the nested structure of stem.type $\in\{$main, sub$\}$

A stemM object has a set of {stemD}, that is written as stemM.D = {stemD}. Figure 1b shows the relationship of stemM and stemD at the top of the PipeTree object at tree.age = 10.

From the relationship of stemM and stemD, we can define stem.type and stem.order. As the branching pattern of *Abies* is monopodial, stems can be classified into two types: main axes and sub-axes, that is, stem.type ($\in$ {main, sub}), and a stemM can and must have only

single stemD of stemD.type = main. All the remaining stem objects are of stemD.type = sub. The order of stem, stem.order ($\in\{0, 1, 2, ...\}$) is defined as follows:

$$\text{stemD.order} = \begin{cases} \text{stemM.order} & \text{if stemD.type} = \text{main}, \\ \text{stemM.order} + 1 & \text{if stemD.type} = \text{sub}. \end{cases}$$

As the order of the original stem of an individual, stem0.order, is equal to zero, the orders of Stem objects in the trunk are always zero, while those of sub-branches are all larger than zero. Figure 1a, b illustrates the order structure of Stem objects.

Let us introduce another property to distinguish Stem class objects. The elongation direction of stem, stem.direction$\in\{$vertical, lateral$\}$, expresses whether the stem is a part of the main trunk or a lateral branch (see Fig. 1b). The recursive inheritance of stem.direction from stemM to stemD can simply defined as follows:

$$\text{stemD.direction} = \begin{cases} \text{stemM.direction} & \text{if stemD.type} = \text{main}, \\ \text{lateral} & \text{if stemD.type} = \text{sub}. \end{cases}$$

All Stem-class objects of stem.age < foliage_max_age (foliage_max_age is given in Table 8) have stem.foliage, a set of needles. The shape of stem.foliage is cylindrical, surrounding stem modules as a metaphor for the bunch of needles.

Below-ground components

As what we know about the below-ground components of plants is much less than what is known of above-ground parts, the modeling of roots inevitably becomes a simplified one. The below-ground part of PipeTree that is constructed only to absorb water from soil is one layer of the grid structure. In other words, two-dimensional discrete distribution of Root class objects represents the below-ground part. At each grid, the local density of roots is divided into two parts: root.fine and root.woody. Water absorption of PipeTree at a grid point depends on the density of fine root, root.fine (g), while woody root, root.woody (g), has no functional contribution in PipeTree. Root class objects are given the ability to grow and expand. The density of roots increases at each grid point, depending on the root density itself and on the allocation of photosynthate from above-ground parts to below-ground parts. Root objects of a tree can expand horizontally by increasing their number. Figure 2 shows an example of Root objects of tree.age = 20.

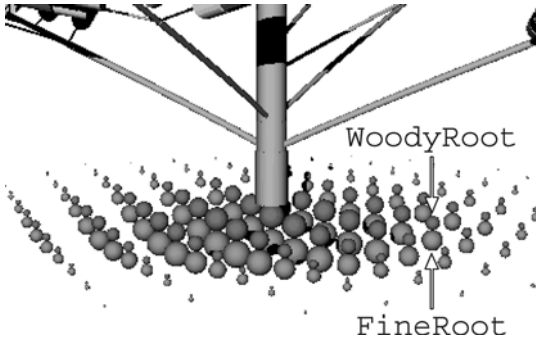

Fig. 2 Root objects of tree.age = 20. A root on grid points consists of fine and wood roots, represented by *balls*. The size of the *ball* indicates the local density of the root

Functional design of PipeTree

During one simulation step, PipeTree carries out the following processes: light capture, photosynthesis, water uptake, water allocation, respiration, allocation of photosynthate, survival check, shoot formation and stem diameter growth. These processes are controlled by resource budget systems under the constraint of structural and morphological restrictions. For an object, the range of resources is restricted to itself and its ''descendants,'' that is the set of objects existing in its distal direction. Additionally, the shoot formation of PipeTree is controlled by some morphological rules described later. Therefore resource allocation that violates the rules is not available. In this section, we briefly describe each process of PipeTree in a simulated abiotic environment (Table 1).

Light capture and photosynthesis

The total amount of light assimilation of a tree depends on the light capture at each stem.foliage. In PipeTree, every stem.foliage of stem.age = 0 (that is, Stem objects at branch terminals) has one light sensor set on the upper side of stem.foliage to evaluate the local light intensity, I (μmol PPFD $\text{m}^{-2}\,\text{s}^{-1}$). To decrease the amount of computation, the stem.foliage objects of stem.age > 0 refer to I of her youngest descendant of stem.type = main. The local light intensity depends on the light distribution of the celestial hemisphere and the distribution of Stem objects in the simulated space, which represents within- and between-tree competition for light.

The method of local light evaluation in PipeTree can be compiled into a sort of ''ray-tracing'' method developed for computer graphics. This is one of the most popular methods for functional–structural models (e.g. Sieväen et al. 1997; Perttunen et al. 1998) and for forest simulators (e.g. Pacala et al. 1993, 1996). For each light beam (or ''ray''), a light-beam tracing program checks for the existence of objects intercepting light. In this model, all Stem objects (with or without stem.foliage) have the ability to cut the light beam perfectly, that is, one hit kills the entire beam. Local light intensity at each light sensor is evaluated as the total intensity of all light beams that survive. The direction and intensity of a light beam are given by a corresponding light source in the hemisphere. The light sources represent an average value of indirect light; details are shown in Table 1.

Table 1 Parameters for simulated environment

Parameter name	Value and units
*xyz*_min	−160, −160, 0 (cm)
*xyz*_max	+160, +160, 1,500 (cm)
Note: These two vectors of (x, y, z) are the minimum and maximum points of the simulation plot for the stand situation, respectively. The boundary planes of x and y are both periodic for light calculation and branch growth. The boundary planes of z are absorptive. The periodic boundary plane shifts in parallel with the opposite boundary, while the absorptive boundary plane terminates the tracking of the light beam. For the simulation of the single-tree situation, no boundary is assumed	
I_{max}	2,000 μmol PPFD m^{-2} s^{-1}
Note: Maximum PPFD density. The product of I_{max} and local light intensity (in normalized value in [0, 1]) is equal to I in Eq. 1	
*n*_latitude	9
*n*_longitude	9
phi_min	0.1π (radian)
gradient_factor	3.0
Note: These four parameters are the properties of the distribution of light intensity in the celestial hemisphere. *n*_latitude and *n*_longitude are the partition numbers in the direction of latitude and longitude of the sky hemisphere, respectively. The number of light sources is the product of these two. Phi_min is the minimum elevation angle of light sources. The normalized intensity of the light source is given by gradient_factor, that is, the relative intensity of the light source at the zenith against the point at phi_min. As the light intensity so defined has no bias in the hemisphere, we can interpret it as a simulation of full or diffused light without any direct light	
precipitation	1,000 mm
Note: Annual precipitation. We assume that all water that falls in the simulation plot can be used by the trees	

Table 2 Parameters[a] for photosynthesis and respiration

Parameter name	Value and units
*p*_max	8.5 μmol CO_2 m^{-2} s^{-1}
Note: Maximum photosynthetic rate, P_{max} in Eq. 1	
f	0.05 μmol CO_2 μmol^{-1} PPFD
Note: The coefficient of light I, f in Eq. 1	
q	0.8 s m^2 μmol PPFD μmol CO_2^{-1}
Note: Degree of non-orthogonality, q in Eq. 1	
assimilation_wp	0.01 MPa^{-1}
Note: The degree of decrease in photosynthetic rate by stem.Ψ, water potential of stem. The assimilation rate per second, $A(I)$ in Eq. 1 is multiplied by exp(−assimilation_wp×stem.Ψ)	
converter	0.21
Note: This is the constant, $C_{A \to M}$ in Eq. 4, to convert the assimilation rate per second (μmol CO_2 m^{-2} s^{-1}) into annual production rate (μmol CO_2 g^{-1} $year^{-1}$)	
respiration_foliage	0.85 μmol CO_2 m^{-2} s^{-1}
respiration_wood	1.1×10^{-2} g cm^{-2} $year^{-1}$
Note: The respiration rate is leaf-area based, while the respiration rate of stem (r_s in body) is proportional to surface area of stem (stem.A_s) defined in text	
water_use_efficiency	250 g g^{-1}
Note: The estimate is based on the literature such as Kimura et al. (1960)	

[a]Most of these parameters relate to Eq. 1. The photosynthetic curves specified by these estimates are shown in Fig. 3. The estimates are based on the literature such as Kuroiwa (1960)

By evaluating the local light intensity at every stem, the potential photosynthetic rate (i.e. without water stress) of all Stem objects per second under the local light intensity I is estimated by applying the nonrectangular hyperbola function (Thornley 1976),

$$A(I) = \frac{fI + P_{max} - \sqrt{(fI + P_{max})^2 - 4fIqP_{max}}}{2q} \quad (1)$$

where $A(I)$ (μmol CO_2 m^{-2} s^{-1}) is the photosynthetic rate per second; f (μmol CO_2 μmol^{-1} PPFD) is the coefficient of I; P_{max} is the maximum photosynthetic rate at light saturation point; and q is the degree of the convexity of the curve. Tables 1 and 2 give the estimates of parameters of photosynthesis, and Fig. 3 shows the relationship between light intensity and photosynthetic rate.

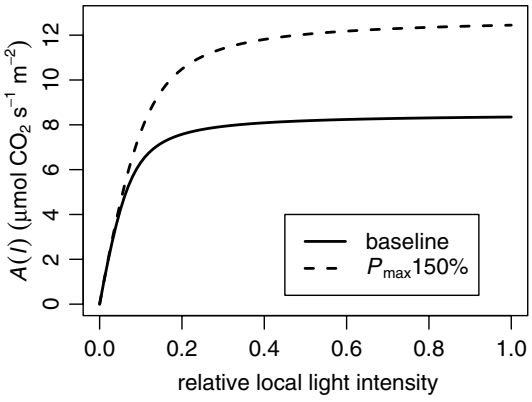

Fig. 3 Photosynthetic curves for PipeTree. The functional form is given by Eq. 1. The *horizontal axis* is relative local light intensity, and the *vertical axis* is photosynthetic rate (μ mol CO_2 m^{-2} s^{-1}). *Solid* and *dashed curves* correspond to baseline (maximum photosynthetic rate = 8.5) and P_{max} enhancement simulation (maximum photosynthetic rate = 12.8), respectively. The estimates for other parameters are shown in Tables 1 and 2

Water uptake and allocation

Realized photosynthetic rate at stem.foliage is not only restricted by local light intensity but by water availability. We employed a model in which assimilation rate was proportional to the ratio of water uptake to water requirement. This model is equivalent to one where water-use efficiency (WUE, Table 2) is constant. Therefore, realized assimilation rate, $A^*(I)$, can be derived as $A^*(I) = A(I) \times \text{stem}.W_u/\text{stem}.W_r$ where $\text{stem}.W_u$ (g s^{-1}) is water-uptake rate and $\text{stem}.W_r$ (g s^{-1}) is the required water given by $A(I)$/WUE from the definition of WUE. The modification to $A(I)$ is interpreted as meaning the realized photosynthetic rate $A^*(I)$ is limited by both the available amount of light and water at the foliage. The multiplication factor of water, $\text{stem}.W_u/\text{stem}.W_r$ is equal to or smaller than 1, because the water uptake, $\text{stem}.W_u$, never exceeds the water requirement, $\text{stem}.W_r$. This depends on the water absorption process described as follows.

The total water requirement of a tree is evaluated by a recursive procedure to sum up the whole W_r of stem objects. Suppose stemM is a mother stem and stemM.D = {stemD} is the set of all daughters of stemM. The total water requirement for stemM is

$$\text{stemM}.W_r = \text{stemM.foliage}.W_r + \sum_{\text{stemD} \in \text{stemM.D}} \text{stemD}.W_r,$$

where $\text{stemM.foliage}.W_r$ (g) is the water requirement of stemM.foliage given by $A(I)$/WUE.

Let us illustrate the outline of water capture and allocation in PipeTree. The total amount of water captured by a tree depends on the area and density of root objects. The volume taken up by a tree is the summation of each water absorption by a root object. At each grid point, root objects from separate tree objects compete for water against every other tree. The uptake of each root object is proportional to the local- or grid-scale density (biomass) of root and total W_r. The water-capture process for below-ground parts determines the total amount of water that can be used by a tree. The parameter values for water distribution are described in Table 3.

The basic rule for water distribution in PipeTree is simple: proportional division, that is, $\text{stem}.W_u$ is proportional to the product of $\text{stem}.W_r$ and the water-uptake rate of the tree, $\text{tree}.W_u$ (g s^{-1}) ($\text{stem}.W_u\text{P}\text{stem}.W_r \times \text{tree}.W_u$). The water allocation to stemD is

$$\text{stemD}.W_u = \text{stemM}.W_u \times \frac{\text{stemD}.W_r}{\text{stemM}.W_r}.$$

The procedure is applied recursively until the $\text{stem}.W_u$ for all stem objects has been evaluated.

The water-distribution process simultaneously derives the distribution of water potential for all Stem objects. The water potential of each stem, $\text{stem}.\Psi$, is recursively defined in the direction from root to shoot terminals. From the definitions of alive and dead areas of stem, only $\text{stem}.A_a$ contributes to water distribution. The recursive formulas to calculate $\text{stem}.\Psi$ are

$$\text{stemD}.\Psi = \text{stemM}.\Psi + c_g \Delta H + \frac{E \times \text{stemD.length}}{k_s \times \text{stemD}.A_a}, \quad (2)$$

$$\text{stem0}.\Psi = \Psi_{soil} + \frac{E}{k_r} + \frac{E \times \text{stem0.length}}{k_s \times \text{stem0}.A_a}, \quad (3)$$

where ΔH (cm) is the difference in height between stemD and stemM; E (g s^{-1}) is the flux of water in stemM; c_g (MPa cm^{-1}) is a constant of the effect of gravity; k_s (MPa $s\ g^{-1}\ cm^{-1}$) and k_r (MPa $s\ g^{-1}$) are the conductance constants for Stem and Root, respectively; and Ψ_{soil} (MPa) is the water potential of soil. These functional models were developed based on the modeling of hydraulic constraints in Magnani et al. (2000). In Table 4, the values of these parameters are shown.

Respiration and photosynthate allocation

Photosynthate at each stem is changed into the annual surplus production (Saeki 1960) and is transferred to other parts of the tree. The surplus production of stem, $\text{stem}.P(I)$ (g $year^{-1}$), is defined as

$$\text{stem}.P(I) = (\text{stem}.A^*(I) - r_f) \times C_{A \to M} \times \text{stem.foliage.weight} \quad (4)$$

where $\text{stem}.A^*(I)$ is the $A^*(I)$ of stem; r_f (μmol CO_2 m^{-2} s^{-1}) is the respiration rate of foliage; $C_{A \to M}$ is a conversion constant from (μmol CO_2 m^{-2} s^{-1}) to (μmol CO_2 g^{-1} $year^{-1}$).

In the next step, the maximum possible amount of photosynthate for stem is recursively evaluated as

Table 3 Parameters for Root object

Parameter name	Value and units
*c*_respiration Note: Annual turnover rate of fine root. Here we equate the turnover of fine root with fine root respiration, as both of them consume photosynthate at unknown rates	0.10 g g^{-1}
*c*_density	7.0 g^{-1}
*c*_distance Note: These two parameters are for the rate of Root formation. The rate at grid *i* is proportional to two factors: local crowding at grid *i* and the local density of mother Root objects. The inhibition of Root growth (in density) by local crowding is expressed by a functional form, $1-\exp(-c\_\text{density}\times w_i)$, where w_i is the local density of Root objects at grid *i*. The growth rate of Root objects at grid *i* is proportional to the density of mother Root objects, which is a weighted sum of local density of Root objects $\sum_{j\in\mathbf{G}} w_{i,j}$, where **G** is the set of all grid points and $w_{i,j}$ is the local density at grid *j* weighted by a function of distance *i*–*j*. The functional form of $w_{i,j}$ is $w_j \exp(-c\_\text{distance}\times d_{i,j})$, where $d_{i,j}$ is the distance between the centers of grids *i* and *j*	0.05 cm^{-1}
*c*_water Note: Water uptake rate is proportional to $1-\exp(c\_\text{water}\times D_r)$ where D_r (g cm^{-2}) is local density of fine root	7.0 g^{-1}
*c*_conversion Note: The conversion coefficient from fine root to woody root	0.10 g g^{-1}
number_fake_grid Note: Number of *x*- and *y*-grids for root system	(50, 50)

Table 4 Parameters[a] for water conductance

Parameter name	Value and units
total_time Note: Approximated total photosynthetic time from May–October, 12 h×90 days. This value is used to calculate water requirement per second	8.21×10^6 s
water_potential_soil Note: Water potential of soil, Ψ_{soil} in Eq. 3	−0.5 MPa
const_wp_grav Note: The effect of gravity, c_g in Eq. 2	9.8×10^{-5} MPa cm^{-1}
conductance_root Note: The conductance of root, k_r in Eq. 2	1.0×10^4 MPa s g^{-1}
conductance_stem Note: The conductance of stem, k_s in Eq. 2	5.0 MPa s g^{-1} cm^{-1}

[a]These parameters relate to Eqs. 2 and 3 and are based on literature such as Magnani et al. (2000)

$$\text{stem}.Q = \text{stem}.P(I) + \sum_{\text{stemD}\in\text{stem.D}} (\text{stemD}.Q - r_s \times \text{stemD}.A_s), \quad (5)$$

where stem.Q is the maximum amount of available photosynthate that the stem can consume and r_s (g cm^{-2}) is the coefficient of stem respiration. The estimate for r_s is shown in Table 2. The first term on the right side is 0 if the stem has no foliage, while the second term represents the transfer of photosynthate from the daughter Stem objects after their respiration loss is reduced. The photosynthate virtually lumped together is the resource that grows up and constructs the above- and below-ground parts of PipeTree.

The model for allocation of photosynthate between above- and below-ground parts is plastic and adaptive. The allocating "ratio" between them is changed at every simulation time step. The share of the below-ground part increases under the condition that total water demand of the above-ground part is larger than total water uptake, while it decreases if water uptake exceeds demand. We adopted the following functional form to determine the fraction of photosynthate for Root objects, u_{new}, which depends on water requirement and uptake for the original stem (i.e. stem0.W_r and stem0.W_u) and u, the fraction in the previous time step of the simulation:

$$u_{new} = \frac{1}{1+\exp[-(\text{stem0}.W_r/\text{stem0}.W_u + \log u - \log(1-u) - 1)]}. \quad (6)$$

The functional form is shown in Fig. 4. As defined in the equation, the below-ground fraction does not change (i.e. $u_{new} = u$) if stem0.W_r and stem0.W_u are equivalent.

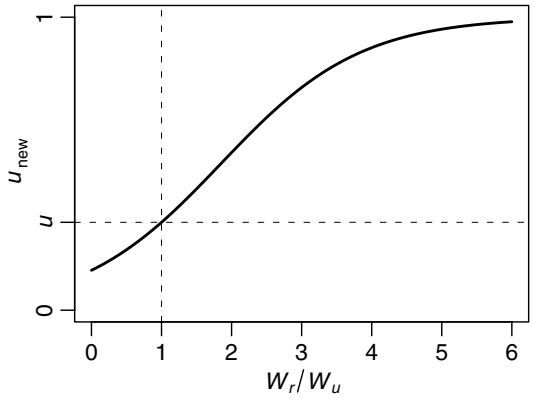

Fig. 4 Annual change in photosynthate allocation between above- and below-ground components as defined by Eq. 6. Suppose the ratio of below- to above-ground components is u at a simulation time step. The *horizontal axis* is the ratio of water requirement (W_r) to realized uptake (W_u) under u. The *vertical axis* shows the allocation to below-ground at the next step, u_{new}. The allocation becomes $u_{new} > u$ if water uptake is insufficient, and $u_{new} < u$ under conditions of water excess. Note that the curve defined by Eq. 6 always contains the point (1, u) for any u

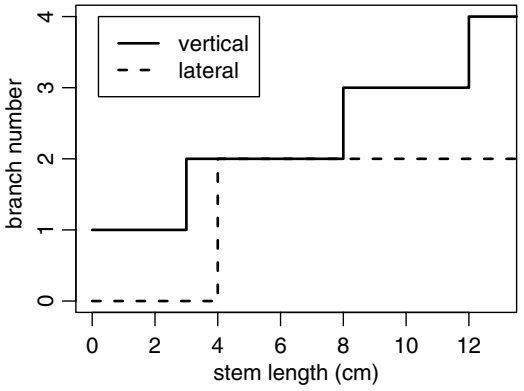

Fig. 5 Relationship between mother stem.length and number of buds (or number of daughter Stem objects). *Solid* and *dashed lines* correspond to vertical and lateral classes of stems, respectively. The branch number (or number of daughter stems) increases with the length of the mother stem for vertical type, while the possible number of branches is either zero or two for Stem objects of stem.type = sub. These values are inferred from literature such as Kohyama (1980) and Kohyama's field observations around Mt. Shimagare (unpublished data)

Survival check

The mortality process of Stem is one of the most difficult but important parts of PipeTree. Because we have no information on the event, we employed one of the simplest models, in which the annual mortality of each stem is independently (i.e. with no correlation to other objects) determined only by the availability of photosynthate for stem, that is, stem.Q_{max} defined in Eq. 5. The functional form is

$$\text{stem.mortality} = \exp(-c\_\text{mortality} \times \text{stem}.Q), \qquad (7)$$

where c_mortality is the coefficient of mortality rate (see Table 6). At every time step (1 year) for each stem in the tree, the alive status, stem.alive ($\in$\{TRUE, FALSE\}), is evaluated by the Bernoulli process.

After ending the procedure of checking stem survival, we recursively apply a function that the alive status of the daughter stem (stemD.alive) is changed by that of the mother's status (stemM.alive). This simulates that the death of a basal part of a branch or a tree kills its whole distal part. The value of stem.alive is recursively evaluated from stem0 (the origin stem of tree), that is, stemD.alive = FALSE if stemM.alive = FALSE. It is clear that stem0.alive = FALSE indicates the death of the tree.

Shoot formation and diameter growth

The formation of a shoot module (that is, stem with stem.foliage) requires PipeTree to solve several equations that seek the consistent allocation of photosynthate under morphological constraints. The process can be divided into three steps: setting the number of Bud class objects for main axes and sub-axes, evaluating scores for all Bud and Stem objects, and allocating photosynthate between newly created shoots and radial growth of preexisting Stem objects. Implicit numerical solvers are developed to find the best allocation between elongation growth of the branch and radial growth of the supporting part.

The branch number of a stem depends only on stem.length as shown in Fig. 5. This is equal to the number of Bud objects, primordia of the stem, in PipeTree. These Bud objects have type ($\in$\{main, sub\}) property similar to the Stem object. The set of Bud objects of a stem includes one bud of bud.type = main. The branching angle for each Bud shown in Table 5 depends on bud.type.

The angles of newly created Stem objects are given by the angles of "modifiers" in Table 5 with rotate function applied. The rotate function is defined as follows (Fig. 6). First, the angles in the global polar coordinates of a daughter stem are given as a copy of those of mother stem. Let us represent this as s, a set of azimuth angles ($s.\theta$) and elevation angles ($s.\phi$). The sets of angles shown in Table 5 are called modifiers represented as m. Both s and m are unit vectors in three-dimensional space. To modify s by m, we prepare two additional unit vectors, $v1$ and $v2$, defined as $(v1.\theta,\ v1.\phi) = (s.\theta,\ s.\phi + 0.5\pi)$ and $(v2.\theta,\ v2.\phi) = (s.\theta + 0.5\pi,\ 0)$, respectively. The rotation of s can be done by the following transformation (see Fig. 6):

$$s' = \sin(m.\phi) \times s + \cos(m.\phi) \times [\sin(m.\theta) \times v1 + \cos(m.\theta) \times v2],$$

where s' is the rotated vector. The angles of s are fixed once the values are set.

The next step in the allocation process is "scoring" the stem and bud using the equations and parameters in

Table 5 Angles for newly created Stem class objects. The set of (θ, ϕ) represents the angles of azimuth and elevation

Parameter name	Value and units
modifier_vertical	0.75π, 0.50π (radian)
modifier_lateral	1.50π, 0.498π (radian)
Note: These vectors of angles of azimuth and elevation determine the rotation angle between stem of mother and daughter, that is, the branching angle of the main (non-lateral) shoot. The origin for stemD rotation is the terminal point of stemM. The three-dimensional angle for stemD elongation is given by the rotate function as defined in the text	
branching_vertical	—, 0.15π (radian)
Note: Branching_vertical gives the angles of elevation of lateral branches of the leader shoot of PipeTree. As the angles of azimuth for these lateral shoots depend on the number of them, the angle between two adjacent shoots is always maximized (e.g. 0.5π for four lateral shoots)	
branching_lateral	0.03π, 0.10π (radian)
branching_lateral	0.97π, 0.10π (radian)
Note: The branching angles for lateral shoots of lateral stems are given by these two vectors of angles of azimuth and elevation. The sets correspond to "right" and "left" side branching, respectively	
branching_range_vertical	0.20π, 0.02π (radian)
branching_range_lateral	0.00π, 0.05π (radian)
Note: These vectors of radian indicate the ranges of "noise" in branching angles of azimuth and elevation. The branching angle is the sum of branching_X (X in vertical and lateral) and a random variable from the uniform distribution of ranges of branching_range_X	

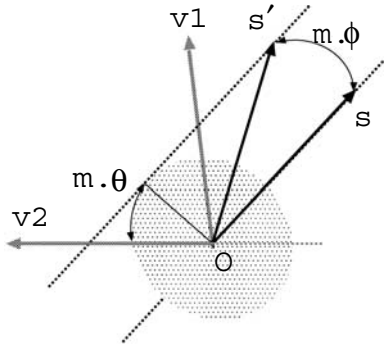

Fig. 6 Polar coordinates to rotate a daughter stem attached the top of her mother stem (*0*). The azimuth and rotation angles of a unit vector *s* are equal to those of the mother's. Vectors *v*1 and *v*2 are both orthogonal to *s* as defined in the text. Given a modifier defined by m.θ and m.ϕ, the rotated vector *s*′ is obtained from the coordinates defined by vectors *s*, *v*1 and *v*2

Table 6. These scores represent the relative intensity of sink function. The score of the stem is proportional to the product of the photosynthetic rate of the stem and a decreasing function of stem.order. The factor of stem.order is a model of apical dominance in PipeTree. In contrast, the scoring of Bud objects must take into account the apical dominance at the shoot level. In *Abies*, it is well known that resource allocation between main axes and sub-axes changes depending on the local light environment (Kohyama 1980). Kohyama (1980) reported that the crown of *Abies* becomes "umbrella-shaped" under dense canopies (i.e. dark environment). This can be explained by the change in apical dominance of the leader shoot of an individual tree. In order to simulate the response to light, we introduced an allocation rule based on local light intensity, shown in Fig. 7. The allocation to main axis of vertical branch (=trunk) decreases sharply under dark conditions, whereas less plasticity to light is assumed for horizontal branches.

The final step of shoot formation is photosynthate allocation under morphological constraints. There are two types of competition for photosynthate: among Stem objects in the tree and among Bud objects in the stem. As mentioned above, the scores for each Stem and Bud object represent the intensity of sink, that is, the amount of photosynthate allocated to an object is proportional to the score of the object. The allocation is subject to the law of conservation of photosynthate. Photosynthate allocation is also constrained by morphological rules. At Stem level, the rule of the pipe model (Shinozaki et al. 1964a, b) is applied such that the law of conservation in the "alive" area of the stem before and after branching is satisfied at every branching point in the tree. In order to check whether the pipe model rule is met at all branching points, the diameter of newly created Stem objects under a given photosynthate must be specified. As we defined the relationship between length and diameter of stem as shown in Fig. 8 and Table 8 based on literature such as Kohyama (1980) and the parameters for needle foliage as in Table 8, the diameter of a newly created stem under a given amount of photosynthate can be calculated by implicit numerical method. Taking into account everything mentioned above, the consistent allocation of photosynthate for every time step is established by a trial and error method of numerical calculation.

Table 6 Parameters for stem scoring (for photosynthate competition between terminal Stem class objects)

Parameter name	Value and units
order_factor	0.15
Note: This is used in the score evaluation for each stem. The score is defined as stem.score = stem.$P(I)$ × exp(−order_factor × stem.order) where stem.$P(I)$ and stem.order are annual net production and branch order of stem, respectively. Their details are described in the text. The functional form of stem.score is specified by a trial and error process. Finally, we adopted the simplest model, in which stem.score depends only on stem.order and not on other factors (e.g. photosynthetic rate and local light intensity)	
dark_inhibition_power	5.0
bud_main_dark_vertical	0.00
bud_main_light_vertical	0.85
bud_main_dark_lateral	0.60
bud_main_light_lateral	0.75
Note: These parameters are used in resource allocation between main buds and sub-buds for vertical and lateral stems. Let us suppose X∈ {vertical, lateral}. The fraction to main bud of stem of X is defined as bud_main_dark_X+ pow(I, dark_inhibition_power) × (bud_main_light_X − bud_main_dark_X) where pow(a, b) represents a^b and I is the local light intensity at stem. The fraction change dependent on I is shown in Fig. 5	
c_mortality	1.5×10^2 g^{-1}
Note: Coefficient of the available photosynthate for a stem as shown in Eq. 7	

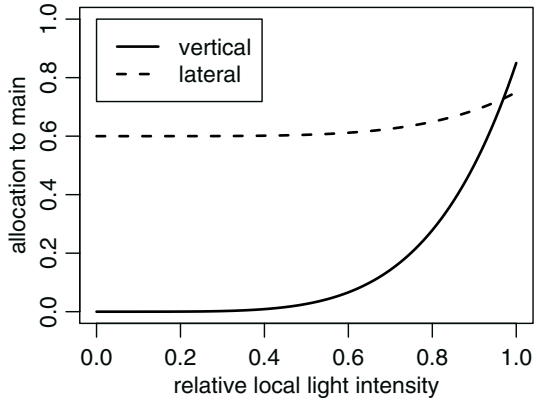

Fig. 7 Relationship between local light intensity of stem (*x-axis*) and the fraction of photosynthate allocation to "main axis" at new shoot formation (*y-axis*). As photosynthate allocation of *Abies* is changed conditionally with light intensity (Kohyama 1980), we employed a functional form (shown in Table 6) such that the curves in the figure can be generated

Simulation procedure

We ran the PipeTree simulator for three types of situations: single tree, multiple-tree stand and P_{max} enhancement. In the single-tree situation, a PipeTree object grows up from a single stem and root. Virtually no spatial limitations exist. This is done to calibrate parameters of PipeTree by comparing the data of single isolates of *Abies* observed around Mt. Shimagare.

After the parameter calibration in the single-tree situation, the simulation of a PipeTree population including 30 individual "clones" was run under the stand situation. The area of the simulation plot is approximately 10 m^2 (3.2×3.2 m quadrat) as described in Table 1. It is therefore an overcrowded initial condition of *Abies* regeneration compared to what is usually observed on Mt. Shimagare (Kohyama and Fujita 1981). The distribution of individuals is random on 10-cm grid points. The range of difference in age among individuals is 20 years, that is, all Tree objects gradually appear during the first 20 simulation steps. The age distribution is uniform. The configuration of tree.age = 0 is the same as that of the single-tree situation. The stand simulation is performed to demonstrate whether the characteristics of the *Abies* population observed on Mt. Shimagare can be generated using PipeTree without modifying the parameters obtained in the single-tree situation. For simplicity (and economical considerations in calculations), we removed PipeTree objects that could not grow in height during simulation run. This rule can be translated as a tree that loses its "leader shoot," that is, the stem at top of the tree (in other words, stem of stem.type = main and stem.order = 0 and stem.age = 0).

The final situation of P_{max} enhancement is almost the same as the stand situation except the maximum photosynthetic rate, P_{max} in Eq. 1, is increased by 50%, caused by, for example, CO_2 enrichment for all individuals. The relationship between local light intensity and photosynthetic rate under the enhancement situation is shown in Fig. 3. This was done to evaluate the feasibility of using the functional–structural model with ecological details under changing environments.

Simulation results

Snapshots of a simulation underway are shown in Fig. 9. For the stand situation (Fig. 9b), the pruning up of the lowest crown is observed, whereas the tree in the single situation (Fig. 9a) generates a conical crown with no pruning up of lower branches.

Table 7 Parameters for shoot formation

Parameter name	Value and units
d_length_power	1.1
d_length	62.0 cm
c_wp_length	25.0 MPa^{-1}
wp_length50	−0.59 MPa
Note: The length of stem, stem.length, is given in the following equation including the above parameters: $L = \frac{d\_length \times D^{d\_length\_power}}{1+\exp(-c\_wp\_length \times (W - wp\_length50))}$ where L, D and W, are stem.length, stem.diameter and stem.Ψ , respectively. The length of the stem monotonically increases with diameter, and monotonically decreases with stem.Ψ, as shown in Fig. 7	
density_wood	0.4 g cm^{-3}
Note: The value (constant for all Stem objects) is specified based on Kohyama (1980). This is required to calculate stem.weight from stem.volume	
pipe_bundle_min_length	0.5 cm
Note: Lower bound of the length of stem object. All the stems for which stem.length is smaller than pipe_bundle_min_length are removed before they grow. This is an ad hoc criterion to decrease the number of shoots	

Table 8 Parameters for needle foliage

Parameter name	Value and units
area_foliage	25.0 g cm^{-2}
Note: Here the rule of th epipe model (the law of conservation in area) is applied so that the amount of needle foliage is proportional to the area of stem. The conversion constant is derived from Kohyama (1980)	
foliage_max_age	3 year
needle_cylinder_radius	1.2 cm
Note: The value of foliage_max_age is based on Kohyama (1980) in which the age distribution of needles attached to a shoot is given. We assume foliage_max_age is constant as an approximated model of foliage. As mentioned in the text, the shape of needle foliage is cylindrical as an approximation of real needles	
eye_rotate_vertical	0.00, 0.50π (radian)
eye_rotate_lateral	0.50π, 0.50π (radian)
Note: These vectors of angles relate to the location of the eye and light sensor to evaluate local light intensity at each stem. The first and second values in the vector represent angles of azimuth and elevation of eye from the root of stem, respectively	

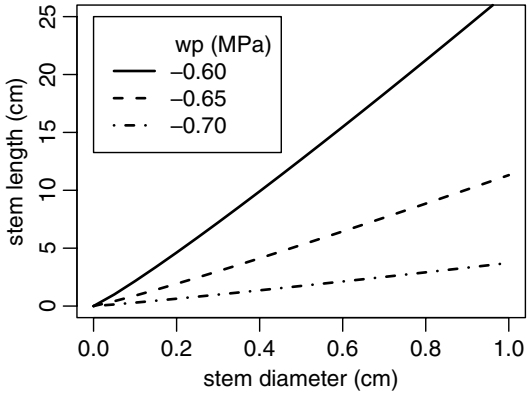

Fig. 8 Relationship between length and diameter of a newly created stem depending on water potential at the mother stem. We assumed that stem.length decreased with decreasing water potential. The functional form and parameter values are shown in Table 7

The results for the single-tree situation are shown in Fig. 10 using the data of single isolated trees on dwarf-bamboo grassland around Mt. Shimagare plots. The trunk diameter is measured at 10% of the height of the tree both in field observations and in the simulation. This indicates that the parameters for PipeTree given in the tables are suitable candidates for reconstructing the trunk diameter–height relationship.

The results for the stand situation (and the field measurements that correspond) are shown in Figs. 11 and 12. The relationship between diameter and height generated for the PipeTree population (Fig. 11b) is similar to the pattern obtained from field observations (Fig. 11a; Kohyama and Fujita 1981; Kohyama et al. 1990) in terms of (1) correspondence of diameter–height change to stand age and (2) plasticity in diameter–height relationship for single-tree (Fig. 10) and stand situations. At the same time, we can see some differences

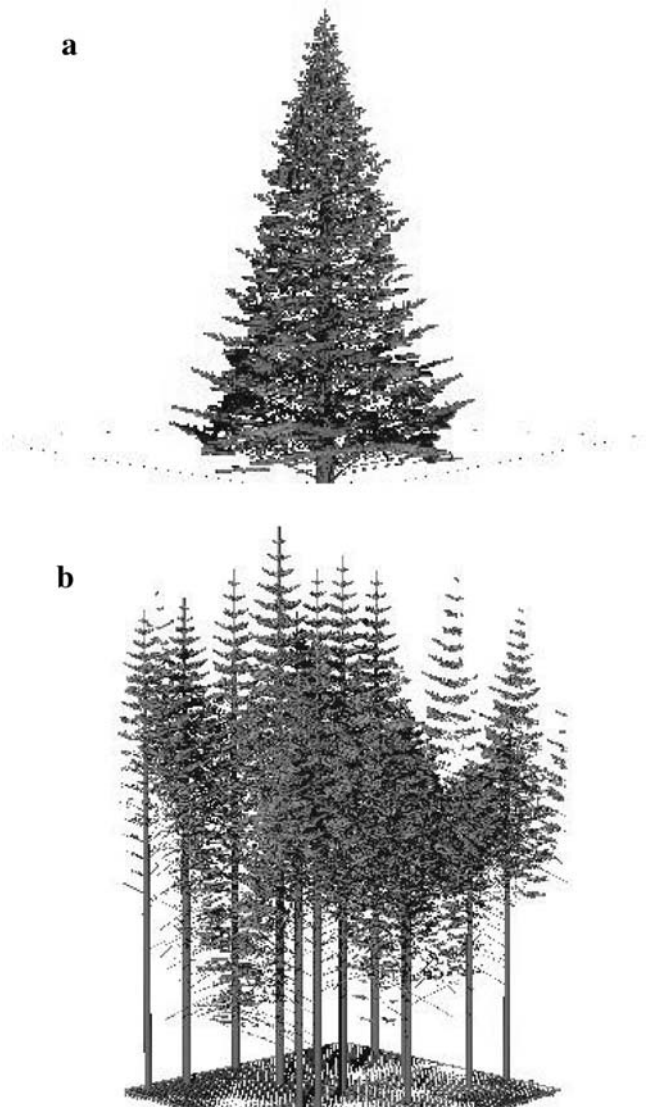

Fig. 9 Three-dimensional snapshot of PipeTree growth. **a** A PipeTree of tree.age = 40 grows up under single-tree situation. **b** A PipeTree stand at simulation timestep 44. Note that the *x*- and *y*-boundaries are all periodic

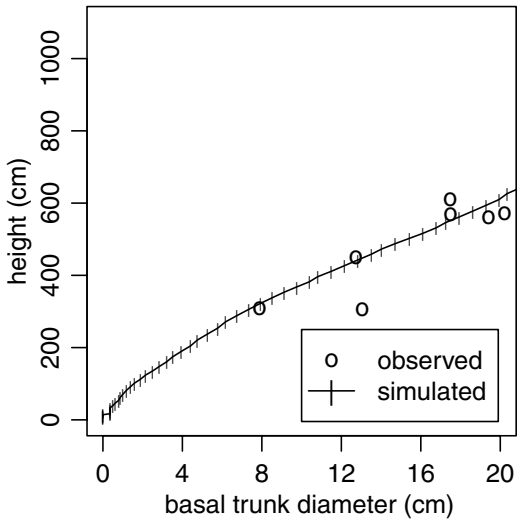

Fig. 10 Relationship between basal trunk diameter and top height for trees that grow in isolated conditions. The trunk diameter is measured at 10% of the height of the tree both in field observations and in the simulation. *Circles* represent field measurements around Mugikusa Pass near Mt. Shimagare in 1978. *Solid curve* shows the diameter–height relationship generated by a PipeTree simulation under single-tree setting. *Vertical ticks on the curve* mark annual observations. The age of PipeTree at *right end* of the figure is about 50 years

between observed and simulated patterns. The observed diameter–height curve in Fig. 11a is slightly convex, whereas that simulated in Fig. 11b is rather concave. The time change in total basal area per land area ($m^2\ m^{-2}$) of the PipeTree stand shown in Fig. 12a slightly underestimates that of a real *Abies* stand in the first 40 years, whereas it rather overestimates it after 40 years. Figure 12b plots the relationship between the time change of tree density and stand biomass. The phenomenon of the self-thinning rule, corresponding to the broken line in Fig. 12b, is reproduced in the stand simulation, as well as in field observations (Kohyama and Fujita 1981).

The results for the P_{max} enhancement situation are shown in Fig. 13. Figure 13a can be interpreted to mean that a 50% increase in P_{max} doubles the net primary production (NPP) of the PipeTree stand (baseline represents stand situation). The NPP of a tree is evaluated as the difference between total acquired photosynthesis (gross primary production, GPP) and total respiration. Therefore NPP is equal to stem0.*Q* for 1 year in PipeTree. Figure 13b suggests that doubling NPP is comparable to doubling basal area. The enhanced P_{max} also accelerated the growth in height. The height growth in the P_{max} enhancement situation is about 50% faster than that of the baseline situation.

Discussion

In the present study, we demonstrated the feasibility of using a functional–structural model (FSM) to evaluate ecosystem functions at the stand level. The PipeTree simulator generates patterns similar to what we observed in the subalpine forest on Mt. Shimagare, such as diameter–height relationship and time change in basal area with stand age (Figs. 11, 12).

In comparison with FSMs already proposed (e.g. Takenaka 1994; Sievänen et al. 1997; Perttunen et al. 1998; Raulier et al. 1999), PipeTree differs in that an assessment of water availability at every component changes its functional behavior. Through the trial and error process for PipeTree development, water dynamics in the tree are incorporated to suppress the growth of terminals, that is, the leader shoots of the trunk and branches, as the length of trunk and branches lengthens. As this relationship to water stress expressed by water potential is consistent with recent studies of tree physiology (e.g. Magnani et al. 2000), we suggest that the

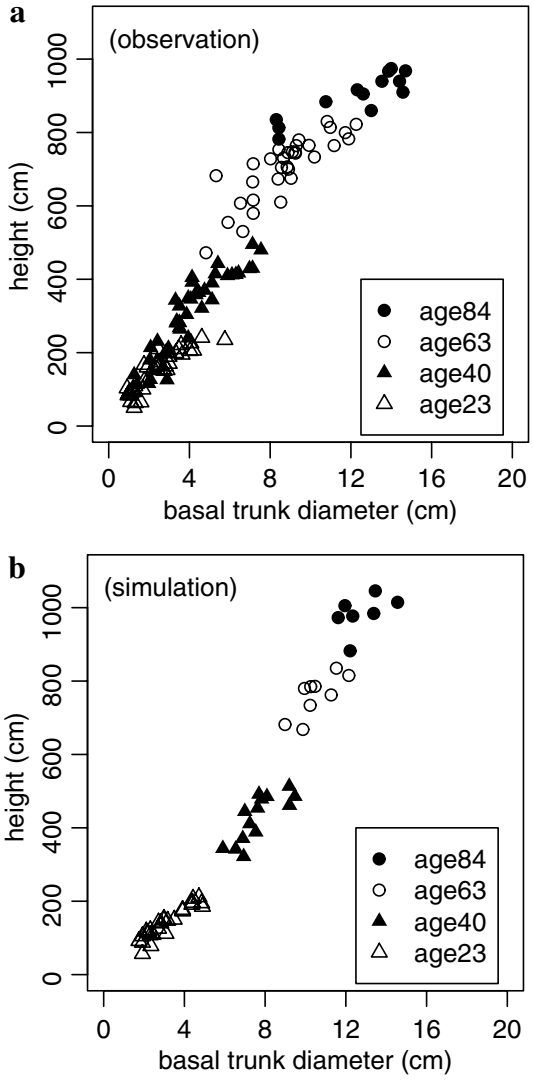

Fig. 11 Relationship between tree basal trunk diameter and height in a dense stand. The diameter is measured at 10% of the height of the tree both in field observations and the simulation. *Open* and *closed triangles* and *circles* indicate diameter–height relationship of all trees that are alive at each observation time. **a** Field measurements from the research of Mt. Shimagare (Kohyama and Fujita 1981; Kohyama et al. 1990). **b** A PipeTree simulation starting from a population of 30 individuals in a 10-m^2 stand

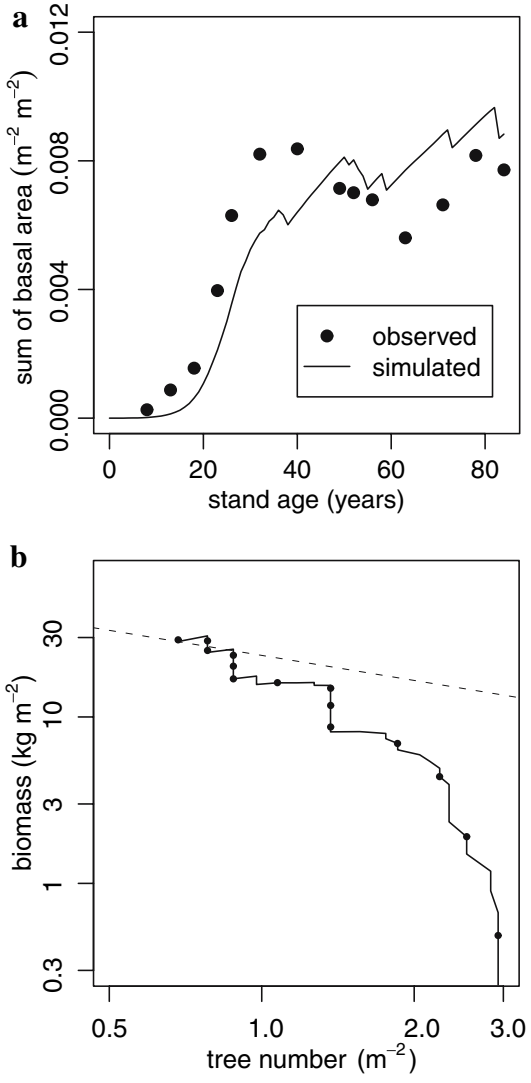

Fig. 12 Comparison of differences in basal area and tree density between field measurements and PipeTree simulation (one trial). **a** Time change of basal area. *Closed circles* are the field measurements on Mt. Shimagare (Kohyama and Fujita 1981). *Solid curve* represents the result of the PipeTree simulation. **b** Relationship between the density of PipeTree objects in 10-m^2 stand and the total above-ground biomass of survived trees. *Solid curve* shows the trajectory of time change in simulation. *Closed circles* mark 5-year observations. *Dashed line* represents a "self-thinning" line. The equation of the line is $y = 8.0 \times 10^5 x^{0.5}$ where x and y are total number and biomass of trees in the simulation plot (10 m^2), respectively

present model is a natural extension of prior FSMs and has the potential for scaling-up from single trees to populations and terrestrial ecosystems.

The present simulator provides a powerful tool for ecological studies both at the individual and stand scales. At the individual scale, it proves that "whole individual form" or the allometric relationship between trunk diameter and tree height can be reconstructed with only local interactions of components. The pattern is a consequence of the integration of resource competition and allocation under morphological constraints and local allometric formulas for the terminal shoots. This could be true as well at the stand scale because the simulated stand is just an ensemble of independent PipeTree objects without any additional population-level rules for interactions among trees. Therefore, the present results suggest that higher-scale ecological patterns can emerge slowly from lower-scale patterns, such as physiological and morphological rules (Levin 1992). The scale gaps among shoots, individual trees and populations can be connected by computer-intensive methodology.

Computer power throws light on multiscale problems in ecology, but the limitations of computing still matter.

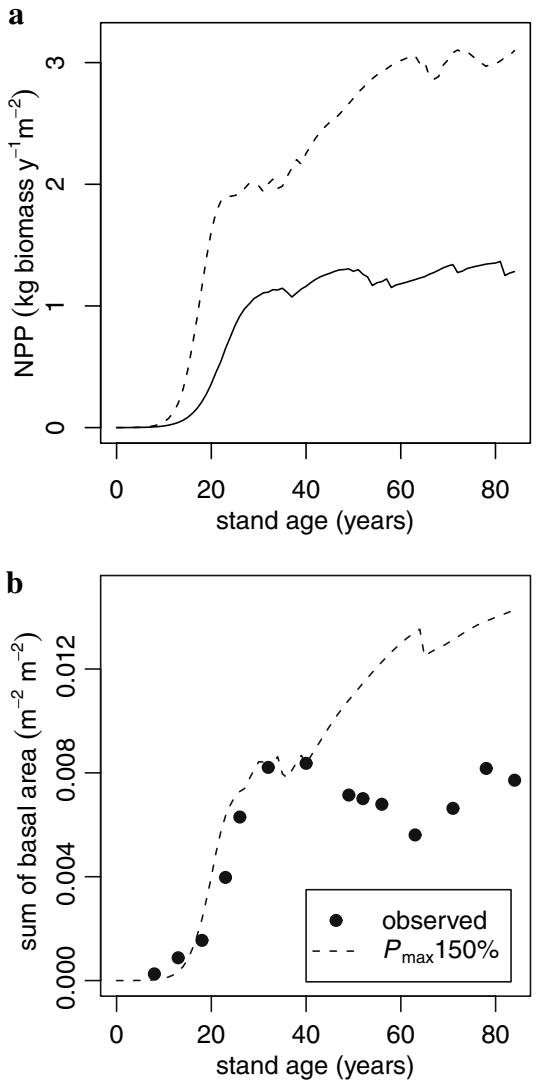

Fig. 13 Results of P_{max} enhancement experiment with 50% increase in maximum photosynthetic rate (P_{max} in Eq. 1) over baseline simulation (see Fig. 3). **a** Time change in NPP. *Solid* and *dashed curves* correspond to baseline and P_{max} enhancement simulation, respectively. **b** Time change in basal area. *Closed circles* represent the field measurements on Mt. Shimagare (Kohyama and Fujita 1981) as in Fig. 12a. *Dashed curve* indicates the result of PipeTree simulation under P_{max} enhancement

In our PipeTree simulation, we could increase neither the size of population nor the number of trials. Although the validity of the parameters and process models must be checked by many more trials with larger populations, this is not technically easy. As the most rate-limiting step of PipeTree is the estimation of local light intensity in three-dimensional space, which consumes approximately 95% of total simulation time, we may focus on the improvement of the algorithm of light calculation.

The field measurements and biological/ecological information to be embedded into PipeTree are not always sufficiently reliable. One of the most important processes in PipeTree is the probability of the death of the stem (at the individual level) and the tree (at the population level). Whereas the details of the survivorship curve for *Abies* have already been phenomenologically revealed (Kohyama and Fujita 1981), the process models of mortality in PipeTree are far from satisfactory. At the shoot level, more detailed research is required to detect factors controlling shoot mortality. The data suggest that the mortality of *Abies* trees in even-height stands is still considerable 60 years after establishment. Although our assumption that a PipeTree cannot survive after losing its leader shoot works in this study, more observations on the characteristics of *Abies* in self-thinning stands are needed.

The limitations of computer power and available data cause many simplifications in the modeling of PipeTree. As the physical environment of simulation is constant both in day and in year, the annual production of PipeTree is evaluated as a simple integration of "averaged" production per second. Although the reproduction of *Abies* could be of considerable importance in discussing the problem of resource allocation within a tree, we were not able to model it due to the lack of data. The validation of these simplifications (both by field and theoretical research) would be a worthwhile next step in the study.

The limitations of computation bring about another approximation in the evaluation of local light environment in PipeTree in that the light intensity at the current-year stem is equal to the mother-stem objects. This could result in the overestimation of the GPP of the tree. The effect of overestimated GPP may be reflected in time changes in basal area as shown in Fig. 13b. The results of the stand or baseline situation show, however, no extreme violation from observations (Figs. 9, 10, 11, 12). This suggests that there are other reasons for the overestimation of mortality or respiration in above- and below-ground parts.

The results obtained in the P_{max} enhancement situation (Fig. 13) are interesting because they suggest the limitations and capabilities of our approach. The doubling in NPP due to 50% increase in photosynthetic rate (Fig. 13a) could be counterintuitive. Figure 13b gives us a possible explanation that the doubling of NPP is related to the doubling of BA that is nearly proportional to the amount of needle foliage as assumed in the pipe model (Table 8). This can be simply explained in that total respiration of a tree is larger than the half of GPP. What we obtained is

$$\begin{aligned} &\mathrm{NPP} = \mathrm{GPP} - r && \text{(baseline situation)} \\ &2\mathrm{NPP} = 1.5\mathrm{GPP} - (r + \Delta r) && (P_{max}\text{ enhancement situation}) \end{aligned}$$

where r (kg biomass year^{-1}) is total respiration at stand level and Δr (kg biomass year^{-1}) is the increase in respiration in the P_{max} enhancement situation. Suppose $r > 0$ and $\Delta r > 0$, and these equations are always true if $\Delta r = r - 0.5\mathrm{GPP}$. The difference, Δr, must be positive, because the supporting part of the tree increases in the P_{max} enhancement situation as shown in Fig. 11b. For $\Delta r > 0$, the condition $r > 0.5\mathrm{GPP}$ is required. We could, however, doubt whether the doubled NPP is an artifact

caused by inadequate assumptions, because no *Abies* forest of over 1% BA has ever been reported in Japan. Fortunately, a sufficiently long research history exists for subalpine *Abies* stands, and it is an interesting question whether BA tends to increase with time when CO_2 enrichment proceeds.

Considering all of the above, we conclude that one of the advantages in using functional–structural models is the evaluation and validation of the "scaling-up" modeling in the field of plant ecology. Ecologists in the field of tree ecology have proposed many models which end at each level, including physiological, shoot, individual and stand models. Such models work only at the level of interest. We suspect, however, that such inconsistency depends on the simplified modeling neglecting the interactions among other levels. Suppose we make a phenomenological model for an *Abies* stand without physiological and morphological constraints. The modeling would be much easier than that of PipeTree, but at the same time, it would be difficult to answer questions on phenomena at different levels, such as the stand dynamics under P_{max} enhancement. The "reconstruction" strategy of the functional–structural model has the potential to reveal the processes under unobserved situations while checking results by comparing piecemeal knowledge of the physiology and ecology of *Abies*. In the quest for models with fewer inconsistencies, we know this paper is just the starting point of modeling an *Abies* forest, hence further improvements by validation in observed and unobserved situations should be our future work for PipeTree.

Acknowledgements We sincerely thank the following people for their helpful comments and suggestions: Kouki Hikosaka, Kyoko Kato, Tsuyoshi Kobayashi, Takeshi Seki, Testuo Shirota, Akihiro Sumida, Maki Suzuki, Akio Takenaka, Naoaki Tashiro, and Kiyoshi Umeki. The development and analysis of PipeTree consists only of free and/or open-source software distributed via the internet. We thank and admire those who develop and maintain it. This work was partially supported by a Grant-in-Aid from the Ministry of Education, Culture, Sports, Science and Technology of Japan (No. 15770006).

References

Bugmann H (2001) A review of forest gap models. Clim Change 51:259–305

Hurtt GC, Moorecroft PR, Pacala SW, Levin SA (1998) Terrestrial models and global change: challenges for the future. Global Change Biol 4:581–590

Ito A, Oikawa T (2002) A simulation model of the carbon cycle in land ecosystem (Sim-CYCLE): a description based on dry-matter production theory and plot-scale validation. Ecol Model 151:147–179

Kimura M, Mototani M, Hogetsu K (1960) Ecological and physiological studies on the vegetation of Mt Shimagare. VI. Growth and dry matter production of young *Abies* stand. Bot Mag Tokyo 81:287–296

Kohyama T (1980) Growth pattern of *Abies mariesii* saplings under conditions of open-growth and suppression. Bot Mag Tokyo 93:13–24

Kohyama T (1993) Size-structured tree populations in gap-dynamic forest—the forest architecture hypothesis for the stable coexistence of species. J Ecol 81:131–143

Kohyama T, Fujita N (1981) Studies on the *Abies* population of Mt Shimagare. I. Survivorship curve. Bot Mag Tokyo 94:55–68

Kohyama T, Hara T, Tadaki Y (1990) Patterns of trunk diameter tree height and crown depth in crowded *Abies* stands. Ann Bot 65:567–574

Kuroiwa S (1960) Ecological and physiological studies on the vegetation of Mt. Shimagare. IV. Some physiological functions concerning matter production in young *Abies* trees. Bot Mag Tokyo 73:133–141

Levin SA (1992) The problem of pattern and scale in ecology. Ecology 73:1943–1967

Magnani F, Mencuccini M (2000) Grace I age-related decline in stand productivity: the role of structural acclimation under hydraulic constraints. Plant Cell Environ 23:251–263

Monsi M, Saeki T (1953) Über den Lichtfaktor in den Pflanzengesellschaften und seine Bedeutung für die Stoff-produktion. Jpn J Bot 14:22–52

Moorecroft PR, Hurtt GC, Pacala SW (2001) A method for scaling vegetation dynamics: the ecosystem demography model (ED). Ecol Monogr 71:557–586

Oikawa T, Saeki T (1977) Light regime in relation to plant population geometry. I. A Monte Carlo simulation of light microclimates within a random distribution foliage. Bot Mag Tokyo 90:1–10

Oshima Y, Kimura M, Iwaki H, Kuroiwa S (1958) Ecological and physiological studies on the vegetation of Mt. Shimagare. I. Preliminary survey of the vegetation of Mt. Shimagare. Bot Mag Tokyo 71:289–301

Pacala SW, Canham CD, Silander JAJ (1993) Forest models defined by field measurements. I. The design of a northeastern forest simulator. Can J For Res 23:1980–1988

Pacala SW, Canham CD, Silander JAJ, Kobe RK, Ribbens E (1996) Forest models defined by field measurements: estimation error analysis and dynamics. Ecol Monogr 66:1–43

Perttunen J, Sievänen R, Nikinmaa E (1998) LIGNUM: a model combining the structure and the functioning of trees. Ecol Model 108:189–198

Raulier F, Berner PY, Ung C (1999) Canopy photosynthesis of sugar maple (*Acer saccharum*): comparing big-leaf and multilayer extrapolations of leaf-level measurements. Tree Physiol 19:407–420

Roux XL, Lacointe A, Escobar-Gutiérrez A, Dizès SL (2001) Carbon-based models of individual tree growth: a critical appraisal. Ann For Sci 58:469–506

Saeki T (1960) Interrelationships between leaf amount light distribution and total photosynthesis in a plant community. Bot Mag Tokyo 73:55-63

Shinozaki K, Yoda K, Hozumi K, Kira T (1964a) A quantitative analysis of plant form—the pipe model theory. I. Basic analysis. Jpn J Ecol 14:97–105

Shinozaki K, Yoda K, Hozumi K, Kira T (1964b) A quantitative analysis of plant form—the pipe model theory. II. Further evidence of the theory and its application to forest ecology. Jpn J Ecol 14:133–139

Sievänen R, Nikinmaa E, Perttunen J (1997) Evaluation of importance of sapwood senescence on tree growth using the model LIGNUM. Silv Fin 31:329–340

Sievänen R, Nikinmaa E, Nygren P, Ozier-Lafontaine H, Perttunen J, Hakula H (2000) Components of functional–structural tree models. Ann For Sci 57:399–412

Sitch S, Smith B, Prentice IC, Arneth A, Bondeau A, Cramer W, Kaplan JO, Levis S, Lucht W, Sykes MT, Thonicke K, Venevsky S (2003) Evaluation of ecosystem dynamics, plant geography and terrestrial carbon cycling in the LPJ dynamic global vegetation model. Global Change Biol 9:161–185

Takenaka A (1994) A simulation model of tree architecture development based on growth response to local light environment. J Plant Res 107:321–330

Thornley JHM (1976) Mathematical models in plant physiology. Academic, London, 86-110

Ecol Res (2005) 20: 271–277
DOI 10.1007/s11284-005-0042-0

ORIGINAL ARTICLE

Tsutom Hiura

Estimation of aboveground biomass and net biomass increment in a cool temperate forest on a landscape scale

Received: 9 September 2004 / Accepted: 29 October 2004 / Published online: 2 April 2005

Abstract I clarified aboveground biomass (AGB), net biomass increment (NBI) and its spatial heterogeneity in a cool temperate forest on a landscape scale (> 2,200 ha). The relationships among AGB, NBI, and the size frequency distribution of trees of each stand were examined by combining an analysis of vegetation using aerial photographs, and data from 146 inventory plots (28.8 ha in total). This area included natural broad-leaved stands, harvested broad-leaved stands, and artificial conifer plantations. A $-3/2$ power distribution density function was applied to the individual mass frequency distribution of each plot. Estimated AGB in carbon (C) equivalent was 480–5,615 g C m^{-2} (3,130 g C m^{-2} on average), and NBI was -98 to 436 g C m^{-2} $year^{-1}$ (83.0 g C m^{-2} $year^{-1}$ on average). NBI had a single significant relationship with the reciprocal of theoretical maximum individual mass, while NBI was not significantly related to AGB. My results showed that, on a landscape scale, AGB and NBI strongly depend on the size structure of forest stands.

Keywords Aerial photograph · Remote sensing · MNY method · Distribution density function · Broad-leaved forest

Introduction

Forest ecosystems are thought to be carbon storage on a global scale (Dixon et al. 1994). Nevertheless, there is still considerable uncertainty about carbon stocks or carbon fixation in forest ecosystems and about the relationships between the carbon fixation ability and forest structure (Clark and Clark 2000; House et al. 2003). We are aware of the problems involved in extrapolations from plot data to a landscape or regional scale. On a landscape scale, forests are composed of mosaic patches that are at different developmental stages (Watt 1947), and their spatio-temporal structure is further complicated by human impacts such as logging and plantations. However, good stands with above average biomass and productivity are often chosen for ecological studies. Therefore, we have to note that both detailed plot studies and large-scale inventories take into account the full range in the variability of forest structure.

Aboveground biomass (AGB) and net biomass increment (NBI) are two important parts of the carbon budget of a forest ecosystem (Shibata et al. 2005). There are various methods for estimating AGB and NBI of forests, and remote sensing techniques are suitable for estimating the biomass on a large scale (Lefsky et al. 2002). However, there is some room for improvement in remote sensing to analyze small-scale patterns and processes such as stand development and its spatial heterogeneity (Schimel 1995; Drake et al. 2003). Furthermore, the remote-sensing data have to be ground-truthed at the landscape scale. It will be possible to estimate the forest biomass explicitly by combining the advantages of various methods (Fournier et al. 2003). To scale up from individual trees to a landscape, it is crucial to clarify the relationships among AGB, NBI, and forest structure. The frequency distribution of individual tree sizes needs to be investigated in relation to biomass because aboveground carbon stocks are primarily determined by the distribution of trees (Hozumi et al. 1968; Kohyama 1991; Kikuzawa 1999). However, there are still many problems in scaling up from this approach (Jarvis 1995).

I clarified AGB, NBI and its spatial heterogeneity in a cool temperate forest, northern Japan, on a landscape scale (> 2,200 ha). The relationships among AGB, NBI, and the size frequency distribution of trees in each stand were examined by combining an aerial photograph analysis of vegetation and data from many inventory plots.

T. Hiura
Tomakomai Research Station,
Field Science Center for Northern Biosphere,
Hokkaido University,
Tomakomai 053-0035, Japan
E-mail: hiura@exfor.agr.hokudai.ac.jp
Tel.: +81-144-332171
Fax: +81-144-332173

Methods

Study area

Tomakomai Experimental Forest (TOEF; 42°40′N, 141°36′E) is located on flat land and has an area of 2,715 ha. Mean monthly temperatures range from −3.2 to 19.1°C, and annual precipitation is 1,450 mm. Snow cover reaches a depth of 50 cm from December to March. This forest was formed on 2 m-deep volcanic ash that accumulated after Mt. Tarumae erupted in 1669 and 1739, and has very shallow soil (Igarashi 1987; Sakuma and Sato 1987). About 100 tree species and 300 herbaceous species were recorded in TOEF in 1916 (Kudo and Yoshimi 1916). The dominant tree species are *Quercus crispula* Blume, *Acer mono* Maxim., *Sorbus alnifolia* (Sieb. Et Zucc.) C. Koch, and *Tilia japonica* (Miq.) Simonkai (Hiura et al. 1998; Hiura 2001). Half the area of TOEF was disturbed by a catastrophic typhoon in 1954 (Mishima et al. 1958; Osawa 1992). A part of the disturbed area was replanted with *Larix leptolepsis* (Sieb. et Zucc.) Gordon, *Abies sachalinensis* (Fr. Schm.) Masters, or *Picea glehnii* (Fr. Schm.) Masters. About 1.2 million cubic meters of logs have been harvested from TOEF in the 100 years since its establishment (Hiura 2002). As a result of the harvest and the disturbance, the mature forest stands in TOEF are fragmented and limited in area.

Field survey

TOEF has around 300 permanent forest plots with areas ranging from 0.01 to 10 ha. I selected 146 square plots with areas of 0.1–0.4 ha (mainly 0.2 ha) to keep a spatial homogeneity and a sufficient number of individuals for the analysis in each plot. The census area was 28.8 ha in total. The plots were set up between 1981 and 1991 in areas that included secondary stands disturbed by a typhoon, mature stands, harvested stands, and plantations. The species names of the trees and diameters at breast height (DBH) were recorded for all living trees with DBH >10 cm. Recensus was done at each plot 7 or 8 years after the initial census. The elevation of these plots is 50–80 m asl, and each plot is on a flat plateau or a gentle slope ($<15°$ slope).

Analysis

Natural forests were categorized by the combination of the number of crown layers (one, two, or three), the type of tree (deciduous broad-leaved, evergreen conifer, or mixed stand), the tree density (low, intermediate, or high), the tree height (<5, 5–10, 10–15, 15–20, or >20 m), and the crown diameter (small, medium, or large) using aerial photographs taken in 1994 (Table 1). There were 58 types of vegetation out of a possible 405 combinations. For plantations, I categorized the stands by tree height (<5, 5–10, 10–15, 15–20, or >20 m), and four types of vegetation were found. This information was entered into a geographic information system.

Table 1 Area, number of plots, mean basal area (BA), and mean AGB for each forest type in TOEF

Forest type	Area (ha)	Number of plots	Mean BA ($cm^2\ m^{-2}$)	Mean AGB ($g\ C\ m^{-2}$)
A-1	41.19	4	6.9	1,466
III-M-D-4-l	45.54	4	12.1	2,561
I-B-D-3-s	457.89	39	12.2	2,555
A-2	111.03	9	12.3	2,717
I-B-D-4-m	5.41	1	12.5	2,646
I-B-D-4-l	5.66	1	12.7	2,718
III-C-D-3-s	0.15	1	12.9	2,779
III-B-D-1-s	1.16	1	13.0	2,812
III-B-I-3-m	4.04	1	13.0	2,887
A-3	117.41	3	13.5	2,703
III-M-D-3-m	31.60	1	13.7	2,864
III-B-D-2-m	4.39	1	13.9	2,850
III-B-D-3-l	200.42	5	14.2	3,056
III-M-D-3-l	8.37	3	14.4	3,125
A-4	255.46	27	14.8	3,210
III-B-D-3-m	341.16	17	15.3	3,323
I-B-D-1-s	10.32	1	15.4	3,365
III-B-D-5-l	3.48	1	15.4	3,515
I-B-D-3-m	64.86	4	15.7	3,369
III-M-D-2-m	0.42	1	15.7	3,539
I-M-D-2-s	3.44	1	16.3	3,617
III-B-D-4-m	31.11	2	16.4	3,609
III-B-D-4-l	416.19	14	16.8	3,762
I-B-D-2-s	30.97	2	17.9	3,938
II-M-D-3-m	2.22	1	18.0	4,113
III-B-D-3-s	46.47	1	19.9	4,434
Total	2,240.36	146 (28.8 ha)	14.4	2,661

Forest type: Roman numerals indicate the number of crown layers. First capital letters indicate the dominant life form: *B* broad-leaved; *C* conifer; *M* mixed. Second capital letters indicate the tree density: *D* high; *I* intermediate. Arabic numbers indicate the dominant tree height classes: *1* height <5 m; *2* height 5–10 m; *3* height 10–15 m; *4* height 15–20 m; *5* height >20 m. Small letters indicate the dominant crown size classes: *s* small; *m* medium; *l* large. *A-1*, *A-2*, *A-3*, and *A-4* indicate artificial plantations which have the dominant height classes 1, 2, 3, and 4, respectively

The 146 forest plots were categorized into 26 types of vegetation out of the 62 types which appeared. The 26 types are the ones listed in Table 1. The area of the 26 vegetation types that were actually sampled using plots was 2,240.36 ha in total, which corresponded to 92% of forest cover in TOEF. The plantation type which had the smallest biomass (A-1, 41.19 ha) was excluded from the NBI analysis because the tree mortality was extremely high due to a disturbance during the census period.

Individual tree mass was estimated from DBH using the following allometric functions.

Tree height (H) for conifers (Hiura et al. 1996),

$$1/H(\mathrm{m}) = 1/0.596 \cdot \mathrm{DBH}(\mathrm{cm})^{1.202} + 1/38.5$$

Tree height for deciduous broad-leaved trees (Hiura et al. 1998),

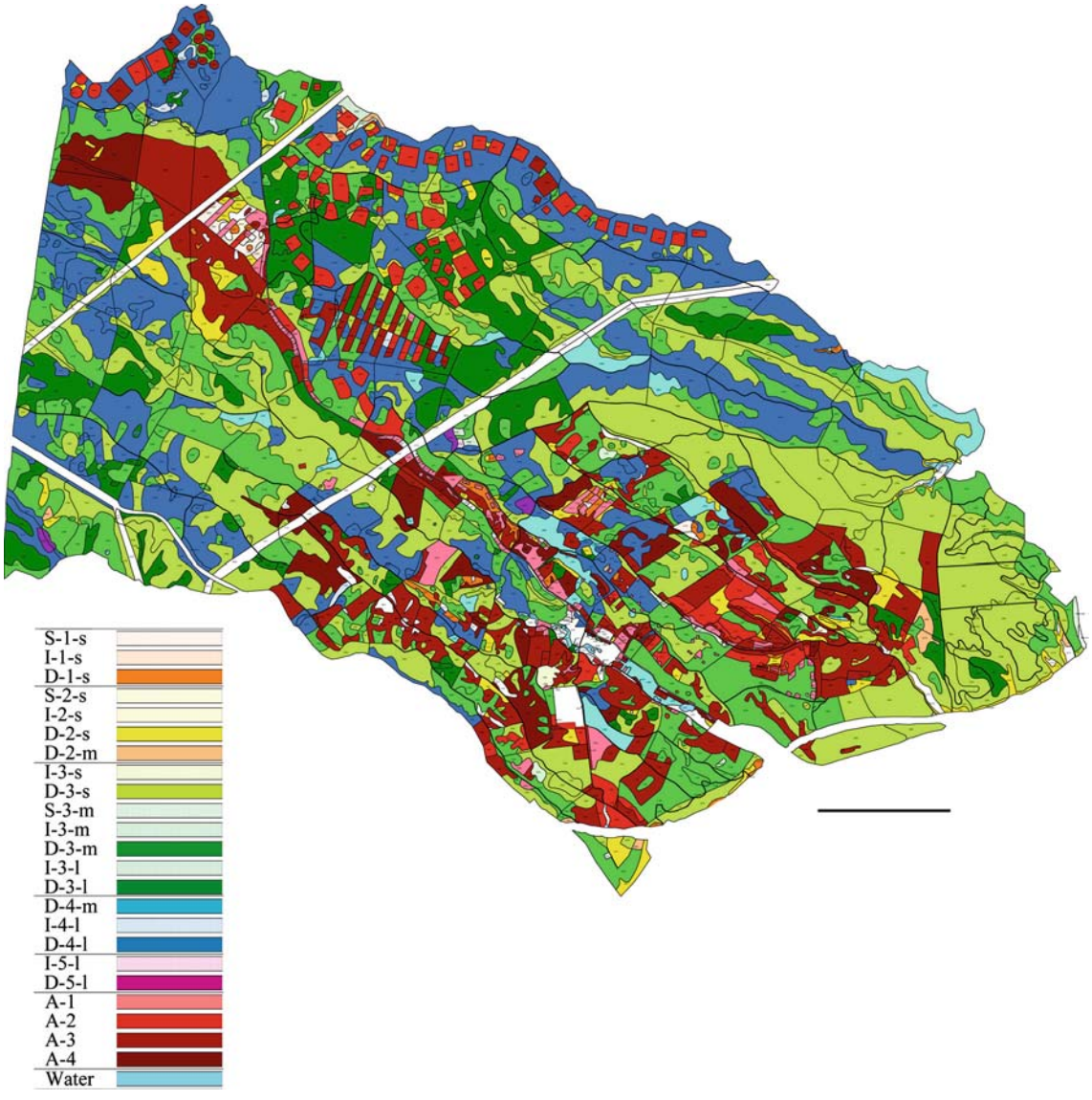

Fig. 1 Vegetation map of Tomakomai Experimental Forest (TOEF) categorized by tree density, tree height, and dominant crown size. *First capitals* indicate the stand density: *D* dense, *I* intermediate, *S* sparse. *Numbers* indicate the dominant tree height classes: *1* height < 5 m, *2* height 5–10 m, *3* height 10–15 m, *4* height 15–20 m, *5* height > 20 m. *Lowercase letters* indicate the dominant crown size classes: *s* small, *m* medium, *l* large. *A* artificial forest, *Water* surface of the water. A *horizontal bar* indicates a scale of 1 km

$$1/H(\mathrm{m}) = 1/2.04 \cdot \mathrm{DBH}(\mathrm{cm})^{0.830} + 1/29.93$$

Stem mass (W_s), branch mass (W_b), and leaf mass (W_l) for evergreen conifers (Shidei 1960),

$$\mathrm{W}s(\mathrm{g}) = 28.47(D^2H(\mathrm{cm}^2\,\mathrm{m}))^{0.919}$$
$$\mathrm{W}b(\mathrm{g}) = 3.938(D^2H(\mathrm{cm}^2\,\mathrm{m}))^{0.928}$$
$$\mathrm{W}l(\mathrm{g}) = 6.117(D^2H(\mathrm{cm}^2\,\mathrm{m}))^{0.851}$$

Stem mass, branch mass, and leaf mass for *Larix* spp. (Shibuya et al. 2000),

$$\mathrm{W}s(\mathrm{g}) = 87.498(D^2H(\mathrm{cm}^2\,\mathrm{m}))^{0.848}$$
$$\mathrm{W}b(\mathrm{g}) = 38.994(D^2H(\mathrm{cm}^2\,\mathrm{m}))^{0.674}$$
$$\mathrm{W}l(\mathrm{g}) = 14.355(D^2H(\mathrm{cm}^2\,\mathrm{m}))^{0.600}$$

Stem and branch mass (W_c) and leaf mass for broad-leaved trees (Takahashi et al. 1999),

$$\mathrm{W}c(\mathrm{g}) = 53.025(D^2H(\mathrm{cm}^2\,\mathrm{m}))^{0.893}$$
$$\mathrm{W}l(\mathrm{g}) = 1.064(D^2H(\mathrm{cm}^2\,\mathrm{m}))^{0.904}$$

NBI was determined by the function,

$$\mathrm{NBI}(\mathrm{gC}\cdot\mathrm{m}^{-2}\,\mathrm{year}^{-1}) = \Delta y - \Delta D$$

where y is the increment of biomass of living trees, and D is dead biomass produced during the census period. Carbon content was assumed to be 50% of the biomass although there are minor differences in carbon content among species (Lamlom and Savidge 2003). The NBI values of the harvested forest stands were corrected by the biomass decrement due to harvesting during the

census period. The biomass decrement was estimated from the DBH values of the logged trees. Therefore, in harvested stands, the growth and mortality of harvested trees from the time of harvest to the time of the final census were not included in determining the NBI values. Thirty-two plots were harvested during the census period. The total logged biomass was 35,293.78 kg C, which corresponds to an average harvest of 83.68 g C m^{-2} $year^{-1}$. Spatial distribution of NBI in TOEF was extrapolated from the vegetation map and the average NBI value of plots in the same vegetation type.

The $-3/2$ power distribution of the MNY method (Hozumi et al. 1968) was applied to the individual mass distribution of each plot, and the distribution density function was determined by the least square method. Where

$$Y = \int_{w}^{w\max} w\phi(w)\mathrm{d}w$$
$$N = \int_{w}^{w\max} \phi(w)\mathrm{d}w$$
$$M = Y/N$$

Y is apparently the biomass of a partial population consisting of those trees whose mass is in the range between the maximum mass of a stand and a given value of w. N is the density of the partial population stated above. M is the mean tree mass of the partial population. The distribution function is expressed as

$$\phi(w) = (\sqrt{B}/2A)w^{-3/2}$$

where A and B are constants. The theory gives A as the reciprocal of the stand biomass and B as the reciprocal of the maximum individual mass in the plot (Hozumi et al. 1968). We can be more than 95% sure that the tree size pattern be expressed successfully with the $-3/2$ power distribution with tree samples of only the largest 20% in the even-aged stand (Osawa and Abaimov 2001). Therefore, it is reliable to analyze the tree size distribution by using trees with DBH > 10 cm. All statistical analysis was carried using SYSTAT ver.5 (1992).

Results

A map of the spatial distribution of the 62 vegetation types in TOEF (Fig. 1) shows that one-third of the area was secondary successional stands (S-1-s to D-3-l), one-third was a plantation (A-1 to A-4), and the rest of the area was mature forest stands (D-4-m to D-5-l). This map, made from a high-resolution image, is available from http://pc3.nrs-unet.ocn.ne.jp/~exfor/Toef/EcolRes2005fig1.pdf. In the146 plots, the initial number of individuals was 17,451 in total, and the observed maximum size was 114.0 cm in DBH for *T. japonica*. Estimated AGB was 480–5,615 g C m^{-2} (3,130 g C m^{-2} on average), NBI was -98 to 436 g C m^{-2} $year^{-1}$ (83.0 g C m^{-2} $year^{-1}$ on average), and mean basal area was 6.9–19.9 cm^2 m^{-2} (14.43 cm^2 m^{-2} on average). Both AGB and NBI of the plots showed normal frequency distributions (Fig. 2).

The spatial distribution of NBI in TOEF (Fig. 3) shows that high and low NBI stands create a complex spatial structure. The average NBI and AGB values by vegetation type were weakly and negatively correlated ($r = -0.569$, $P = 0.003$, $n = 25$).

The goodness of fit for application of the $-3/2$ power function to individual mass frequency distributions in each plot was high [Fig. 4 for representation; $R^2 = 0.961 \pm 0.004$ (mean ± SE), $n = 144$], although the goodness of fit was relatively low in two plots in which the maximum DBH was over 100 cm ($R^2 = 0.694$ and 0.532). This means that the application of the distribution density function used in this study was relevant, and the theoretical value of the maximum individual mass was very similar to the actual value, especially for young stands. If the Gompertz function was applied to the data including broad-leaved stands and plantations, NBI had a significant relationship to the reciprocal of B (theoretical maximum individual mass T_{max}) [Fig. 5b,

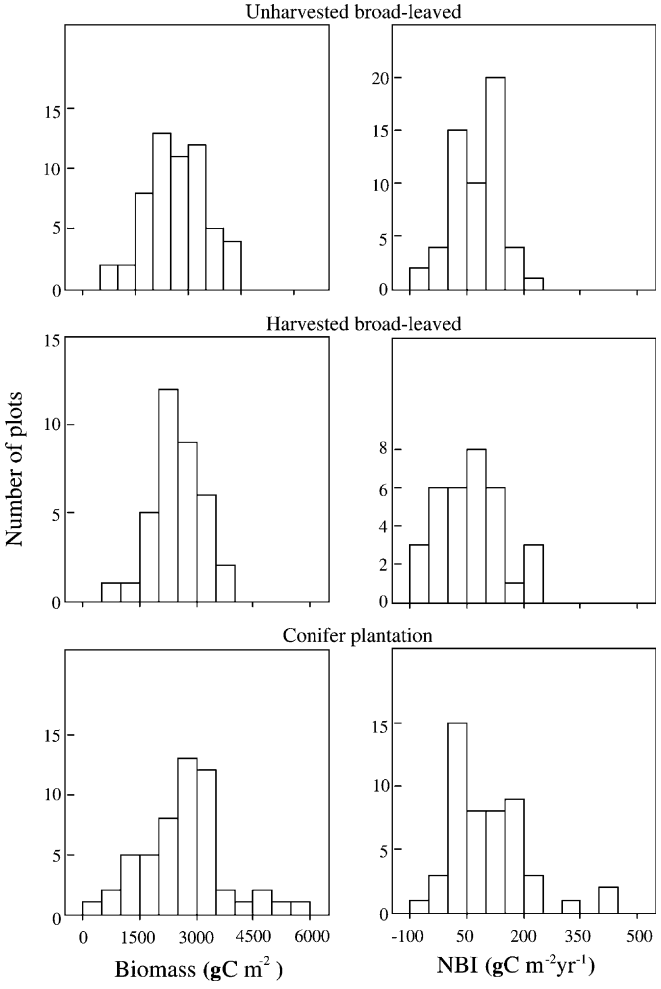

Fig. 2 Frequency distribution of aboveground biomass (AGB; *left panel*) and net biomass increment (NBI; *right panel*) in TOEF. *Upper*, *middle*, and *low panels* show unharvested broad-leaved, harvested broad-leaved, and conifer plantation stands, respectively

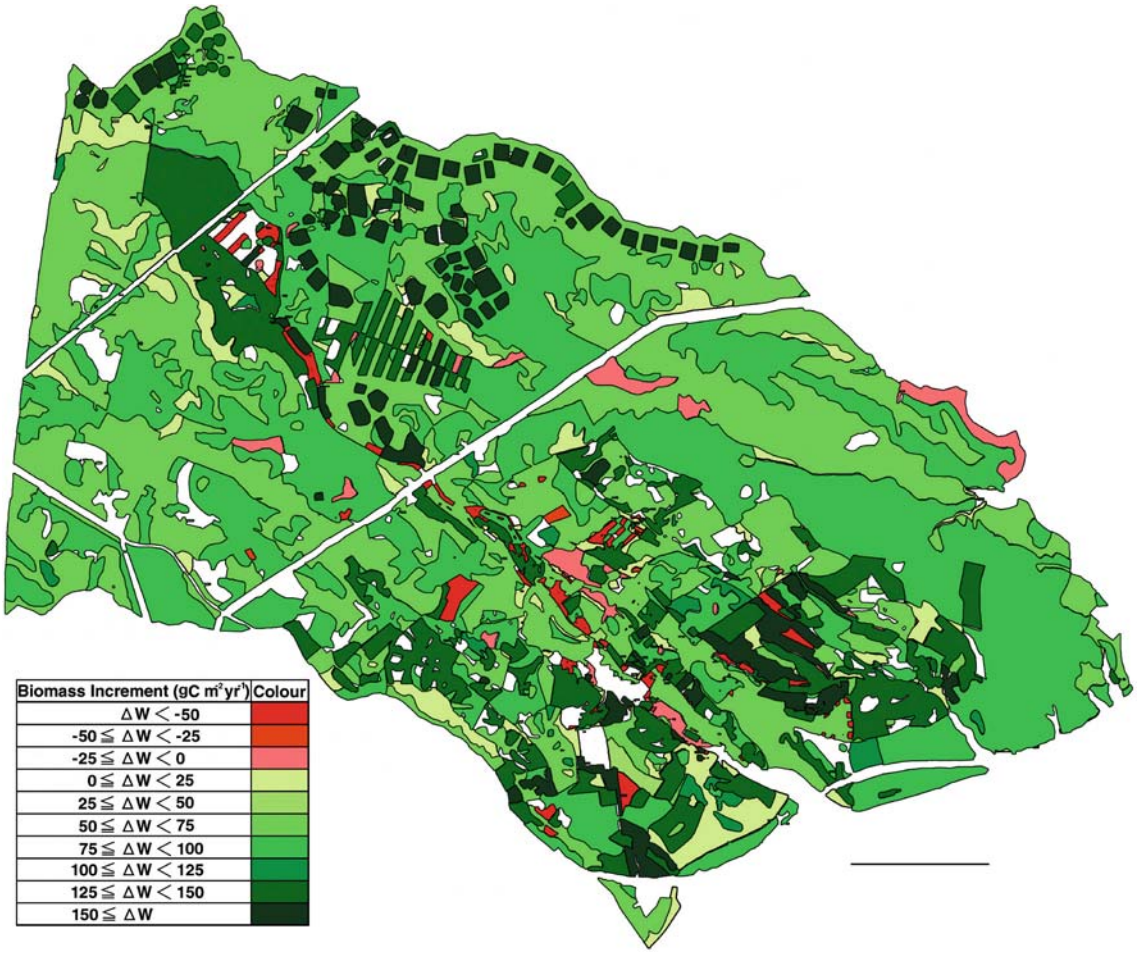

Fig. 3 Estimated spatial distribution of NBI in TOEF. A *horizontal bar* indicates a scale of 1 km

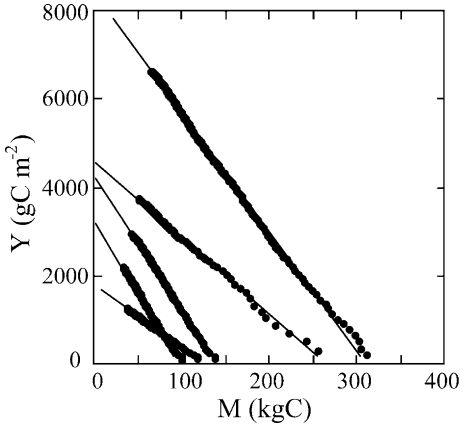

Fig. 4 Some representative examples of the goodness of fit of the $-3/2$ power function to the individual mass frequency distribution of each stand. Y is apparently the biomass of a partial population which consisted of those trees whose mass is in the range between the maximum mass of a stand and a given value of w. M is the mean tree mass of the partial population

NBI $= 240.92 - 30.72 \ln(T_{max})$, $F = 9.528$, $P = 0.002$], while NBI did not have a significant relationship to AGB (Fig. 5a, $F = 0.387$, $P = 0.535$). The significant relationship between NBI and $1/B$ yields a T_{max} of 2,546 kg C when NBI is zero. NBI also had a significant negative relationship to the actual maximum individual mass (R_{max}) [NBI $= 205.33 - 23.40 \ln(R_{max})$, $F = 5.704$, $P = 0.018$].

Discussion

Several studies have reported AGB values on a landscape scale for cool temperate or boreal forests in the northern hemisphere. Those are 2,325–11,689 g C m^{-2} for 20- to 100-year-old stands of *Larix* forest in China (Zhou et al. 2002), 1,650–8,900 g C m^{-2} for broad-leaved and conifer mixed forest in Canada (Fournier et al. 2003), 4,300 g C m^{-2} for coniferous forest in Canada (Banfield et al. 2002), and 3,650 g C m^{-2} for boreal forest in Canada (Ranson et al. 1997). The average AGB of TOEF (3,130 g C m^{-2}; range 480–5,615 g C m^{-2}) was lower than these values. TOEF is composed mainly of secondary forests created after a typhoon in 1954 and young plantations, and small areas of mature stands (Fig. 1). Most variations in stand structure, such as variations in biomass or individual size

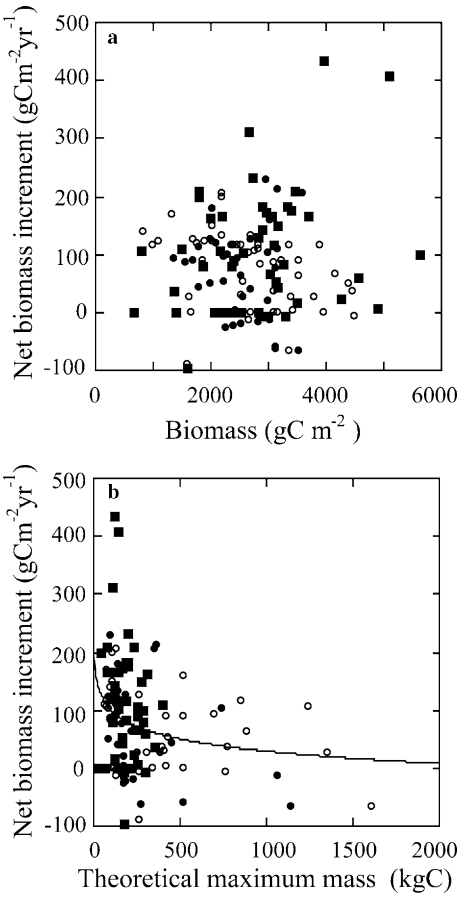

Fig. 5 Relationships between NBI and AGB (**a**) and NBI and the theoretical maximum individual mass (**b**). *Open circles* indicate unharvested broad-leaved forests, *closed circles* indicate harvested broad-leaved forests, and *closed squares* indicate plantations. The curve indicates a statistically significant relationship fitted to the Gomperz equation ($F = 9.528$, $P = 0.002$)

distribution, in mature forests on a landscape scale seem to be due to differences in soil condition or topography (Clark and Clark 2000). However, the variation in the natural forest in TOEF should reflect the disturbance history because the soil condition is very uniform and the topography is very flat. Thus, it can be assumed that the low AGB in TOEF is mainly due to the young age of the stands. Furthermore, the number of plots in the mature forest was low, and the basal area of the vegetation type which had the highest biomass was 19.9 $cm^2\ m^{-2}$. This value is considerably smaller than the value for a 9-ha forest plot in a mature forest in TOEF (26.3 $cm^2\ m^{-2}$) (Hiura et al. 1998). In addition, trees having DBH values less than 10 cm were neglected in the present study. Because the number of plots in the mature forest was low, and because the small trees were neglected, the given AGB will be slightly less than its true value.

AGB estimated from inventory plots can be compared with values estimated by remote-sensing techniques such as lidar remote sensing (Lefsky et al. 2002). NBI at the level of plots had a negative relationship with the maximum individual size, while NBI was not significantly related to AGB (Fig. 5). These results show that analyses based on the maximum size of individuals should lead to a better estimate of NBI than analyses based on AGB in lidar remote sensing. In areas of young stands where the tree density is high, large trees dominate the light environment in a stand, and inhibit growth of small trees (Weiner 1984; Kikuzawa 1999). In addition, if leaf mass of large individuals does not increase any more (Kira and Shidei 1967), the productivity of an individual tree should decrease with tree size because the mass-based photosynthetic rate decreases with tree size (Thomas and Winner 2002; Nabeshima and Hiura 2004). These appear to be the reasons for the negative relationship between NBI and the maximum tree size of stands in TOEF that was dominated by young stands. Therefore, the maximum size could be thought to be an index of the stand development.

NBI does not directly correspond to net primary production; rather it is the difference between net primary production and mortality. However, the NBI for TOEF in this study (−98 to 436 g C $m^{-2}\ year^{-1}$, 83 g C $m^{-2}\ year^{-1}$ on average) was comparable to the NBI for a deciduous broad-leaved forest in Japan (Maruyama 1977; 113–237 g C $m^{-2}\ year^{-1}$, and the net primary production in the forest was 292–491 g C $m^{-2}\ year^{-1}$). The T_{max} value when NBI was zero calculated from the fitted curve in Fig. 5b corresponded to a tree having a DBH of 120 cm, and this size corresponded to the maximum tree size observed in this study. This means that aboveground growth and mortality will be balanced when the stand development is sufficient. A previous study assumed that primary production decreases with stand development, and eventually reaches zero (Kira and Shidei 1967). However, primary production should never reach zero even in the most developed old growth forest, because tree mortality will certainly occur whenever the stands develop.

My results show that, on a landscape scale, not only AGB but also NBI depend strongly on the size structure of forest stands. In the future, measurements of other components of carbon budgets in forest ecosystems, such as litter fall and soil respiration relative to stand development, will enable the construction of a functional model for estimating the net ecosystem productivity on a landscape scale.

Acknowledgements I thank the staff of TOEF for their help during the field survey, T. Itagaki for his analysis of aerial photographs, and Y. Fukushima and E. Nabeshima for their data management. This work was partly supported by grants from the Ministry of Education, Science, Sports, and Culture of Japan (09NP1501, 12740418, and 15208014). This paper was also partly funded by the Japanese Government (IGBP-MESSC program, 2nd phase), and contributes to TEMA, a GCTE core-research project.

References

Banfield GE, Bhatti JS, Jiang H, Apps MJ (2002) Variability in regional scale estimates of carbon stocks in boreal forest ecosystems:results from West-Central Alberta. For Ecol Manage 169:15–27

Clark DB, Clark DA (2000) Landscape-scale variation in forest structure and biomass in a tropical rain forest. For Ecol Manage 137:185–198

Dixon RK, Brown S, Houghton RA, Solomon AM, Trexler MC, WisniewskiI J (1994) Carbon pools and flux of global forest ecosystems. Science 263:185–190

Drake JB, Knox RG, Dubayah RO, Clark DB, Condit R, Blairi JB, Hofton M (2003) Above-ground biomass estimation in closed canopy Neotropical forests using lidar remote sensing:factors affecting the generality of relationships. Global Ecol Biogeogr 12:147–159

Fournier RA, Luther JE, Guindon L, Lambert MC, Piercey D, Hall RJ, Wulder MA (2003) Mapping aboveground tree biomass at the stand level from inventory information: test cases in Newfoundland and Quebec. Can J For Res 33:1846–1863

Hiura T (2001) Stochasticity of species assemblage of canopy trees and understorey plants in a temperate secondary forest created by major disturbances. Ecol Res 16:887–893

Hiura T (2002) Recent research advances related to forest dynamics and biodiversity in Hokkaido University Forests. Eurasian J For Res 5:113–118

Hiura T, Sano J, Konno Y (1996) Age structure and response to fine-scale disturbances of *Abies sachalinensis*, *Picea jezoensis*, *Picea glehnii*, and *Betula ermanii* growing under the influence of a dwarf bamboo understory in northern Japan. Can J For Res 26:289–297

Hiura T, Fujito E, Ishii T, Naniwa A, Sugata S, Ishida K, Murakami M, Kato E, Maeno H, Fukushima Y, Sakai T (1998) Stand structure of a deciduous broad-leaved forest in Tomakomai Experimental Forest, based on a large-plot data. Res Bull Exp For Hokkaido Univ 55:1–10

House JI, Prentice IC, Ramankutty N, Houghton RA, Heimann M (2003) Reconciling apparent inconsistencies in estimates of terrestrial CO_2 sources and sinks. Tellus B Chem Phys Meteorol 55:345–363

Hozumi K, Shinozaki K, Tadaki Y (1968) Studies on the frequency distribution of the weight of individual trees in a forest stand I. A new approach toward the analysis of the distribution function and the $-3/2$th power distribution. Jpn J Ecol 18:10–20

Igarashi Y (1987) Vegetational succession in the Tomakomai Experimental Forest area. Res Bull Hokkaido Univ For 44:405–427

Jarvis PG (1995) Scaling processes and problems. Plant Cell Environ 18:1079–1089

Kikuzawa K (1999) Theoretical relationships between mean plant size, size distribution and self thinning under one-sided competition. Ann Bot 83:11–18

Kira T, Shidei T (1967) Primary production and turnover of organic matter in different forest ecosystems of the western Pacific. Jpn J Ecol 17:70–87

Kohyama T (1991) Simulating stationary size distribution of trees in rain forests. Ann Bot 68:173–180

Kudo Y, Yoshimi T (1916) Flora of Tomakomai Experimental Forest, Hokkaido University. Res Bull Tohoku Emp Univ For 3:1–62

Lamlom SH, Savidge RA (2003) A reassessment of carbon content in wood:variation within and between 41 North American species. Biomass Bioenerg 25:381–388

Lefsky MA, Cohen WB, Harding DJ, Parker GG, Acker SA, Gower ST (2002) Lidar remote sensing of above-ground biomass in three biomes. Global Ecol Biogeogr 11:393–399

Maruyama K (1977) Comparison of forest structure, biomass and net primary productivity between the upper and lower parts of beech forest zone. In: Shidei T, Kira T (eds) Primary productivity of Japanese forests—productivity of terrestrial communities. University of Tokyo Press, Tokyo, pp186–201

Mishima T, Taniguchi S, Taniguchi M, Hishinuma Y (1958) The actual states of wind damage in the Tomakomai Experimental Forest of Hokkaido University. Res Bull Hokkaido Univ For 19:1–39

Nabeshima E, Hiura T (2004) Size dependency of photosynthetic water and nitrogen use efficiency and hydraulic limitation in *Acer mono*. Tree Physiol 24:745–752

Osawa A (1992) Development of a mixed-conifer forest in Hokkaido, northern Japan, following a catastrophic windstorm: a "parallel" model of plant succession. In: Kelty MJ (ed) The ecology and silviculture of mixed-species forests. Kluwer, Amsterdam, pp 29–52

Osawa A, Abaimov AP (2001) Feasibility of estimating stem size distribution from measurement on the largest trees in even-aged pure stands. Can J For Res 31:910–918

Ranson KJ, Sun GQ, Lang RH, Chauhan NS, Cacciola RJ, Kilic O (1997) Mapping of boreal forest biomass from spaceborne synthetic aperture radar. J Geophys Res Atmos 102:29599–29610

Sakuma T, Sato F (1987) Dynamics of inorganic elements in soils under deciduous forests. Res Bull Hokkaido Univ For 44:537–552

Schimel DS (1995) Terrestrial ecosystems and the carbon-cycle. Global Change Biol 1:77–91

Shibata H, Hiura T, Tanaka Y, Takagi K, Koike T (2005) Carbon cycling and budget at a forested basin in southwestern Hokkaido, northern Japan. Ecol Res 20 (this issue)

Shibuya M, Yajima S, Takahashi K, Sasaoka E, Sugiura T, Tsuno Y, Sawamoto T, Hatano R (2000) Biomass, primary production, and litter decomposition rate in eastern Siberia. In: Takahashi K (ed) Studies on the effects of forest fire on the biodiversity and carbon cycling in northern Eurasian biome. Kaken Report, pp 65–75

Shidei T (1960) Studies on the productivity of the forest. I. Essential needle-leaved forests on Hokkaido. Kokusaku Pulp Industry Co

SYSTAT (1992) Statistics, version 5.2 edition. SYSTAT, Evanston, IL

Takahashi K, Yoshida K, Suzuki M, Seino T, Tani T, Tashiro N, Ishii T, Sugata S, Fujito E, Naniwa A, Kudo G, Hiura T, Kohyama T (1999) Stand biomass, net production and canopy structure in a secondary deciduous broad-leaved forest, northern Japan. Res Bull Hokkaido Univ For 56:70–85

Thomas SC, Winner WE (2002) Photosynthetic differences between saplings and adult trees:an integration of field results by meta-analysis. Tree Physiol 22:117–127

Watt AS (1947) Pattern and process in the plant community. J Ecol 35:1–22

Weiner J (1984) Neighborhood interference amongst *Pinus rigida* individuals. J Ecol 72:183–195

Zhou GS, Wang YH, Jiang YL, Yang ZY (2002) Estimating biomass and net primary production from forest inventory data: a case study of China's *Larix* forests. For Ecol Manage 169:149–157

Section 2
Latitudinal/altitudinal transect of East Asia

Ecol Res (2005) 20: 279–286
DOI 10.1007/s11284-005-0043-z

ORIGINAL ARTICLE

Shin-ichiro Aiba · Masaaki Takyu · Kanehiro Kitayama

Dynamics, productivity and species richness of tropical rainforests along elevational and edaphic gradients on Mount Kinabalu, Borneo

Received: 9 September 2004 / Accepted: 15 December 2004 / Published online: 25 February 2005

Abstract We studied the dynamics of nine tropical rainforests on Mount Kinabalu, Borneo, at four elevations (700, 1,700, 2,700 and 3,100 m) on various edaphic conditions for four 2-year periods over 8 years (1995–2003), and examined the relationships with above-ground productivity. Mean growth rate of stem diameter, basal area turnover rate and estimated recruitment rate (using growth rate and size distribution) correlated with productivity among the nine forests in all periods. These rates based on growth rates of surviving stems appeared to be good measures of stand turnover. However, observed recruitment rate and mortality (and turnover rate as mean of these rates) based on direct observation of recruits and deaths did not correlate with productivity in some periods. These rates may not be useful as measures of stand turnover given small sample size and short census interval because they were highly influenced by stochastic fluctuation. A severe drought associated with the 1997–1998 El Niño event inflated mortality and depressed mean growth rate, recruitment rate and basal area turnover rate, but had little effect on the correlations between these rates (except mortality) and productivity. Across broad elevational and edaphic gradients on Mount Kinabalu, forest turnover, productivity and species richness correlated with each other, but the causal interpretation is difficult given the different histories and species pools among forests at different elevations.

Keywords Growth · Mortality · Productivity · Recruitment · Turnover

S. Aiba (✉)
Faculty of Science, Kagoshima University,
Kagoshima 890-0065, Japan
E-mail: aiba@sci.kagoshima-u.ac.jp
Tel.: +81-99-2858166
Fax: +81-99-2594720

M. Takyu
Faculty of Regional Environmental Science,
Tokyo University of Agriculture,
Sakuragaoka 1-1-1, Setagaya-ku,
Tokyo 156-8502, Japan

K. Kitayama
Center for Ecological Research,
Kyoto University, Kamitanakami-Hirano,
Otsu 520-2113, Japan

Introduction

Based on a worldwide analysis of humid tropical forests, Phillips et al. (1994) showed that tree species richness correlated with stem turnover rate (mean of recruitment and mortality rates) and with basal area turnover rate, and argued that these rates were measures of productivity. Because turnover rate is far easier to measure than productivity, research on interesting questions involving productivity, such as diversity-productivity relationship, will be greatly facilitated if turnover rate can be used as a surrogate of productivity. However, the linkage between turnover and productivity was questioned (Sheil 1996; Condit 1997), and to our knowledge there has been no study that directly examined the relationship between turnover and productivity for tropical forests. Weaver and Murphy (1990) showed that both above-ground productivity and turnover rate diminished with increasing elevation on a subtropical mountain in Puerto Rico, but this could not be tested statistically because there were only three plots.

On Mount Kinabalu, Borneo, the highest mountain in southeast Asia between the Himalayas and New Guinea, we have been conducting tree censuses at nine permanent plots every 2 years since 1995. These plots are established at four elevations and on different edaphic conditions that reflect diverse geological substrates. A direct estimate of above-ground net primary productivity is available in these plots because litterfall was also monitored, and it has been shown that elevation (as a surrogate of temperature) and edaphic

conditions (as a surrogate of soil nutrient conditions) synergistically determine productivity (Kitayama and Aiba 2002; Takyu et al. 2003; Kitayama et al. 2004). Stand dynamics during 1995–1999 were analysed by Aiba and Kitayama (2002). In this paper, we study variation in stand dynamics (turnover rates as well as growth rates) among the nine plots over 8 years (1995–2003), and examine the relationship with productivity.

On Mount Kinabalu, a severe drought occurred in 1997–1998 in association with the El Niño–Southern Oscillation event, and growth rates and mortality were significantly affected by the drought (Aiba and Kitayama 2002). It is necessary to consider the impact of the drought in order to study stand dynamics (Sheil 1995; Phillips 1995). We therefore calculated growth and turnover rates for each of four 2-year census intervals, of which one (1997–1999) included the drought (drought period) and the other three (1995–1997, 1999–2001 and 2001–2003) did not (non-drought periods). This is also because long census intervals underestimate turnover (recruitment and mortality) rates due to population heterogeneity within a stand and unrecorded mortality of recruits (Sheil 1995; Sheil and May 1996; Kohyama and Takada 1998). We also calculated recruitment rate and mortality over the entire study period (1995–2003) because short census intervals, when combined with small sample sizes, may lead to stochastic fluctuation in these rates. Finally, we will demonstrate the correlation between productivity and species richness for our plots, and discuss the relationships among forest turnover, productivity and species richness.

Methods

Study sites

The geological substrates of Mount Kinabalu (4,095 m, 6°05′N, 116°33′E) are dominated by Tertiary sedimentary rock below c. 3,000 m and by granite above that. Ultrabasic (or serpentine) rock and unconsolidated Quaternary sediment are distributed as patches at some elevations. We selected a total of nine study sites of primary forests on gentle sideslopes ($\leq 27°$) at four common elevations (700, 1,700, 2,700 and 3,100 m) on these substrates (Table 1). At each elevation, we have a pair of sites on ultrabasic versus non-ultrabasic substrate (Tertiary sedimentary rock at 700, 1,700 and 2,700 m and granite at 3,100 m), and at 1,700 m we have an additional site on Quaternary sediment. Selecting the two (or three) sites on different substrates at exactly the same elevation was not always possible due to heterogeneous distribution of the substrate and precipitous topography. Reflecting diverse geology, edaphic conditions differ greatly between two (or three) forests at the same elevation. In short, soil fertility (in terms of biologically available nitrogen and phosphorus) is the lowest on ultrabasic rock, intermediate on Tertiary sedimentary rock (or granite), and the highest on Quaternary sediment at each elevation (Kitayama and Aiba 2002; Takyu et al. 2002; Kitayama et al. 2004). Annual mean temperature (24.3°C at 550 m) decreases with increasing elevation following a lapse rate of 0.55°C per 100 m (Kitayama and Aiba 2002). Mean annual rainfall varies little with elevation, and was ample ($> 2{,}000$ mm) everywhere except during the drought. The El Niño drought occurred from late 1997 to early 1998, and the climatic departure from normal conditions seemed to become greater with increasing elevation (Aiba and Kitayama 2002). According to our measurements using climatic stations at the four elevations, the drought culminated in March to April 1998: the lowest 30-day running totals (the sum of rainfall of a particular day and the preceding 29 days) were 14.4 mm at 550 m, 0.9 mm at 1,560 m, 1.0 mm at 2,650 m and 0.6 mm at 3,270 m. Forest structure and floristic composition of these sites were analysed by Aiba and Kitayama (1999), Aiba et al. (2002) and Takyu et al. (2002).

Table 1 Characteristics of the nine study plots, established at four common elevations on different geological substrate of Mount Kinabalu, Borneo

Common elevation (m)	Geological substrate	Abbreviation	Exact elevation (m)	Plot area (ha)	Basal area (m^2 ha^{-1})[a]	Stem density (ha^{-1})[a]	Above-ground net primary productivity (kg m^{-2} $year^{-1}$)	Litterfall rate (kg m^{-2} $year^{-1}$)
700	T	07S	650	1.00[b]	36.2	1,064	1.91	1.11
700	U	07U	700	1.00	40.7	1,175	1.72	1.11
1,700	T	17S	1,560	0.50	40.0	1,730	1.22	0.80
1,700	Q	17Q	1,860	1.00	49.3	2,045	1.35	0.94
1,700	U	17U	1,860	0.20	49.9	3,535	0.81	0.63
2,700	T	27S	2,590	0.25	53.5	2,116	0.78	0.53
2,700	U	27U	2,700	0.20	41.5	3,775	0.73	0.59
3,100	G	31S	3,080	0.20	64.0	3,665	0.82	0.63
3,100	U	31U	3,050	0.06	25.1	4,383	0.20	0.16

T Tertiary sedimentary; *U* ultrabasic; *Q* Quaternary sedimentary; *G* granitic rocks
[a]For stems ≥4.8 cm dbh
[b]Trees in a large gap (0.14 ha area) were excluded from analysis

Permanent plot censuses

At each of the nine study sites we have established a permanent plot (Table 1, 0.06–1.00 ha area) and conducted the first tree census from October 1995 to August 1996 (1995 census). The subsequent censuses were conducted biennially (in 1997, 1999, 2001 and 2003) from September to December. In each tree census, care was taken to enable correct remeasurement. A point without any stem irregularities was selected at around breast height (1.3 m above ground), the girth measured to the nearest millimetre, and the tree marked with spray paint. Stem diameter at breast height (dbh cm) was calculated as the girth divided by π. Multiple stems were measured separately. Buttressed stems were measured well above the protrusion. Death of stems, and new recruits, were recorded in the second and later censuses. In the two lowland plots (07S and 07U, see Table 1 for the abbreviations of the plots), all stems ≥10 cm dbh (31.4 cm girth) were measured in 1-ha plots; stems 10 cm > dbh≥4.8 cm (15 cm girth) were measured in two 10×100-m (0.1-ha) transects laid within the plots. In the seven plots at ≥1,700 m, all stems ≥4.8 cm dbh were measured. In the 07S plot, a large canopy gap (0.14 ha area) was formed by tree falls between the 1995 and 1997 censuses. Trees in this part of the plot were excluded from the analysis.

Calculating growth and turnover rates

Growth rate (cm $year^{-1}$) was calculated as absolute difference in dbh between two censuses divided by census interval (days between census midpoints divided by 365). Mean growth rates were computed for two dbh classes (4.8–10 and ≥10 cm) separately because stems < 10 cm dbh were measured in subsamples in the two lowland plots. Mortality (% $year^{-1}$) was calculated as percentage of fatalities per year (Sheil et al. 1995). Recruitment rate (% $year^{-1}$) was calculated in the symmetrical form to mortality (Sheil et al. 2000). These formulations yielded virtually identical values to those obtained from logarithmic models used by Phillips et al. (1994). We used both observed and estimated number of recruits outgrowing the minimum dbhs that were defined arbitrarily. Estimation of number of recruits was done by Gf estimation (Kohyama and Takada 1998). The Gf estimate of the number of recruits per area at the midpoint (6 and 11 cm) of the minimum size classes (5–7 and 10–12 cm) is the stem density f in the minimum size class multiplied by average growth rate G of survivors within the size class divided by the class width (2 cm). Stem turnover rate (% $year^{-1}$) was calculated as mean of mortality and observed recruitment rates (Phillips et al. 1994). Basal area turnover rate (cm^2 m^{-2} $year^{-1}$) was calculated as the increase by the growth of surviving stems divided by the census interval. These rates were computed for two minimum dbhs (≥4.8 and ≥10 cm, except Gf estimate of recruitment rate where minimum dbhs were ≥6 and ≥11 cm) to take into account the small sample sizes for stems < 10 cm dbh in the two lowland plots (07S and 07U) and for stems ≥10 cm dbh in the 31U plot. For the two lowland plots, the number of stems (survivors, fatalities and recruits) for < 10 cm dbh were multiplied by the sample area for ≥10 cm dbh divided by one for < 10 cm dbh, and these area-corrected values were added to values for ≥10 cm dbh to calculate mortality and recruitment rate for stems ≥4.8 cm (or ≥6 cm for Gf estimate of recruitment rate).

Checking the error

In the second and later censuses, some stems far larger than the minimum dbh were recorded as recruits. These stems might have been overlooked in the previous censuses. We determined the valid record of dbh of the recruit that showed maximal growth rates in each plot (usually stems of the fast-growing species that showed high growth rates in successive censuses). We assumed that a recruit was present (but overlooked) in the previous censuses if dbh of that recruit was greater than dbh of the valid recruit, and predicted the dbh in the previous censuses using mean growth rate of that stem (or assigned the same dbh if that stem was recorded only once). Some stems that had been considered as dead in one or more censuses were found alive in subsequent censuses. Dbh of such stems was interpolated using growth rate between the preceding and subsequent censuses. Stems with dbh predicted by the above-mentioned methods, as well as stems that showed negative growth of > 5%, were omitted from the calculation of mean growth rate (Condit et al. 1993), but were included in the calculation of observed recruitment rate and basal area turnover rate.

Productivity and species richness

Litterfall monitoring started in February 1996 in all plots (April 1996 in the 17Q plot), and ended in July 1999 in the 07U plot (but continued in the other plots). Above-ground net primary productivity (ANPP) was estimated by above-ground biomass increment for surviving stems (1995–1997) plus fine litterfall (excluding branches > 2 cm girth) for the period before the culmination of the drought (before February 1998) (Clark et al. 2001). Temporal change in productivity was not considered due to the lack of litterfall data after July 1999 in the 07U plot. The productivity values with litterfall from February 1996 to February 1998 for all plots except the 17Q plot were cited from Kitayama and Aiba (2002). Kitayama et al. (2004) reported the productivity values with litterfall from November 1996 to November 1997 for the 17T and 17Q plots. From the ratio of the 17Q to 17T plots during this period, we estimated the productivity value of the 17Q plot with litterfall from February 1996 to February 1998. Small contribution of

biomass increment by recruits was neglected in these estimates, and this might produce slight underestimates.

The relationship between productivity and various rates of forest dynamism (log-transformed when appropriate) was examined using Pearson correlations for each of the four census intervals and also for the entire study period in the case of observed recruitment and mortality rates. The ANPP may correlate with mean growth rate, Gf estimate of recruitment rate or basal area turnover rate simply because all of these rates were calculated from the same data, i.e. growth rates of surviving stems. Therefore, we used litterfall rate as a surrogate of productivity when examining the correlations involving these rates. It is noted that similar results were obtained if we used ANPP, because ANPP correlated highly with litterfall rates among the nine plots ($r = 0.98$, $P < 0.001$). Differences in regression lines for forest dynamics against productivity among periods were examined by analysis of covariance (ANCOVA). Differences in intercepts were tested after homogeneity of slopes was confirmed. We used both arcsine-transformed and non-transformed values for recruitment and mortality rates, and obtained similar results. Only the results using non-transformed values were reported. Finally, we evaluated species richness of each plot using Fisher's α, a diversity index that is relatively independent of sample size (Rosenzweig 1995; Condit et al. 1996; Aiba et al. 2002), citing the data from Aiba et al. (2002).

Results

Among various rates of forest dynamism, mean growth rates for both dbh classes (4.8–10 and ≥10 cm) and basal area turnover rates for both minimum dbhs (≥4.8 and ≥10 cm) significantly correlated with productivity among the nine plots in all of the four census intervals (Table 2, $r \geq 0.75$, all $P < 0.05$, examples for ≥10 cm dbh in Fig. 1a and b).The Gf estimates of recruitment rate for both minimum dbhs (≥6 and ≥11 cm) also correlated with productivity in all intervals ($r \geq 0.59$, examples for ≥11 cm dbh in Fig. 1c) although the correlations were marginally insignificant in one period for each minimum dbh (1999–2001 for ≥6 cm dbh and 1995–1997 for ≥11 cm dbh). It is noted that all of these rates are based on growth rates of surviving stems. However, observed recruitment rates (both ≥4.8 cm and ≥10 cm dbh) only correlated significantly with productivity in some intervals, and mortalities (both ≥4.8 cm and ≥10 cm dbh) did not in any of the four intervals ($r \leq 0.66$, all $P > 0.05$) (examples for ≥10 cm dbh in Fig. 1d, e). Reflecting this, turnover rates (mean of observed recruitment and mortality rates) did not necessarily significantly correlate with productivity in some intervals for both minimum dbhs.

Periods when observed recruitment rate significantly correlated with productivity were not consistent between the two minimum dbhs (1995–1997 for ≥4.8 cm dbh, and 1997–1999 and 2001–2003 for ≥10 cm dbh). In the case of observed recruitment rate ≥10 cm dbh, the insignificant correlations with productivity were partly because of outlying values from the 31U plot (Fig. 1d). In this plot, the sample size for ≥10 cm dbh was small (54–58 stems in each census), and the few recruits observed (two and three stems) resulted in exceptionally large recruitment rates during 1995–1997 and 1999–2001. Exclusion of the 31U plot improved the correlation between observed recruitment (and also turnover) rate (≥10 cm dbh) and productivity among the other

Table 2 Pearson correlation coefficients between productivity (litterfall rate or above-ground net primary productivity) and various rates of forest dynamism for each of four census intervals (ns $P > 0.05$; * $P < 0.05$; ** $P < 0.01$; *** $P < 0.001$), and the results of ANCOVA for the difference in the regression lines for forest dynamism against productivity among intervals

Productivity and dynamism	Dbh (cm)	Census intervals				*P* (ANCOVA)	
		1995–1997	1997–1999	1999–2001	2001–2003	Slope	Intercept
Litterfall rate (kg m^{-2} $year^{-1}$)							
Mean growth rate (cm $year^{-1}$)[a]	4.8–10	0.87**	0.89**	0.82**	0.94***	0.63	0.16
Mean growth rate (cm $year^{-1}$)[a]	≥10	0.93***	0.94***	0.92***	0.94***	0.55	0.009
Basal area turnover rate (cm^2 m^{-2} $year^{-1}$)	≥4.8	0.83**	0.81**	0.75*	0.85**	0.89	0.005
Basal area turnover rate (cm^2 m^{-2} $year^{-1}$)	≥10	0.87**	0.84**	0.82**	0.84**	0.90	0.01
Gf estimate of recruitment rate (% $year^{-1}$)	≥6	0.75*	0.68*	0.59ns	0.71*	0.90	0.84
Gf estimate of recruitment rate (% $year^{-1}$)	≥11	0.63ns	0.80**	0.96***	0.93***	0.18	0.98
Above-ground net primary productivity (kg m^{-2} $year^{-1}$)							
Observed recruitment rate (% $year^{-1}$)	≥4.8	0.69*	0.56ns	0.21ns	0.65ns	0.21	0.002
Observed recruitment rate (% $year^{-1}$)	≥10	0.20ns	0.93***	0.15ns	0.94***	0.04	0.61
Observed recruitment rate (% $year^{-1}$)[b]	≥10	0.92**	0.89**	0.62ns	0.94***	0.07	0.32
Mortality rate (% $year^{-1}$)	≥4.8	0.35ns	−0.03ns	0.53ns	0.20ns	0.68	0.02
Mortality rate (% $year^{-1}$)	≥10	0.26ns	0.30ns	0.66ns	0.55ns	0.43	0.01
Mortality rate (% $year^{-1}$)[b]	≥10	0.50ns	0.52ns	0.57ns	0.25ns	0.58	0.02
Turnover rate (% $year^{-1}$)	≥4.8	0.68*	0.29ns	0.64ns	0.58ns	0.69	0.23
Turnover rate (% $year^{-1}$)	≥10	0.24ns	0.65ns	0.59ns	0.85**	0.32	0.33
Turnover rate (% $year^{-1}$)[b]	≥10	0.85**	0.72*	0.65ns	0.77*	0.99	0.07

[a]Log-transformed because this yielded a better fit for the regression
[b]Excluding the 31U plot that had a small sample size

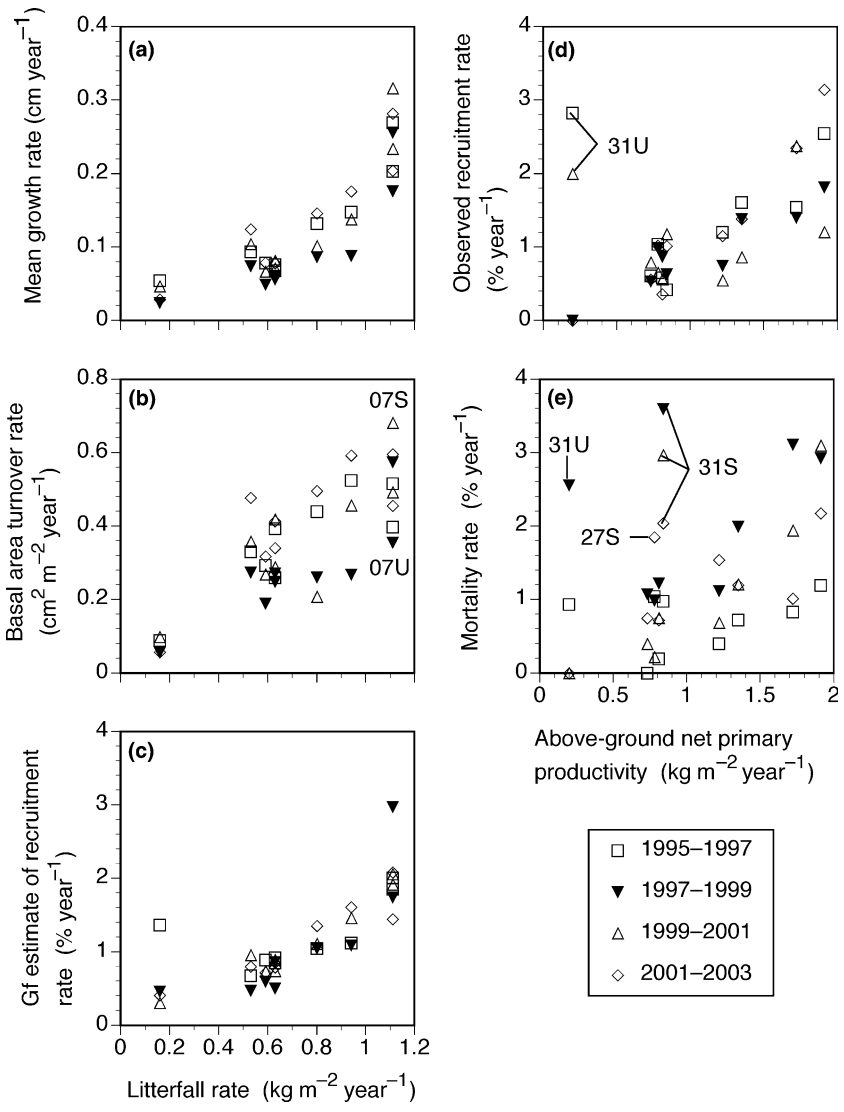

Fig. 1 The relationships between above-ground productivity (litterfall rate or above-ground net primary productivity, kg m^{-2} year^{-1}) and various rates of tree growth and stand turnover for stems ≥10 cm dbh during four 2-year periods among nine plots on Mount Kinabalu, Borneo. The 1997–1999 period included the El Niño drought. Outliers explained in the text were indicated by plot abbreviations (Table 1). **a** Mean growth rates of dbh (cm year^{-1}); **b** basal area turnover rate (cm^2 m^{-2} year^{-1}); **c** Gf estimates of recruitment rates (% year^{-1}); **d** observed recruitment rates (%year^{-1}); **e** mortality (% year^{-1})

eight plots, but the correlations were still insignificant for 1999–2001 for both recruitment and turnover rates. It might be that small sample sizes are problematic only when census intervals are short. We therefore calculated the observed recruitment rate over all 8 years (1995–2003). We used cumulative number of recruits by including stems that had been recruited and died during this period in order not to underestimate recruitment rate (and counting only once when a stem was recruited twice by shrinkage and subsequent growth). Observed recruitment rates over 8 years significantly correlated with productivity for both minimum sizes, even when the 31U plot was included (Fig. 2a, $r = 0.68$ for ≥4.8 cm dbh and $r = 0.84$ for ≥10 cm dbh, both $P < 0.05$).

The small sample size for ≥10 cm dbh in the 31U plot also resulted in fluctuation in short-term (2-year) mortality (Fig. 1e). However, exclusion of the 31U plot did not improve the correlation between mortality (≥10 cm dbh) and productivity, reflecting unexpectedly high mortalities in two other plots (27S and 31S). We calculated mortality over 8 years (1995–2003) to remove the effects of short census intervals. As for recruitment rate, we used the cumulative number of fatalities by including the death of recruits. Mortalities over 8 years correlated with productivity, but the correlations were insignificant (Fig. 2b, $r = 0.32$ for ≥4.8 cm dbh and $r = 0.58$ for ≥10 cm dbh, both $P > 0.05$). We identified two factors that collapsed the correlations between mortality over 8 years and productivity. One is unexpectedly low mortality in the 07U plot for ≥4.8 cm dbh. This reflected the small sample size for 4.8–10 cm dbh (133–152 stems in each census) and few fatalities (only three stems over 8 years) recorded in this size class. The other is that mortalities (both ≥4.8 cm and ≥10 cm dbh) in two plots (27S and 31S) were unexpectedly high. Close inspection of data (Figs. 1e, 2b) indicated that mortality became elevated especially at smaller dbh (< 10 cm dbh) during and after the drought period (1997–1999) in these plots. When these outliers were excluded, the correlations between mortality over 8 years (1995–2003) and productivity became significant

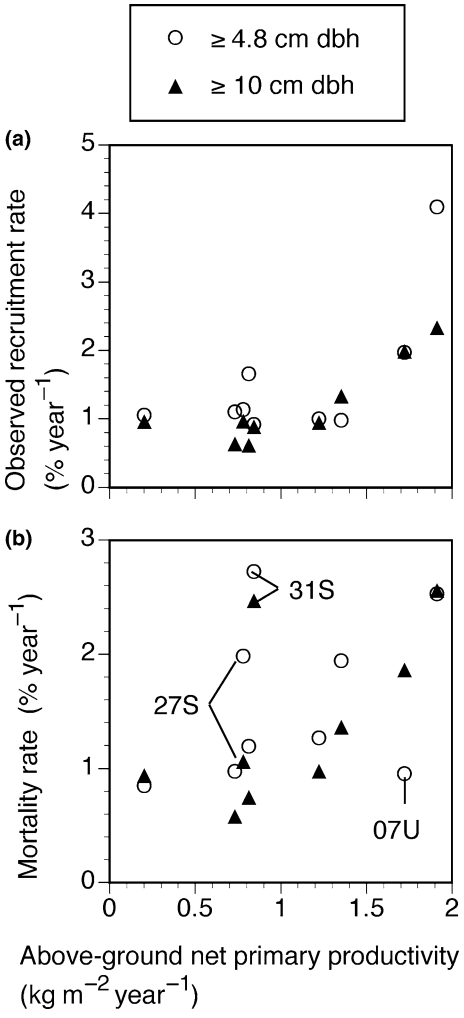

Fig. 2 The relationships between above-ground net primary productivity (kg m^{-2} $year^{-1}$) and observed recruitment or mortality rates over 8 years (1995–2003) for stems ≥4.8 cm and ≥10 cm dbh. Outliers explained in the text were indicated by plot abbreviations (Table 1). **a** Observed recruitment rates (% $year^{-1}$); **b** mortality (% $year^{-1}$)

($r = 0.93$, $P < 0.01$, for ≥4.8 cm dbh, excluding 07U, 27S and 31S plots; $r = 0.83$, $P < 0.05$, for ≥10 cm dbh, excluding 27S and 31S plots).

Mean growth rates (≥10 cm dbh), basal area turnover rates (both ≥4.8 and ≥10 cm dbh), observed recruitment rates (≥4.8 cm dbh) and mortality (both ≥4.8 and ≥10 cm dbh) differed among four census intervals when intercepts of the regression lines against productivity were compared (Table 2, ANCOVA, $P < 0.05$). During the drought interval (1997–1999), mean growth rates, basal area turnover rates and observed recruitment rates were depressed, and mortality was inflated (examples in Fig. 1). As was pointed out earlier, the drought elevated mortality in the 27S and 31S plots in particular, and the effects could be recognized even after the drought. If we examined temporal patterns in the correlations between various rates of forest dynamism and productivity (Table 2), there was no consistent pattern in comparison

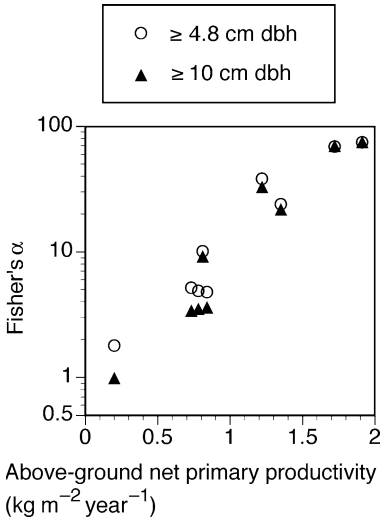

Fig. 3 The relationship between productivity (kg m^{-2} $year^{-1}$) and Fisher's α for stems ≥4.8 cm and ≥10 cm dbh

between drought period versus non-drought periods. Therefore, the drought had little effect on the correlations between these rates (except mortality) and productivity.

Sample-size adjusted index of species richness (Fisher's α) showed a highly significant correlation with productivity for both minimum dbhs (Fig. 3, $r = 0.96$, $P < 0.001$ for both ≥4.8 cm and ≥10 cm dbh, using log-transformed Fisher's α). Therefore, forest turnover, productivity and species richness correlated with each other across broad elevational and edaphic gradients on Mount Kinabalu.

Discussion

The present results demonstrated that some measures of stand dynamics correlated with productivity among forests across broad elevational and edaphic gradients on a single tropical humid mountain. Among various measures tested, mean growth rate and turnover rates based on growth rates of surviving stems (Gf estimate of recruitment rate and basal area turnover rate) highly correlated with productivity. However, turnover rates based on direct observations of recruits and fatalities did not necessarily correlate with productivity. So, our results generally support the argument of Phillips et al. (1994) on turnover-productivity relationship, but the stem turnover rate they used (mean of observed recruitment and mortality rates) may not be universally useful as a measure of stand dynamics.

Among three measures highly correlated with productivity, mean growth rate showed the strongest correlations, and the other two rates (Gf estimate of recruitment rate and basal area turnover rate) showed similar magnitudes of correlation with one another. Mean growth rate may be the best measure of stand productivity, although it has not been used previously.

Phillips et al. (1994) stated that basal area turnover rate was a direct measure of productivity. However, this rate was unexpectedly small in the two lowland plots (07S and 07U) during non-drought periods in the present results (Fig. 1b), reflecting the relatively small basal areas in these plots (Table 1). Generally, tropical lowland forests exhibit smaller basal areas than montane forests (Edwards and Grubb 1977; Tanner 1980; Weaver and Murphy 1990; Lieberman et al. 1996; Aiba and Kitayama 1999). So, basal area turnover rate may not be a good measure of forest productivity when comparing montane and lowland forests.

Why did mean growth rate and turnover rates based on growth rates of surviving stems correlate highly with productivity, while observed rates of recruitment and mortality did not? The former measures are based on average values of relatively large samples of observations, and therefore are likely to yield relatively unbiased estimates for the populations. By contrast, the latter ones rest upon relatively rare events that are highly unpredictable in both space and time, and these rates, observed in small samples during short time intervals, fluctuate greatly in a stochastic manner. This was exemplified by recruitment and mortality rates for ≥10 cm dbh in the 31U plot and by mortality for ≥4.8 cm dbh in the 07U plot in the present results (Figs. 1d, e, 2b). Phillips et al. (1994) used turnover rates as the mean of recruitment and mortality rates to dampen the effects of such fluctuation. However, in our case, turnover rate as well as observed recruitment and mortality rates did not always correlate with productivity. Lengthening the time interval could diminish the short-term fluctuation for recruitment rate, but did not make the correlation for mortality significant (Fig. 2). We noted that the correlations between these rates and productivity were usually positive, although they were insignificant. So, increasing the number of plots may yield significant positive correlations.

Observed recruitment is also affected by an incomplete census that results in recruits being overlooked in one or more censuses and a sudden recruitment of large stems in subsequent censuses. Although we have tried to correct for this, errors might still remain especially for ≥4.8 cm dbh. We suggest that direct counts of recruits and fatalities may not be useful as measures of turnover rate because they are highly influenced by stochastic fluctuation and methodological errors, especially when the sample size is small and the census interval is short. The Gf estimation of recruitment rate developed by Kohyama and Takada (1998) is a powerful tool to resolve such problems, but there is no appropriate method for mortality estimation.

Phillips and Gentry (1994), Phillips (1996) and Phillips et al. (2004) suggested that tropical tree populations experienced increased rates of mortality and recruitment in the latter part of the 20th century. In our short-term data set, there was no clear temporal increase in turnover rates, the impact of the drought was overriding. As was pointed out by the present results, as well as our earlier analysis (Aiba and Kitayama 2002), the severe 1997–1998 El Niño drought inflated mortality, and reduced growth rate, recruitment rate and basal area turnover rate. Long-term mortalities (1995–2003) were greater than expected in the two high-altitude plots (27S and 31S) on non-ultrabasic substrates (Fig. 2b), and this appeared to be partly due to the long-term impact of the drought. Similar long-term effects could be detected when temporal correlations in individual stem growth rates were examined for all nine plots (S. Aiba, unpublished data). However, the present results also indicated that the drought had little effect on the correlation between turnover rates (except mortality) and productivity. The correlation between stand turnover and productivity appeared to be so strong that even the impact of a severe drought could not confound it.

The present results also indicated that forest turnover, productivity and species richness correlated with each other. This seems to support a general pattern at regional to global scales for forest ecosystems (Phillips et al. 1994; Bellingham et al. 1999; Burslem and Whitmore 1999; Waide et al. 1999), but the causal interpretation of this pattern is difficult. We could not assume that forests at different elevations have the same species pools, because these forests have experienced different histories (Sheil 1996). Forest zonation has shifted along the mountain slope during past climatic changes (Morley 2000), and each forest still might not have reached equilibrium conditions. Forests at higher elevations may be less species-rich, simply because they have smaller species pools reflecting more severe past climatic disturbance. Also, there are circular relationships among forest turnover, productivity and species richness: for example, high species richness can be both a cause and a result of high productivity (Waide et al. 1999). Alternatively, apparent correlations among these attributes may be the product of an unidentified common cause: for example, both high turnover and species richness could be ascribed to the early successional status of the forest (Sheil 1996). Comparing sites with the same species pool (at the same elevation on a mountain) at the same successional stage would be the first step towards untangling the cause and effect behind these correlations.

Acknowledgements We would like to thank Datuk Lamri Ali, Mr Francis Liew, Dr Jamili Nais, Mr Maklarin Lakim and Ms Rimi Repin of Sabah Parks for their generous support for our study. We also thank Prof Takashi Kohyama for his comments on the manuscript.

References

Aiba S, Kitayama K (1999) Structure, composition and species diversity in an altitude-substrate matrix of rain forest tree communities on Mount Kinabalu, Borneo. Plant Ecol 140:139–157

Aiba S, Kitayama K (2002) Effects of the 1997–1998 El Niño drought on rain forests of Mount Kinabalu, Borneo. J Trop Ecol 18:215–230

Aiba S, Kitayama K, Repin R (2002) Species composition and species-area relationships of trees in nine permanent plots in altitudinal sequence on different geological substrates of Mount Kinabalu. Sabah Parks Nature J 5:7–69

Bellingham PJ, Stewart GH, Allen RB (1999) Tree species richness and turnover throughout New Zealand forests. J Veg Sci 10:825–832

Burslem DFRP, Whitmore TC (1999) Species diversity, susceptibility to disturbance and tree population dynamics in tropical rain forest. J Veg Sci 10:767–776

Clark DA, Brown S, Kicklighter DW, Chambers JQ, Thomlinson JR, Ni J (2001) Measuring net primary production in forests: concepts and field methods. Ecol Appl 11:356–370

Condit R (1997) Forest turnover, diversity, and CO_2. Trends Ecol Evol 12:249–250

Condit R, Hubbell SP, Foster RB (1993) Identifying fast-growing native trees from the Neotropics using data from a large, permanent plot census plot. For Ecol Manag 62:123–143

Condit R, Hubbell SP, LaFrankie JV, Sukumar R, Manokaran N, Foster RB, Ashton PS (1996) Species-area and species-individual relationships for tropical trees: a comparison of three 50-ha plots. J Ecol 84:549–562

Edwards PJ, Grubb PJ (1977) Studies of mineral cycling in a montane rain forest in New Guinea. I. The distribution of organic matter in the vegetation and soil. J Ecol 65:943–969

Kitayama K, Aiba S (2002) Ecosystem structure and productivity of tropical rain forests along altitudinal gradients with contrasting soil phosphorus pools on Mount Kinabalu, Borneo. J Ecol 90:37–51

Kitayama K, Aiba S, Takyu M, Majalap N, Wagai R (2004) Soil phosphorus fractionation and phosphorus-use efficiency of a Bornean tropical montane rain forest during soil aging with podozolization. Ecosystems 7:259–274

Kohyama T, Takada T (1998) Recruitment rates in forest plots: Gf estimates using growth rates and size distribution. J Ecol 86:633–639

Lieberman D, Lieberman M, Peralta R, Hartshorn GS (1996) Tropical forest structure and composition on a large-scale altitudinal gradient in Costa Rica. J Ecol 84:137–152

Morley RJ (2000) Origin and evolution of tropical rain forests. John Wiley and Sons Ltd, Chichester

Phillips OL (1995) Evaluating turnover in tropical forests: response. Science 268:894–895

Phillips OL (1996) Long-term environmental change in tropical forests: increasing tree turnover. Environ Conserv 23:235–248

Phillips OL, Baker TR, Arroyo L, Higuchi N, Killeen TJ, Laurance WF, Lewis SL, Lloyd J, Malhi Y, Monteagudo A, Neill DA, Núñez Vargas P, Silva JNM, Terborgh J, Vásquez Martínez R, Alexiades M, Almeida S, Brown S, Chave J, Comiskey JA, Czimczik CI, Di Fiore A, Erwin T, Kuebler C, Laurance SG, Nascimento HEM, Olivier J, Palacios W, Patiño S, Pitman NCA, Quesada CA, Salidas M, Torres Lezama A, Vinceti B (2004) Pattern and process in Amazon tree turnover, 1976–2001. Phil Trans R Soc Lond B 359:381–407

Phillips OL, Gentry AH (1994) Increasing turnover through time in tropical forests. Science 263:954–958

Phillips OL, Hall P, Gentry AH, Sawyer SA, Vázquez R (1994) Dynamics and species richness of tropical rain forests. Proc Natl Acad Sci USA 91:2805–2809

Rosenzweig ML (1995) Species diversity in space and time. Cambridge University Press, Cambridge

Sheil D (1995) Evaluating turnover in tropical forests. Science 268:894

Sheil D (1996) Species richness, tropical forest dynamics and sampling: questioning cause and effect. Oikos 76:587–590

Sheil D, Burslem DFRP, Alder D (1995) The interpretation and misinterpretation of mortality rate measures. J Ecol 83:331–333

Sheil D, Jennings S, Savill P (2000) Long-term permanent plot observations of vegetation dynamics in Budongo, a Ugandan rain forest. J Trop Ecol 16:765–800

Sheil D, May RM (1996) Mortality and recruitment rate evaluations in heterogeneous tropical forests. J Ecol 84:91–100

Takyu M, Aiba S, Kitayama K (2002) Effects of topography on tropical lower montane forests under different geological conditions on Mount Kinabalu, Borneo. Plant Ecol 159:35–49

Takyu M, Aiba S, Kitayama K (2003) Changes in biomass, productivity and decomposition along topographical gradients under different geological conditions in tropical lower montane forests on Mount Kinabalu, Borneo. Oecologia 134:397–404

Tanner EVJ (1980) Studies on the biomass and productivity in a series of montane rain forests in Jamaica. J Ecol 68:573–588

Waide RB, Willig MR, Steiner CF, Mittelbach G, Gough L, Dodson SI, Juday GP, Parmenter R (1999) The relationship between productivity and species richness. Annu Rev Ecol Syst 30:257–300

Weaver PL, Murphy PG (1990) Forest structure and productivity in Puerto Rico's Luquillo Mountains. Biotropica 22:69–82

Ecol Res (2005) 20: 287–296
DOI 10.1007/s11284-005-0044-y

ORIGINAL ARTICLE

**Masaaki Takyu · Yasuhiro Kubota · Shin-ichiro Aiba
Tatsuyuki Seino · Takashi Nishimura**

Pattern of changes in species diversity, structure and dynamics of forest ecosystems along latitudinal gradients in East Asia

Received: 11 October 2004 / Accepted: 1 January 2005 / Published online: 3 March 2005

Abstract We examined effects of seasonality of climate and dominant life form (evergreen/deciduous, broad-leaf/coniferous) together with energy condition on species diversity, forest structure, forest dynamics, and productivity of forest ecosystems by comparing the patterns of changes in these ecosystem attributes along altitudinal gradients in tropical regions without seasonality and along a latitudinal gradient from tropical to temperate regions in humid East Asia. We used warmth index (temperature sum during growing season, WI) as an index of energy condition common to both altitudinal and latitudinal gradients. There were apparent differences in patterns of changes in the ecosystem attributes in relation to WI among four forest formations that were classified according to dominant life form and climatic zone (tropical/temperate). Many of the ecosystem attributes—Fisher's alpha of species-diversity indices, maximum tree height and stem density, productivity [increment rate of aboveground biomass (AGB)], and population and biomass turnover rates—changed sharply with WI in tropical and temperate evergreen broad-leaved forests, but did not change linearly or changed only loosely with WI in temperate deciduous broad-leaved and evergreen coniferous forests. Values of these ecosystem attributes in temperate deciduous broad-leaved and evergreen coniferous forests were higher (stem density was lower) than those in tropical and temperate evergreen broad-leaved forests under colder conditions (WI below 100°C). Present results indicate that seasonality of climate and resultant change in dominant life form work to buffer the effects of energy reduction on ecosystem attributes along latitudinal gradients.

Keywords Species diversity · Aboveground net primary productivity · Forest dynamics · Forest structure · Latitude

M. Takyu (✉)
Tokyo University of Agriculture, 1-1-1 Sakuragaoka,
Setagaya, Tokyo 156-8502, Japan
E-mail: m1takyu@nodai.ac.jp
Tel.: +81-3-5477-2291
Fax: +81-3-5477-2291

Y. Kubota
Faculty of Education, Kagoshima University,
Korimoto, Kagoshima 890-0065, Japan

S. Aiba
Faculty of Science, Kagoshima University,
Korimoto, Kagoshima 890-0065, Japan

T. Seino
Center for Ecological Research, Kyoto University,
Kamitanakami Hirano-cho, Ohtsu,
Shiga 520-2113, Japan

T. Nishimura
Yokohama Institute for Earth Sciences,
3173-25 Showa-machi, Kanazawa, Yokohama,
Kanagawa 236-0001, Japan

Introduction

A latitudinal gradient from tropical to boreal regions is not only an energy gradient but also a gradient of duration of growing season. As the growing season shortens and latitude increases, dominant life forms of forest ecosystems change from evergreen broad-leaved trees through deciduous broad-leaved trees to coniferous trees (Holdridge 1947; Kira 1976; Ohsawa 1995). In tropical regions, evergreen broad-leaved trees dominated across the altitudinal gradients despite the decline in air temperature because there was no seasonality in climate (Whitmore 1990; Kitayama 1992).

Many previous studies on changes in forest ecosystem attributes along latitudinal gradients have focused on the relationships with energy rather than on the relationships with seasonality of climate and/or dominant life forms. Net primary productivity has been estimated using actual evapotranspiration (e.g., Miami model of Lieth 1975; Chikugo model of Uchijima and Seino 1985). The species–energy hypothesis explains that energy availability may

constrain the number of species that can coexist in a community (Hutchinson 1959; Adams and Woodward 1989; Currie 1991). However, since life form is an adaptation to seasonality of climate, the pattern of changes in ecosystem attributes along latitudinal gradients may be affected by dominant life forms of forest ecosystems. Deciduousness is an adaptive leafing phenology to achieve sufficient productivity during the hot summer in temperate regions (Kikuzawa 1991). It is well known that conifers have greater maximum tree size and lifespan than broad-leaved trees (Waring and Franklin 1979; Suzuki and Tsukahara 1987). These differential functions among life forms may work as a buffer to the effects of energy reduction on productivity and biomass along a latitudinal gradient, and ecosystem attributes may be different depending on forest formations with different dominant life forms. Accordingly, we have to consider the effects of seasonality of climate and resultant change in dominant life form on ecosystem attributes to understand latitudinal changes in forest ecosystems.

Recently, many studies have examined patterns in ecosystem attributes at global scales using databases of plot-level forest inventory data (Adams and Woodward 1989; Currie 1991; Phillips et al. 1994; Cornelissen 1996; Reich and Bolstad 2001). However, there are few studies that have focused on the geographical patterns in East Asia (Ohsawa 1995; Kohyama 1999). In East Asia, the humid climate extends continuously from tropical to boreal regions without deserts at middle latitudes. This condition provides us good opportunities to examine the effects of air temperature on ecosystem attributes without considering the effects of seasonality of precipitation. The objectives of this study were to examine the effects of seasonality of climate and the resultant differences in dominant life form on species diversity, structure, dynamics, and productivity of forest ecosystems along a latitudinal gradient in humid East Asia.

In the present study, in order to distinguish the effects of seasonality and dominant life forms from the effects of energy condition, we compared the patterns of changes in ecosystem attributes along a latitudinal gradient from tropical to boreal regions with the patterns of changes along altitudinal gradients in tropical regions.

Methods

We collected tree census data by using the database PlotNet, which includes plot-level forest inventory data from equatorial regions in Southeast Asia to boreal regions in East Asia (http://eco1.ees.hokudai.ac.jp/~plotnet/db/). From the study plots collected, we chose 48 plots that met the following conditions: more than 1,000 mm of annual precipitation, primary forest with no record of logging, more than 1,000 m^2 in plot area (Appendix 1). We used plots with large areas because some ecosystem attributes vary depending on plot area, especially species diversity and forest dynamics. However, the effects of plot area may not be excluded completely because half of the plots were less than 1 ha in area. We used census data collected from 1990–2001 for trees≥10 cm in diameter at breast height (DBH). Since seven plots lacked recensus data and 27 plots lacked litterfall data, sample sizes were different among analyses (Table 1).

For forest structural attributes, maximum DBH and tree height (H), stem density, and aboveground biomass (AGB) were calculated. AGB was estimated from allometric regressions between aboveground tree mass and $DBH^2 \times H$ reported for each forest formation in previous studies (Appendix 2). For some plots without tree height data, allometric regressions between aboveground tree mass and DBH were adopted for the estimation of AGB. Aboveground net primary production (ANPP) was calculated as annual increment in AGB of surviving trees between two censuses (AGB increment rate) plus mean annual fine litterfall. Fine litterfall included all organs greater than 2 mm in diameter (leaves and branches less than about 2 cm in diameter and flowers, fruits, and dust); it was collected by litter traps that were made of 1- or 2-mm mesh and were cone- or rectangular-shaped with a 0.5-m^2 opening. Fisher's alpha and Shannon-Wiener's H' were calculated as species diversity indices.

Mortality (mt), recruitment (rc), population turnover (pt), and biomass turnover (bt) rates were calculated as attributes of forest dynamics from the following equations:

Table 1 Number of sampled plots for species diversity and attributes of forest structure and dynamics

Formation type	Species diversity	Maximum tree size	AGB	Population dynamics	AGB increment	ANPP
Temperate deciduous broad-leaved forests	11	12	12	8	8	4
Temperate evergreen coniferous forests	14	15	15	13	14	2
Temperate evergreen broad-leaved forests	8	9	9	8	8	4
Tropical evergreen broad-leaved forests	11	12	12	11	11	11
Total	44	48	48	40	41	21

$$mt = 100[\ln(No) - \ln(Ns)]/t$$

$$rc = 100[\ln(Nf) - \ln(Ns)]/t$$

$$pt = (mt + rc)/2$$

$$bt = \text{annual AGB increment}/\text{AGB}$$

where No = number of stems at start, Ns = survived stems, Nf = final stems (survived stems + recruits), and t = census span (year).

As an index of energy condition, we used warmth index (WI, Kira 1948):

$$\text{WI} = \sum(\text{MMAT} - 5)$$

where MMAT is monthly mean air temperature for months with a mean above 5°C. We did not use actual evapotranspiration (AET) as an index of energy condition, though many previous studies have. AET explained well the changes in ANPP along both temperature and humidity gradients (Lieth 1975), since it is a function of net radiation and saturation deficit. However, AET is independent of altitude, and it cannot explain changes in ecosystem attributes along an altitude gradient, since solar radiation is generally independent of altitude. Therefore, we used WI as an index of energy condition common to both latitudinal and altitudinal gradients. Since study plots used in this study were located in humid regions, we did not need to consider the effects of deficiency of precipitation. For 26 plots below 1,000 m in altitude, WI significantly correlated with AET when we estimated AET from monthly mean air temperature and precipitation following Takahashi (1979) ($r^2 = 0.78$). Annual temperature range (mean temperature of the warmest month minus the coldest month) was used as an index of seasonality of climate. Although day length during the growing season may change in relation to annual temperature range along a latitudinal gradient, effects of day length could not be distinguished from effects of annual temperature range in this study.

Figure 1 shows latitudinal changes in WI, annual temperature range, and relative basal area of evergreen broad-leaved trees (RBA-EB) for the 48 plots. WI ranged from 20.3°C month in boreal coniferous forests to 261.1°C month in tropical lowland rain forests. As annual temperature range increased above 20°C and WI fell below 80°C month in temperate regions, RBA-EB decreased from 100 to 0% abruptly, and deciduous broad-leaved and evergreen coniferous trees predominated. In tropical regions, evergreen conifers increased as WI decreased below 100°C month, but evergreen, broad-leaved trees predominated in all plots but one. Therefore, we divided vegetation types into four formations based on the climatic zone and dominant life form: tropical evergreen broad-leaved forests, temperate (warm-temperate) evergreen broad-leaved forests, temperate (cool-temperate) deciduous broad-leaved forests, and temperate (cool-temperate and boreal) evergreen coniferous forests, and we compared the pattern of changes for ecosystem attributes along WI among the four formations in this study.

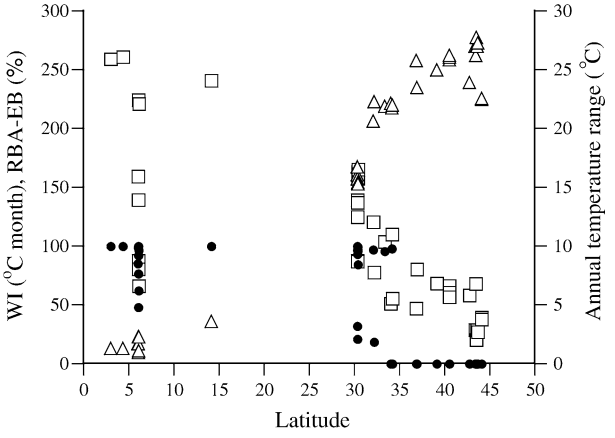

Fig. 1 Latitudinal changes in warmth index (WI, *open squares*), annual temperature range (*open triangles*), and relative basal area of evergreen broad-leaved trees (RBA-EB, *closed circles*) for the 48 study plots

To compare ecosystem attributes among the four formations, correlation between ecosystem attributes and WI in each formation was tested by ANOVA, and slopes and intercepts of regression lines against WI were compared by Bonferroni test after ANCOVA. To test the effects of energy condition, seasonality of climate, and dominant life forms on ecosystem attributes, multiple regression analysis was adopted. In this analysis, three explanatory variables were used: WI as an index of energy condition, annual temperature range as an index of seasonality of climate, and RBA-EB as an index of dominant life form.

Results

The species diversity indices, Fisher's alpha and Shannon-Wiener's H' (data not shown), increased with increasing WI in each formation (ANOVA, $P < 0.01$; Fig. 2). For Fisher's alpha, the slope of the regression line against WI for temperate deciduous broad-leaved and evergreen coniferous forests was significantly looser than for tropical and temperate evergreen broad-leaved forests (ANCOVA, $P < 0.01$). The slope of the regression for the temperate deciduous broad-leaved and evergreen coniferous forests was greater than for the tropical and temperate evergreen broad-leaved forests at a comparable WI under colder conditions (WI < 100°C month). For Shannon-Wiener's H', neither the slopes nor the intercepts of the regression lines against WI were significantly different among the four formations.

For forest structural attributes, there were apparent differences among the four formations. Maximum DBH increased with increasing WI in each formation (ANOVA, $P < 0.01$; Fig. 3a), but the slope of the regression line against WI was greater for the temperate deciduous broad-leaved and evergreen coniferous forests

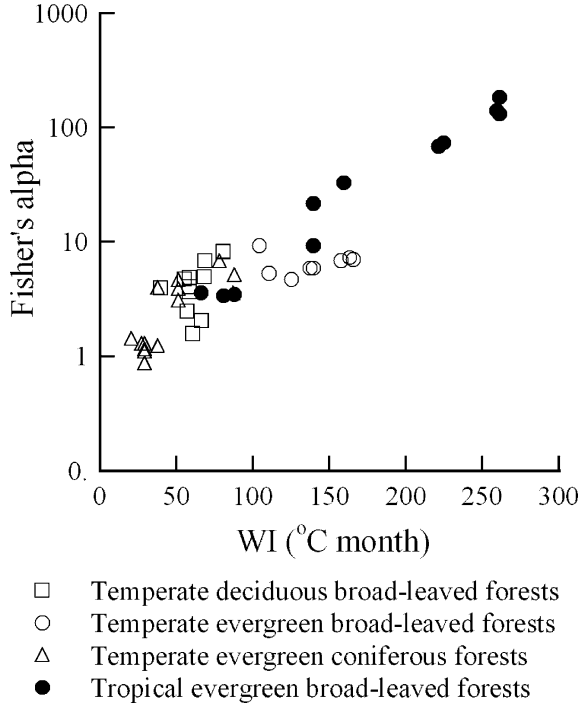

Fig. 2 Changes in species diversity (Fisher's alpha) of four forest formations in relation to WI

than for the tropical and temperate evergreen broad-leaved forests (ANCOVA, $P < 0.05$). Maximum tree height increased with increasing WI in tropical and temperate evergreen broad-leaved forests (ANOVA, $P < 0.01$), but showed similar values and no significant relationships with WI in temperate deciduous broad-leaved and evergreen coniferous forests (ANOVA, $P > 0.05$; Fig. 3b). Thus, maximum tree height was higher in temperate deciduous broad-leaved and evergreen coniferous forests than in tropical and temperate evergreen broad-leaved forests under colder conditions (WI < 100°C month).

Stem density decreased with increasing WI in tropical and temperate evergreen broad-leaved forests (ANOVA, $P < 0.01$) while it varied independently of WI in temperate deciduous broad-leaved and evergreen coniferous forests (ANOVA, $P > 0.05$; Fig. 3c). For stem density, the intercept of the regression line against WI for the tropical and temperate evergreen broad-leaved forests was significantly greater than that for the temperate deciduous broad-leaved and evergreen coniferous forests (ANCOVA, $P < 0.01$). The low stem density under colder conditions in temperate deciduous broad-leaved and evergreen coniferous forests was explained by the decrease in stem density of small trees (10 cm ≤ DBH < 15 cm) at low WI (Fig. 4).

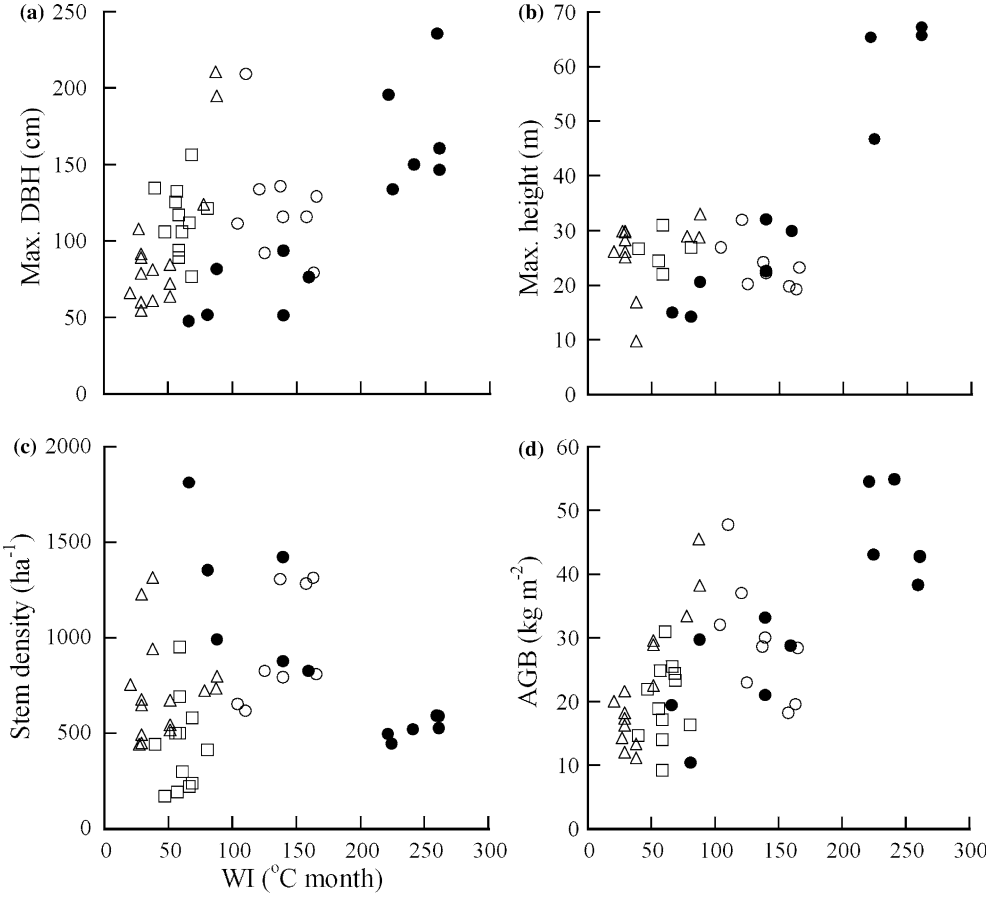

Fig. 3 Changes in forest structural attributes in four forest formations in relation to WI. **a** Maximum DBH. **b** Maximum tree height. **c** Stem density of trees≥10 cm in DBH. **d** Aboveground biomass (AGB). *Symbols* are the same as Fig. 2

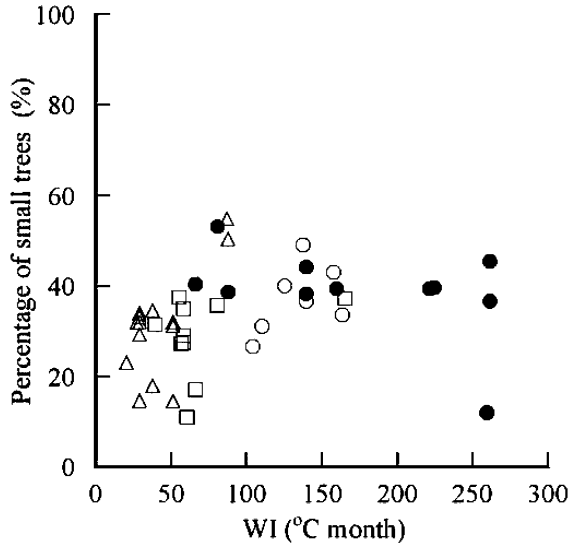

Fig. 4 Changes in percentage of small trees (10 cm ≤ DBH Symbols are the same as Fig. 2

AGB increased with increasing WI in each formation (ANOVA, $P < 0.01$; Fig. 3d), and there were no significant differences in slopes and intercepts of the regression lines among the four formations. Accordingly, the distribution of carbon in biomass differed among the four formations. Under colder conditions (WI < 100°C month) in temperate deciduous broad-leaved and coniferous forests, a greater part of the assimilated carbon was concentrated in a few large canopy trees rather than small trees. In contrast, under colder conditions in tropical and temperate evergreen broad-leaved forests, canopy trees were smaller but had greater stem density, with assimilated carbon shared among a greater number of trees.

ANPP was positively correlated with WI for the 21 plots for which ANPP data was available (ANOVA, $P < 0.01$; Fig. 5a). However, we could not compare among the four formations due to the small sample size. Therefore among the four formations, we compared AGB increment rate, which is recognized to be a good estimate for ANPP (Clark et al. 2001). AGB increment rates in temperate deciduous broad-leaved and evergreen coniferous forests were similar and had no significant relationship with WI (ANOVA, $P > 0.05$), while increment rates in tropical and temperate evergreen broad-leaved forests increased with WI (ANOVA, $P < 0.01$; Fig. 5b). AGB increment rates in temperate deciduous broad-leaved and evergreen coniferous forests were greater than those in tropical and temperate evergreen broad-leaved forests at WI below 100°C month.

In tropical and temperate evergreen broad-leaved forests, mortality, recruitment rate, and population turnover rates increased with increasing WI, but one plot showed a high rate below 80°C month of WI (Fig. 6). In contrast, these attributes of forest dynamics varied independently of WI in temperate deciduous broad-leaved and evergreen coniferous forests (ANOVA,

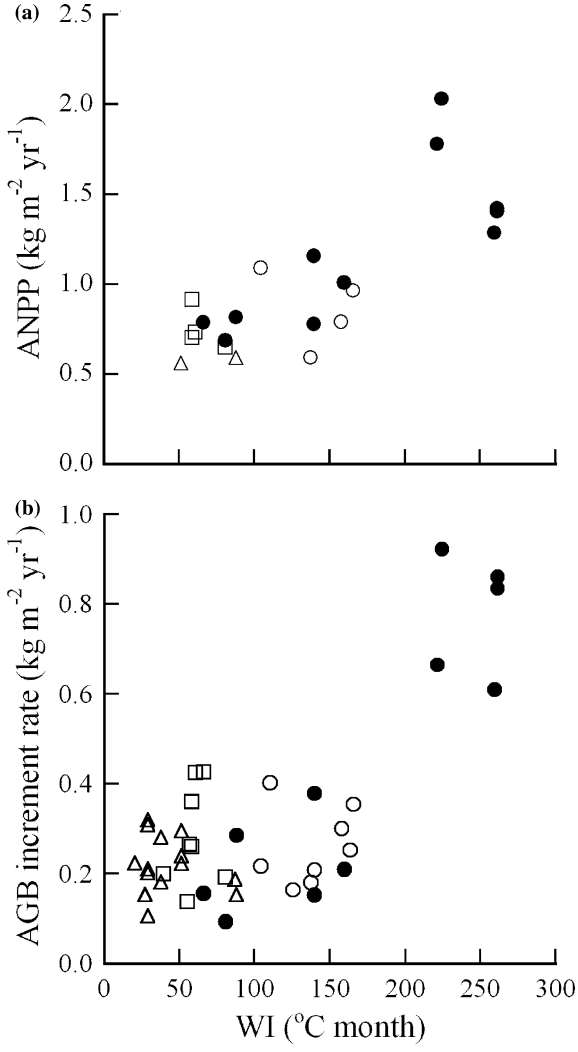

Fig. 5 Changes in **a** aboveground net primary productivity and **b** aboveground biomass increment rate (AGB increment rate) in four forest formations in relation to WI. *Symbols* are the same as Fig. 2

$P > 0.05$). Biomass turnover rate, which was independent of population turnover rate, showed a pattern similar to population turnover rates. Values for these four attributes of forest dynamics tended to be higher in temperate deciduous broad-leaved and evergreen coniferous forests than in tropical and temperate evergreen broad-leaved forests under colder conditions (WI < 100°C month).

Multiple regression analysis was significant in clarifying the variance in 10 of 12 ecosystem attributes. For 6 of the 10 attributes—Fisher's alpha, maximum tree height, stem density, AGB increment rate, population turnover rate, and biomass turnover rate—multiple regression analysis demonstrated that RBA-EB together with WI explained a significant amount of the variance (Table 2). For these six attributes, regression against WI was not significant or the slopes of the regression lines were significantly looser for the temperate deciduous broad-leaved and evergreen coniferous forests compared to those for the tropical and temperate evergreen

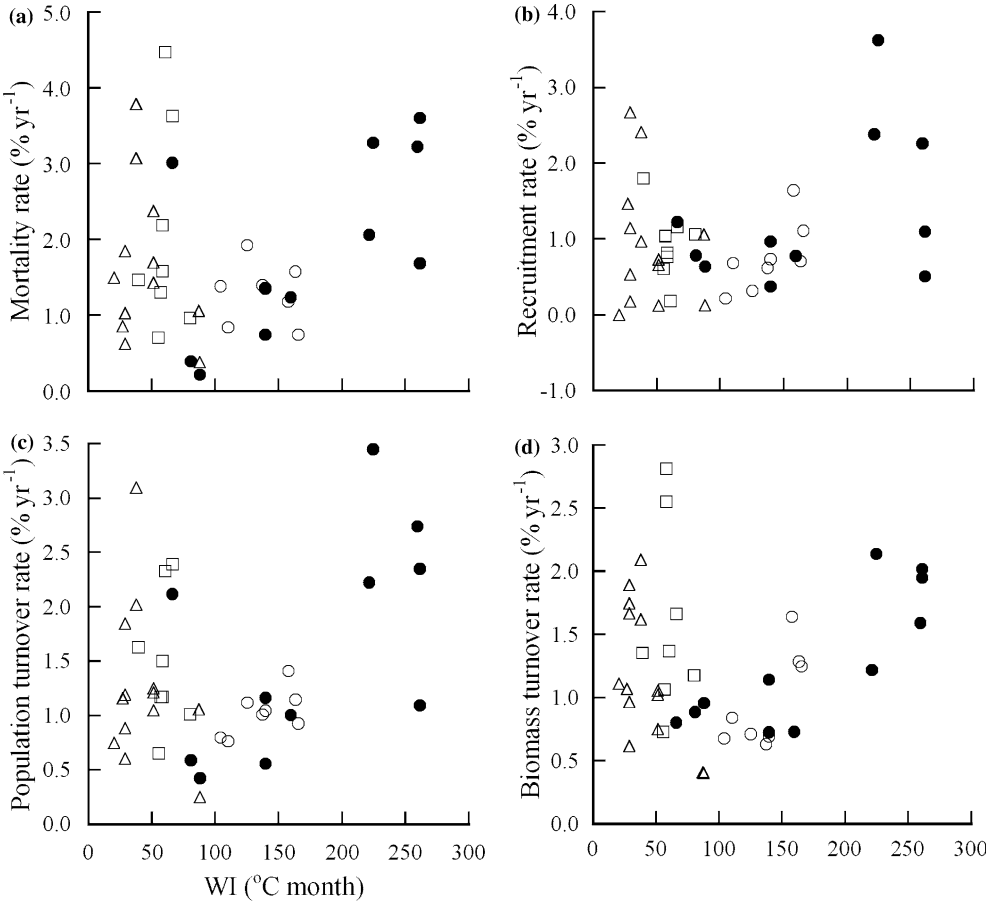

Fig. 6 Changes in forest dynamics in four forest formations in relation to WI. **a** Mortality rate. **b** Recruitment rate. **c** Population turnover rate = (mortality + recruitment rate)/2. **d** Biomass turnover rate = AGB increment rate/AGB. *Symbols* are the same as Fig. 2

broad-leaved forests. Annual temperature range played a significant role in only three attributes—Shannon-Wiener's H', maximum DBH, and stem density.

Discussion

The pattern of changes in ecosystem attributes in relation to WI was distinctively different for two groups of formations. One group included tropical and temperate evergreen broad-leaved forests, and the other included temperate deciduous broad-leaved and evergreen coniferous forests. Multiple regression analysis demonstrated that not only energy condition but also seasonality of climate and dominant life form significantly contributed to explaining the variance in many ecosystem attributes in humid East Asia. Dominant life form, especially, affected ecosystem attributes much more than seasonality

Table 2 Results of multiple regression analysis between forest ecosystem attributes as criterion variables and three explanatory variables: warmth index (*WI*), annual temperature range (*Temp range*), and relative basal area of evergreen broad-leaved trees (*RBA-EB*). Coefficient of determination (r^2) and probability of significance (P) for the multiple regression and number of samples (n) are shown for each attribute. Standard regression coefficient and probability of significance for the three explanatory variables are also shown

Attribute	n	r^2	P	Standard regression coefficient			Probability		
				WI	Temp range	RBA-EB	WI	Temp range	RBA-EB
Fisher's alpha	44	0.79	0.00	1.29	−0.17	−0.72	0.00	0.18	0.00
Shannon-Wiener's H'	43	0.82	0.00	0.74	−0.40	−0.19	0.00	0.00	0.18
Max. DBH	48	0.39	0.00	1.04	0.50	−0.17	0.00	0.02	0.48
Max. tree height	35	0.64	0.00	1.40	0.07	−0.82	0.00	0.69	0.00
Stem density	47	0.44	0.00	−1.09	−0.63	0.76	0.00	0.00	0.00
AGB	48	0.50	0.00	0.77	0.17	0.08	0.00	0.34	0.70
ANPP	21	0.62	0.00	0.78	−0.09	−0.07	0.00	0.68	0.81
AGB increment rate	41	0.65	0.00	1.33	0.10	−0.62	0.00	0.53	0.00
Mortality rate	40	0.17	0.09	0.76	0.04	−0.66	0.02	0.87	0.04
Recruitment rate	40	0.13	0.15	0.57	−0.14	−0.47	0.07	0.58	0.13
Population turnover rate	40	0.21	0.03	0.84	−0.04	−0.71	0.01	0.86	0.02
Biomass turnover rate	41	0.23	0.02	0.90	0.16	−0.79	0.00	0.51	0.01

of climate. These results indicate that seasonality of climate and resultant changes in dominant life form work to buffer the effects of energy reduction on ecosystem attributes along a latitudinal gradient. As well, the effects of dominant life form are more important than the direct effects of seasonality of climate in many cases.

AGB increment rates of temperate deciduous broad-leaved and evergreen coniferous forests did not decrease with decreasing WI, while those of tropical and temperate evergreen broad-leaved forests did. Reich (1993) compared net photosynthetic capacity, leaf N concentration, and specific leaf area in relation to leaf lifespan among some formations, and showed that values for these three leaf traits were higher in deciduous broad-leaved trees than in evergreen broad-leaved trees. Accordingly, deciduous broad-leaved trees achieve high photosynthetic capacity per unit time by allocating much N to leaves, which may contribute to the greater annual productivity of temperate deciduous broad-leaved forests than tropical and temperate evergreen broad-leaved forests under colder conditions (WI < 100°C month) despite the shorter growing season. Although day length during growing season increased with increasing latitude and may contribute to the high productivity in forests at high latitudes, we could not examine the effects of day length on productivity in this study. The higher concentration of leaf N leads to higher litter decomposition rates in temperate deciduous broad-leaved forests compared to tropical and temperate evergreen broad-leaved forests (Cornelissen 1996). The high productivity and decomposition rate may provide the basis for the high biomass turnover rate in temperate deciduous broad-leaved forests.

Stem density in temperate deciduous broad-leaved and evergreen coniferous forests was lower than in tropical and temperate evergreen broad-leaved forests at a comparable WI due to the low density of small trees, though stem density varied independently of WI in temperate deciduous broad-leaved and evergreen coniferous forests. This suggests that large canopy trees may share a greater part of the resources and suppress small trees in temperate deciduous broad-leaved and evergreen coniferous forests. Takyu et al. (1994) showed that shrub species had much higher mortality and recruitment rates than canopy species in a temperate coniferous forest. Temperate evergreen conifers generally have a longer lifespan and greater maximum tree size than deciduous and evergreen broad-leaved trees (Waring and Franklin 1979; Suzuki and Tsukahara 1987). The high population turnover rate of temperate evergreen coniferous forests may result from the high population turnover rate of shrub species due to severe suppression by large canopy trees, although we could not compare the differences in population turnover rates between canopy and shrub species in our data set. However, we could not deny the effect of variation in gap formation among study plots on the forest dynamics in temperate evergreen coniferous forests, since attributes of forest dynamics varied independently of WI in this forest formation. Since the death of large canopy trees in coniferous forests may create large gaps, attributes of forest dynamics may vary if a study plot includes large gaps. On the other hand, high productivity due to the exclusive use of resources and the long lifespan of large canopy trees may result in the high AGB increment rate of temperate evergreen coniferous forests under colder conditions.

This study is a preliminary step in examining the effects of seasonality of climate and resultant changes in dominant life form using a database of forest inventory data; however, the database is not yet adequate for data from East Asia. The development of networks among forest ecologists and the accumulation of forest inventory data are necessary for understanding patterns and mechanisms of changes in ecosystem attributes along a latitudinal gradient and for monitoring changes in ecosystems in East Asia due to global climatic changes.

Acknowledgements We thank Prof. T. Kohoyama and Prof. T. Nakashizuka for their valuable comments. We would also like to thank the following people who allowed us to use their plot data: Dr. H. Ida, Dr. K. Takahashi, Dr. A. C. Luna, Dr. K. Niiyama, Dr. T. Masaki, Dr. N. Akashi, Dr. M. Nakagawa, Dr. T. Manabe, Dr. Y. Kominami, Dr. Abd. Rahman Kassim, and Dr. Nur Supardi Md. Noor. Research in Pasoh Forest Reserve was supported by an NIES/FRIM/UPM Joint Research Project grant (Global Environment Research Program, Ministry of the Environment, Japan).

Appendix 1

Table 3 List of study plots

Plot name	Region/country	Latitude	Longitude	Altitude (m)	Plot area (m^2)	Reference
Pasoh	Peninsular Malaysia/Malaysia	2°59′N	102°19′E	100	60,000	Niiyama et al. (2003)
Lambir CBP	Sarawak/Malaysia	4°2′N	113°5′E	200	80,000	Nakagawa et al. (2000)
Lambir Crane	Sarawak/Malaysia	4°2′N	113°5′E	200	40,000	Nakagawa et al. (2000)
Kinabalu 07T	Sabah/Malaysia	6°03′N	116°42′E	650	10,000	Aiba and Kitayama (1999)
Kinabalu 07U	Sabah/Malaysia	6°06′N	116°42′E	700	10,000	Aiba and Kitayama (1999)
Kinabalu 17T	Sabah/Malaysia	6°N	116°32′E	1,560	10,000	Takyu et al. (2002)
Kinabalu 17Q	Sabah/Malaysia	6°01′N	116°32′E	1,860	10,000	Takyuet al. (2002)
Kinabalu 17U	Sabah/Malaysia	6°03′N	116°36′E	1,860	2,000	Aiba and Kitayama (1999)
Kinabalu 27T	Sabah/Malaysia	6°03′N	116°32′E	2,590	2,500	Aiba and Kitayama (1999)
Kinabalu 27U	Sabah/Malaysia	6°03′N	116°32′E	2,700	2,000	Aiba and Kitayama (1999)
Kinabalu 31T	Sabah/Malaysia	6°05′N	116°33′E	3,080	2,000	Aiba and Kitayama (1999)
Mt.Makiling long-term monitoring plot	Luzon Island/Philippines	14°08′N	121°11′E	400	40,000	Luna et al. (1999)
Yakushima AIK	Kagoshima/Japan	30°23′N	130°38′E	170	5,000	Aiba (unpublished)
Yakushima KAW	Kagoshima/Japan	30°21′N	130°24′E	200	2,500	Aiba et al. (unpublished)
Yakushima HAN	Kagoshima/Japan	30°22′N	130°23′E	280	5,000	Aiba (unpublished)
Yakushima KOY1	Kagoshima/Japan	30°18′N	130°27′E	700	2,500	Aiba and Kohyama (1997)
Yakushima KOY2	Kagoshima/Japan	30°18′N	130°27′E	540	2,500	Aiba and Kohyama (1997)
Yakushima ANB	Kagoshima/Japan	30°19′N	130°36′E	570	5,000	Aiba (unpublished)
Yakushima ARA	Kagoshima/Japan	30°18′N	130°34′E	1,180	5,000	Aiba (unpublished)
Yakushima MIG	Kagoshima/Japan	30°19′N	130°29′E	1,200	10,000	Akashi et al. (unpublished)
Kirishima	Kagoshima/Japan	31°7′N	130°27′E	1,140	10,000	Kubota (unpublished)
Aya	Miyazaki/Japan	32°04′N	131°09′E	400	40,000	Tanouchi and Yamamoto (1995)
Ohkuchi	Kagoshima/Japan	32°8′N	130°32′E	490	4,700	Tanouchi et al. (1994)
Mt. Tatera	Nagasaki/Japan	34°08′N	129°13′E	170	40,000	Miura et al. (2001)
Ohdaigahara	Nara/Japan	34°11′N	136°04′E	1,450	10,000	Akashi and Nakashizuka (1999)
Ohdaigahara Belt 1	Nara/Japan	34°N	136°E	1,550	4,000	Nakashizuka (1991)
Ohdaigahara Belt 2	Nara/Japan	34°N	136°E	1,550	2,000	Nakashizuka (1991)
Ohdaigahara Belt 3	Nara/Japan	34°N	136°E	1,550	2,000	Nakashizuka (1991)
Ogawa	Ibaraki/Japan	36°54′N	140°35′E	555	60,000	Nakashizuka and Matsumoto (2002)
Kayanodaira	Nagano/Japan	36°5′N	138°3′E	1,500	10,000	Ida (unpublished)
Kanumazawa Riparian Research Forest	Iwate/Japan	39°06′N	141°52′E	430	47,100	Suzuki et al. (2002)
Shirakami Akaishizawa	Aomori/Japan	40°3′N	140°7′E	380	10,000	Nakashizuka (unpublished)
Shirakami Kumagera	Aomori/Japan	40°3′N	140°7′E	520	10,000	Nakashizuka (unpublished)
Shirakami Kushiishione	Aomori/Japan	40°3′N	140°7′E	624	10,000	Nakashizuka (unpublished)
Tomakomai Horonai	Hokkaido/Japan	42°43′N	141°34′E	90	12,000	Wada and Ribbens (1997)
Tomakomai Horonai hills	Hokkaido/Japan	42°43′N	141°34′E	90	6,800	Seino (unpublished)
Tomakomai Midori-no-tunnnel	Hokkaido/Japan	42°43′N	141°34′E	90	10,000	Kohyama et al. (1999)
Nukabira	Hokkaido/Japan	43°21′N	143°09′E	1,000	22,500	Takahashi (1994)
Taisetsu onsen	Hokkaido/Japan	43°21′N	143°1′E	1,000	18,000	Kubota et al. (1994)
Nopporo	Hokkaido/Japan	43°25′N	141°32′E	100	1,200	Seino (unpublished)
Taisetsu nipesotu	Hokkaido/Japan	43°29′N	143°04′E	1,400	1,200	Kubota (1995)
Taisetsu 13–1	Hokkaido/Japan	43°31′N	143°12′E	1,000	2,000	Kubota (1995)
Taisetsu 13–2	Hokkaido/Japan	43°31′N	143°12′E	1,000	1,600	Kubota (1995)
Taisetsu mikuni	Hokkaido/Japan	43°34′N	143°08′E	1,000	2,000	Kubota (1995)
Tokachigawa	Hokkaido/Japan	43°39′N	142°57′E	1,100	65,000	Kubota and Nagaike (unpublished)
Shiretoko 1	Hokkaido/Japan	44°04′N	145°02′E	200	22,500	Kubota (2000)
Shiretoko 2	Hokkaido/Japan	44°04′N	145°02′E	250	1,600	Kubota (unpublished)
Shiretoko 3	Hokkaido/Japan	44°04′N	145°02′E	250	1,600	Kubota (unpublished)

Appendix 2

Table 4 Allometric regressions among aboveground tree mass Wt (kg), stem diameter DBH (cm), and tree height H (m) in each forest formation. Wt is total of stem (Ws), branch (Wb), and leaf weights (Wl)

Ws	Wb	Wl	Reference
Cool-temperate/boreal mixed coniferous and deciduous broad-leaved forests			
$\ln W\text{s} = 0.884\ln(\text{DBH}^2H) - 3.089$	$\ln W\text{b} = 0.917\ln(\text{DBH}^2H) - 4.939$	$\ln W\text{l} = 0.904\ln(\text{DBH}^2H) - 6.846$	Takahashi et al. (1999)
$\ln W\text{s} = 2.424\ln\text{DBH} - 2.505$	$\ln W\text{b} = 2.572\ln\text{DBH} - 4.453$	$\ln W\text{l} = 2.500\ln\text{DBH} - 6.288$	Takahashi et al. (1999)
Boreal/subalpine coniferous forests			
$W\text{s} = 0.02847(\text{DBH}^2H)^{0.919}$	$W\text{b} = 0.003938(\text{DBH}^2H)^{0.928}$	$W\text{l} = 0.006117(\text{DBH}^2H)^{0.8506}$	Research group on forest productivity of the four universities (1960)
$W\text{s} = 0.04653\text{DBH}^{2.550}$	$W\text{b} = 0.006468\text{DBH}^{2.570}$	$W\text{l} = 0.009640\text{DBH}^{2.356}$	
Cool-temperate deciduous forests			
$W\text{t} = 0.00158(\text{DBH}^2H)^{0.865}$, H (cm)			Nakashizuka (1984)
$W\text{s} + b = 0.122\text{DBH}^{2.380}$		$W\text{l} = 0.0303\text{DBH}^{1.72}$	Ikushima (1964)
Warm-temperate mixed coniferous and broad-leaved forests			
For *Abies firma*			
$W\text{s} = 0.0871(\text{DBH}^2H)^{0.8269}$	$W\text{b} = 0.0088(\text{DBH}^2H)^{0.9216}$	$W\text{l} = 0.0160(\text{DBH}^2H)^{0.7466}$	Nakao (1985)
For *Tsuga sieboldii*			
$W\text{s} = 0.0361(\text{DBH}^2H)^{0.9184}$	$W\text{b} = 0.0155(\text{DBH}^2H)^{0.8979}$	$W\text{l} = 0.0790(\text{DBH}^2H)^{0.8196}$	Nakao (1985)
For deciduous broad-leaved trees			
$W\text{s} = 0.0875(\text{DBH}^2H)^{0.8581}$	$W\text{b} = 0.0134(\text{DBH}^2H)^{0.9917}$	$W\text{l} = 0.0080(\text{DBH}^2H)^{1.0383}$	Nakao (1985)
For evergreen broad-leaved trees			
$W\text{s} = 0.0495(\text{DBH}^2H)^{0.9274}$	$W\text{b} = 0.0134(\text{DBH}^2H)^{0.9917}$	$W\text{l} = 0.0190(\text{DBH}^2H)^{0.6785}$	Nakao (1985)
For *Abies firma* with DBH ≥30 cm without tree height data			
$\log W\text{s} = 1.8071\text{logDBH} - 0.0515$	$\text{Log } W\text{b} = 2.4586\text{logDBH} - 1.9471$	$\log W\text{l} = 1.7083\text{logDBH} - 1.1837$	Ando et al. (1977)
For *Abies firma* with DBH			
$\log W\text{s} = 2.4748\text{logDBH} - 1.1222$	$\log W\text{b} = 2.5308\text{logDBH} - 2.0537$	$\log W\text{l} = 2.7036\text{logDBH} - 2.6844$	Ando et al. (1977)
For *Tsuga sieboldii* without tree height data			
$\log W\text{s} = 2.1845\text{logDBH} - 0.7232$	$\log W\text{b} = 3.0895\text{logDBH} - 2.8608$	$\log W\text{l} = 2.4057\text{logDBH} - 2.7498$	Ando et al. (1977)
For broad-leaved trees without tree height data			
$\text{logWs} = 2.5857\text{logDBH} - 1.2268$	$\log W\text{b} = 2.6560\text{logDBH} - 1.8546$	$\log W\text{l} = 1.7433\text{logDBH} - 1.6735$	Ando et al. (1977)
Warm temperate evergreen broad-leaved forests			
$W\text{t} = 0.0303D_{0.1}^2H$, $D_{0.1} = 0.941\text{DBH} + 0.734$		Nagano (1978)	
$W\text{s} + b = 0.119\ \text{DBH}^{2.390}$		$W\text{l} = 0.0236\text{DBH}^{1.93}$	Kimura (1960)
Tropical evergreen broad-leaved forests			
$W\text{s} = 0.02903(\text{DBH}^2H)^{0.9813}$	$W\text{b} = 0.1192W\text{s}^{1.059}$	$W\text{l} = 0.09146(W\text{s} + W\text{b})^{0.7266}$	Yamakura et al. (1986)
$W\text{t} = \exp(-2.134 + 2.530\ln\text{DBH})$			Brown (1997)

References

Adams JM, Woodward FI (1989) Patterns in tree species richness as a test of the glacial extinction hypothesis. Nature 339:699–701

Aiba S, Kitayama K (1999) Structure, composition and species diversity in an altitude-substrate matrix of rain forest tree communities on Mount Kinabalu, Borneo. Plant Ecol 140:139–157

Aiba S, Kohyama T (1997) Crown architecture and life-history traits of 14 tree species in a warm-temperate rain forest: significance of spatial heterogeneity. J Ecol 85:611–624

Akashi N, Nakashizuka T (1999) Effects of bark-stripping by Sika deer (*Cervus nippon*) on population dynamics of a mixed forest in Japan. For Ecol Manage 113:75–82

Ando T, Chiba K, Nishimura T, Tanimoto T (1977) Temperate fir and hemlock forests in Shikoku. In: Shidei T, Kira T (eds) Primary productivity of Japanese forests (JIBP synthesis 16). University of Tokyo Press, Tokyo, pp 213–244

Brown S (1997) Estimating biomass and biomass change of tropical forests. A primer. FAO Forestry Paper 134. A Forest Resource Assessment Publication

Clark DA, Brown S, Kicklighter DW, Chambers JQ, Thomlinson JR, Ni J, Holland EA (2001) Net primary production in tropical forests: an evaluation and synthesis of existing field data. Ecol Appl 11:371–384

Cornelissen JHC (1996) An experimental comparison of leaf decomposition rates in a wide range of temperate plant species and types. J Ecol 84:573–582

Currie DJ (1991) Energy and large-scale patterns of animal- and plant-species richness. Am Nat 137:27–49

Holdridge LR (1947) Determination of world plant formations from simple climatic data. Science 105:367–368

Hutchinson GE (1959) Homage to Santa Rosalia, or why are there so many kind of animals? Am Nat 93:145–159

Ikushima I (1964) Productive structure of tree communities. In: National Park Agency of Japan (ed) Report on scientific research of Mount Ohyama in Tanzawa Mountains. Kanagawa Prefecture, Yokohama, pp 106–125

Iwasa Y, Sato K, Kakita M, Kubo T (1993) Modeling biodiversity: latitudinal gradient of forest species diversity. In: Schulze ED, Mooney HA (eds) Biodiversity and ecosystem function. Springer, Berlin Heidelberg New York, pp 433–451

Kikuzawa K (1991) A cost-benefit analysis of leaf habit and leaf longevity of trees and their geographical pattern. Am Nat 138:1250–1263

Kimura M (1960) Primary production of the warm-temperate laurel forest in the southern part of Oosumi Peninsula, Kyushu, Japan. Misc Rep Res Inst Nat Res 52–53:36–47

Kira T (1948) On the altitudinal arrangement of climatic zones in Japan (in Japanese). Kanti-Nogaku 2:142–173

Kira T (1976) Terrestrial ecosystems, ecological studies 2 (in Japanese). Kyoritu Shuppan, Tokyo

Kitayama K (1992) An altitudinal transect study of the vegetation on Mount Kinabalu, Borneo. Vegetatio 102:149–171

Kohyama T, Suzuki E, Aiba S, Seino T (1999) Functional differentiation and positive feedback enhancing plant biodiversity. In: Kato M (ed) The biology of biodiversity. Springer, Berlin Heidelberg New York Tokyo, pp 179–191

Kubota Y (1995) Effects of disturbance and size structure on the regeneration process in a sub-boreal coniferous forest, northern Japan. Ecol Res 10:135–142

Kubota Y (2000) The spatial dynamics of regeneration in a conifer/broadleaf mixed forest in northern Japan. J Veg Sci 11:633–640

Kubota Y, Hiura T, Konno Y (1994) Stand structure and growth patterns of understory trees in a coniferous forest, Taisetsuzan National Park, Japan. Ecol Res 9:333–341

Lieth H (1975) Modeling the primary productivity of the world. In: Lieth H, Whittaker RH (eds) Primary productivity of the biosphere. Springer, Berlin Heidelberg New York Tokyo, pp 237–263

Luna AC, Osumi K, Gascon AF, Lasco RD, Palijon AM, Castillio ML (1999) The community structure of a logged-over tropical rain forest in Mt. Makiling Forest Reserve, Philippines. J Trop For Sci 11:446–458

Miura M, Manabe T, Nishimura N, Yamamoto S (2001) Forest canopy and community dynamics in a temperate old-growth evergreen broad-leaved forest, south-western Japan: a 7-year study of a 4-ha plot. J Ecol 89:841–849

Nagano M (1978) Dynamics of stand development. In: Kira T, Ono Y, Hosokawa T (eds) Biological production in a warm-temperate evergreen oak forest of Japan (JIBP synthesis 18). University of Tokyo Press, Tokyo, pp 21–32

Nakagawa M, Tanaka K, Nakashizuka T, Ohkubo T, Kato T, Maeda T, Sato K, Miguchi H, Nagamasu H, Ogino K, Teo S, Hamid AA, Seng LH (2000) Impact of severe drought associated with the 1997–1998 El Nino in a tropical forest in Sarawak. J Trop Ecol 16:355–367

Nakao T (1985) Ecological studies of *Abies* and *Tsuga* forests in Kyushu, Japan. Bull Miyazaki Univ For 25:1–156

Nakashizuka T (1984) Regeneration process of climax beech (*Fagus crenata*) forests V. Population dynamics of beech in a regeneration process. Jpn J Ecol 34:411–420

Nakashizuka T (1991) Population dynamics of coniferous and broad-leaved trees in a Japanese temperate mixed forest. J Veg Sci 2:413–418

Nakashizuka T, Matsumoto Y (2002) Diversity and interaction in a temperate forest community. Springer, Berlin Heidelberg New York Tokyo

Niiyama K, Kassim AR, Iida S, Kimura K, Ripin A, Appanah S (2003) Regeneration of a clear-cut plot in a lowland dipterocarp forest in Pasoh Forest Reserve, Peninsular Malaysia. In: Okuda T, Manokaran N, Matsumoto Y, Niiyama K, Thomas SC, Ashton PS (eds) Pasoh: ecology of a lowland rain forest in Southeast Asia. Springer, Berlin Heidelberg New York Tokyo, pp 559–568

Ohsawa M (1995) Latitudinal comparison of altitudinal changes in forest structure, leaf-type, and species richness in humid monsoon Asia. Vegetatio 121:3–10

Phillips OL, Hall P, Gentry AH, Sawyer SA, Váquez R (1994) Dynamics and species richness of tropical rain forests. Proc Natl Acad Sci USA 91:2805–2809

Reich PB (1993) Reconciling apparent discrepancies among studies relating life span, structure and function of leaves in contrasting plant life forms and climates: 'the blind men and the elephant retold'. Funct Ecol 7:721–725

Reich PB, Bolstad P (2001) Productivity of evergreen and deciduous temperate forests. In: Roy J, Saugier B, Mooney HA (eds) Terrestrial global productivity. Academic, San Diego, pp 245–283

Research group on forest productivity of the four universities (1960) Studies on the productivity of the forest. Part I. Essential needle-leaved forests of Hokkaido. Kokusaku Pulp, Tokyo

Runkle JR (1989) Synchrony of regeneration, gaps, and latitudinal differences in tree species diversity. Ecology 70:546–547

Suzuki E, Tsukahara J (1987) Age structure and regeneration of old growth *Cryptomeria japonica* forests on Yakushima Island. Bot Mag Tokyo 100:223–241

Suzuki W, Osumi K, Masaki T, Takahashi K, Daimaru H, Hoshizaki K (2002) Disturbance regimes and community structure of a riparian and an adjacent terrace stand in the Kanumazawa Riparian Research Forest, northern Japan. For Ecol Manage 157:285–301

Takahashi K (1979) Estimate of evapotranspiration based on monthly temperature and precipitation (in Japanese). Tenki 26:759–762

Takahashi K (1994) Effect of size structure, forest floor type and disturbance regime on tree species composition in a coniferous forest in Japan. J Ecol 82:769–773

Takahashi K, Yoshida K, Suzuki M, Seino T, Tani T, Tashiro N, Ishii T, Sugata S, Fujito E, Naniwa A, Kudo G, Hiura T, Kohyama T (1999) Stand biomass, net production and canopy structure in a secondary deciduous broad-leaved forest, northern Japan. Res Bull Hokkaido Univ For 56:70–85

Takyu M, Ohsawa M, Ozaki K, Ohtsuka Y, Yoshida N, Honma K, Ono M, Egusa K (1994) Community dynamics of a *Cryptomeria japonica* forest during 10 years in the Yakushima wilderness area, Yakushima island, southern Japan. In: Environment Agency, Nature Conservation Bureau (ed) Long term ecological studies in the Yakushima wilderness area and its surrounding areas, 1994 reports (in Japanese with English summary). Nature Conservation Society of Japan, Tokyo, pp 3–19

Takyu M, Aiba S, Kitayama K (2002) Effects of topography on tropical lower montane forests under different geological conditions on Mount Kinabalu, Borneo. Plant Ecol 159:35–49

Tanouchi H, Yamamoto S (1995) Structure and regeneration of canopy species in an old-growth evergreen broad-leaved forest in Aya district, southwestern Japan. Vegetatio 117:51–60

Tanouchi H, Sato T, Takeshita K (1994) Comparative studies on acorn and seedling dynamics of four Quercus species in an evergreen broad-leaved forest. J Plant Res 107:153–159

Thornthwaite CW (1948) An approach toward a rational classification of climate. Geogr Rev 21:633–651

Uchijima Z, Seino H (1985) Agroclimatic evaluation of net primary productivity of natural vegetations. I. Chikugo model evaluating net primary productivity. J Agr Meteorol 40:343–352

Wada N, Ribbens E (1997) Japanese maple (*Acer palmatum* var. *matsumurae*, Aceraceae) recruitment patterns:seeds, seedlings, and saplings in relation to conspecific adult neighbors. Am J Bot 84:1294–1300

Waring RH, Franklin JF (1979) Evergreen coniferous forests of the Pacific Northwest. Science 204:1380–1386

Whitmore TC (1990) An introduction to tropical rain forests. Clarendon Press, Oxford

Yamakura T, Hagiwara T, Sukardjo S, Ogawa H (1986) Aboveground biomass of tropical rain forest stands in Indonesian Borneo. Vegetatio 68:71–82

Ecol Res (2005) 20: 297–304
DOI 10.1007/s11284-005-0045-x

ORIGINAL ARTICLE

Akio Takenaka

Local coexistence of tree species and the dynamics of global distribution pattern along an environmental gradient: a simulation study

Received: 21 September 2004 / Accepted: 19 December 2004 / Published online: 9 March 2005

Abstract A spatially explicit tree-based model was used to demonstrate the effects of a mechanism promoting multiple-species coexistence on the development of vegetation zonation and its response to climate change. Temporal fluctuation in reproduction was incorporated as the mechanism, which facilitates the persistence of less competitive species. Four hypothetical tree species with different temperature dependencies of seed production were randomly located over a landscape represented by 2,000×40 cells. Each cell can sustain a single tree at most. A zonal distribution pattern emerged corresponding to the temperature gradient along the long axis of the landscape. When there was a temporal variation in seed production, species became distributed over a wider range than that when seed production was constant. When the whole landscape was warmed, the distribution range of each species shifted towards the cool end of the landscape. However, the migration was retarded due to competition for vacant spaces with the remnant species which had dominated the location before the warming. Temporal fluctuation in reproduction facilitated the migration because it enhanced the persistence of minority species and, thus, the invasion and establishment of new species in the area dominated by other species.

Keywords Climate change · Environmental gradient · Forest · Simulation · Species coexistence · Temporal fluctuation in reproduction

A. Takenaka
National Institute for Environmental Studies,
16-2 Onogawa, Tsukuba 305-8506, Japan
E-mail: takenaka@nies.go.jp
Tel.: +81-29-8502474
Fax: +81-29-8502577

Introduction

Vegetation zonation is widely observed both along latitudinal and vertical climate gradients (Woodward 1987; Ohsawa 1993, 1995). Such zonation reflects the absence of a super-plant species that dominates under all climatic conditions. Each individual species has a limited range of conditions for the successful completion of its lifecycle. Such a range, defined in the absence of interspecific competition, is called a fundamental niche (Silvertown 2004). Generally, plants are not found all over their fundamental niches. The range of environmental conditions under which a species is actually observed is called a realized niche. The role of interspecific competition in the determination of the realized niche is quite likely to be very important, but has not been quantitatively examined many times.

The spatial distribution patterns of individual plant species are not static. They are known to have shifted in response to global climate change during the last glacial period (Webb 1992; Webb and Bartlein 1992; Malanson 1993). The speed of movement of vegetational zones after the last glacial period has been estimated from pollen analysis and plant macro fossil data (e.g. Gear and Huntley 1991; Lavoie and Payette 1996; Müller et al. 2003). The estimated rate exceeds 100 m $year^{-1}$ for many tree genera (Clark 1998). Infrequent long-distance dispersal is suspected to play an important role in the rapid movement of the distribution range of tree species (Clark 1998; Clark et al. 1998; Higgins and Richardson 1999).

The speed of the distribution range shift in response to climate change is limited not only by seed dispersal processes, but also by interspecific competition (e.g. Dullinger et al. 2004). The expansion of the range is affected by competition with originally dominant species around the front line. However, again, not many studies have explicitly examined the effects of competition on the rate of migration of plant species populations. Among the few is a study by Kohyama and Shigesada

(1995) using a size structure model of forest dynamics. They suggested that resident species which had been dominant in a local community considerably slow the rate of invasion of another species which would otherwise dominate at the equilibrium state. Interspecific competition retards the growth of local population size of invading species.

The model by Kohyama and Shigesada does not include any explicit mechanism for species coexistence. If some mechanisms give an advantage to locally minor species, that would accelerate the shift of vegetation zonation. In addition, the mechanism also widens the realized niche of individual species because small populations of the species around its distribution border are less likely to go extinct. To understand the development and dynamics of vegetation zonation, consideration of among-species competition and the coexistence mechanisms of multiple species are indispensable.

The objective of the present study was to demonstrate that the processes relevant to the coexistence of multiple species are closely related to the development of the realized niche of trees along an environmental gradient, and also related to the response of the distribution range to climate change. Various hypotheses have been proposed to explain species diversity and apparent coexistence of trees in a forest community (Tilman 1999; Hubbell 2001; Nakashizuka 2001). In the present model, temporal fluctuation of reproduction (Chesson and Warner 1981) was incorporated as a mechanism of multiple-species coexistence.

Methods

Model

To simulate the development and dynamics of the spatial distribution pattern of individual tree species, a spatially explicit tree-based model is used. The landscape is represented by a 2D lattice. A tree-based model is better for dealing with stochastic processes and local interaction among individual trees. The model is not calibrated using measured data, because the emphasis is on the demonstration of the close relationships between species coexistence and species distribution pattern, rather than predictions from real forests.

The lattice representing the landscape contains 80,000 (2,000×40) cells. Each cell can sustain at most a single tree. A temperature gradient is assumed along the long axis of the lattice. The length of the axis, 2,000 cells, is not long enough to represent an actual latitudinal gradient, but long enough to represent an actual altitudinal gradient along mountain slopes.

Each tree is characterized by its age and species. The mortality rate is 2% $year^{-1}$, irrespective of age. The maximum longevity is 100 years. Dead trees are immediately removed from the landscape, leaving vacant cells ready for the establishment of new seedlings. Newly established seedlings take 20 years to mature and start seed production.

The number of seeds a tree produces depends on temperature. The local temperature is represented by a hypothetical warmth index. The larger the index, the warmer the climate. The temperature dependency of the fecundity is represented by a convex second order function of the warmth index (Fig. 1). Among-species differences in temperature dependency are represented by species-specific parameters of the convex function. No seeds are produced if the function gives a negative value. Life history processes other than seed production do not depend on temperature conditions.

Temporal fluctuation in reproduction is incorporated into the model as a mechanism of species coexistence. Chesson and Warner (1981) showed that, theoretically, multiple species of territorial or sessile organisms competing for space coexist stably if reproduction by each species is temporally variable, individuals are polycarpic, and the species' populations have overlapping generations. Under these conditions, the vacant places formed after the death of adults are occupied by a species which happens to reproduce at that time, given that other non-reproducing species do not interfere. This process is called winning-by-forfeit (Hurtt and Pacala 1995) or winning-by-default (Webb and Peart 2001). If the temporal variation in reproduction is large enough, a rare species can occasionally increase its population size considerably by winning-by-default.

In the present model, seed production of each tree species fluctuates annually in an all-or-none manner. The seed production is synchronized within species. At every time step representing a year, whether or not a species will reproduce is determined for each species randomly based on the probability of reproduction. All species have the same probability of seed production, but the masting is mutually independent among species. The number of seeds a mature tree produces in a reproductive year is adjusted so that 1,000 seeds are produced per year on average.

Generally, the density of seeds dispersed from a parent tree decreases with distance from the tree (Wilson 1993). In this model, the density of seeds dispersed from

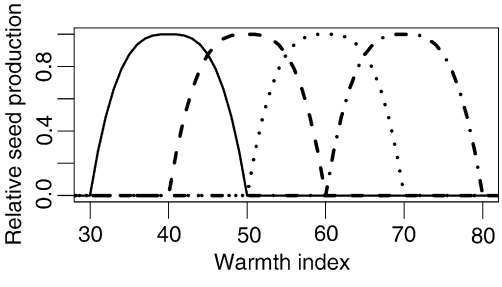

Fig. 1 Dependencies of mean annual seed production of four tree species on a hypothetical warmth index. Different lines represent different tree species. Lower values on the warmth index indicate cooler climates

a parent tree to a given cell over a distance, d, is given by:

$$\text{Seed density} = k \exp(-1.2\, d),$$

where k is an adjustable constant. The infinite tail of the negative exponential function is truncated at a given cutoff distance, denoted as $D_{\max}$. The constant k is adjusted so that the total number of dispersed seeds equals the number of seeds produced by the parent tree. In addition to seeds dispersed following the above distribution function, some trees disperse 1% of their seeds to a randomly selected cell over a distance longer than $D_{\max}$. This process is incorporated to simulate rare long-distance seed dispersal, which is suspected to play an important role in the migration of vegetation. The probability of long-distance dispersal is a changeable parameter.

After determining the number of seeds dispersed to all cells, their fate is decided. In a cell already occupied by an established tree, all seeds fail to establish. No persistent seed bank is formed. In a vacant cell, a single seed is randomly chosen from all seeds dispersed into the cell and allowed to establish as a seedling.

Simulation

Initially, four species with different temperature dependencies were distributed over the 2D lattice. All cells were occupied by mature trees aged from 20 to 100 years. The four species were represented by the same number of trees, i.e., 20,000 individuals from each, to occupy the 80,000 cells of the lattice. The 80,000 trees were located randomly over the landscape, irrespective of their species and age. The temperature dependencies of seed production are shown in Fig. 1.

A gradient of warmth index was set along the long axis of the landscape (Fig. 2). After 2,000 years from the initiation of the simulation, the warmth index was increased by 0.1 every year over the entire landscape to simulate global warming. The warming process continued for 100 years so that the warmth index increased by 10 from the initial condition. After that, the climate was kept constant for 4,900 years. In total, the simulation was carried out for 7,000 years. All four species were able to produce seeds in some part of the landscape both before and after the warming (Fig. 3).

The effects of the frequency of seed production, seed dispersal range, and long-distance seed dispersal were tested. The set of tested parameters is shown in Table 1. Simulation was carried out on a personal computer equipped with a 2 GHz CPU. Each run took one to several hours, depending on the setting of parameters. For each run, the species and age of tree in each cell were recorded at 10-year intervals.

Results

Distribution pattern under fixed condition

As each tree species has a limited warmth index range for seed production, trees outside the range disappeared soon after the initiation of the simulation because of the maximum longevity of individual trees. After that, the distribution range of each species continued to shrink for several hundred years and then stabilized. At this time of apparent equilibrium, a clear zonation of species emerged (Fig. 4). The calculation was repeated several times for each set of parameters, but no apparent differences were observed. In the following, figures representing a single run are shown (Figs. 4, 5, and 6).

The width of the overlap of neighboring species' populations was affected by the temporal fluctuation in

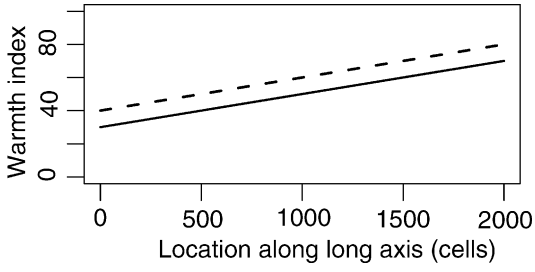

Fig. 2 Distribution of hypothetical warmth index along the long axis of a hypothetical landscape. The left hand side is the cool end. The *solid line* represents the initial condition which lasts for 2,000 years and the *broken line* the warmer conditions from 2,100 to 7,000 years. The warming process takes place at a constant rate during the period from 2,000 to 2,100 years

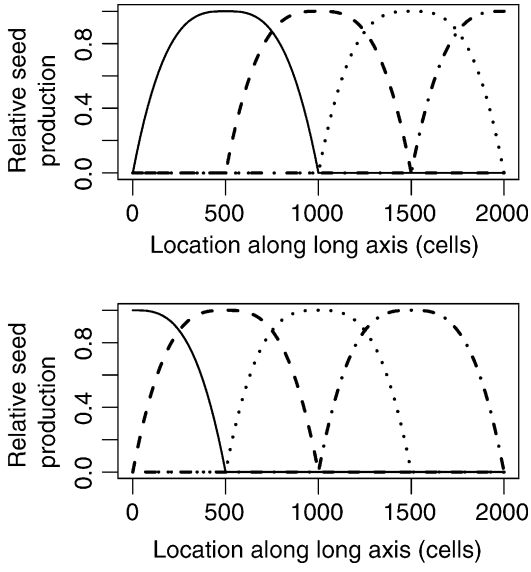

Fig. 3 Mean annual seed production of mature trees of four species along the long axis of the hypothetical landscape. Different *lines* represent different species. The left hand side is the cool end. *Top*, during the period before warming (from the start to year 2,000); *bottom*, during the period after warming (from 2,100 to 7,000 years)

Table 1 Parameters used for the simulation study. The values given in the right-hand column apply to all tree species

Constant parameters	
Years for tree maturation	20 years
Maximum longevity	100 years
Tree mortality	0.02 year^{-1}
Distance of long seed dispersal	40 cells' distance
Percentage of seeds for long-distance dispersal	1%
Varied parameters	
Probability of seed production in a given year	1.0, 0.5, 0.25 year^{-1}
D_{max} (maximum distance that a seed can disperse from the parent tree)	4, 8 cells
Probability a tree disperse some of its seeds over a long distance in a given year	0, 0.5

seed production (Fig. 4). When all mature trees produce seeds every year (probability of seed production was 1.0 year^{-1}), a distinct border between neighboring populations emerged, with a narrow transitional zone. In any area of the landscape, species that showed the highest fecundity dominated locally and excluded species less adapted to the local environment. Two species rarely coexisted at any point in the landscape. Thus, realized distribution range of individual species was confined to areas where the species can surpass any other species by higher seed production (Figs. 3 and 4).

When there was temporal variation in seed production (i.e., probability of reproduction was 0.5 or 0.25 year^{-1}), the transitional zone between neighboring species' populations was remarkably wide. The competitive exclusion of less-adapted species was hindered. The distribution range of individual species was closer to the potential distribution range than in the case when there was no temporal fluctuation in reproduction. Local species diversity was higher in most parts of the landscape.

Irrespective of the frequency of seed production, seed dispersal distance had scarcely any effect on the width of the transitional zone. Rare long-distance dispersal did not have any effect, either.

Response to warming

The response of the distribution range of individual species to warming is shown in Fig. 5. After the simulated warming, trees located near the warm end of their distribution range swiftly disappeared because they were no longer able to reproduce under the new temperature conditions. The vacant area was then occupied by other species which can reproduce there. In 3,000 years, zones of vacant cells among neighboring populations were observed when there was no fluctuation in seed production (Fig. 5, left column). This was because the disappearance of the former population occurred over too wide an area for instantaneous occupation by other species. The invasion of the species more adapted to the new local conditions in the vacant area was limited by seed dispersal.

As the front of the species population expanded towards the cool end of the landscape, the population met the warm end of the population of the species more adapted to cool conditions. Even in the cells where the invading species was able to produce more seeds than the remnant, locally less-adapted species, they did not

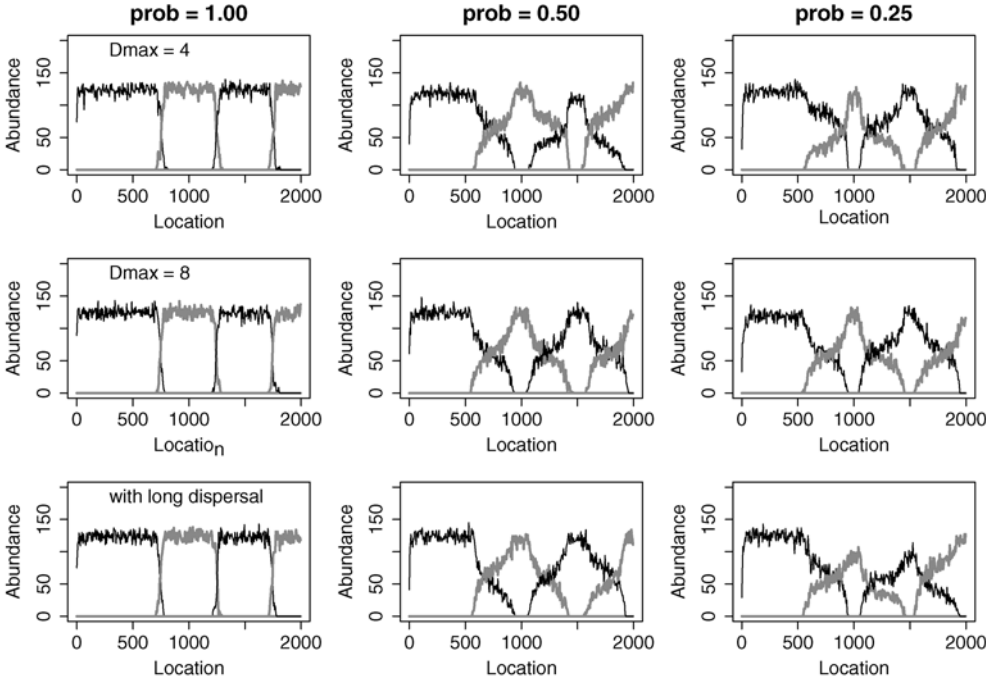

Fig. 4 Distribution range of the populations of four tree species 2,000 years after the initiation of the simulation. The left hand side is the cool end. The maximum distance of normal seed dispersal (D_{max}) is four cells (*top*), eight cells (*middle*), and four-cell dispersal with long-distance dispersal (*bottom*). In the *left column*, mature trees of all species produce seeds every year (prob = 1.0); in the *center column*, each species produces seeds once every 2 years on average (prob = 0.5); in the *right column*, each species produce seeds once every 4 years on average (prob = 0.25). The abundance is the number of trees of individual species in a 5×40-cell area across the landscape

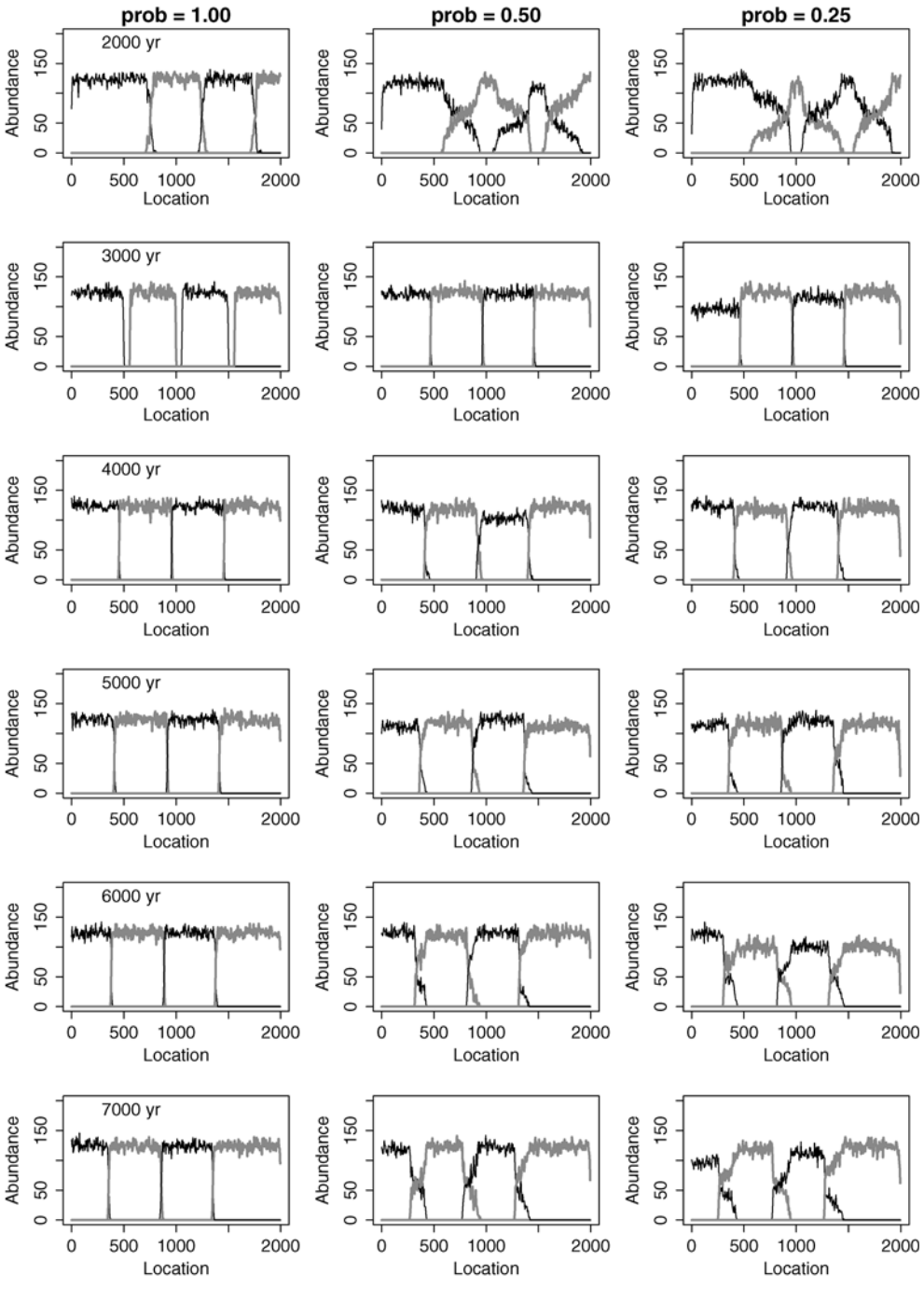

Fig. 5 Distribution range of the populations of four tree species after warming. Distribution from 2,000 to 7,000 years are shown at 1,000-year intervals (from top to bottom). The warming process takes place during the period 2,000–2,100 years. The left hand side is the cool end. The maximum distance of normal seed dispersal is four cells. In the *left column*, mature trees of all species produce seeds every year. In the *center column*, each species produces seeds once every 2 years on average. In the *right column*, each species produces seeds once every 4 years on average. The abundance is the number of trees of individual species in a 5×40-cell area across the landscape

take over the less adapted one instantly. The invaders had to wait for the stochastic death of the less-adapted but not sterile trees. Further, vacant cells left after the death of trees were not freely available to the invading species. As long as the remaining trees from the less-adapted species could produce some seeds, the seeds of invaders had to compete with them for space. The seeds from distant parental trees of invaders are likely to be outnumbered by the currently dominant species. This process caused delayed expansion of invading species.

The delay of invasion was distinct when all mature trees reproduced every year, but there was much less delay when there was temporal fluctuation in seed production. In the latter case, the front of the expanding species swiftly penetrated through the occupying species. The small number of seeds dispersed from distant parent trees can occupy available canopy gaps occasionally due to the winning-by-default mechanism. This penetration does not cause local exclusion of the original inhabitants. The less-adapted but formerly dominant species still remains as a minor component of the local community. Its persistence is also due to the effect of fluctuating reproduction. As a result, wide zones of overlap between neighboring species appeared again. This

pattern did not change, even when the simulation was continued for longer than 7,000 years (data not shown).

Long-distance seed dispersal accelerated the formation of the overlap zone when there was temporal fluctuation in seed production (Fig. 6, right column). When seeds were produced constantly, the border between neighboring species remained distinct irrespective of the occurrence of long-distance seed dispersal (Fig. 6, left column).

Discussion

When there is no fluctuation in seed production, the present model produced similar patterns to those reported by Kohyama and Shigesada (1995), who used a size-structured model of forest dynamics. The transitional zones between the distribution ranges of neighboring populations are narrow, and the realized distribution ranges along the environmental gradient hardly cover the "fundamental niche". Further, the migration rate of vegetational zones in response to climate change was much slower than that expected when there is no among-tree competition for space and expansion is limited only by seed dispersal.

When temporal fluctuation in seed production was incorporated, however, the behavior of the current model was different from that of Kohyama and Shigesada. As less-fecund species can survive by the winning-by-default mechanism, the realized distribution range of individual species was closer to the fundamental niche (Fig. 4). Moreover, the front of expanding species swiftly penetrated into the population of the originally resident species (Figs. 5 and 6).

Generally, the most competitive species in a community is expected to exclude other species competing for a single limited resource (Levins 1979). The high tree-species diversity often observed in forest ecosystems is apparently paradoxical. Researchers have proposed various mechanisms for this coexistence of tree species (Tilman 1999; Nakashizuka 2001). The temporal fluctuation of the production of propagules by sessile or territorial organisms is one of those (Chesson and Warner 1981). The present results are not likely to depend specifically on the fluctuation of reproduction. Any mechanism promoting the persistence of minor or less-adapted tree species is likely to widen the realized niches, and also facilitate the migration of a species' distribution range in response to environmental change. Incorporation of such mechanisms into the size-structured forest model as used by Kohyama and Shigesada (1995) is worth testing to validate the generality of the present results. The major difference between the present model and that of Kohyama and Shigesada lies in the implementation of competition. In the present model, the competition is at the scale of the size of a single tree and in an all-or-none manner. In the size-structured model, the competition is among size classes, and spatially averaged. This may lead to different behavior when fluctuating reproduction is incorporated.

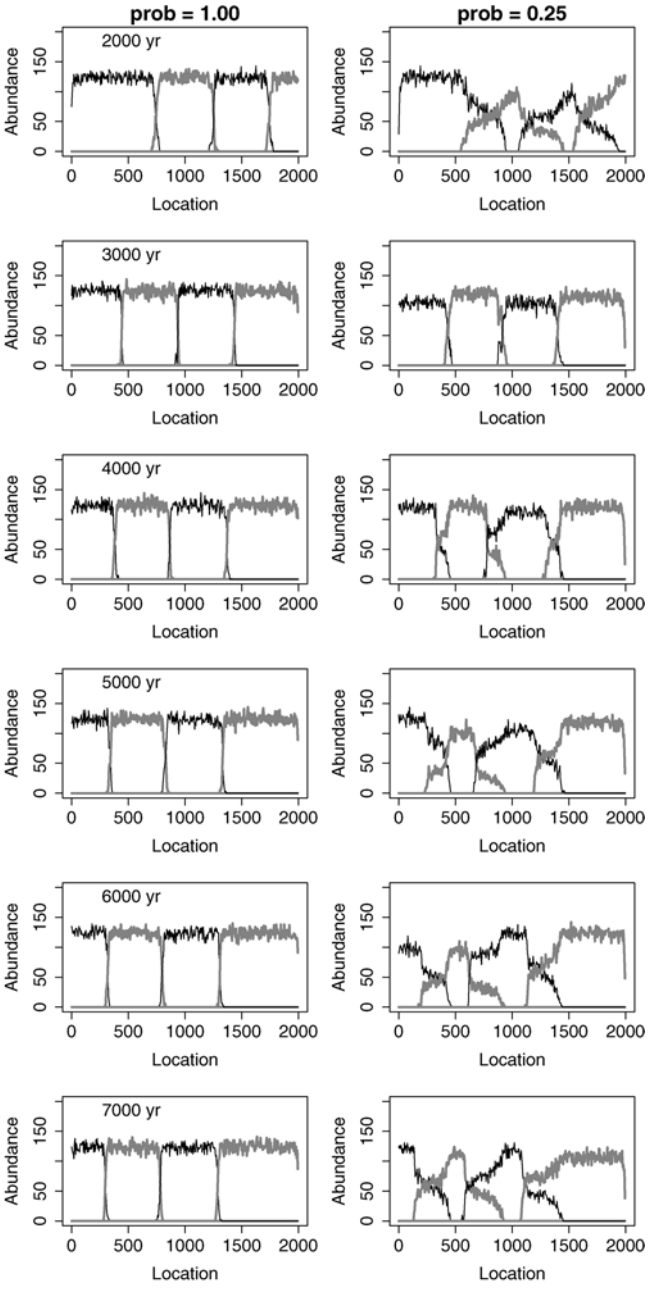

Fig. 6 Distribution range of the population of four tree species after warming when seeds are occasionally dispersed over a long distance. Distribution from 2,000 to 7,000 years are shown at 1,000-year intervals (from *top to bottom*). The warming process takes place during the period 2,000–2,100 years. The left hand side is the cool end. The maximum distance of normal seed dispersal (D_{max}) is four cells, and rare long-distance dispersal also occurs. In the *left column*, mature trees of all species produce seeds every year; in the *right column*, each species produces seeds once every 4 years on average. The abundance is the number of trees of individual species in a 5×40-cell area across the landscape

The incorporation of fluctuation of seed production of trees synchronized within species is justified

because it is a frequently observed phenomenon (Kelly 1994; Herrera et al. 1998; Shibata et al. 2002). However, the contribution of this phenomenon to species coexistence in real forests has not been quantified. Long-term observation is needed to explore the mechanisms responsible for the coexistence of tree species (Nakashizuka et al. 1995; Clark et al.1999; Connell and Green 2000).

In recent years, efforts have been made to combine global climate models with vegetation models considering interactions between climates and vegetation (Peng 2000). Such models can be used to simulate the distribution of vegetation under varying global climates, and to predict vegetation responses to climates in the past and future. As the global carbon budget is predicted to be much influenced by the migration of vegetation (Solomon and Kirilenko 1997), the coupling model is also needed to simulate the global carbon balance. The correlation between climate and vegetation has been studied and used to predict the future vegetation pattern at equilibrium (e.g., Iverson and Prasad 1998, 2001). However, the predicted rate of climate change in the near future is too high for vegetation zonation to catch up without delay. As demonstrated in this study, local processes affecting species diversity are likely to affect the transitional dynamics of vegetation zonation in response to climate change. For a realistic prediction of future responses of vegetation to global climate change, the modes of competition within local community should be carefully considered.

In the present study, only seed production was assumed to be affected by the climatic condition. In reality, other processes, such as growth, survival, frequency of reproduction, successful fertilization, and seedling establishment, are all likely to be affected by climate change. Climate dependencies of different life history processes may affect the dynamics of species' distribution ranges in different ways. For example, less frequent seed production near the border of the potential distribution range will provide more opportunities for other species to invade by winning-by-default. On the other hand, McKone et al. (1998) predicted less variance of seed production in mast-seeding plant species in response to the predicted global warming. That may cause reduced species diversity as a result of weakened effects of the winning-by-default mechanism. In the understanding of migration processes under the changing climate, we should pay attention to the climatic effects on interactions among species in various aspects.

References

Chesson PL, Warner RR (1981) Environmental variability promotes coexistence in lottery competitive systems. Am Nat 117:923–943

Clark JS (1998) Why trees migrate so fast: confronting theory with dispersal biology and the paleorecord. Am Nat 152:204–224

Clark JS, Fastie C, Hurtt G, Jackson ST, Johnson C, King GA, Lewis M, Mynch J, Pacala S, Prentice C, Schupp EW, Webb T III, Wyckoff P (1998) Reid's paradox of rapid plant migration. Bioscience 48:13–24

Clark JS, Beckage B, Camill P, Cleveland B, HilleRisLambers J, Lichter J, McLachlan J, Mohan J, Wyckoff P (1999) Interpreting recruitment limitation in forests. Am J Bot 86:1–16

Connell JH, Green PT (2000) Seedling dynamics over thirty-two years in a tropical rain forest tree. Ecology 81:568–584

Dullinger S, Dirnbock T, Grabherr G (2004) Modelling climate change-driven treeline shifts: relative effects of temperature increase, dispersal and invasibility. J Ecol 92:241–252

Gear AJ, Huntley B (1991) Rapid changes in the range limits of Scots Pine 4000 years ago. Science 251:544–547

Herrera CM, Jordano P, Guitián J, Traveset A (1998) Annual variability in seed production by woody plants and the masting concept: reassessment of principles and relationship to pollination and seed dispersal. Am Nat 152:576–594

Higgins SI, Richardson DM (1999) Predicting plant migration rates in a changing world: the role of long-distance dispersal. Am Nat 153:464–475

Hubbell SP (2001) The unified neutral theory of biodiversity and biogeography. Princeton University Press, Princeton and Oxford

Hurtt GC, Pacala SW (1995) The consequences of recruitment limitation: reconciling chance, history and competitive differences between plants. J Theor Biol 176:1–12

Iverson LR, Prasad AM (1998) Predicting abundance of 80 tree species following climate change in the eastern United States. Ecol Monogr 68:465–485

Iverson LR, Prasad AM (2001) Potential changes in tree species richness and forest community types following climate change. Ecosystem 4:186–199

Kelly D (1994) The evolutionary ecology of mast seeding. Trends Ecol Evol 9:465–470

Kohyama T, Shigesada M (1995) A size-distribution-based model of forest dynamics along a latitudinal environmental gradient. Vegetatio 121:117–126

Lavoie C, Payette S (1996) The long-term stability of the boreal forest limit in subarctic Quebec. Ecology 77:1226–1223

Levins R (1979) Coexistence in a variable environment. Am Nat 114:765–783

Malanson GP (1993) Comment on modeling ecological response to climatic change. Clim Change 23:95–105

McKone MJ, Kelly D, Lee WG (1998) Effect of climate change on mast-seeding species: frequency of mass flowering and escape from specialist insect seed predators. Global Change Biol 4:591–596

Müller UC, Pross J, Bibus E (2003) Vegetation response to rapid climate change in Central Europe during the past 140,000 yr based on evidence from the Furamoos pollen record. Quat Res 59:235–245

Nakashizuka T (2001) Species coexistence in temperate, mixed deciduous forests. Trends Ecol Evol 16:205–210

Nakashizuka T, Iida S, Masaki T, Shibata M, Tanaka H (1995) Evaluating increased fitness through dispersal: a comparative study on tree populations in a temperate forest, Japan. Ecoscience 2:245–251

Ohsawa M (1993) Latitudinal pattern of mountain vegetation zonation in southern and eastern Asia. J Veg Sci 4:13–18

Ohsawa M (1995) Latitudinal comparison of altitudinal changes in forest structure, leaf-type, and species richness in humid monsoon Asia. Vegetatio 121:3–10

Peng C (2000) From static biogeographical model to dynamic global vegetation model: a global perspective on modelling vegetation dynamics. Ecol Model 135:33–54

Shibata M, Tanaka H, Iida S, Abe S, Masaki T, Niiyama K, Nakashizuka T (2002) Synchronized annual seed production by 16 principal tree species in a temperate deciduous forest, Japan. Ecology 83:1727–1742

Silvertown J (2004) Plant coexistence and the niche. Trends Ecol Evol 19:605–611

Solomon AM, Kirilenko AP (1997) Climate change and terrestrial biomass: what if trees do not migrate? Global Ecol Biogeogr Lett 6:139–148

Webb T III (1992) Past changes in vegetation and climate: lessons for the future. In: Peters RL, Lovejoy TE (eds) Global warming and biological diversity. Yale University Press, New Haven, pp 59–75

Tilman D (1999) Diversity by default. Science 283:495–496

Webb T III, Bartlein PJ (1992) Global changes during the last 3 million years: climatic controls and biotic responses. Annu Rev Ecol Syst 23:141–173

Webb CO, Peart DR (2001) High seed dispersal rates in faunally intact tropical rain forest: theoretical and conservation implications. Ecol Lett 4:491–499

Wilson MF (1993) Dispersal mode, seed shadows, and colonization patterns. Vegetatio 107/108:261–280

Woodward FI (1987) Climate and plant distribution. Cambridge University Press, Cambridge

Ecol Res (2005) 20: 305–312
DOI 10.1007/s11284-005-0046-9

ORIGINAL ARTICLE

Takashi Kohyama

Scaling up from shifting-gap mosaic to geographic distribution in the modeling of forest dynamics

Received: 5 October 2004 / Accepted: 13 January 2005 / Published online: 1 April 2005

Abstract Shifting-gap mosaic is incorporated into the dynamic model of size-structured forests along geographic gradients. In the model named SAL (size–age–location), a forest at a geographic location has a patch-age structure, which approximates the shifting-gap mosaic, and a tree-size structure in each patch of the forest. Growth and recruitment occur in each patch and are regulated by patch-scale crowding in terms of upper basal area. Seed production depends on the basal area density of mother trees at the forest scale. Seeds are dispersed to neighboring locations of the geographic landscape. After a century-long "warming" treatment, a resident forest zone prevented, over several millennia, an invading forest zone from achieving a steady-state range of geographic distribution. Introducing the gap mosaic into the model did not make substantial changes in the response of latitudinal forest zones to the warming treatment, but only moderately accelerated the migration speed of invader species. Temporal fluctuation in seed production without interspecific synchronization, or the lottery effect, did not facilitate the migration of invader species at all.

Keywords Gap mosaic · Global warming · Latitudinal gradient · Simulator · Temporal fluctuation

Introduction

Forest ecosystems, with a high capacity for primary production, provide the major stock of biomass on earth. Long-term biomass dynamics have been successfully described by so-called forest-gap models, which incorporate the processes of tree physiology and demography in forest ecosystems (Bugmann 2001). An aspect for the next generation of forest dynamic models is to scale models up from the patch scale to the regional and global scales to allow for the reasonable prediction of geographic change in vegetation distribution. Though most gap models keep the spatial scale of interest basically at a crown size of 100–400 m^2, some models deal with landscape-level, patch-mosaic forest dynamics (Pacala et al. 1996; Liu and Ashton 1998). Large computational power is required for scaling these models up to regional and global scales (Friend et al. 1997).

An alternative approach is to derive a model of partial differential equations from the stochastic gap model (Kohyama 1993; Hurtt et al. 1998; Kohyama et al. 2001; Moorcroft et al. 2001), and to apply this model across large scales. These models approximate the shifting-patch mosaic of forest landscapes according to the age distribution of patches with different tree-size structures, wherein the creation of tree-fall gaps corresponds to the "death" of a patch of a particular age and the simultaneous "birth" of a gap, resetting the patch age to zero. Tree-size structure is developed with patch aging, and the demography of trees in each patch is regulated by patch-scale tree-size structure. The application of this type of model successfully reproduced the observed structure and dynamics of actual forests.

Geographic-scale models of forest dynamics must predict the shift of geographic forest zones along latitudinal and altitudinal gradients. With the parameterization of thermal response of demographic processes of each species, interaction and competitive exclusion among species along thermal gradients may be described. As seed dispersal is the basis for any species to migrate to new locations, spatial dispersal of seeds must be parameterized in this type of model.

As an attempt at modeling forest zone dynamics along geographic gradients, Kohyama and Shigesada (1995) proposed a geographically extended model of

T. Kohyama
Frontier Research Center for Global Change,
Japan Agency for Marine-Earth Science and Technology,
3137-25 Showamachi, Kanazawa-ku,
Yokohama 236-0001, Japan

T. Kohyama
Graduate School of Environmental Earth Science,
Hokkaido University, Sapporo 060-0810, Japan
E-mail: kohyama@ees.hokudai.ac.jp
Tel.: +81.11.706.2260
Fax: +81.11.706.4954

stand-structure dynamics. Geographic landscape is expressed by spatial location, along which environmental gradients can be defined. Seed dispersal in geographic space was formulated as a kind of diffusion process. In the model, the forest had no patch mosaic feature and was expressed only according to tree-size structure (or vertical foliage structure without horizontal heterogeneity). Kohyama and Shigesada's model described the geographic range of forest zones that had wider potential thermal adaptation, but were competitively excluded by better-performing neighboring forest zones. Following a century-long warming process, they predicted that a resident forest type adapted to a cool environment remarkably prevented the migration of an invasive forest type adapted to warm environment, over several millennia after the warming, even allowing for a high potential of seed dispersal.

This paper proposes the combination of the patch-mosaic model (Kohyama 1993; Kohyama et al. 2001) and the geographic distribution model (Kohyama and Shigesada 1995), and examines whether or not the gap-mosaic feature of forest landscapes facilitates the migration rate of species and the shift of forest zones with climatic change. Gap dynamics may mitigate interspecies competition, thereby promoting the adaptive shift of forest zones. A high rate of gap formation may also suppress the recruitment success of invasive species. Therefore, it is worth examining the effect of the shifting-gap mosaic using the gap-mosaic, geographic model.

Takenaka (2005) introduced an individual-tree-based, lattice model of large-scale forest dynamics, where a unit cell corresponds to the size of a single tree canopy. Takenaka assumed thermal gradients in the lattice-structured landscape. He demonstrated the possible effect of interspecies asynchronized reproduction (which was synchronized within species across geographic scales) on the migration acceleration of an invasive forest zone into a resident zone through the "lottery" effect (Chesson and Warner 1981). The lottery effect states that successful regeneration of less frequent invasive species is guaranteed on the vacant cell during their mast years when the abundant resident species produce no seed. In the real forest landscape, however, a new tree-fall gap providing a regeneration site for tree species may not necessarily guarantee the regeneration success of invaders during their mast years because seedlings of invasive species must compete against the resident seedling pool communities. The model proposed here can simulate this situation. Testing Takenaka's prediction using the present model is thus another purpose of this paper.

The model

Tree distribution at a particular time (t) is expressed along three dimensions reflecting different spatial scales of forest landscapes: tree size (x), which defines the vertical foliage profile in a patch; patch age (a), which defines the shifting-patch mosaic in a forest at a particular geographic location; and geographic location (l), which defines the geographic distribution range of forest species. The overall model is composed of two submodels: one describing the dynamics of tree-size structure specific to species i at patch of age a at the forest at location l, $f_i(t, l, a, x)$; and the other describing the proportion of patches of age a within the forest at location l, $S(t, l, a)$. The model is a combination of the following earlier models: size-structured population (Suzuki 1966; Sinko and Streifer 1967), patch-structured population (Levin 1976), and population dispersal (Skellam 1951), and is the first attempt at combining all of these ecological processes (Fig. 1). I name the present model SAL (size–age–location). All parameters for the modeling framework and simulation are listed in Table 1.

Let $f_i(t, l, a, x)$ be the density of trees per unit forest area of species i with size x (trunk diameter of breast height or any other size dimension) of patch age a, at geographic location l, at time t. The tree density $f_i(t, l, a, x)$ is defined on a per-forest-area basis; therefore the integration of $f_i(t, l, a, x)$ with respect to patch age a corresponds to the forest-scale tree-size structure per unit forest area, at site l. Per-area density at each patch scale is thus described by $f_i(t, l, a, x)/S(t, l, a)$.

The time-dependent change of $f_i(t, l, a, x)$ is described by patch-scale demographic processes, namely tree-size growth, tree mortality and reproduction, patch aging and gap formation, and the movement over geographic location through seed dispersal. We define $G_i(t, l, a, x)$ as the size growth rate of trees of size x; $\gamma(l, a)$ as the gap formation rate (or the death rate of the patch of age a which is reborn at patch age 0), $\mu_i(t, l, a, x)$ as the mortality of trees of size x in the stand of age a independent of gap-formation events, and $R_i(t, l)$ as the rate of mature seed production by mother trees of species i across a patch-dynamic landscape of the forest at t. These demographic processes can change with geographic location l of the forest. Demographic functions G_i, μ_i, and R_i are time dependent, because they can be regulated by instantaneous tree-size structure.

The dynamics of tree populations with size structure and shifting-patch mosaic, along a geographic/environmental gradient, are modeled by the equation (cf. Kohyama 1993):

$$\frac{\partial f_i(t,l,a,x)}{\partial t} = -\frac{\partial [G_i(t,l,a,x) f_i(t,l,a,x)]}{\partial x} - \frac{\partial f_i(t,l,a,x)}{\partial a} - \gamma(l,a) f_i(t,l,a,x) - \mu_i(t,l,a,x) f_i(t,l,a,x). \quad (1)$$

Detail for deriving Eq. 1 (without l dimension) are shown in Moorcroft et al. (2001). The first term of the right side of Eq. 1 corresponds to size upgrowth, the second term describes patch aging, the third and fourth terms are patch death by gap formation and tree death without gap formation, respectively.

Let us assume that seed rain of a particular species is uniformly mixed within a forest, and that seed dispersal occurs between neighboring locations. This assumption

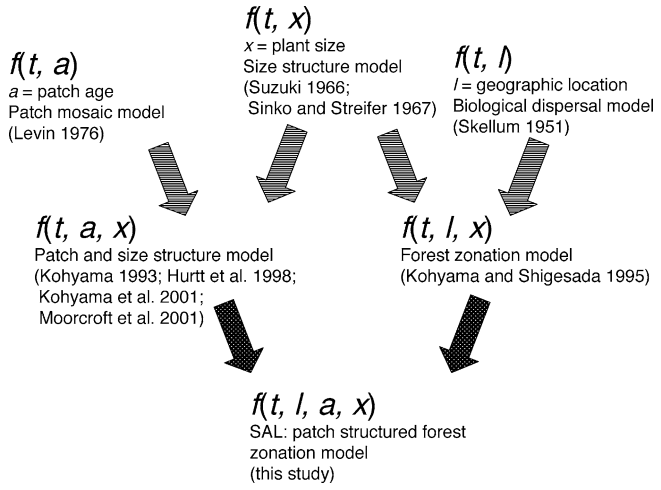

Fig. 1 Outline of preceding models of structured biological populations and the present model, which combines all of them

will be reasonable because patch mosaic represents approximately a 10-m-radius resolution (at the scale of forest-gap models), and the resolution of geographic locality employed here is 100 km (usual grid size for dynamic global vegetation models). The boundary condition of Eq. 1 with respect to size x at $x=0$, or seed production, is

$$G_i(t,l,a,0)f_i(t,l,a,0) = \varepsilon_i(t,l,a)S(t,l,a) \times \left[R_i(t,l) + m_i\frac{\partial R_i(t,l)}{\partial l} + p_i\frac{\partial R_i(t,l)}{\partial l^2}\right], \quad (2)$$

where

$$R_i(t,l) = \int_0^\infty \int_0^\infty \phi_i(t,l,x)f_i(t,l,a,x)\,\mathrm{d}x\mathrm{d}a. \quad (3)$$

Kohyama and Shigesada (1995) give a full explanation of the right side of Eq. 2, defining the movement through seed dispersal along location. They present the relationship between the diffusion-like expression of Eq. 2 and the explicit distribution function of seed dispersal for finer resolution of geographic location. Equation 2 introduces two parameters to describe seed dispersal: m_i (km) is the average spatial drift of seed rain from seed source, and p_i (km^2) is half of the spatial variance of seed dispersal of species i, both defined for a unit seed-production event. The parameter ϵ_i (t, l, a) of Eq. 2 defines the capacity for establishment success of species i, which can be a function of patch-scale crowding. Equation 3 formulates the forest-level seed production over tree size and patch mosaic of species i in a forest. The parameter ϕ_i (t, l, x) expresses the per-capita fecundity, the instantaneous rate of seed production for a tree of size x at location l at time t. In this paper, temporal fluctuation of seed production is taken into account in ϕ_i (t, l, x), as demonstrated later.

Another boundary condition of Eq. 1 with respect to patch age a, at $a=0$, which defines the advance regeneration at gap patch, is formulated as in Kohyama (1993)

$$f_i(t,l,0,x) = n_i(x)\int_0^\infty \gamma(l,a)f_i(t,l,a,x)\,\mathrm{d}a. \quad (4)$$

The function n_i (x) defines the species-specific probability of survival of populations beyond the gap-formation event, or advance regeneration, and $\gamma(l, a)$ expresses the gap-formation rate. Tree mortality at patch age a was therefore the summation of mortality related to and not related to gap formation: $[1- n_i(x)]\gamma(l, a)+\mu_i(t, l, a, x)$.

The landscape-level patch-age dynamics are expressed by the usual differential equation for age-structured populations (Kohyama 1993)

$$\frac{\partial S(t,l,a)}{\partial t} = -\frac{\partial S(t,l,a)}{\partial a} - \gamma(l,a)S(t,l,a), \quad (5)$$

where $S(t, l, a)$ is the distribution density function of a patch at age a at location l at time t; therefore the primitive of $S(t, l, a)$ is unity, conserving forest-land area. Patch birth rate, or the rate of gap formation, corresponds to the summation of patch death as

$$S(t,l,0) = \int_0^\infty \gamma(l,a)S(t,l,a)\,\mathrm{d}a. \quad (6)$$

The gap formation rate $\gamma(l, a)$ is common to Eqs. 1 and 4 in the submodel describing size-structure dynamics, and Eqs. 5 and 6 in the submodel describing patch-age dynamics.

Simulation

The same assumption as in Kohyama and Shigesada (1995) for the simulation was used here, in addition to the inclusion of gap-mosaic landscape of forests and temporal fluctuation in reproduction.

The environmental gradient along geographic location was set to demonstrate thermal gradient along a latitudinal transect. A parabolic response of relative vigor of species i, $v_i(l)$, along one-dimensional geographic location l was set as

$$v_i(l) = v_i^* - 4\times10^{-7}(l - l_i^*)^2, \quad (7)$$

for a non-negative range of $v_i(l)$, otherwise $v_i(l)=0$. The parameter l_i^* (km) denotes the optimal location of species i, where the species exhibits its maximum vigor at v_i^*. Three representative dominant species of forest zones were simulated, representing tropical rain forest species ($i=1$), warm-temperate rain forest species ($i=2$) and cool-temperate deciduous forest species ($i=3$). The sets of optimal location and maximum vigor, (l_i^* v_i^*), were set at (4,000; 1), (3,000; 0.75), and (2,000; 0.5) for $i=1,2$, and 3, respectively, at the initial stable thermal environmental condition (from $t=0$ to $t=10{,}000$ simulation years).

Table 1 Symbols used in the model and simulation

Symbol	Definition	Units
Parameters		
t	Time	year
x	Tree size in trunk basal diameter	cm
a	Patch age	year
l	Geographic location	km
i	Species identifier	Dimensionless
Tree-size structure and demography		
$f_i(t, l, a, x)$	Tree-size structure at patch age a	$cm^{-1}\ m^{-2}\ year^{-1}$
$G_i(t, l, a, x)$	Growth rate of tree at size x at patch age a	$cm\ year^{-1}$
$\mu_i(t, l, a, x)$	Tree mortality not related to gap formation	$year^{-1}$
$B(t, l, a, x)$	Upper basal area above x of all species at patch age a	$cm^2\ m^{-2}$
$B_i(t, l)$	Total basal area density of species I at forest scale	$cm^2\ m^{-2}$
$R_i(t, l)$	Recruitment rate at $x=0$	$m^{-2}\ year^{-1}$
$\phi_i(t, l, x)$	Fecundity of tree at size x at location l	$year^{-1}$
$\epsilon_i(t, l, a)$	Index of recruitment success at patch age a	Dimensionless
$n_i(x)$	Fraction of trees surviving through gap formation	Dimensionless
$\sigma_i(t)$	Multiplier defining mast and inter-mast years	Dimensionless
Patch-age structure and dynamics		
$S(t, l, a)$	Frequency of patch at age a of the forest at location l	$year^{-1}$
$\gamma(l, a)$	Gap formation rate	$year^{-1}$
Geographic-scale performance		
$v_i(l)$	Relative vigor of species i at location l	Dimensionless
v_i^*	Maximum relative vigor of species i	Dimensionless
l_i^*	Location with maximum vigor for species i	km
m_i	Average drift of seed dispersal	km
p_i	Half of variance of seed dispersal	km^2

Relative vigor was multiplied by growth and reproductive rates to characterize location-specific species traits; otherwise, species parameters were set as described below.

The range of potential geographic niches can be described as the range along l with positive $v_i(l)$. [Actually $v_i(l)$ should be above the minimum positive value to compensate for tree mortality, so that population can be sustained.] At the boundary of identical relative vigor between two adjacent species $v_i(l) = v_{i+1}(l)$; the identical demographic functions in growth, recruitment and mortality were realized on the present assumption. At any location apart from this boundary, one species is superior to the other in terms of larger $v_i(l)$, where the superior species excludes inferior species through interspecific competition in the present model (Kohyama 1993). Therefore, the realized niche is defined by the range of geographic location l where $v_i(l)$ of the target species is larger than that of the other species. Actually, tails of distribution beyond this competitive boundary, caused by regular seed rain from the edge of distribution, slightly widen the realized distribution range (Kohyama and Shigesada 1995).

Global warming causes a latitudinal shift in the thermal environment of a geographic location. The century-long warming experiment was set between $t = 10{,}000$ and $t = 10{,}100$ simulation years, during which the optimal location of each species l_i^* was decreased 7 km every year, resulting in a 700-km shift over 100 years of warming. The maximum vigor v_i^* was kept unchanged. After $t = 10{,}100$ year, the thermal condition was set as stable at a new "warm-earth" scenario until $t = 30{,}000$. Figure 2 shows the calculated potential and realized niches from Eq. 7 for species 2, representing the warm-temperate rain forest during the simulation period.

The upper basal area of all species above tree size x ($cm^2\ m^{-2}$) for patch-scale tree-size structure,

$$B(t, l, a, x) = \frac{\pi}{4} \frac{1}{S(t, l, a)} \int_x^\infty y^2 \sum_i f_i(t, l, a, y)\, \mathrm{d}y, \qquad (8)$$

was employed to describe the degree of patch-scale crowding on the tree growth rate at size x. Growth-rate function $G_i(t, l, a, x)$ was

$$G_i(t,l,a,x) = v_i(l)0.08x[1 - 0.2\ln x - 0.005B(t,l,a,x)], \quad (9)$$

where parameters were based on field observations for tropical rain forests (Kohyama 1991).

The per-capita seed production, ϕ_i (t, l, x), was assumed to be proportional to tree basal area. Therefore, the basal area density of target species across a patch-mosaic landscape,

$$B_i(t,l) = \frac{\pi}{4}\int_0^\infty \int_0^\infty x^2 f_i(t,l,a,x)\,\mathrm{d}x\,\mathrm{d}a, \quad (10)$$

characterizes the forest-scale annual seed production of species i (cf. Eq. 3), thus

$$R_i(t,l) = \sigma_i(t)v_i(l)0.003B_i(t,l), \quad (11)$$

where the parameter 0.003 (cm^{-2} year^{-1}) was estimated by Kohyama (1991). To examine the effect of mast-year phenomena on species distribution shift, the mast-seeding multiplier σ_i (t) was introduced here, with the difference approximation of t by $\Delta t = 1$ (year) in the overall simulation. For the no-mast-seeding case, $\sigma_i(t) = 1$ every year. In the mast-seeding case, seed year was synchronized across geographic location within species at an average return interval of 4 years, and asynchronously among species. Randomly visiting seed year yields [(interseed-year interval + 1) × annual average seed production.

Dispersal parameters in Eq. 2 were set common among species in the simulation where $m_i = 0$ km, assuming no directional drift component brought about by prevailing wind, gravity (along altitudinal gradient) etc., and $p_i = 100$ km^2 caused by two-directional seed dispersal, for every species. The parameter p_i corresponds to one half of the variance of the seed-dispersal function around the seed-source location as stated above. A variance of 200 km^2 in seed dispersal represents an extreme performance of long-distance seed dispersal.

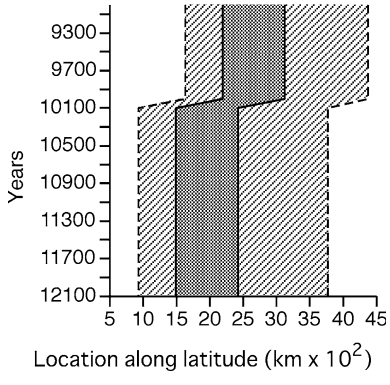

Fig. 2 Potential niche, defined for the range with positive $v_2(l)$ of Eq. 7, and realized niche, where $v_2(l)$ is larger than that of other species, for the species representing warm-temperate rain forest $i = 2$ (where $v_2^* = 0.75$ and $l_2^* = 3{,}000$ km and 2,300 km before and after warming, respectively) under the present global-warming scenario. The potential niche is the *striped zone within broken lines*; the realized niche is the *shaded zone within solid lines*. These niches are defined to be steady-state ones, and they can be different from the simulated temporary pattern in Fig. 3 due to a time-delay effect

The patch-specific establishment success was suppressed by patch-scale basal area density of all species as

$$\varepsilon_i(t,l,a) = \exp[-0.06B(t,l,a,0)], \quad (12)$$

where the parameter value 0.06, set common across species, was estimated by Kohyama (1991).

Gap-formation rate, $\gamma(l, a)$, was set constant at 0.01 year^{-1}, independent of either a or l. Tree mortality was also set constant at 0.01 year^{-1} across geographic location for every species, independent of either crowding or size. Therefore, μ_i $(t, l, a, x) = 0$ (year^{-1}) and $n_i(x) = 0$ in the gap-dynamic case so that all tree mortality was linked with gap formation, whereas μ_i $(t, l, a, x) = 0.01$ year^{-1} and $n_i(x) = 1$ in gap-averaged case (the same as in Kohyama and Shigesada 1995), so that all mortality was independent of gap formation, and tree-size structure at any patch became identical irrespective of patch age as a dummy variable (Kohyama et al. 2001).

Regulation of demographic processes according to tree-size structure at patch scale made it impossible to solve the present model analytically. Simulation with difference approximation of the SAL model was employed to predict geographic-scale forest dynamics as follows. Backward difference approximation was employed for the differential with respect to x and a in Eqs. 1 and 5, and bilateral difference approximation was used for second-order differential with respect to l in Eq. 2. One-year time interval was used for t, 4-cm interval for tree size x, 20 years for patch age a, and 100-km interval for location l. Initial condition at $t = 0$ was that all patch conditions were gap or in the youngest patch-age class, and each species was represented by 0.0001 m^{-2} trees of the smallest tree size in every geographic location. The steady-state condition across geographic scales was independent of initial condition; a small initial cohort at any location within the potential distribution niche, defined by Eq. 7, resulted in the identical steady-state distribution, or realized geographic niche, of each species. Each simulation (with and without gap mosaic, with and without mast seeding) was run over 30,000 years, for pre-warming (0–10,000 years), warming (10,000–10,100), and post-warming (10,100–30,000) periods. Source code of simulation in C++ is available at http://hosho.ees.hokudai.ac.jp/~kohyama/SAL/.

Results and discussion

The main question of the present simulation is whether or not the shifting-gap mosaic of landscape (by provid-

ing vacant sites for regeneration) or mast seeding (by providing temporarily available regeneration sites) facilitates the speed of the forest boundary movement in response to a global-warming treatment. To test this particular question, results with gap dynamics where no trees survive over gap formation, $n_i(x) = 0$ irrespective of x, were compared with those without patch dynamics, where $n_i(x) = 1$ irrespective of x. For gap-dynamic forests, both constant annual seed production and mast seeding with 4-year average return interval were simulated. Here only the results of the intermediate species representing warm-temperate rain forest ($i = 2$), surrounded by tropical rain forest species ($i = 1$) and cool-temperate deciduous species ($i = 3$) are shown because the results apply to any forest zone surrounded by neighbor zones.

Figure 3 illustrates the response in distribution range to warming treatment in each simulation. Geographic distribution was shown in terms of species-specific basal area density at forest scale, $B_i(t, l)$, for the warm-temperate rain forest species, $i = 2$. In every simulation, the resident forest responded immediately in basal area density (and therefore biomass) to warming, with a delay of only another century, irrespective of whether or not neighboring forest zone species existed.

Compared to the biomass change in resident forests, the edge shift of forest zones exhibited a longer response to warming treatment. In neighbor-free situations, it took another century or so for the warmer edge of the target species to shift by the failure of reproduction and vegetative growth. The cooler-edge expansion took more time due to the limitation of seed-dispersal capacity. The new cooler edge, however, is exploited within one-half millennium. There was no visible difference in the distribution range shift among gap-averaged, gap-mosaic, and gap-mosaic plus mast-seeding situations (Fig. 3, upper panels).

When the target species distribution was restricted by the competitive situation with neighboring species (or forest zones), the simulation results were different from those without neighbor species. The distribution edge movement was retarded along both warmer and cooler edges. As the resident part responded somewhat immediately to warming, a relatively gentle increase in abundance along the warmer side (due to the decline in relative vigor there) and a sharp decline in the abundance along the cooler side (due to improved relative vigor and failure of migration) characterized the distribution for a long while. Even two millennia after warming, the target species could not achieve the steady-state distribution. The difference between gap-averaged simulation, gap-dynamic one, and gap-dynamic plus mast-seeding one was not obvious (Fig. 3, lower panels).

To quantify the time delay of the distribution-range movement, Fig. 4 illustrates the time course of the relative difference in temporary geographic distribution from the final state geographic distribution. The relative difference was defined by

$$\frac{1}{2}\frac{\int_{500}^{4500} |B_i(t, l) - B_i(t_{\max}, l)| \mathrm{d}l}{\int_{500}^{4500} B_i(t_{\max}, l)\ \mathrm{d}l}$$

where $t_{\max}$ was set at year 30,000, for the geographic range of $l = 500$–$4{,}500$ km, which was wide enough to cover the entirety of the target-species distribution (cf. Fig. 2). This index is 1 for perfect separation, and 0 for perfect coincidence.

Three simulations without neighbor species showed almost the same time course in Fig. 4, where a 10% difference from the final-state distribution was achieved

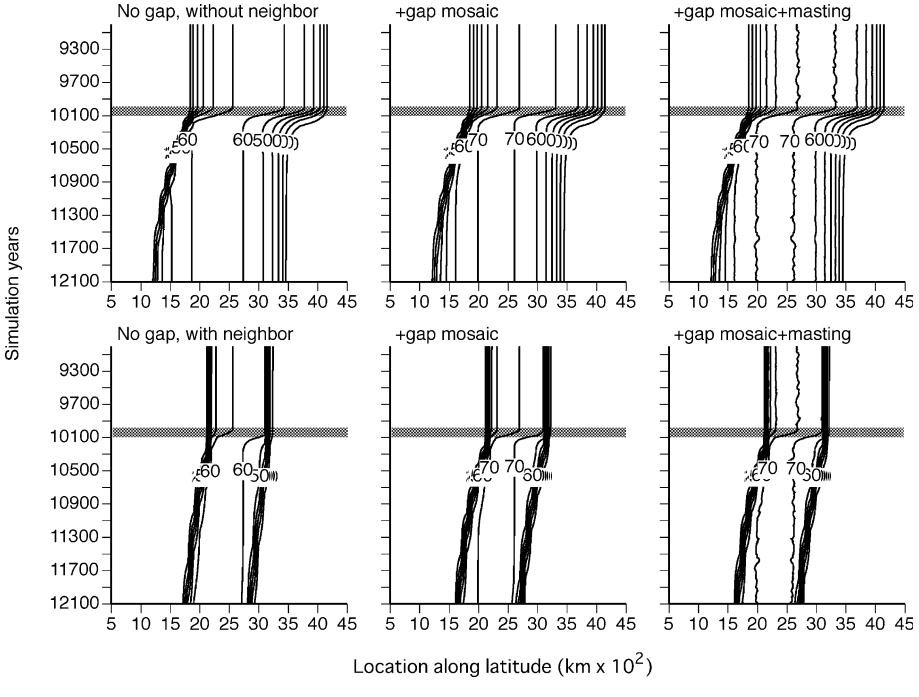

Fig. 3 Time course of the simulated distribution range of warm-temperate rain forest species. *Upper panels* no neighbor zones; *lower panels* with right-side neighboring tropical rain forest zone and left-side cool-temperate deciduous forest zone (their distributions not shown). From *left* to *right*, in *upper and lower panels*, no gap-mosaic model, gap-mosaic model, and gap-mosaic model with temporal fluctuation in seed production. Warming treatment during year 10,000–10,100 (*shaded belts*) resulting in a 700-km leftward shift. The distribution is presented in forest-scale basal area density, with a contour interval of 10 cm m^{-2}

300 years after warming ended, in year 10,100 and a 5% difference after 700 years. With neighboring species, the gap-averaged forest simulation (as in Kohyama and Shigesada 1995) took 5,900 years for the difference to be decreased to 10% and 8,900 years to 5%. The gap-dynamic forest with and without mast seeding showed almost the same trajectory. The case representing gap-dynamic and annual seeding took 3,600 years for a 10% difference and 6,900 years for a 5% difference. The gap-dynamic, mast-seeding situation required a slightly longer period toward convergence, 3,700 years for 10% difference and 7,200 years for 5% difference. Therefore, forest gap dynamics moderately facilitated migration, and mast-seeding showed no effect, or slightly retarded the speed of migration when a neighboring forest zone species was present.

Takenaka (2005) simulated vegetation change with a warming scenario similar to this study, applying a lattice model of multi-species forest dynamics. The model assumed that a single cell corresponded to the space for a single tree, and that regeneration occurred only on vacant cells created by the death of trees. Therefore, the shifting-gap mosaic feature of forest dynamics was introduced in a simplified form (either vacant or occupied). In his model, only seed production was the function of thermal conditions unlike the present model where rates of seed production and tree growth were functions of thermal conditions. Takenaka (2005) showed the millennia-scale delay in the distribution boundary shift with neighbor species, in response to a century-long warming, which agrees with the present results. He also reported, however, that mast-seeding phenomena with asynchrony among species remarkably facilitated the migration speed of invasive species into the zone occupied by resident species. The latter result is completely contrary to that of this study. This disagreement is caused by the fact that successful establishment of seedlings in the present model did not guarantee regeneration and growth to adult tree size because the patch-scale crowding effect, even at gap patch, prevented seedling upgrowth. In Takenaka's model, on the other hand, random occupancy of vacant cells resulted in regeneration success into mother trees. Such simplification of the regeneration process in the Takenaka lattice model enabled the lottery mechanism of migration to work. It is doubtful if this mechanism allows for forest tree species to adapt to rapid environmental change, because a tree must succeed across stages within a heavily structured forest landscape, as is modeled in this study. To predict the response of forest zones to environmental change, further examination is needed through comparison among models of different types. For instance, the present simulation results, carried out along a one-dimensional geographic gradient, may be modified when two-dimensional geographic space is introduced.

The present model has a wide applicability for a variety of ecological-scaling questions. At a finer scale than the present latitudinal zonation aspect, the model can describe the relationship among species differing in their geographic optima and distribution ranges. The gap-dynamic model at the forest scale has successfully reproduced the dynamics of a warm-temperate rain forest (Kohyama 1993), a cool-temperate mixed forest (Hurtt et al. 1998), and tropical rain forests (Kohyama et al. 2001; Moorcroft 2001). An accumulated database of permanent plots across geographic gradients will enable us to parameterize the demographic performance of species along gradients. Through the present model describes demographic processes according to physiological parameters as in Moorcroft et al. (2001), it provides a basis for global-scale functional modeling of vegetation dynamics.

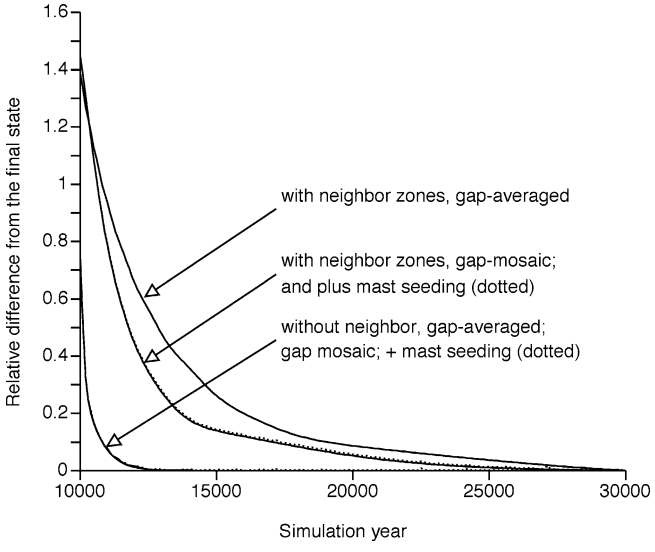

Fig. 4 Time course of the temporary geographic distribution of warm-temperate rain forest species toward final-state distribution (at year 30,000). The change in relative difference between temporary distribution and final distribution (≥1 for perfect separation, 0 for perfect overlap) is plotted against time with the period of warming (year 10,000–10,100) and that of post-warming (year 10,100–30,000)

Acknowledgements I thank George Hurtt, Takuya Kubo, Matthew Potts, Hisashi Sato, and Akio Takenaka for providing valuable comments and suggestions on this study. I particularly appreciate that Akio inspired the examination of mast-seeding phenomenon through his on-going study (Takenaka 2005).

References

Bugmann H (2001) A review of forest gap models. Clim Change 51:259–305

Chesson PL, Warner RR (1981) Environmental variability promotes coexistence in lottery competitive systems. Am Nat 117:923–943

Friend AD, Stevens AK, Knox RG, Cannell MGR (1997) A process-based, terrestrial biosphere model of ecosystem dynamics (Hybrid v3.0). Ecol Model 95:249–287

Hurtt GC, Moorcroft PR, Pacala SW, Levin SA (1998) Terrestrial models and global change; challenges for the future. Global Change Biol 4:581–590

Kohyama T (1991) Simulating stationary size distribution of trees in rain forests. Ann Bot 68:173–180
Kohyama T (1993) Size-structured tree populations in gap-dynamic forest: the forest architecture hypothesis for the stable coexistence of species. J Ecol 81:131–143
Kohyama T, Shigesada N (1995) A size-distribution-based model of forest dynamics along a latitudinal environmental gradient. Vegetatio 121:117–126
Kohyama T, Suzuki E, Partomihardjo T, Yamada T (2001) Dynamic steady state of patch-mosaic tree-size strucuture of a mixed dipterocarp forest regulated by local crowding. Ecol Res 16:85–98
Levin SA (1976) Population dynamic models in heterogeneous environments. Annu Rev Ecol Syst 7:287–311
Liu J, Ashton PS (1998) FORMOSAIC: an individual-based spatially explicit model for simulating forest dynamics in landscape mosaics. Ecol Model 106:177–200
Moorcroft PR, Hurtt GC, Pacala SW (2001) A method for scaling vegetation dynamics: the ecosystem demography model (ED). Ecol Monogr 71:557–586
Pacala SW, Canham CD, Saponara J, Silander JA, Kobe RK, Ribbens E (1996) Forest models defined by field measurements: estimation, error analysis and dynamics. Ecol Monogr 66:1–43
Sinko JW, Streifer W (1967) A new model for age-size structure of a population. Ecology 48:910–918
Skellam JG (1951) Random dispersal in theoretical populations. Biometrika 38:196–218
Suzuki T (1966) Forest transition as stochastic process I. J Jpn Forest Soc 48:436–439
Takenaka A (2005) Local coexistence of tree species and global distribution pattern along environmental gradient: a simulation study. Ecol Res 20, present issue

Section 3
Monitoring and modeling atmosphere–forest–soil processes

Ecol Res (2005) 20: 313–324
DOI 10.1007/s11284-005-0047-8

ORIGINAL ARTICLE

**Satoru Takanashi · Yoshiko Kosugi · Yumiko Tanaka
Masato Yano · Tatsuya Katayama · Hiroki Tanaka
Makoto Tani**

CO_2 exchange in a temperate Japanese cypress forest compared with that in a cool-temperate deciduous broad-leaved forest

Received: 15 September 2004 / Accepted: 14 December 2004 / Published online: 9 March 2005

Abstract To examine the characteristics of carbon exchange in coniferous forests, we analysed the seasonal and diurnal patterns of CO_2 exchange, as measured using the eddy covariance method, in a Japanese cypress forest in the Kiryu Experimental Watershed (KEW) in central Japan. The net CO_2 exchange data during periods of low-friction velocity conditions and during periods of missing data were interpolated. The daily CO_2 uptake was observed throughout the year, with maximum values occurring in early summer. Periods of low carbon uptake were seen in late summer owing to high respiratory CO_2 efflux. The diurnal and seasonal patterns of daytime CO_2 exchange at KEW were compared with those in a cool-temperate deciduous forest of the Tomakomai Experimental Forest (TOEF) in Japan. The environmental differences between evergreen and deciduous forests affected the seasonal patterns of carbon uptake. Although there were great differences in the mean monthly air temperatures between the sites, the mean monthly daytime carbon uptake was almost equal at both sites during the peak growing period. The carbon-uptake values at the same PAR level were greater before noon than after noon, especially at TOEF, suggesting the stomatal regulation of carbon uptake.

Keywords CO_2 exchange · Eddy covariance · Photosynthesis · Respiration · Temperate conifer forest

S. Takanashi (✉) · Y. Kosugi · M. Yano · T. Katayama
H. Tanaka · M. Tani
Laboratory of Forest Hydrology,
Division of Environmental Science and Technology,
Graduate School of Agriculture, Kyoto University,
Kyoto 606-8502, Japan
E-mail: takanash@kais.kyoto-u.ac.jp
Tel.: +81-75-7536089
Fax: +81-75-7536088

Y. Tanaka
Tomakomai Experimental Forest Research Station,
Field Science Center for Northern Biosphere,
Hokkaido University, Tomakomai,
Hokkaido 053-0035, Japan

Present address: M. Yano
Climate Change Mitigation Policy Group,
Environmental Policy Consulting Department,
UFJ Institute Ltd., 1-11-7 Shimbashi,
Minato-ku, Tokyo 105-8631, Japan

Present address: T. Katayama
NTT Communications Co., Tokyo, Japan

Present address: H. Tanaka
Hydrospheric Atmospheric Research Center,
Nagoya University, Furo-cho,
Chikusa-ku, Nagoya 464-8601, Japan

Introduction

Understanding the characteristics of diurnal and seasonal phasing and the amplitudes of ecosystem flux is very important for evaluating the roles of forests in the sequestration of CO_2 and related environmental changes, including global warming. Carbon dioxide exchange between the atmosphere and an ecosystem is described by net ecosystem exchange (NEE), which represents the difference between the uptake of CO_2 during photosynthesis and the emission of CO_2 during ecosystem respiration. These two components of NEE are large and are important for understanding the global carbon budget (Law et al. 1999; Buchmann 2002). Carbon dioxide fluxes from a forest to the atmosphere, which are measured by the eddy covariance approach, can provide direct estimates of the phasing and amplitude of ecosystem processes. The values of NEE have been estimated by the eddy covariance method for various vegetation types of different ages, including evergreen, deciduous, broad-leaved, and coniferous vegetation (e.g., Valentini et al. 2000; Baldocchi et al. 2001). In Japan, the CO_2 flux has also been reported for several sites (e.g., Yamamoto et al. 1999; Ohtani et al. 2001; Watanabe et al. 2001; Saigusa et al. 2002; Hirano et al. 2003; Kominami et al. 2003; Nakai et al. 2003).

However, the analyses and comparisons of diurnal and seasonal phasing and amplitudes of CO_2 fluxes among various forest types have not been sufficient. Recent reports have indicated that eddy covariance measurements made under stable nighttime conditions may not be reliable because of poor mixing (Goulden et al. 1996; Baldocchi et al. 1997; Law et al. 1999). However, during daytime under well-mixed conditions, the eddy covariance method is a good tool for analysing changes in NEE in response to changing environmental conditions at different time scales, including half-hourly, daily, monthly, and inter-annually, as well as for the comparison of CO_2 exchange characteristics of various forests.

Baldocchi and Vogel (1996) compared the CO_2 flux over a period of 2 days in relation to absorbed photosynthetically active radiation (PAR) and vapour-pressure deficit in a temperate broad-leaved forest and in a boreal pine forest. They pointed out the effects of temperature, vapour-pressure deficit, and surface wetness on the radiation-dependency of forest CO_2 exchange. Falge et al. (2002) analysed seasonal patterns of maximum daytime uptake and maximum nighttime release using eddy covariance data of FLUXNET forests and found remarkable parallels within and between the above functional vegetation types with regard to their seasonal patterns of maximum diurnal CO_2 uptake and release. To understand the characteristics of CO_2 exchange in different forests under various environmental conditions, long-term diurnal and seasonal patterns of eddy CO_2 flux at a variety of sites should be precisely analysed and compared, coupling physiological processes with major environmental factors.

In this study, we estimated the value of NEE, ecosystem respiration (F_{RE}), and gross primary production ($GPP = NEE + F_{RE}$), interpolating nighttime fluxes under low-friction velocity. We also showed the diurnal and seasonal phasing and amplitudes of daytime CO_2 fluxes in relation to responses to changing PAR. We compared the CO_2 exchange in a temperate coniferous forest with that in a cool-temperate broad-leaved deciduous forest in order to analyse the CO_2 exchange characteristics of these two forests in relation to the different environmental conditions.

Materials and methods

Site information

Kiryu Experimental Watershed

Observations were conducted at the Kiryu Experimental Watershed (KEW) in central Japan (34°58′N, 135°59′E; Fig. 1a). The entire experimental watershed covers 5.99 ha and ranges in elevation from 190–255 m. A meteorological observation tower is located in a small catchment (0.68 ha) within the experimental watershed. The vegetation consists mainly of the evergreen conifer *Chamaecyparis obtusa* Sieb. et Zucc. (Japanese cypress) planted in 1959 (13.9 m average height; 21.1 m maximum height; 43 m^2 ha^{-1} basal area; 1,853 stems ha^{-1}), which represents 92% of the total basal area.

Pinus densiflora Sieb. et Zucc., the natural regeneration of afforested trees, and several deciduous broad-leaved tree species are sparsely present. In recent years, *P. densiflora* stands have declined as a result of pine-wilt disease (Hobara et al. 2001). *Eurya japonica* Thunb. is dominant on the forest floor. The total leaf-area index (LAI), measured using an LAI-2000 (Licor, Lincoln, NE, USA), ranges between 4.5 and 5.5, with little seasonal fluctuation. The topographic map in Fig. 1b illustrates the mild inclination of approximately 9.2° to the north. The area surrounding the observation tower is national forest, and planted *C. obtusa* is currently the dominant species. The daytime wind direction is mainly

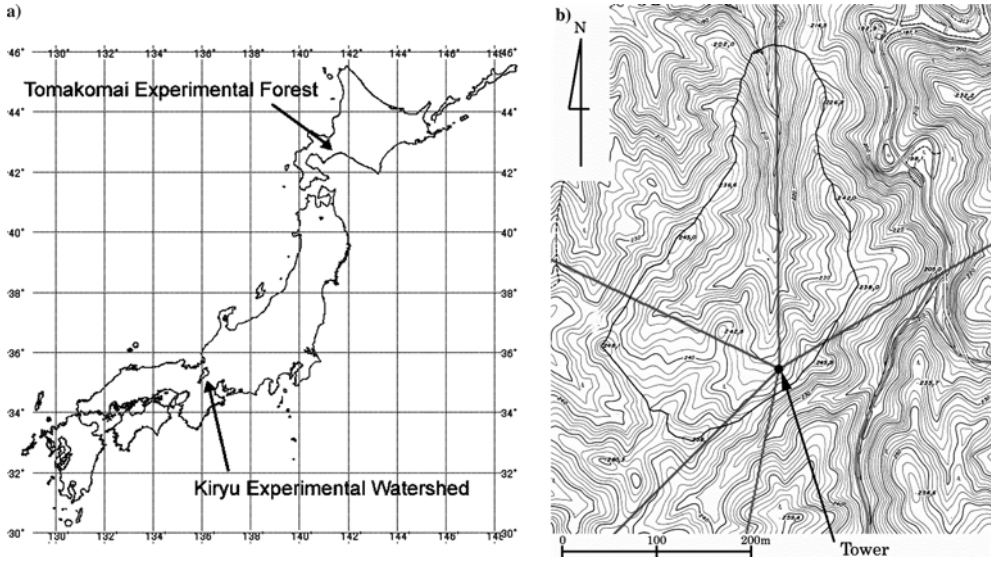

Fig. 1 Location of the study site (**a**) and topographic map of the area around the observation tower in the Kiryu Experimental Watershed (KEW) (**b**). The five *grey lines* represent the boundary of the five fans toward which the sonic wind vectors *u* and *w* were rotated

from the north, while the nighttime wind direction is from the south. The forest fetch in a northwest direction is approximately 750 m, and those in the other directions exceed 2,000 m. Based on the model by Schuepp (1990), the percentages of data for which >80% of the measured flux can be expected to come from within the actual forest are 92% during the daytime and 81% during the nighttime. The mean annual air temperature from 1997–2001 was 14.0°C, and the mean annual precipitation from 1972–2001 was 1,645 mm. The climate is warm temperate with rainfall distributed throughout the year, peaking in summer, and with little snowfall in winter.

Tomakomai Experimental Forest

We compared the flux data for the Japanese cypress forest at KEW with the flux data for a cool-temperate deciduous broad-leaved forest at Tomakomai Experimental Forest (TOEF) in southwestern Hokkaido, the northernmost island of the Japanese archipelago (42°41′N, 141°34′E). The dominant species around the observation tower include *Quercus crispula* Blume, *Phellodendron amurense* Rupr., *Acer mono* Maxim., *Cornus controversa* Hemsl., and *Ostrya japonica* Sarg. The average tree height is approximately 13 m. *Dryopteris crassirhizoma* Nakai is distributed throughout the forest floor. Fukushima et al. (1998) reported that total LAI of TOEF, calculated by multiplying the leaf number of each species by the average leaf area within a 15-m square plot in a mature forest, was 7.59. Takahashi et al. (1999) reported that total LAI, estimated by felling all trees within a 10-m square plot in a secondary forest in TOEF, was 5.1. LAI measured with a plant canopy analyser (LAI-2000, Licor) ranged from 5–6 in peak growing periods. The mean monthly temperatures range from −3.2 to 19.1°C, and the annual precipitation is 1,450 mm. Snow cover reaches a depth of 50 cm from December to March (Hiura 2001).

Measurements

Kiryu Experimental Watershed

The CO_2 flux above the temperate coniferous forest at KEW was measured at a height of 28.5 m on the observation tower. The measurements discussed here were made from 1 January 2001 to 31 December 2002. Wind speed and temperature were observed with a three-axis sonic anemometer (DAT-310 or DA-600T, Kaijo). The carbon dioxide concentration was monitored with a closed-path CO_2/H_2O analyser (LI-6262 or LI-7000, Licor) or with an open-path CO_2/H_2O analyser (LI-7500, Licor) after 30 April 2002. A closed-path infrared gas analyser (IRGA) was installed on the tower platform so as to minimise the tube length. Sampled air was drawn through a Bev-a-line plastic tube (3 m long, 3 mm i.d.) with a pump into the CO_2 analyser. The average time for calculating the CO_2 covariance and friction velocity was 30 min. Based on measurements of mean vertical wind speed over the long term, we assumed the practical surface to be a complex of five fans from the observation tower, and rotated the sonic wind vectors u and w toward the surface (see Fig. 1b). The time lag for CO_2 was determined after every instance of maintenance and data collection to maximise the covariance between the vertical wind velocities in the closed-path system. The median of the optimised time lag for each 30-min interval was used as a constant for each period. The linear trend of the CO_2 concentration was removed. Spike data values outside of the ± 3.5SD threshold were replaced with the interpolated values. When four or more consecutive points were detected, they were not considered spikes. Data beyond the range values (e.g., caused by an analogue communication error) were also replaced. If the number of spikes or data beyond the range exceeded 1% of the total number of data points for each element, then the 30-min flux data were considered unacceptable. The Webb, Pearman, and Leuning (WPL) correction for the effect of air-density fluctuation (Webb et al. 1980) was made for data with an open-path system but not for data with a closed-path system, as described by Leuning and Moncrieff (1990). We sampled the fluctuation of CO_2 in terms of mole fractions calculated by IRGA software with a closed-path system, which includes the dilution correction owing to water vapour (Aubinet et al. 2000). Based on cospectral analysis, the tube attenuation at high frequency in the case of the closed-path system was corrected.

The downward PAR above the canopy was measured with a quantum sensor (LI-190SA, Licor) installed at the observation tower. To interpolate the missing PAR data during the period from 1 January to 30 June 2001, we used a regression equation obtained from the relationship between solar radiation and PAR during the second half of 2001. The observation tower was equipped with instruments to measure air temperature and air humidity (HMP45C, VAISALA, Finland), and precipitation was measured with a tipping bucket rain gauge (RT-5, Ikeda Keiki) at the meteorological station near the tower. The periods during which micro-meteorological data were missing were 12 days in June and 5 days in September 2001. In this study, daytime is defined as having a PAR value of >5 μmol m^{-2} s^{-1}, and nighttime as PAR <5 μmol m^{-2} s^{-1}.

Tomakomai Experimental Forest

The meteorological observation tower (33 m tall) was equipped with instruments to measure the downward PAR above the canopy (ML-020P, Eko), the air temperature at a height of 19 m (TS-801, Ogasawara Keiki), the air humidity at 19 m (P-HMP-45D, Ogasawara Keiki), and precipitation (B-011, Yokogawa Dens-

hikiki). At the flux observation tower (21 m tall), located in the northwest part of TOEF, the wind speed and temperature were observed with a three-axis sonic anemometer (DAT-300, Kaijo), and the CO_2 concentration was monitored with a closed-path CO_2/H_2O analyser (LI-6262, Licor). Sample air was drawn through a 25-m tube with a 0.63-cm radius (SYNFLEX, Nitta Moore, Tokyo, Japan) at a rate of 17 l min^{-1} and sent through an external filter and an air dryer (DH-109, Komatsu Electronics, Tokyo, Japan) to a sample cell of the IRGA. Turbulence signals were low-pass filtered at a cut-off frequency of 4 Hz to avoid aliasing and were recorded at 10 Hz. The double rotation method was applied to the sonic anemometer velocities (McMillen 1988; Kaimal and Finnigan 1994). The average time for calculating the CO_2 covariance was 30 min. Noise and spikes in the raw data set were removed using the model from EUROFLUX (Højstrup 1993; Vickers and Mahrt 1997).

Analyses

Nighttime CO_2 fluxes ($F_{c,\ night}$), which directly reflect ecosystem respiration at night, depend on temperature; however, $F_{c,\ night}$ is probably underestimated during periods of poor mixing conditions, when the CO_2 concentration changes or CO_2 storage drains down the sloped terrain below the eddy-flux measurement level (Goulden et al. 1996; Greco and Baldocchi 1996; Lavigne et al. 1997; Law et al. 1999; Saigusa et al. 2002; Nakai et al. 2003). Therefore, we investigated the relationship between $F_{c,\ night}$ and air temperature at a height of 20 m for two friction velocity (u_*) classes at KEW. In this study, the low-friction velocity (poor mixing) condition is defined as $u_* < 0.3$ m s^{-1}, and the high-friction velocity condition is defined as $u_* \geq 0.3$ m s^{-1}. This threshold value was tentatively determined from the relationship between CO_2 flux and u_*, given the available data, and we analysed the sensitivity of the annual NEE to different threshold values (see Fig. 5). For these analyses, we used the nighttime CO_2 flux data from 1 May to 31 December 2002, which were measured with an open-path gas analyser. The percentages of data under low- and high-friction velocity conditions were 63 and 37%, respectively (Fig. 2).

The values of $F_{c,\ night}$ increased exponentially with air temperature, and the values of $F_{c,\ night}$ under low-friction velocity conditions were smaller than those under high-friction velocity conditions. The best-fitting lines are shown in Fig. 2 with the Arrhenius function, which expresses the temperature dependency of $F_{c,\ night}$ as follows:

$$F_{c,\ night} = f(T_{ref}) \exp\left(\frac{\Delta H_a (T_{air} - 298.15)}{298.15 R T_{air}}\right) \quad (1)$$

where $f(T_{ref})$ is the reference value of a given parameter at a temperature of 25°C (= 298.15 K), ΔH_a is the energy of activation, R is a gas constant, and T_{air} is the air temperature at a height of 20 m.

The typical seasonal behaviour of daytime CO_2 fluxes is reflected in the seasonal development of radiation and temperature for differing biomes (Falge et al. 2002). By analogy with the light-photosynthesis curve in the field of plant physiology, a nonrectangular hyperbola

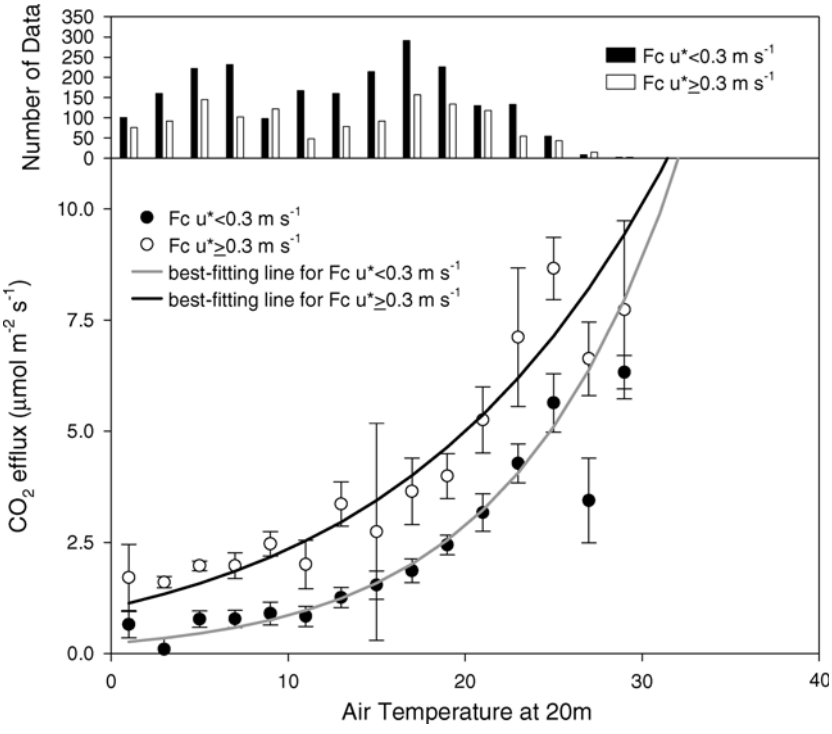

Fig. 2 Relationship between the air temperature at a height of 20 m and nighttime CO_2 fluxes for two friction velocity classes. Data were averaged in the range of 2°C. The number, averaged value, and standard error are shown. *Lines* denote best-fitting curves based on the Arrhenius function (Eq. 1)

(Eq. 2) was fitted to each month (e.g., Johonson and Thornley 1984; Cannell and Thornley 1998; Caton et al. 1999):

$$F_{\mathrm{c,\ day}} = \frac{\alpha I + F_{\mathrm{GPP,sat}} - \sqrt{(\alpha I + F_{\mathrm{GPP,sat}})^2 - 4\theta\alpha I F_{\mathrm{GPP,sat}}}}{2\theta} - F_{\mathrm{RE,\ day}} \quad (2)$$

where α is the photosynthetic efficiency, I is the incident PAR on the canopy, $F_{\mathrm{GPP,\ sat}}$ is the gross primary productivity at light saturation, θ is the convexity of the function, and $F_{\mathrm{RE,\ day}}$ is ecosystem respiration during the day. The three parameters for monthly daytime CO_2 flux data ($F_{\mathrm{GPP,\ sat}}$, $F_{\mathrm{RE,\ day}}$, α) were estimated by nonlinear regression. The value of θ was fixed to 0.9. Based on leaf-level knowledge, the value of θ (typically around 0.9 for many leaves, including Japanese cypress; unpublished data) is only affected by the gradient in light absorption and photosynthetic capacity within the leaf and the changes in the photosynthesis rate, which shifts from electron-transport-limited to Rubisco-limited at low irradiances (Cannell and Thornley 1998). We estimated $F_{\mathrm{RE,\ day}}$ with an optimisation procedure, rather than fixing it with average $F_{\mathrm{c,\ night}}$ for each month. One of the reasons for this was that some studies (Lloyd et al. 1995; Shapiro et al. 2004) have reported that leaf-level respiration in light conditions is significantly lower than in the dark. This equation, with parameters for each month, was used to fill gaps, and seasonal patterns were analysed.

To interpolate data during missing periods, as well as under low-friction velocity conditions at nighttime, we used the following three methods:

1. Gaps not filled: The data of missing daytime periods (daytime gaps) or missing nighttime periods were not filled. The raw data during periods of low-friction velocity conditions at nighttime were used for the annual CO_2 exchange estimation.
2. Nighttime gaps filled: Daytime gaps were not filled, whereas the data during missing nighttime periods and under low-friction velocity conditions (nighttime gaps) were filled by Eq. 1 using parameters for $F_{\mathrm{c,\ night}}$ under high-friction velocity.
3. Both daytime and nighttime gaps filled: Using the parameter sets for each month, daytime gaps were filled by Eq. 2, and nighttime gaps were filled as in (2) above.

To estimate the annual CO_2 exchange, the daily totals of CO_2 flux ($F_{\mathrm{c,\ daily}}$) data were calculated. If we could obtain data covering more than 80% of a day, we calculated $F_{\mathrm{c,\ daily}}$ by multiplying the mean 30-min CO_2 flux of that day by 48. The time periods for which we could not obtain data covering more than 80% of the day, including eddy flux, friction velocity, air temperature, and PAR, using each of the three methods because of missing data, were (1) 177, (2) 178, and (3) 15 days in 2001, and (1) 90, (2) 84, and (3) 0 days in 2002. These data were filled by the average $F_{\mathrm{c,\ daily}}$ of the year.

Results

Micro-meteorological environment in KEW

The seasonal changes in the micro-meteorological and hydrological environments at KEW in 2001 and 2002 are shown in Fig. 3 (black bars and lines indicate the data from KEW); the changes in CO_2 flux (F_c) are shown in Fig. 4. PAR for sunny days was recorded as approximately 2,000 μmol m^{-2} s^{-1} in summer and 1,000 μmol m^{-2} s^{-1} in winter. No clear differences were found in the seasonal changes in PAR between the two years, except in July 2001 when there were more clear days than in July 2002. The average air temperature at a height of 20 m was 13.7°C in 2001, with a minimum of −5.2°C in January and a maximum of 35.3°C in July. The average air temperature was 14.4°C in 2002, with a minimum of −3.6°C in January and a maximum of 34.4°C in July. The air temperature in summer was similar for both years. The differences in the average air temperatures were caused mainly by the higher temperatures in winter and early spring of 2002 (January, February, and March). Annual precipitation, which fell mostly in summer, was 1,438 mm in 2001 and 1,179 mm in 2002. In this watershed, the precipitation measured in 2002 was the lowest recorded in 31 years, except for 1,030 mm in 1994. Nevertheless, even in the driest years, a permanent groundwater supply maintains stream runoff from the experimental watershed (5.99 ha). During 2001, a rainy June was followed by a dry summer (July and August) and a rainy September, all of which represent typical seasonal changes in a normal year. In 2002, a dry June was followed by a rainy July and a dry August and September. The vapour-pressure deficit in June and September in 2002 was higher than that in 2001. Net CO_2 uptake (from the atmosphere to the ecosystem) was observed throughout the year at this forest, indicating CO_2 sequestration even in winter. In both years, the maximum values of F_c (approximately −40 μmol m^{-2} s^{-1}) were reached in early summer, similar to PAR; however, periods of low carbon uptake were observed in late summer because of high respiratory CO_2 efflux, the maximum values of which reached approximately 15 μmol m^{-2} s^{-1} in August. In summer 2002, the results showed lower soil moisture conditions than in 2001, but no significant effect on the CO_2 flux above the canopy was found.

The effect of friction velocity on the estimation of NEE

The annual NEE (for 2001 and 2002 respectively) estimated by each of the three methods described in the

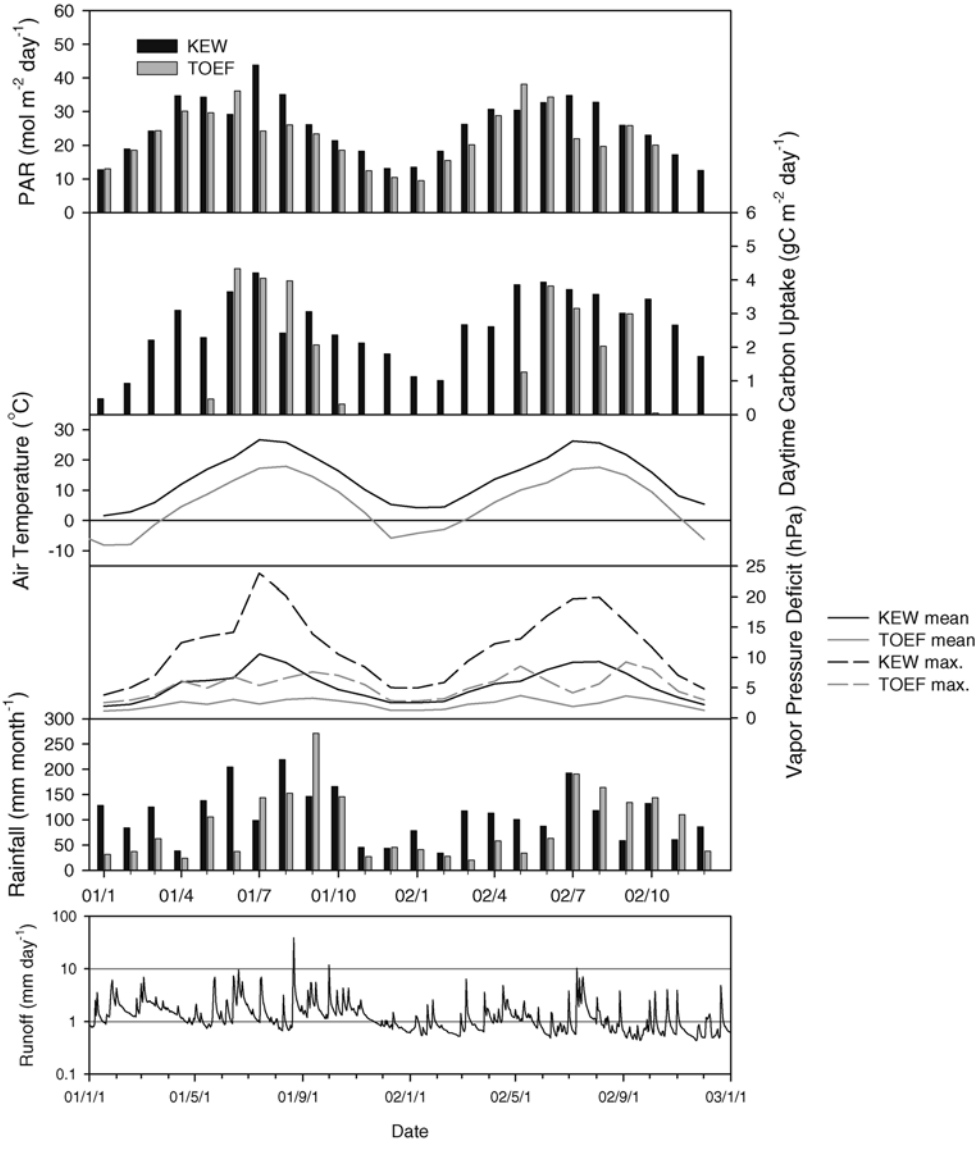

Fig. 3 Monthly seasonal changes in micro-meteorological and hydrological factors in both the temperate coniferous forest (KEW) and the cool-temperate deciduous broad-leaved forest (TOEF). Monthly means of the daily sum of PAR and daytime carbon uptake, daily mean air temperature, daily mean and maximum vapour-pressure deficit, and monthly totals of rainfall at both sites are shown. The daily total of runoff at KEW is also shown

analysis section was: (1) (gaps not filled), 700.9 and 746.3 g C m^{-2} $year^{-1}$; (2) (nighttime gaps filled), 412.2 and 502.3 g C m^{-2} $year^{-1}$; and (3) (both daytime and nighttime gaps filled), 477.1 and 480.3 g C m^{-2} $year^{-1}$. The friction velocity threshold values control the fraction of available nighttime data and influence the parameters in Eq. 1, thereby influencing the annual NEE estimation. Therefore, we tested the sensitivity of the annual NEE for different u_* thresholds (Fig. 5). With an increasing u_* threshold, the annual carbon uptake decreases, although at a large u_* threshold, the number of available data decreases. Figure 5 shows that within the range of the previously reported thresholds for a forest (0.15–0.45 m s^{-1}; e.g., Goulden et al. 1996; Lavigne et al. 1997; Falge et al. 2001; Griffis et al. 2003; Hirano et al. 2003; Knohl et al. 2003; Carrara et al. 2004; Chambers et al. 2004; Cook et al. 2004), the total annual NEE ranges between 435 and 592 g C m^{-2} $year^{-1}$, but no significant differences in the annual NEE were found between the two years, despite differences in precipitation. We also estimated the annual F_{RE} for the two study years as −990.9 g C m^{-2} $year^{-1}$ in 2001 and −1,129 g C m^{-2} $year^{-1}$ in 2002, using method 3 (respiration in the daytime was fixed to $F_{RE,\,day}$ of each month); the estimated GPP was 1,468 g C m^{-2} $year^{-1}$ in 2001 and 1,609 g C m^{-2} $year^{-1}$ in 2002.

Seasonal patterns of daytime CO_2 flux compared with that in a cool-temperate deciduous forest

To compare seasonal patterns and magnitudes of daytime CO_2 flux in a temperate coniferous forest to those in a cool-temperate deciduous broad-leaved forest in Japan, the monthly means of total daily

PAR, daytime carbon uptake, daily mean air temperature, daily mean and maximum vapour-pressure deficit, and monthly rainfall in KEW and TOEF were compared, as shown in Fig. 3. The daytime carbon uptake was calculated with the total daily CO_2 flux data (gaps not filled) during the daytime. The daily totals of PAR above both sites were similar, except for the low PAR period owing to fog at TOEF in July and August. The values of the mean monthly air temperature at TOEF were approximately 8°C lower than those at KEW. At KEW, daytime carbon uptake was observed throughout the year; the peaks were reached in June or July at approximately 3–4 g C m^{-2} $year^{-1}$. At TOEF, leaves flushed at the beginning of May and fell at the beginning of October, with little year-to-year fluctuation based on measurements of PAR transmittance from the top of the canopy to the forest floor (unpublished data, Tanaka). During peak growing periods, the daytime carbon uptake at TOEF was approximately 3–4 g C m^{-2} day^{-1}, and the values in the deciduous season were negative or close to zero. The differences between the evergreen conifer and deciduous broad-leaved forests influenced the seasonal patterns of daytime carbon uptake, although daytime carbon uptake was almost equal between the forests during the peak growing period despite large differences in mean monthly air temperature.

For a more precise comparison of CO_2 fluxes between the two sites, including diurnal and seasonal changes, the relationship between PAR and CO_2 flux was determined, as shown in Fig. 6. The seasonal changes in parameters for the nonrectangular hyperbola function (Eq. 2, fitted to all the daytime data) are shown in Fig. 7. The temperate evergreen coniferous forest absorbed CO_2 throughout the year, while the cool-temperate deciduous broad-leaved forest absorbed CO_2 only during the growing season (June–September). At TOEF, the scatter in the results for April, May, and October can be attributed to forest-floor vegetation (Fig. 6b). The values of $F_{GPP,\,sat}$ and $F_{RE,\,day}$ in the evergreen coniferous forest were slightly greater than those in the

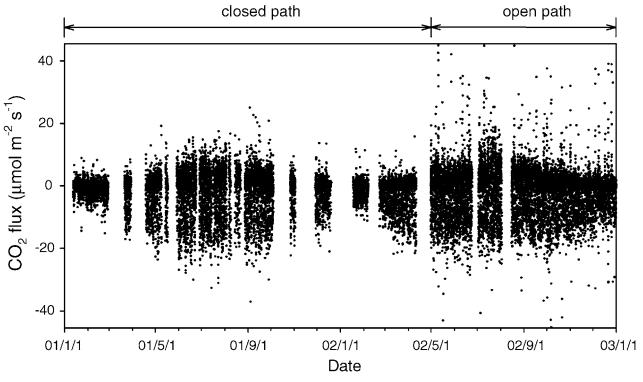

Fig. 4 Seasonal changes in 30-min CO_2 fluxes at KEW. Closed-path data from 1 January 2001 to 30 April 2002 and open-path data from 1 May to 31 December 2002 are shown. *Negative values* indicate CO_2 absorption from the atmosphere to the forest

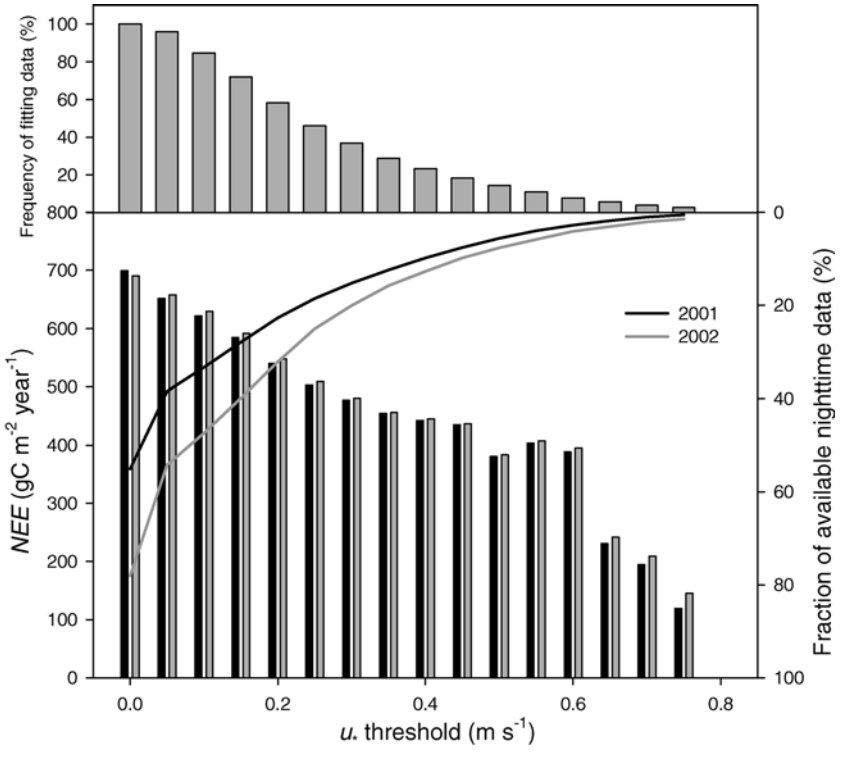

Fig. 5 Sensitivity of yearly NEE estimates to different u_* thresholds. The *bars* indicate the values of NEE, and the *lines* indicate the fraction of nighttime data under higher u_* than that of the threshold conditions for all nighttime data. Frequencies of fitting data to available nighttime data are shown at the top

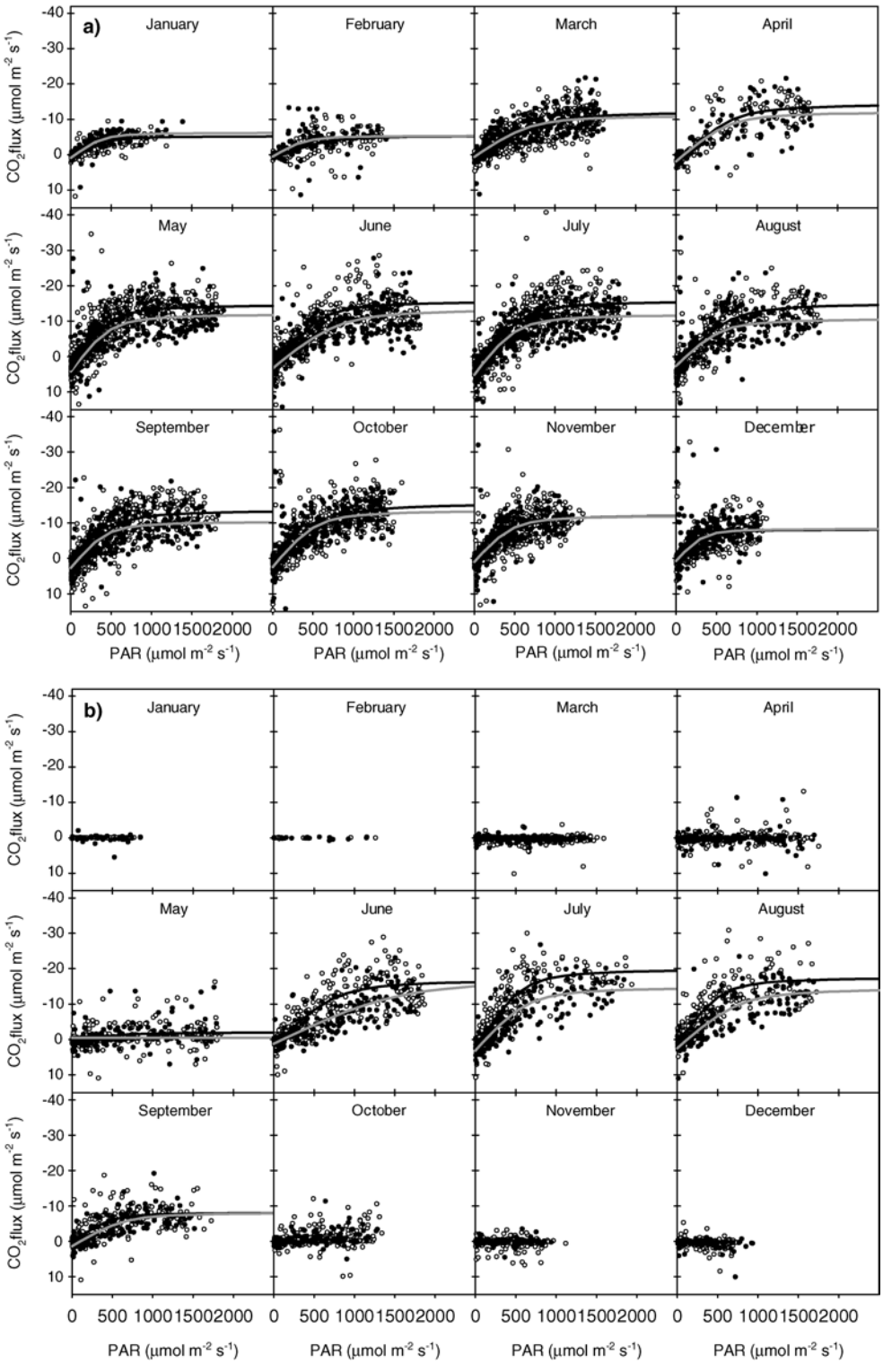

Fig. 6 Relationship between incident PAR and daytime CO_2 flux (*white circles* represent morning data; *black circles* represent afternoon data) in the temperate evergreen coniferous forest in 2002 (**a**) and in the cool-temperate deciduous broad-leaved forest in 2001 (**b**). Best-fitting lines (*black line* represents morning data; *grey line* represents afternoon data) of the nonrectangular hyperbola (Eq. 2) are also shown

deciduous broad-leaved forest. The daytime carbon uptake in the same light environment was greater in the morning than in the afternoon, especially at TOEF. This difference in uptake between morning and afternoon was greater in summer at both sites.

Discussion

The estimated annual NEE in KEW, which is afforested but unmanaged, indicates that this forest has

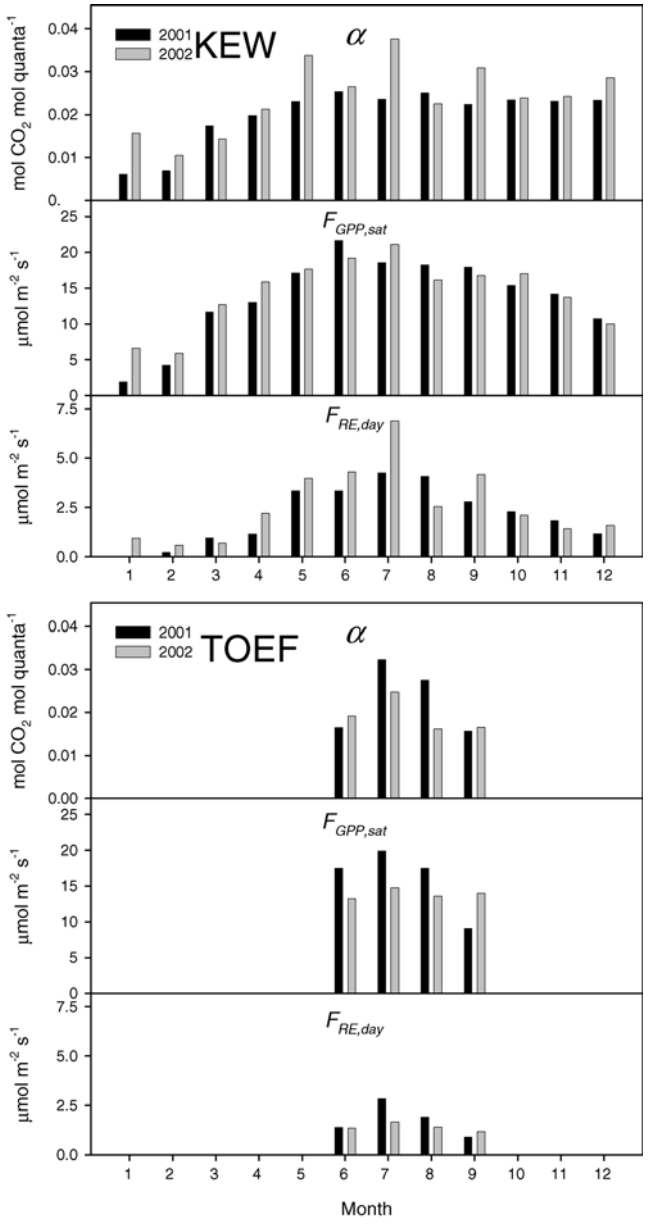

Fig. 7 Seasonal changes in the parameters of the nonrectangular hyperbola function (Eq. 2 fitted to all the daytime data). The parameters of photosynthetic efficiency (α), the gross primary productivity at light saturation ($F_{GPP,\ sat}$), and ecosystem respiration during the day ($F_{RE,\ day}$) are shown

acted as a significant carbon sink, even in a dry year such as 2002. These values of NEE, which are tentative because neither CO_2 storage nor an advection term were taken into account, are greater than those reported for other cool-temperate deciduous broad-leaved forests in Japan (Saigusa et al. 2002; Nakai et al. 2003) and are similar to values seen in European coniferous forests (Valentini et al. 2000). The sensitivity test of annual NEE for different u_* thresholds revealed that annual carbon uptake decreases with increasing u_* threshold. However, the uncertainty of the modelled efflux and the potential risk of 'double counting' increase if CO_2 is stored within the forest under low-friction velocity conditions and flushed under high-friction velocity conditions, which are sometimes observed in the morning (Aubinet et al. 2000; Knohl et al. 2003).

We estimated the monthly parameters of the non-rectangular hyperbola by analogy with the light-photosynthesis curve in the field of plant physiology. In the peak growing season, the values of both $F_{GPP,\ sat}$ and $F_{RE,\ day}$ in the coniferous forest were slightly greater than those in the broad-leaved forest. The absolute values of $F_{RE,\ day}$ remain questionable because we did not evaluate the storage term, which is very sensitive to CO_2 fluxes at low PAR; the storage term is a comparatively large part of CO_2 exchange at low PAR (Grace et al. 1996; Saigusa et al. 2002). Therefore, differences in $F_{RE,\ day}$ at the two sites may be explained by including both ecosystem respiration and the storage-capacity term, which reflects canopy structure, mixing strength, observation height, and other environmental factors.

The difference in the CO_2 flux between the morning and afternoon may reflect a difference in the vapour-pressure deficit between these times (Baldocchi and Vogel 1996); however, the data were classified by time rather than by vapour-pressure deficit under light-saturated conditions, especially at TOEF (Fig. 8). These results suggest that trees control the stomata to maintain their leaf water content, such that canopy-level CO_2 absorption is affected by water loss in the afternoon as opposed to instantly responding to a vapour-pressure deficit. In mature forest stands, limitations by leaf water content have been suggested. Komatsu (2003) showed that the surface conductance for closed coniferous stands decreased with increasing canopy height when no limitation of soil moisture and no significant relationship between the surface conductance and LAI were observed. Regarding the canopy maple trees growing at TOEF, Nabeshima and Hiura (2004) reported that the leaf-level maximum net assimilation rate per unit dry mass and the nitrogen use efficiency decreased and the water use efficiency increased with increasing tree size. Whether a vapour-pressure deficit or a lack of leaf water content is responsible for lower CO_2 absorption during the afternoon, this hysteresis in the light-response curve observed at both sites strongly suggests that daytime CO_2 absorption is affected by stomatal regulation. Therefore, understanding the relationship between water and stomatal responses is very important for the evaluation of carbon balance. For more precise estimates of net ecosystem CO_2 sequestration, we should analyse this hysteresis more precisely by investigating and integrating the CO_2 exchange characteristics of each component. These components should include leaf-level photosynthesis and transpiration; linkages between leaf, trunk, root, and microbial respiration; and environmental factors, including light, temperature and water.

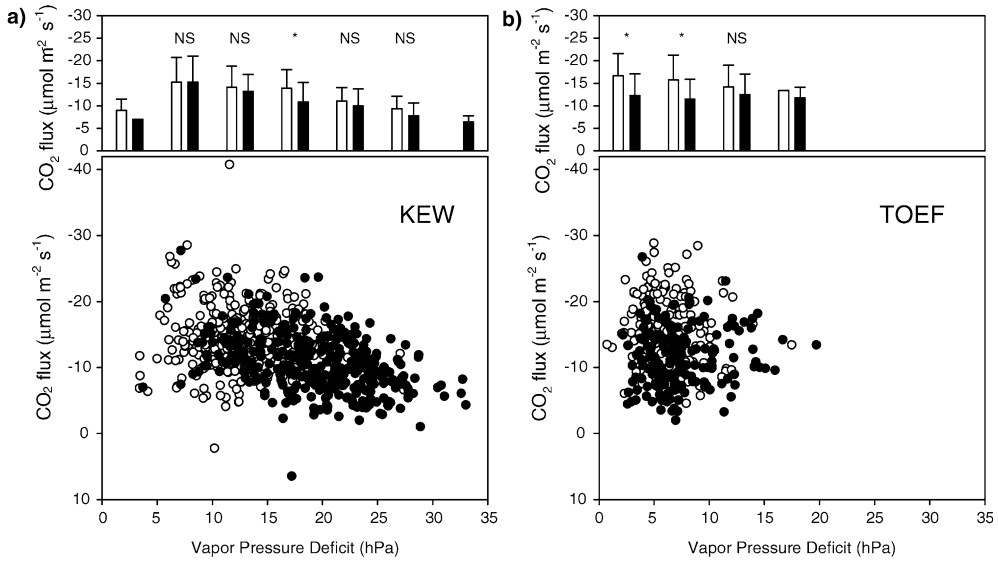

Fig. 8 Comparisons of daytime CO_2 flux between morning data (*white circles*) and afternoon data (*black circles*) at different vapour-pressure deficits under light-saturated conditions (PAR > 800 μmol m^{-2} s^{-1}). Data in June–August 2002 at KEW (**a**) and in June–August 2001 at TOEF (**b**) are shown in the *lower figures*. The *upper figures* illustrate daytime CO_2 flux (*white bars* represent morning data; *black bars* represent afternoon data; *error bars* represent standard deviation) divided into seven vapour-pressure deficit categories. An *asterisk* denotes a significant difference in CO_2 flux between morning data and afternoon at $P < 0.01$ by the *t*-test data. *NS* denotes no significant difference

Conclusions

We investigated the eddy CO_2 fluxes above an evergreen coniferous (Japanese cypress) forest and compared them with data taken above a cool-temperate deciduous broad-leaved forest in Japan. Net CO_2 uptake was observed throughout the year in the evergreen forest, indicating CO_2 sequestration even in winter. The total annual NEE values were 477 and 480 g C m^{-2} $year^{-1}$ in 2001 and 2002 respectively, but no significant differences in annual NEE were found between the years, despite differences in precipitation. However, the absolute values of NEE remain uncertain because of the uncertainty in the threshold values of u_* controlling the estimation of NEE.

The environmental differences between KEW and TOEF showed an effect on the seasonal patterns of carbon uptake. Nevertheless, despite great differences between the mean monthly air temperatures at the sites, the mean monthly daytime carbon uptake was almost equal for the two sites during the peak growing period. The carbon uptake values at the same PAR level were greater before noon than after noon, especially at TOEF, suggesting the stomatal regulation of carbon uptake.

Acknowledgements This work was supported by the Global Environmental Research Fund of the Japanese Environment Agency Grant (No. B-3) and by the IGBP-MESSC as part of the "Response of Terrestrial Watershed Ecosystems to Global Change" project, and contributes to TEMA (Terrestrial Ecosystem and Monsoon Asia) Second Term, a core research of GCTE (Global Change and Terrestrial Ecosystem). We especially thank Masanori Katsuyama for providing the rainfall and runoff data. Many thanks also to Takumi Wada, Tomonori Mitani, Shinjiro Okubo, Naoko Matsuo, Motoko Higuchi, Tomoko Obote, and Hiroyuki Ando for their support in the field observations and for valuable discussion.

References

Aubinet M, Grelle A, Ibrom A, Rannik Ü, Moncrieff J, Foken T, Kowalski AS, Martin P, Berbigier P, Bernhofer C, Clement R, Elbers J, Granier AGT, Morgenstern K, Pilegaard K, Rebmann C, Snijders W, Valentini R, Vesala T (2000) Estimates of the annual net carbon and water exchange of European forests: the EUROFLUX methodology. Adv Ecol Res 30:113–175

Baldocchi DD, Vogel CA (1996) Energy and CO_2 flux densities above and below a temperate broad-leaved forest and a boreal pine forest. Tree Physiol 16:5–16

Baldocchi DD, Vogel CA, Hall B (1997) Seasonal variation of carbon dioxide exchange rates above and below a boreal jack pine forest. Agr For Meteorol 83:147–170

Baldocchi D, Falge E, Gu L, Olson R, Hollinger D, Running S, Anthoni P, Bernhofer C, Davis K, Evans R, Fuentes J, Goldstein A, Katul G, Law B, Lee X, Malhi Y, Meyers T, Munger W, Oechel W, Paw U KT, Pilegaard K, Schmid HP, Valentini R, Verma S, Vesala T, Wilson K, Wofsy S (2001) FLUXNET: a new tool to study the temporal and spatial variability of ecosystem-scale carbon dioxide, water vapor, and energy flux densities. Bull Am Meteorol Soc 82:2415–2434

Buchmann N (2002) Plant ecophysiology and forest response to global change. Tree Physiol 22:1177–1184

Cannell MGR, Thornley JHM (1998) Temperature and CO_2 responses of leaf and canopy photosynthesis: a clarification using the non-rectangular hyperbola model of photosynthesis. Ann Bot 82:883–892

Carrara A, Janssens IA, Yuste JC, Ceulemans R (2004) Seasonal changes in photosynthesis, respiration and NEE of a mixed temperate forest. Agr For Meteorol 126:15–31 (DOI 10.1016/j.agrformet.2004.05.002)

Caton BP, Foin TC, Hill JE (1999) A plant growth model for integrated weed management in direct-seeded rice I. Development and sensitivity analyses of monoculture growth. Field Crops Res 62:129–143 (DOI 10.1016/S0378-4290(99)00010-6)

Chambers JQ, Tribuzy ES, Toledo LC, Crispim BF, Higuchi N, dos Santos J, Araújo AC, Kruijt B, Nobre AD, Trumbore SE (2004) Respiration from a tropical forest ecosystem: partitioning of sources and low carbon use efficiency. Ecol Appl 14:S72–S88

Cook BD, Davis KJ, Wang W, Desai A, Berger BW, Teclaw RM, Martin JG, Bolstad PV, Bakwin PS, Yi C, Heilman W (2004) Carbon exchange and venting anomalies in an upland deciduous forest in northern Wisconsin, USA. Agr For Meteorol 126:271–295 (DOI 10.1016/j.agrformet.2004.06.008)

Falge E, Baldocchi D, Olson R, Anthoni P, Aubinet M, Bernhofer C, Burba G, Ceulemans R, Clement R, Dolman H, Granier A, Gross P, Grünwald T, Hollinger D, Jensen N-O, Katul G, Keronen P, Kowalski A, Lai CT, Law BE, Meyers T, Moncrieff J, Moors E, Munger JW, Pilegaard K, Rannik Ü, Rebmann C, Suyker A, Tenhunen J, Tu K, Verma S, Vesala T, Wilson K, Wofsy S (2001) Gap filling strategies for defensible annual sums of net ecosystem exchange. Agr For Meteorol 107:43–69 (DOI 10.1016/S0168-1923(00)00225-2)

Falge E, Tenhunen J, Baldocchi D, Aubinet M, Bakwin P, Berbigier P, Bernhofer C, Bonnefond J-M, Burba G, Clement R, Davis KJ, Elbers JA, Falk M, Goldstein AH, Grelle A, Granier A, Grünwald T, Guðmundsson J, Hollinger D, Janssens IA, Keronen P, Kowalski AS, Katul G, Law BE, Malhi Y, Meyers T, Monson RK, Moors E, Munger JW, Oechel W, Paw U KT, Pilegaard K, Rannik Ü, Rebmann C, Suyker A, Thorgeirsson H, Tirone G, Turnipseed A, Wilson K, Wofsy S (2002) Phase and amplitude of ecosystem carbon release and uptake potentials as derived from FLUXNET measurements. Agr For Meteorol 113:75–95 (DOI 10.1016/S0168-1923(02)00103-X)

Fukushima Y, Hiura T, Tanabe S (1998) Accuracy of the MacArthur-Horn method for estimating a foliage profile. Agr For Meteorol 92:203–210 (DOI 10.1016/S0168-1923(98)00103-8)

Goulden ML, Munger JW, Fan S-M, Daube BC, Wofsy SC (1996) Measurements of carbon sequestration by long-term eddy covariance: methods and a critical evaluation of accuracy. Global Change Biol 2:169–182

Grace J, Malhi Y, Lloyd J, McIntyre J, Miranda AC, Meir P, Miranda HS (1996) The use of eddy covariance to infer the net carbon dioxide uptake of Brazilian rain forest. Global Change Biol 2:209–217

Greco S, Baldocchi DD (1996) Seasonal variations of CO_2 and water vapour exchange rates over a temperate deciduous forest. Global Change Biol 2:183–197

Griffis TJ, Black TA, Morgenstern K, Barr AG, Nesic Z, Drewitt GB, Gaumont-Guay D, McCaughey JH (2003) Ecophysiological controls on the carbon balances of three southern boreal forests. Agr For Meteorol 117:53–71 (DOI 10.1016/S0168-1923(03)00023-6)

Hirano T, Hirata R, Fujinuma Y, Saigusa N, Yamamoto S, Harazono Y, Takada M, Inukai K, Inoue G (2003) CO_2 and water vapor exchange of a larch forest in northern Japan. Tellus B 55:244–257 (DOI 10.1034/j.1600-0889.2003.00063.x)

Hiura T (2001) Stochasticity of species assemblage of canopy trees and understorey plants in a temperate secondary forest created by major disturbances. Ecol Res 16:887–893 (DOI 10.1046/j.1440-1703.2001.00449.x)

Hobara S, Tokuchi N, Ohte N, Koba K, Katsuyama M, Kim S-J, Nakanishi A (2001) Mechanism of nitrate loss from a forested catchment following a small-scale, natural disturbance. Can J For Res 31:1326–1335

Højstrup J (1993) A statistical data screening procedure. Meas Sci Technol 4:153–157

Johnson IR, Thornley JHM (1984) A model of instantaneous and daily canopy photosynthesis. J Theor Biol 107:531–545

Kaimal JC, Finnigan JJ (1994) Atmospheric boundary layer flows: their structure and measurement. Oxford University Press, New York

Knohl A, Schulze E-D, Kolle O, Buchmann N (2003) Large carbon uptake by an unmanaged 250-year-old deciduous forest in Central Germany. Agr For Meteorol 118:151–167

Komatsu H (2003) Relationship between canopy height and the reference value of surface conductance for closed coniferous stands. Hydrol Process 17:2503–2512 (DOI 10.1002/hyp.5141)

Kominami Y, Miyama T, Tamai K, Nobuhiro T, Goto Y (2003) Characteristics of CO_2 flux over a forest on complex topography. Tellus B 55:313–321 (DOI 10.1034/j.1600-0889.2003.00040.x)

Lavigne MB, Ryan MG, Anderson DE, Baldocchi DD, Crill PM, Fitzjarrald DR, Goulden ML, Gower ST, Massheder JM, McCaughey JH, Rayment M, Striegl RG (1997) Comparing nocturnal eddy covariance measurements to estimates of ecosystem respiration made by scaling chamber measurements at six coniferous boreal sites. J Geophys Res 102:28977–28985

Law BE, Ryan MG, Anthoni PM (1999) Seasonal and annual respiration of a ponderosa pine ecosystem. Global Change Biol 5:169–182 (DOI 10.1046/j.1365-2486.1999.00214.x)

Leuning R, Moncrieff J (1990) Eddy-covariance CO_2 flux measurements using open- and closed-path CO_2 analyzers: corrections for analyzer water vapor sensitivity and damping of fluctuations in air sampling tubes. Bound Layer Meteorol 53:63–76

Lloyd J, Wong SC, Styles JM, Batten D, Priddle R, Turnbull C, McConchie CA (1995) Measuring and modelling whole-tree gas exchange. Aust J Plant Physiol 22:987–1000

McMillen RT (1988) An eddy correlation technique with extended applicability to non-simple terrain. Bound Layer Meteorol 43:231–245

Nabeshima E, Hiura T (2004) Size dependency of photosynthetic water- and nitrogen-use efficiency and hydraulic limitation in *Acer mono*.Tree Physiol 24:745–752

Nakai Y, Kitamura K, Suzuki S, Abe S (2003) Year-long carbon dioxide exchange above a broadleaf deciduous forest in Sapporo, Northern Japan. Tellus B 55:305–312 (DOI 10.1034/j.1600-0889.2003.01413.x)

Ohtani Y, Mizoguchi Y, Watanabe T, Yasuda Y, Okano M (2001) Seasonal change of CO_2 flux above an evergreen needle leaf forest in temperate region, Fujiyoshida, Japan. CGER-Report, Proceedings of the International Workshop for Advanced Flux Network and Flux Evaluation, M-011, pp 129–132

Saigusa N, Yamamoto S, Murayama S, Kondo H, Nishimura N (2002) Gross primary production and net ecosystem exchange of a cool-temperate deciduous forest estimated by the eddy covariance method. Agr For Meteorol 112:203–215 (DOI 10.1016/S0168-1923(02)00082-5)

Schuepp PH, Leclerc MY, MacPherson JI, Desjardins RL (1990) Footprint prediction of scalar fluxes from analytical solutions of the diffusion equation. Bound Layer Meteorol 50:355–373

Shapiro J, Griffin K, Lewis J, Tissue D (2004) Response of *Xanthium strumarium* leaf respiration in the light to elevated CO_2 concentration, nitrogen availability and temperature. New Phytol 162:377–386 (DOI 10.1111/j.1469-8137.2004.01046.x)

Takahashi K, Yoshida K, Suzuki M, Sino T, Tani T, Tashiro N, Ishii T, Sugata S, Fujito E, Naniwa A, Kudo G, Hiura T, Kohyama T (1999) Stand biomass, net production and canopy structure in a secondary deciduous broad-leaved forest, northern Japan. Res Bul Hokkaido Univ For 56:70–85

Valentini R, Matteucci G, Dolman AJ, Schulze E-D, Rebmann C, Moors EJ, Granier A, Gross P, Jensen NO, Pilegaard K, Lindroth A, Grelle A, Bernhofer C, Grünwald T, Aubinet M, Ceulemans R, Kowalski AS, Vesala T, Rannik Ü, Berbigier P, Loustau D, Guðmundsson J, Thorgeirsson H, Ibrom A, Morgenstern K, Clement R, Moncrieff J, Montagnani L, Minerbi S, Jarvis PG (2000) Respiration as the main determinant of carbon balance in European forests. Nature 404:861–865 (DOI 10.1038/35009084)

Vickers D, Mahrt L (1997) Quality control and flux sampling problems for tower and aircraft data. J Atmos Oceanic Technol 14:512–526

Watanabe T, Yasuda Y, Yamanoi K, Ohtani Y, Okano M, Mizoguchi Y (2001) Seasonal variations in energy and CO_2 fluxes over a temperate deciduous forest at Kawagoe, Japan. CGER-Report, Proceedings of the International Workshop for Advanced Flux Network and Flux Evaluation, M-011, pp 11–17

Webb EK, Pearman GI, Leuning R (1980) Correction of flux measurements for density effects due to heat and water vapour transfer. Q J R Meteorol Soc 106:85–100

Yamamoto S, Murayama S, Saigusa N, Kondo H (1999) Seasonal and inter-annual variation of CO_2 flux between a temperate forest and the atmosphere in Japan. Tellus B 51:402–413 (DOI 10.1034/j.1600-0889.1999.00020.x)

Ecol Res (2005) 20: 325–331
DOI 10.1007/s11284-005-0048-7

ORIGINAL ARTICLE

**Hideaki Shibata · Tsutom Hiura · Yumiko Tanaka
Kentaro Takagi · Takayoshi Koike**

Carbon cycling and budget in a forested basin of southwestern Hokkaido, northern Japan

Received: 13 September 2004 / Accepted: 24 November 2004 / Published online: 2 March 2005

Abstract Quantification of annual carbon sequestration is very important in order to assess the function of forest ecosystems in combatting global climate change and the ecosystem responses to those changes. Annual cycling and budget of carbon in a forested basin was investigated to quantify the carbon sequestration of a cool-temperate deciduous forest ecosystem in the Horonai stream basin, Tomakomai Experimental Forest, northern Japan. Net ecosystem exchange, soil respiration, biomass increment, litterfall, soil-solution chemistry, and stream export were observed in the basin from 1999–2001 as a part of IGBP-TEMA project. We found that 258 g C m^{-2} $year^{-1}$ was sequestered annually as net ecosystem exchange (NEE) in the forested basin. Discharge of carbon to the stream was 4 g C m^{-2} $year^{-1}$ (about 2% of NEE) and consisted mainly of dissolved inorganic carbon (DIC). About 43% of net ecosystem productivity (NEP) was retained in the vegetation, while about 57% of NEP was sequestered in soil, suggesting that the movement of sequestered carbon from aboveground to belowground vegetation was an important process for net carbon accumulation in soil. The derived organic carbon from aboveground vegetation that moved to the soil mainly accumulated in the solid phase of the soil, with the result that the export of dissolved organic carbon to the stream was smaller than that of dissolved inorganic carbon. Our results indicated that the aboveground and belowground interaction of carbon fluxes was an important process for determining the rate and retention time of the carbon sequestration in a cool-temperate deciduous forest ecosystem in the southwestern part of Hokkaido, northern Japan.

Keywords Carbon biogeochemistry · Climate change · Eddy flux · Forest ecosystem · Net ecosystem productivity

H. Shibata (✉)
Northern Forestry and Development Office,
Field Science Center for Northern Biosphere,
Hokkaido University, 250 Tokuda, Nayoro 096-0071, Japan
E-mail: shiba@exfor.agr.hokudai.ac.jp
Tel.: +81-1654-24264
Fax: +81-1654-37522

T. Hiura · Y. Tanaka
Tomakomai Research Station,
Field Science Center for Northern Biosphere,
Hokkaido University, Takaoka, Tomakomai 053-0035, Japan

K. Takagi
Teshio Experimental Forest,
Field Science Center for Northern Biosphere,
Hokkaido University, Toikanbetsu, Horonobe,
Teshio 098-2943, Japan

T. Koike
Southern Forestry and Development Office,
Field Science Center for Northern Biosphere,
Hokkaido University, N9 W9, Kita-ku,
Sapporo 060-0809, Japan

Present address: Y. Tanaka
Institute of Low-Temperature Science,
Hokkaido University, N19 W8, Kita-ku,
Sapporo 060-0819, Japan

Introduction

Global climate change and increased levels of atmospheric carbon dioxide (CO_2) have motivated the scientific community and the public to ponder questions such as "How much carbon can be sequestered by a forest and where in the forest does this occur?" The quantification of carbon budget and cycling is a useful research tool with which to assess the role of forest vegetation and soil in carbon accumulation in the ecosystem. Given the close relationship that exists between the carbon dynamics of forest ecosystems and productivity within the ecosystems, the study of carbon dynamics has become a fundamental component of the research conducted by ecosystem ecologists since the international biological program (IBP) that was conducted late 1960 to the 1970s (Cole and Rapp 1981). However, quantification of the actual carbon sequestration rate in forest ecosystems is complicated by the difficulty associated with measuring

the rate of CO_2 exchange between the atmosphere and ecosystem. Eddy correlation techniques for assessing CO_2 flux over the forest canopy provide quantitative information on net photosynthesis and respiration (for both vegetation and microorganisms), or net ecosystem exchange (NEE) (Baldocchi et al. 2001).

NEE, measured using eddy flux at the boundary between the canopy and the atmosphere, corresponds to the net flux of CO_2 ($=b+c+d-a$, in Fig. 1) including photosynthesis and respiration and provides an indication of how much carbon was sequestered in the ecosystem. However, while NEE provides useful quantitative information on ecosystem functioning associated with carbon sequestration, it cannot be used to derive how this sequestered carbon is partitioned in the terrestrial ecosystem. Given that the difference in turnover time for carbon in soil and in vegetation is markedly different (Malhi et al. 1999; Chapin et al. 2002), it is very important to assess the internal cycling and partitioning of carbon in the vegetation and soil separately. It is thus essential to compare the carbon budget ($=$NEE$-h$, in Fig. 1) and the internal cycling ($=$c, d, e, f and g in Fig. 1) in the same basin over the same period. In a previous study associated with the internal partitioning of carbon in ecosystems, Malhi et al. (1999) indicated that carbon distribution and cycling in forest ecosystems are highly dependent upon climate and vegetation type. However, studies that have integrated monitoring of the carbon budget and cycling in the same basin over the same period of time have rarely been conducted to date. In Asia particularly, biogeochemical assessments of eddy CO_2 flux and internal cycling and budget have been particularly limited (Yamamoto et al. 1999), despite unique climatic and other environmental characteristics that distinguish the region from the relatively well-studied forests of the northeastern US and northwestern Europe.

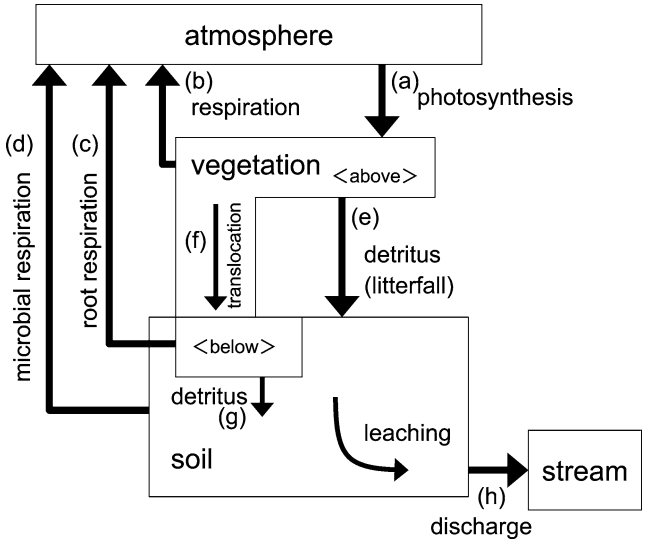

Fig. 1 Outline of the carbon budget and cycling in vegetation–soil–stream ecosystem

In addition, the forest studied in this paper has been recognized as an ecosystem sensitive to environmental changes and stresses because the forest is located on infertile, young volcanic soil in a transient zone from temperate to sub-boreal. Quantitative analysis of the carbon dynamics will not only provide fundamental information about the biogeochemical processes of ecosystems, but will also contribute to our understanding of the impact of carbon sequestration on ecosystem functioning and the effect that this might have on global climate change. The objectives of this study therefore were to (1) quantify the carbon budget and cycling and (2) understand the quantitative role of the vegetation and soil in carbon sequestration in a forest basin.

Methods

Study site

This study was conducted in the Horonai stream basin in the Tomakomai Experimental Forest (Hokkaido University), located in southwestern Hokkaido, northern Japan (42°40′N, 141°36′E). The Horonai stream is a first-order stream with a basin area of 9.4 km^2. The mean annual precipitation is approximately 1,200 mm and the mean annual temperature is 7.1°C. The vegetation in the basin is cool-temperate forest, mainly dominated by secondary deciduous forests that colonized the area after a typhoon in 1954. Approximately 50 tree species co-exist, including *Quercus mongolica* var. *crispula*, *Acer mono*, *Acer palmatum* ssp. *matsumurae*, and *Magnolia hyporeuca* (Hiura 2001). The predominant soil type is volcanic Regosols (Andic Udipsamments) (Soil Survey Staff 1994). The parent material of the soil is clastic pumice and sand that was deposited by eruptions of Mt. Tarumae in 1667 and 1739 (Sakuma 1987). Other detailed characteristics of the vegetation, soil and streams of the area have been described by Shibata et al. (1998, 2001), Takahashi et al. (1999) and Hiura (2001).

Net ecosystem exchange (NEE)

CO_2 fluxes between atmosphere and canopy (NEE) were measured from 1999–2001 by applying the eddy correlation method above the canopy layer from a 21-m-high observation tower (Tanaka et al. 2001). The mean height of the vegetation around the tower was approximately 13 m. Atmospheric CO_2 concentration was measured by the closed-path system using a nondispersive infrared carbon dioxide (NDIR-CO_2) sensor (LI-COR 6262, Li-Cor, NE, USA). An ultrasonic anemometer (DAT-600, Kaijo, Tokyo, Japan) and CO_2/H_2O fluctuation meter (AH-300, Kaijo) were used for the measurement of the fluxes.

Biomass and litterfall

We used long-term inventory data collected for the Tomakomai Research Station of Hokkaido University to calculate the stand volume of various forest stands in the study area. The investigated plot was 1 ha in area, and the stand volume and mortality of the aboveground vegetation were measured at 1-year intervals. Both aboveground and belowground biomasses of the stand were estimated by combining the measured stand volume and applying an allometric growth equation for each species derived from harvesting research previously conducted in the study basin (Takahashi et al. 1999). A more detailed description of the vegetation and the methods used to estimate biomass at the landscape scale was described by Hiura (2001, 2005).

Litter traps (1 m^2) were used to collect litterfall from vegetation with 25 replicates in a representative secondary stand in the study area. These samples were collected at monthly intervals from 1999–2001, and dried and weighed (Hiura 2005).

Soil respiration

A closed-chamber system and NDIR sensor (LI-6200, Licor, NE, USA) were used to measure soil respiration (Yanagihara et al. 2000). Twelve circular chambers (71.6 cm^2) were installed in forest stands that were considered representative of the study area. Soil respiration and surface soil temperature (0–10 cm) were measured using a 10-cm-long sensor at monthly intervals during periods of no snowfall from 1999–2000. The relationship between soil respiration and soil temperature was derived empirically and used to extrapolate annual soil respiration using the continuous soil surface temperature data—one of the long-term meteorological parameters collected at the Tomakomai Experimental Forest.

Carbon export from soil to stream

We installed tension-free lysimeters under the forest floor and in mineral soil (1.5 m deep) to collect the soil gravity water. Four lysimeters were thus installed below the forest floor and two lysimeters in the mineral soil at the bank near the middle part of the stream. Stream water was collected from the upper and lower river reaches at 2-week intervals and analyzed for dissolved organic carbon (DOC) and dissolved inorganic carbon (DIC) concentrations using a TOC analyzer (TOC 5000A, Shimadzu, Kyoto, Japan). Particulate organic carbon (POC) (particles > 0.7 μm) was also measured by filtering the stream water collected from the lower stream reaches (Shibata et al. 2001). Total carbon content of the particulate material was analyzed using a CN analyzer (Sumigraph Model NC-900, Sumika Analysis Center, Osaka, Japan).

Stream height was measured continuously using a pressure transducer and data logger at the weir station located at the lower stream reaches. Stream discharge was calculated using an empirical relationship between stream height and observed discharge (Shibata et al. 2001). Carbon flux in the stream was calculated by multiplying the carbon concentrations for DOC, DIC and POC, with discharge. Given that this basin was located in a very flat region, and that along its course, volcanic gravel deposits suggest that the groundwater inflow from the neighboring basin might affect the hydrologic budget, differences in the flux between upper and lower stream reaches were used to quantify net export of DOC and DIC from soil to stream (Shibata et al. 2001). We assumed that the influx of POC from the upper stream reaches was negligible because most of the POC would have been derived from the riparian canopy and the riverbank. Throughfall was collected using a circular funnel (30 cm in diameter) at the riverbank and analyzed for DOC and DIC concentrations. More detailed methods for calculating the contributions of the soil and stream on carbon dynamics were reported by Shibata et al. (2001).

Budget calculation

All carbon-flux measurements were conducted from 1999–2001. Mean fluxes for the 3 years were used in the budget analysis. We used the steady-state budget for vegetation and soil as illustrated in Eqs. 1 and 2, respectively, to analyze the carbon dynamics of the ecosystem. The letters in parenthesis refer to Fig. 1.

$$\mathrm{NEE} - \mathrm{SR} = \mathrm{LF} + \mathrm{AB} + \mathrm{AC} \quad (1)$$

where NEE is net ecosystem exchange ($=b+c+d-a$), SR is soil respiration ($=d+c$), LF is litterfall and mortality of aboveground vegetation ($=e$), AB is aboveground biomass increment and AC is allocation from aboveground to belowground vegetation ($=f$).

$$\mathrm{AC} - \mathrm{BB} + \mathrm{LF} = \mathrm{SR} + \mathrm{DC} + \mathrm{SS} \quad (2)$$

where BB is belowground biomass increment, DC is discharge to stream ($=h$), and SS is carbon storage in organic and mineral soil. Measured carbon fluxes were NEE, SR, LF, AB, BB, and DC, while the estimated carbon fluxes based on these equations were AC and SS. The left side of Eq. 1 (= NEE – SR) corresponds to gross ecosystem exchange (GEE).

Results

Carbon fluxes in the basin

Figure 2 shows the seasonal fluctuation in monthly NEE over the canopy from 1999–2001. Negative values for NEE indicate net CO_2 transport from atmosphere to ecosystem. Atmospheric CO_2 was sequestered mainly

from June to October each year. Maximum estimates of carbon uptake ranged from −80 to −100 g C m^{-2} $month^{-1}$ from June to July (Fig. 2). Annual mean NEE for 3 years was −258 (±36 SD) g C m^{-2} $year^{-1}$.

Soil respiration was observed to fluctuate in response to changes in soil temperature (Fig. 3). The Q_{10} value was 2.7, and the annual flux of soil respiration over 3 years was 592 ± 55 g C m^{-2} $year^{-1}$. The annual flux of soil respiration was approximately two times larger than the NEE in this studied basin. Given the relationship between respiration and NEE, GEE (the net flux of photosynthesis and respiration for the aboveground vegetation) was 850 g C m^{-2} $year^{-1}$.

Litterfall occurred mainly in late summer and fall (October and November) of each year. Annual mean litterfall for the 3 years was 118 g C m^{-2} $year^{-1}$ in the secondary forest stands. The increments of aboveground and belowground biomass and tree mortality measured in the secondary forest stand were 92, 16, and 79 g C m^{-2} $year^{-1}$, respectively. The annual carbon sequestered by the vegetation was 108 g C m^{-2} $year^{-1}$, approximately 42% of the NEE. The sum of the litterfall and mortality for aboveground vegetation was 197 g C m^{-2} $year^{-1}$, accounting for the organic carbon input from the aboveground vegetation to soil surface.

Stream export of DOC, DIC and POC was considered an output of carbon from the terrestrial ecosystem. Annual mean export of dissolved and particulate carbon from soil to stream for 3 years was 4.1 ± 1.8 g C m^{-2} $year^{-1}$ (Fig. 4), and DIC, DOC and POC accounted for 68, 13 and 19% of the total carbon export to the stream. The total export of carbon to the stream corresponded to only 2% of the NEE flux in this basin. DOC concentration was higher in the surface soil water, and tended to decrease with depth of ground (Fig. 5). DIC was a major carbon form in stream water collected from both the upper and lower reaches of the stream.

Carbon budget in the basin

Figure 6 shows the carbon cycling and budget of the basin in the study. Based on the NEE and export to the stream, the annual net carbon sequestration rate in this basin (=NEP) was 254 g C m^{-2} $year^{-1}$. The carbon allocation from the aboveground to belowground vegetation calculated using Eq. 1 was 549 g C m^{-2} $year^{-1}$, corresponding to 65% of GEE. The carbon budget in the soil (Eq. 2) indicated that 146 g C m^{-2} $year^{-1}$ was sequestered in the soil in this basin. The annual carbon sequestration in vegetation and soil accounted for 43 and 57% of NEP, respectively. The total input of carbon from the aboveground and belowground vegetation to the soil was 730 g C m^{-2} $year^{-1}$, including the litterfall, mortality of aboveground vegetation, root detritus and root respiration.

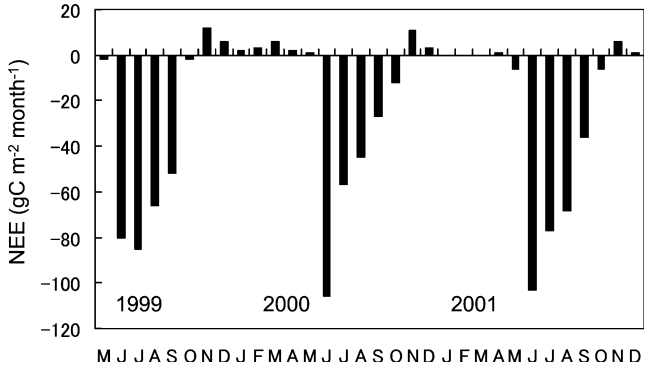

Fig. 2 Seasonal fluctuation in monthly NEE over the forest canopy from 1999–2001. *Negative values* represent net inflow of carbon from atmosphere to canopy

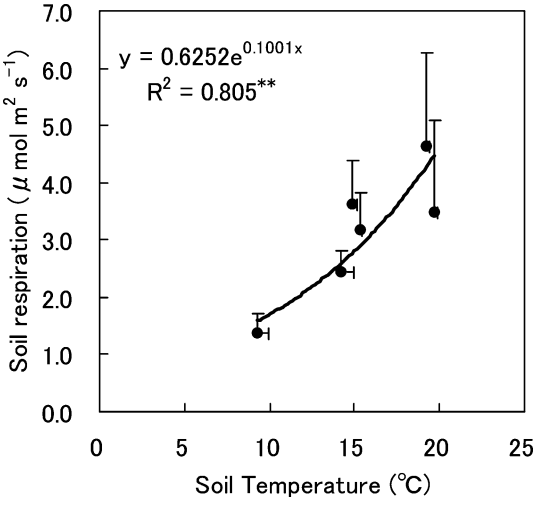

Fig. 3 Relationship between soil respiration and soil surface temperature (0–10 cm). Data were obtained in different months during nonsnowy periods. *Bars* represent standard deviations

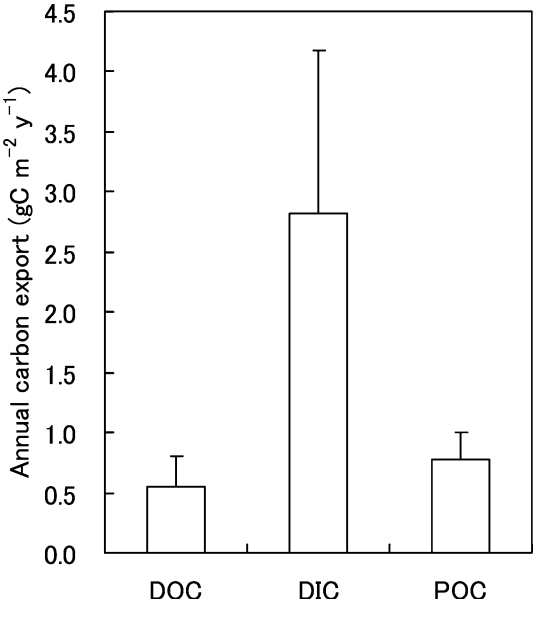

Fig. 4 Annual carbon export from the terrestrial ecosystem to a stream in the Horonai stream basin. Data are mean values obtained after 3 years. *Bar* represents standard deviation

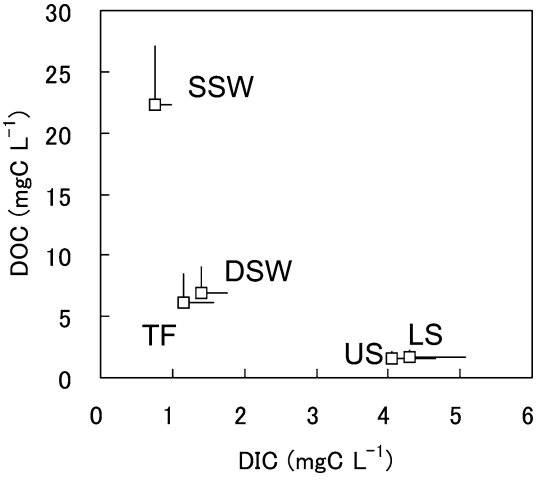

Fig. 5 Mean concentration of DOC and DIC in throughfall (*TF*), surface soil water (*SSW*), deep soil water (*DSW*), upper stream (*US*) and lower stream (*LS*). *Bars* represent standard deviations

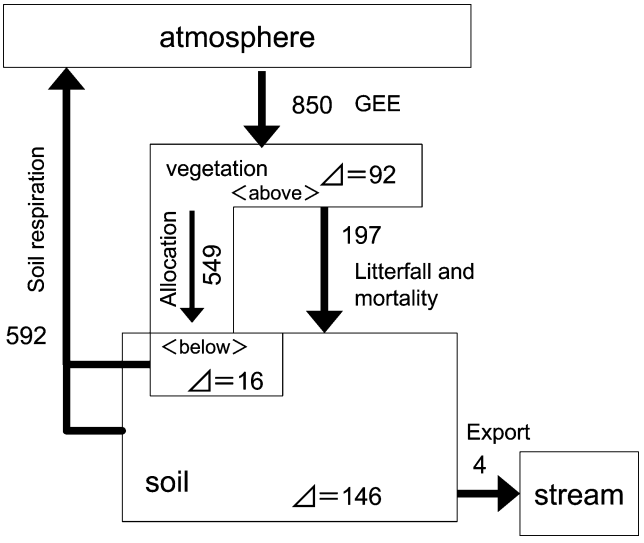

Fig. 6 Annual carbon budget and cycling (g C m^{-2} year^{-1}) in the Horonai stream basin. *Delta values* ($\Delta =$) indicate net accumulation of carbon in aboveground and belowground vegetation and soil. Allocation of carbon from aboveground to belowground vegetation and carbon accumulation of soil are estimated values based on the budget (see details in the text and in Eqs. 1, 2)

Discussion

In the forest basin of this study, net carbon sequestered in the ecosystem is partitioned between the vegetation and soil almost equally on an annual basis. The total litterfall and aboveground tree mortality (197 g C m^{-2} year^{-1}) accounted for 27% of the total carbon input from the vegetation to soil (730 g C m^{-2} year^{-1}). Consequently, the movement of carbon through the roots into the soil was an important pathway for carbon input to the soil. Since, in annual steady-state conditions (no net change in the storage of CO_2 in soil on annual basis), CO_2 input via root respiration to soil would ordinarily be balanced by emissions from the soil surface to the atmosphere, the organic carbon input via root detritus and exudates could be an important form of carbon for the net release of carbon from belowground vegetation to soil. The net increment of root biomass (16 g C m^{-2} year^{-1}, estimated using the allometric growth equation obtained from harvesting measurements) suggested that the increment in very fine root biomass might have been underestimated in this budget. Detailed measurement and estimation methods will be required to clarify the extent of fine and very fine root production with respect to carbon sequestration (Satomura et al. 2003; Shutou and Nakane 2004). Reich and Bolstad (2001) reported that the net primary production of belowground vegetation accounted for 14–80% of the total net primary production in various temperate forest ecosystems.

Raich and Schlesinger (1992) estimated annual soil respiration rates for the various global biomes. The soil respiration rate in our study area fell within the range (647 ± 51 g C m^{-2} year^{-1}) they gave for temperate deciduous forests. In the soil system, DOC decreased with depth of the soil, suggesting that the adsorption and/or decomposition of DOC was the dominant mechanism of DOC retention in ground (Shibata et al. 2001). In general, volcanic pumice is considered to have a relatively high ability to adsorb solutes to the solid phase of soil. We estimated the total carbon pool in the organic and mineral soil using previously reported data (Sakuma 1987; Eguchi et al. 1997). The total carbon pool in soil from the O horizon to 100-cm-deep mineral soil was approximately 5,500 g C m^{-2}, corresponding to values approximately 38 times larger than the annual net carbon sequestration in soil. Assuming most of the organic carbon accumulates within the top 100 cm of soil, the mean residence time of sequestered carbon in soil is approximately 40 years for this basin. DOC concentration in soil water from the mineral soil (1.5 m deep) was still significantly higher than that of stream water (Fig. 5), suggesting that the depletion of DOC in soil water occurred deeper in mineral soil. Consequently, the mean residence time for carbon in soil estimated above could still be an underestimatation in this study. An analysis of the quantitative dynamics in the deeper mineral soil would be a key to understand the buffering function of the soil system on the temporal fluctuations of the carbon input from atmosphere–vegetation system.

Annual mean NEE (−258 g C m^{-2} year^{-1}) in this basin is comparable with that reported for a growing season of similar length (about 150 days) in the worldwide CO_2 flux network (FLUXNET, Baldocchi et al. 2001). However, for the eddy measurements, it should be noted that several uncertainties regarding the applicability of the techniques still remain, including (1) difficulties in measuring eddies during periods of

high atmospheric stability and when the canopy surface is irregular and (2) difficulties measuring the drainage flow of CO_2 across the stream valley (Baldocchi et al. 2001). These uncertainties might affect the estimation of the unmeasured flux; particularly the allocation of carbon from the vegetation to the soil. In addition, we used the compartment model for the carbon budget, which assumes a steady state on an annual basis. It should be noted that actual carbon transport sometimes fluctuates and is transient. For example, the aforementioned buffering function of the soil system against temporal fluctuations in carbon input could be transient.

Hiura (2005) indicated that the secondary forest, which is the dominant vegetation type in this basin, showed higher net biomass increment than the mature forest also found in this basin. The higher sequestration rate of the vegetation and soil in this basin may mean that the forest in the study area was relatively young and at an early stage of succession. Since most of the forest stands in this basin became established after a large disturbance caused by a by typhoon in 1954, the growth rate of the vegetation seems to be still increasing. The soil is also a very young Regosol that developed after the recent eruption of a volcano within the last several centuries. These age characteristics of vegetation and soil would affect the NEP in the basin. Furthermore, since the study area is located near urban and industrial areas (Shibata et al. 1998), the forest ecosystem currently receives slightly elevated amounts of atmospheric nitrogen (4–5 kg N ha^{-1} $year^{-1}$ of bulk deposition, Shibata et al. 1998). The effect of nitrogen deposition as a nutrient input on carbon sequestration needs to be examined more closely to determine if the input of nitrogen from the atmosphere enhances the uptake of carbon in the forest (Lloyd 1999; Nadelhoffer et al. 1999).

Our results suggest that the fundamental characteristics of the parent materials of soil and the chronological attributes of the vegetation and soil—including natural disturbances in the past—were an important factor affecting the current NEP and the partitioning of sequestered carbon in the ecosystem. An integrated regional cross-site analysis of carbon biogeochemistry, including eddy measurements and budgets under the various environmental conditions, would improve our understanding of the role of forest ecosystems in global climate change.

Acknowledgements We would like to thank Ms. Yuko Yanagihara and all of the technical staff of the Tomakomai Research Station, Hokkaido University for their helpful fieldwork and maintenance of the observation instruments. We express our considerable thanks to Prof. Kenkichi Ishigaki and the late Prof. Shigeru Nakano for their constructive advice and their great efforts toward this research program. This study was funded by the Japanese Ministry of Education, Science, Sports, Culture and Technology (B(1)-11213101).

References

Baldocchi D, Falge E, Gu L, Olson R, Hollinger D, Running S, Anthoni P, Bernhofer C, Davis K, Evans R, Fuentes J, Goldstein A, Katul G, Law B, Lee X, Malhi Y, Meyers T, Munger W, Oechel W, Paw KT, Pilegaard K, Schmid HP, Valentini R, Verma S, Vesala T, Wilson K, Wofsy S (2001) FLUXNET: a new tool to study the temporal and spatial variability of ecosystem-scale carbon dioxide, water vapor, and energy flux densities. Bull Am Meteorol Soc 82:2415–2434

Chapin FS III, Matson PA, Mooney HA (2002) Principles of terrestrial ecosystem ecology. Springer, New York

Cole DW, Rapp M (1981) Elemental cycling in forest ecosystem. In: Reichle ED (ed) Dynamic properties of forest ecosystems. Cambridge University Press, Cambridge, pp 341–410

Eguchi S, Sakata T, Hatano R, Sakuma, T (1997) Daily change of CO_2 efflux from the soil of a deciduous broad-leaved forest and its significance as a CO_2 source for vegetation (in Japanese with English summary). Jpn J Soil Sci Plant Nutr 68:138–147

Hiura T (2001) Stochasticity of species assemblage of canopy trees and understory plants in a temperate secondary forest created by major disturbances. Ecol Res 16:887–893

Hiura T (2005) Above-ground biomass and net biomass increment in a cool temperate forest on a landscape scale (this issue). Ecol Res 20

Lloyd J (1999) The CO_2 dependence of photosynthesis, plant growth responses to elevated CO_2 concentrations and their interaction with soil nutrient status. II Temperate and boreal forest productivity and the combined effects of increasing CO_2 concentrations and increased nitrogen deposition at a global scale. Funct Ecol 13:439–759

Malhi Y, Baldocchi DD, Jarvis PG (1999) The carbon balance of tropical, temperate and boreal forests. Plant Cell Env 22:715–740

Nadelhoffer KJ, Emmett BA, Gundersen P, Kjonaas OJ, Koopmans CJ, Schleppi P, Tietema A, Wright RF (1999) Nitrogen deposition makes a minor contribution to carbon sequestration in temperate forests. Nature 398:145–148

Raich JW, Schlesinger WH (1992) The global carbon dioxide flux in soil respiration and its relationship to vegetation and climate. Tellus B 44:81–99

Reich PB, Bolstad P (2001) Productivity of evergreen and deciduous temperate forest. In: Roy J, Saugier B, Mooney HA (eds) Terrestrial global productivity. Academic Press, San Diego, pp 245–284

Sakuma T (1987) Characterization of soils in the tomakomai experiment forest (in Japanese with English summary). Res Bull Coll Exp For Hokkaido Univ 44:749–759

Satomura T, Nakatsubo T, Horikoshi T (2003) Estimation of the biomass of fine roots and mycorrhizal fungi: a case study in a Japanese red pine (*Pinus densiflora*) stand. J For Res 8:221–225

Shibata H, Kirikae M, Tanaka Y, Sakuma T, Hatano R (1998) Proton budgets of forest ecosystems on volcanogenous Regosols in Hokkaido, northern Japan. Water Air Soil Pollut 105:63–72

Shibata H, Mitsuhashi H, Miyake Y, Nakano S (2001) Dissolved and particulate carbon dynamics in a cool-temperate forested basin in northern Japan. Hydrol Process 15:1817–1828

Shutou K, Nakane K (2004) Change in soil carbon cycling for stand development of Japanese cedar (*Cryptomeria japonica*) plantations following clear-cutting. Ecol Res 19:233–244

Soil Survey Staff (1994) Keys to soil taxonomy. USDA Conservation Service, Washington

Takahashi K, Yoshida K, Suzuki M, Seino T, Tani T, Tashiro N, Ishii T, Sugata S, Fujito E, Naniwa A, Kudo G, Hiura T, Kohyama T (1999) Stand biomass, net production and canopy structure in a secondary deciduous broad-leaved forest, northern Japan. Res Bull Hokkaido Univ For 56:70–85

Tanaka Y, Tanaka N, Hatano R (2001) Seasonal variation of carbon dioxide and energy fluxes above a cool, temperate, broad-leaved forest. CGER-Report M-011-2001. In: Proceedings of international workshop for advanced flux network and flux evaluation, Sapporo, Japan, pp 133–137

Yamamoto S, Murayama S, Saigusa N, Kondo H (1999) Seasonal and inter-annual variation of CO_2 flux between a temperate forest and atmosphere in Japan. Tellus 51B:402–413

Yanagihara Y, Koike T, Matsuura Y, Mori S, Shibata H, Satoh F, Masuyagina OV, Zyryanova OA, Prokushkin AS, Prokushkin SG, Abaimov AP (2000) Soil respiration rate on the contrasting north- and south-facing slopes of a larch forest in central Siberia. Eurasian J For Res 1:19–29

Ecol Res (2005) 20: 333–346
DOI 10.1007/s11284-005-0049-6

ORIGINAL ARTICLE

Tetsuya Hiyama · Kiyotaka Kochi · Nakako Kobayashi
Satiraporn Sirisampan

Seasonal variation in stomatal conductance and physiological factors observed in a secondary warm-temperate forest

Received: 14 September 2004 / Accepted: 8 January 2005 / Published online: 16 April 2005

Abstract This study quantified stomatal conductance in a CO_2-fertilized warm-temperate forest. The study considered five items: (1) the characteristics of the diurnal and seasonal variation, (2) simultaneous measurements of canopy-scale fluxes of heat and CO_2 and the normalized difference vegetation index (NDVI), (3) the stomatal conductance of sunlit and shaded leaves, (4) a stomatal conductance model, and (5) the effects of leaf age on stomatal conductance. Sampled plants included evergreen and deciduous species. Stomatal conductance, SPAD, and leaf nitrogen content were measured between March and December 2001. Sunlit leaves had the largest diurnal and seasonal variation in conductance in terms of both magnitude and variability. In contrast, shaded leaves had only low conductance and slight variation. Stomatal conductance increased sharply in new shooting leaves of *Quercus serrata* until reaching a maximum 2 months after full leaf expansion. The seasonal changes in the canopy-scale heat and CO_2 fluxes were similar to the change in the canopy-scale NDVI of the upper-canopy plants. These seasonal changes were correlated with the leaf-level H_2O/CO_2 exchanges of upper-canopy plants, although these did not represent the stomatal conductance in fall completely. Seasonal variations in the leaf nitrogen content and SPAD were similar, except leaf foliation, until day 130 of the year, when the behaviors were completely the opposite. A Jarvis-type model was used to estimate the stomatal conductance. We modified it to include SPAD as a measure of leaf age. The seasonal variation in stomatal conductance was not as sensitive to SPAD, although estimates for evergreen species showed improvements.

T. Hiyama (✉) · K. Kochi · N. Kobayashi · S. Sirisampan
Hydrospheric Atmospheric Research Center,
Nagoya University, Nagoya 464-8601, Japan
E-mail: hiyama@hyarc.nagoya-u.ac.jp
Tel.: +81-52-7893478
Fax: +81-52-7893436

Keywords Stomatal conductance of water vapor · Sunlit and shaded leaves · Jarvis-type model · SPAD · Leaf nitrogen content

Introduction

To understand how terrestrial ecosystems respond to global climate change, several dynamic global vegetation models (DGVM) have been developed (e.g., Foley et al. 1996; Cox 2001; Watanabe et al. 2004). Foley et al. (1998) stated that three elements are crucial for a DGVM: (1) land surface processes [i.e., energy (heat), water, and CO_2 fluxes (balances)], including plant physiological processes, (2) phenological aspects (seasonality of plants), and (3) transient processes of carbon balance and vegetation structure. The key function in the land surface processes is leaf stomatal control. Pursuing mechanistic explanations of stomatal behavior is still an active research target (Watanabe et al. 2004). However, to better understand phenological behaviors, more field measurements combining seasonal analyses of canopy-scale fluxes of heat and CO_2 and leaf-level stomatal control are required.

Stomata are plant organs on the leaf surface that form an important interface for H_2O/CO_2 gas exchange between plants and the atmosphere. Stomata change rapidly depending on environmental conditions. Smith and Hollinger (1991) stated that stomatal behavior is often the most sensitive indicator of plants from a physiological perspective.

The leaf exchange of H_2O can be considered in terms of both stomatal conductance and transpiration. However, the transpiration rates measured in chambers are not useful parameters in themselves because of the difficulty in matching the chamber environment to the outside environment (Jones 1992). Leaf conductance is defined as the proportionality constant between transpiration and the vapor concentration gradient between inside the leaf and the leaf surface (Pearcy et al. 1989).

Stomatal conductance is a part of leaf conductance and is the reciprocal of stomatal resistance, although the conductance is usually used rather than the resistance because the conductance is proportional to the flux, and it expresses the regulatory control exerted by the stomata on transpiration rates. Stomatal conductance can be used to deduce transpiration and photosynthetic activities because they are closely related.

Attempts have been made to improve the accuracy of estimates of stomatal conductance, as it is an important variable in many models. Furthermore, it mirrors plant condition. The most famous and simplest stomatal conductance model is the experimental model of Jarvis (1976), which considered several environmental factors, including the photosynthesis photon flux density (PPFD), air temperature (T), water vapor pressure deficit of air (VPD), soil water potential, atmospheric CO_2 concentration, CO_2 concentration within the stomata, cuticular conductance, and leaf water potential. Recently, a limited number of environmental variables, such as PPFD, T, VPD, and soil water potential, have been used to estimate stomatal conductance based on Jarvis's (1976) concept. Such modified models are called Jarvis-type models (Stewart 1988; Ogink-Hendriks 1995). Yu et al. (1998) considered the Jarvis-type model convenient because it can estimate stomatal conductance in terms of environmental variables. Such models have been broadly used for second-generation schemes for land surface modeling (Sellers et al. 1997; Pitman 2003). These models were also developed to improve the estimation of stomatal conductance. Here, we use a Jarvis-type model to quantify stomatal conductance as it relates to environmental factors.

When considering physiological activities at canopy scale, many assumptions are needed to scale-up measurements made at leaf scale. First, second-generation schemes for land surface modeling, such as SiB2 of Sellers et al. (1992, 1996), were proposed based on the assumption that plants of different heights undergo the same physiological activities. However, this is incorrect in theory and nature (De Pury and Farquhar 1997). Plants in the lower canopy are not as active as upper-canopy plants. Subsequent studies used a multi-layer approach, such as the Penman-Monteith (Monteith 1965) multi-layer model. This separates a forest into multiple layers, which are then integrated to represent a canopy scale. However, multi-layer studies are quite complex in terms of analyses and measurements. More recently, a separate approach to modeling sunlit and shaded leaves was developed. This is an intermediate concept between a big leaf-type model and a multi-layer model. This approach separates a forest into two types of leaves, i.e., sunlit leaves (those exposed to radiation) and shaded leaves (those not exposed). An outstanding advantage of the sunlit and shaded leaf approximation is that it avoids the error due to the rough calculations of a big-leaf model. Moreover, it is less complex than a multi-layer model.

Sirisampan et al. (2003) measured the stomatal conductance of six species in a small warm-temperate forest located within the city of Nagoya, Japan, which has a population exceeding two million. They focused on both multi-layer and sunlit and shaded leaf approaches to see how much in actual measurements each layer or leaf light condition gave the stomatal conductance. They used a Jarvis-type model to estimate stomatal conductance from PPFD, T, VPD, and soil water potential. Using a sensitivity test, they determined that the soil water potential had no effect on the stomatal conductance for each species. In Sirisampan et al. (2003), the Jarvis-type model overestimated stomatal conductance when new leaves were developing in the spring. They suggested that the model might be improved if it included physiological factors, such as leaf age as a limiting factor, as well as environmental factors.

It is also interesting to consider how stomatal behavior differs in different years, especially with a relatively higher atmospheric CO_2 concentration (Oguri and Hiyama 2002). In 2000, the annual mean atmospheric CO_2 concentration for this forest was around 395 ppm (Oguri, personal communication). It is also valuable to compare how canopy-scale data, such as the heat and CO_2 fluxes and NDVI, correspond to leaf-level stomatal behavior.

Therefore, this study quantified the stomatal conductance of water vapor in the same warm-temperate forest as Sirisampan et al. (2003). The study considered five items: (1) the characteristics of the diurnal and seasonal variation, (2) simultaneous measurements of the canopy-scale heat and CO_2 fluxes and the normalized difference vegetation index (NDVI), (3) the stomatal conductance of sunlit and shaded leaves, (4) a stomatal conductance model, and (5) the effects of leaf age on stomatal conductance. We determined the characteristics of stomatal conductance for sunlit and shaded leaves. Using the sunlit- and shaded-leaf approach, many studies have considered photosynthesis, while few have considered transpiration. The analysis of leaf age was used to delineate the effects of a physiological factor on stomatal conductance.

Site description

The experimental site was a warm-temperate forest behind the Hydrospheric Atmospheric Research Center (HyARC) at Nagoya University, Japan (35°10'N, 136°58'E). This forest is in the eastern part of Nagoya and is surrounded by residences and buildings. The forest is a secondary warm-temperate forest within an urban area. Consequently, the forest is exposed to relatively higher atmospheric CO_2 concentrations (Oguri and Hiyama 2002). A map of the site is shown in Fig. 1 of Oguri and Hiyama (2002). Previously, the dominant vegetation at this forest site was pine (*Pinus densiflora*) (Aoki 1997). Currently, the dominant vegetation occupying the upper forest canopy is mostly *Quercus serrata*,

a deciduous species. Most of the middle canopy is composed of evergreen plants (e.g., *Eurya japonica*, *Ilex pedunculosa*, *Ligustrum japonicum*, and *Vaccinium bracteatum*), with some deciduous trees (e.g., *Evodiopanax innovans*). The understory vegetation (hereafter, the lower canopy) consists mainly of young evergreen plants of the species listed above and *Aucuba japonica*.

The mean tree height was 17.8 m in 2001. The leaf area index (LAI) and plant area index (PAI) were 1.5 and 3.0, respectively, for the middle- and lower-canopy trees. During the season when *Q. serrata* was foliated, the LAI and PAI of the upper canopy trees were 4.4 and 5.3, respectively. LAI and PAI for the entire canopy were 1.5 and 3.9 (in the nonfoliated season of *Q. serrata*), and 5.9 and 8.3 (in the foliated season), respectively. These values were obtained from measurements using a fish-eye camera (Hashimoto, personal communication).

A 21-m-high meteorological tower was installed and used to measure stomatal conductance, canopy-scale fluxes, and NDVI (described below). The maximum fetch (around 500 m) was along the dominant wind direction (northwestern). The minimum fetch (around 100 m) was perpendicular to the dominant wind direction. The annual mean air temperature was 15.1°C and the annual precipitation was 1415 mm (obtained using tower measurements from January to December 2001). The annually integrated net ecosystem exchange (NEE) was 2.3 (t C ha^{-1} $year^{-1}$) in 2001 (Muraishi, personal communication).

Methods

Measuring stomatal conductance

The vegetation was grouped by measurement height into four groups: 14.6, 6.4, 5.4, and 0.8 m high. Species with canopies located at 14.6 m were defined as the upper canopy (*Q. serrata*), those at 6.4 and 5.4 m were the middle canopy (*E. japonica*, *I. pedunculosa*, and *V. bracteatum*), and those located at 0.8 m were the lower canopy (*L. japonicum* and *A. japonica*).

Stomatal conductance of water vapor was measured using a null-balance porometer (Model LI-6400, Portable Photosynthesis System, LI-COR) on a leaf scale. In most cases, at least six leaves for each species were measured every hour. Measurements were made from dawn to dusk, with an earlier start in summer because of the earlier sunrise. Monthly observations were carried out from March to December 2001. Note that *Q. serrata* is a deciduous plant, and it was not observed from the end of December until March since there were no exposed leaves on the trees. There are no data for early April because the *Quercus* leaves were too small for measurements.

Stomatal conductance for the upper canopy was measured on 26 April, 29 May, 26 June, 2 August, 12 September, 13 October, 19 November, and 2 December. For the middle canopy, we used data obtained on 20 March, 27 April, 4 June, 4 July, 3 August, 13 September, 14 October, 23 November, and 23 December. For the lower canopy, we used data obtained on 21 March, 28 April, 9 July, 5 August, 17 September, 20 October, 24 November, and 24 December.

Furthermore, measurements of sunlit and shaded *Q. serrata* leaves were distinguished because the high crown density resulted in the self-shading of leaves. Sunlit leaves were exposed to much greater light intensities than were shaded leaves, particularly in summer.

Leaf-scale measurements of the PPFD, T, and VPD within a leaf chamber were made using the inner sensors in the porometer at the same times as the stomatal conductance was measured.

All the sampled plants were within 3 m of the micrometeorological tower. We examined eight trees belonging to six species, including both deciduous and evergreen plants. The height, diameter at breast height (DBH), and crown projection area of the sampled plants are as described in Table 1 of Sirisampan et al. (2003).

Observations of microclimate and canopy-scale fluxes of heat and CO_2

Microclimate

Microclimate data measured above the forest canopy included the incoming solar radiation, net radiation, soil heat flux, air temperature, relative humidity, and precipitation; the soil water potential on the forest floor was also measured. The net radiometer was an MF-11 (Eko) sensor and the soil heat flux plate was an MF-81 (Eko). The measurements, except for the soil water potential, were recorded using an automatic logging system (CR10X, Campbell) at 10-min intervals. The instruments were mounted at the top of the tower (21 m). Soil water potential was measured using tensiometers installed near the tower at depths of 5, 10, 20, 40, and 80 cm. Measurements were generally made during a 1-h period in the afternoon of the day of measurements.

Precipitation was measured on the upper deck of the HyARC building, about 120 m from the tower, using a rain gauge. During instrument failure, precipitation was taken from the monthly meteorological report recorded at the Nagoya local meteorological observatory, 1.5 km from the experimental site.

Canopy-scale fluxes of heat and CO_2

The canopy-scale fluxes of sensible heat and CO_2 were determined using the eddy covariance method. From the residuals of the heat balance equation, the water vapor (latent heat) flux was obtained simultaneously. Detailed descriptions of the derivations and method of correction for the accurate fluxes are given in T. Ohta et al. (per-

sonal communications). The following is a brief explanation of the flux derivations.

A three-dimensional ultrasonic anemometer-thermometer (DA-600, Kaijo, Japan) was used to measure the three-dimensional wind speed and temperature fluctuations, which were recorded at 10-Hz intervals on a magnetic optical (MO) disk using a digital recorder (DR-M3, TEAC). A closed-path CO_2/H_2O gas analyzer (LI-6262, LI-COR) was used to measure the fluctuations in the CO_2 and H_2O densities. The length and inside diameter of the tube for the air intake were 6 m and 4 mm, respectively. The intake rate was 1 L min^{-1} . A temperature/humidity probe (HMP45A, Vaisala) was set for the flux corrections.

The three-dimensional ultrasonic anemometer-thermometer, closed-path CO_2/H_2O gas analyzer, and temperature/humidity probe were installed on the tower at 22 m and the digital recorder was set in a hut located on the forest floor close to the tower.

The equation for the eddy covariance method for calculating the flux (F) is

$$F = \overline{wc} = \overline{w'c'} + \bar{w}\,\bar{c}, \tag{1}$$

where w is the vertical wind speed and c is a scalar, such as temperature (for the sensible heat flux), H_2O density (for the latent heat flux), or CO_2 density (for the CO_2 flux). The bars and primes denote the mean values for a calculation period, and the perturbation from the mean, respectively.

The three-axis rotation algorithm (Kaimal and Finnigan 1994) was used to derive w in streamline coordinates. As we used a closed-path system to measure the turbulent fluctuation of the CO_2/H_2O densities, a time-lag correction was used, but the tube attenuation (i.e., high-frequency correction of the CO_2/H_2O fluctuation) was not corrected. Air density fluctuations were corrected according to Webb et al. (1980).

The CO_2 fluxes were averaged when the PPFD exceeded 50 μmol m^{-2} s^{-1}. In this study, the latent heat fluxes were obtained from the residuals of the heat balance equation. Finally, all of the canopy-scale fluxes were averaged to obtain daily mean values.

Observing the canopy-scale NDVI

In addition to the microclimate observations, described in the Microclimate section, we measured the downward/upward shortwave radiation and the downward/upward PAR (photosynthetically active radiation) at three different heights using albedo-meters (CM3, Kipp & Zonen) and PAR sensors (LI-190A, LI-COR), respectively. Sensors were set at 20.75, 10.70, and 0.90 m, corresponding to the upper, middle, and lower canopies. The signal output from each sensor was recorded using a micro-logger (CR23X, Campbell).

The albedo-meter can sense shortwave radiation (W m^{-2}) ranging from 300–4,000 nm and the PAR sensors can sense PPFD (μmol photon m^{-2} s^{-1}) ranging from 400–700 nm. The PPFD values were converted to PAR (W m^{-2}) by dividing by 4.4. As PAR equals the radiation in the visible range, we assume that the residual (shortwave radiation minus PAR) is the radiation in the near-infrared range. Therefore, this observation produced the downward/upward radiation over the entire shortwave (from 300–4,000 nm), visible (from 300–700 nm), and near-infrared (from 700–4,000 nm) ranges at three heights. We calculated the reflectance over the entire shortwave (ρ_{Rs}, i.e., the albedo), visible (ρ_{PAR}), and near-infrared (ρ_{NIR}) ranges, as follows:

$$\rho_{R_s} = R_s\uparrow / R_s\downarrow, \tag{2}$$

$$\rho_{PAR} = \mathrm{PAR}\uparrow / \mathrm{PAR}\downarrow, \tag{3}$$

$$\rho_{NIR} = \mathrm{NIR}\uparrow / \mathrm{NIR}\downarrow, \tag{4}$$

where $R_s\uparrow$ is the upward shortwave radiation, $R_s\downarrow$ is the downward shortwave radiation, PAR$\uparrow$ is the upward visible radiation, PAR$\downarrow$ is the downward visible radiation, NIR$\uparrow$ is the upward near-infrared radiation, and NIR$\downarrow$ is the downward near-infrared radiation. The values of NIR$\uparrow$ and NIR$\downarrow$ are derived using the following equations:

$$\begin{aligned} \mathrm{NIR}\downarrow &\cong R_s\downarrow - \mathrm{PAR}\downarrow, \\ \mathrm{NIR}\uparrow &\cong R_s\uparrow - \mathrm{PAR}\uparrow. \end{aligned} \tag{5}$$

Finally, NDVI can be derived as:

$$\mathrm{NDVI} = \frac{\rho_{NIR} - \rho_{PAR}}{\rho_{NIR} + \rho_{PAR}}. \tag{6}$$

NDVI ranges from −1 to 1, and the vegetation activity (or chlorophyll density) increases as NDVI approaches 1.

The daily mean values of the three reflectance values (ρ_{Rs}, ρ_{PAR}, ρ_{NIR}) for the three heights were averaged when $R_s\downarrow$ exceeded 400 W m^{-2} at the upper (20.75 m) level, 35 W m^{-2} at the middle (10.70 m) level, and 10 W m^{-2} at the lower (0.90 m) level.

Measuring SPAD

SPAD is an index representing the relative chlorophyll density in a leaf. A SPAD sensor (SPAD-502, Minolta) was used to measure the difference in the absorption rates at 650 nm (red visible band; maximum absorption of chlorophyll) and 940 nm (near-infrared band; no absorption of chlorophyll). The correlation between SPAD and chlorophyll density is high and is represented by a second-order polynomial, which differs among tree species (Hoshino, personal communication). As we measured stomatal conductance using fixed plant bodies for the six species, we could detect seasonal variation in the chlorophyll density of each plant, using the separately measured values of SPAD for each plant.

SPAD was measured on the same day as the stomatal conductance. Additional SPAD measurements were made on 16, 18, 20, 24 April, 11 May, and 11 December

for the upper canopy (*Q. serrata*), 24 January and 26 February for the middle canopy (*E. japonica*, *I. pedunculosa*, and *V. bracteatum*), and 28 January and 27 February for the lower canopy (*L. japonicum* and *A. japonica*) to detect precise seasonal variation. Although different leaves were sampled for the stomatal conductance and SPAD measurements, both measurements were carried out on the same trees.

The numbers of sampled leaves were 6 for *A. japonica*, 8 for *L. japonicum*, and 9–12 for the other species. From January to March, only six leaves of evergreen species were sampled for the SPAD measurements. The leaves sampled for the SPAD measurements were cut and used to measure the leaf nitrogen content (described later). SPAD was measured just after cutting the leaf. For each leaf, 6–10 measurements were made and the averaged values were used in the analyses.

Measuring the leaf nitrogen content

The same leaves were used to measure the leaf nitrogen content and SPAD, although only three leaves of evergreen trees were measured from January to March. All the leaves sampled from January to September were stored frozen (below −40°C) until October 2001, when the leaf nitrogen content was measured for the first time.

First, the sampled leaves were used to measure leaf area (cm^2). Then, the leaves were dried for 3 days using a dryer at 60°C, and the dry leaves were weighed (mg). Finally, the leaves were ground into a powder.

The nitrogen content was preliminarily measured using an elemental analyzer (NA2500, Thermo-electron), which burned the powdered leaves and produced CO_2 and N_2. The gases were separated in an isolation column and analyzed using chromatographic techniques to measure the detection time differences and strength of each gas. Hippuric acid was used as the standard material for the nitrogen content analyses. Using the elemental analyzer, we measured the nitrogen contents of the samples obtained on 24 January, 26 February, and 27 April for *V. bracteatum*; 24 January, 26 February, and 4 June for *I. pedunculosa*; 24 January, 26 February, 4 June, 4 July, and 3 August for *E. japonica*; and 27 February and 9 July for *L. japonicum*. Unfortunately, when the carbon content of the leaves was high, the samples did not combust completely. Therefore, we could not determine precise nitrogen contents for the samples obtained on 27 April for *V. bracteatum*, 26 February for *I. pedunculosa*, and 4 July and 3 August for *E. japonica*.

We measured the nitrogen contents of the other samples using a CN analyzer (MT-700, Yanaco), which also burned the powdered leaves and produced CO_2 and N_2 separately. This analyzer was capable of burning materials containing more carbon. The analyzer measured the difference in the electrical resistance between completely CO_2-absorbed sample gas (containing N_2 gas from the samples) and the original sample gas (non-absorbed CO_2 and N_2 gas from the samples). Hippuric acid was also used as the standard material for the nitrogen content analyses.

Finally, we calculated the leaf nitrogen content per unit leaf area (area-based leaf nitrogen content; N_a) and that per unit leaf weight (mass-based leaf nitrogen content; N_m).

Stomatal conductance model

Jarvis-type stomatal conductance model

To quantify how environmental factors affect stomatal conductance, the experimental stomatal conductance model introduced by Jarvis (1976) is very useful and was therefore used here. This Jarvis-type model is a function of the incident photon flux density of PAR or PPFD, VPD, T, and soil water potential (Stewart 1988; Ogink-Hendriks 1995). Sirisampan et al. (2003) concluded that soil water potential could be removed from consideration at this observation site, since its effect was insignificant in predicting stomatal conductance. Therefore, the stomatal conductance model used here was

$$g_{sw} = g_{sw\,max}\, f(Q) f(D) f(T), \tag{7}$$

where g_{sw} is the stomatal conductance of water vapor (mol H_2O m^{-2} s^{-1}), g_{swmax} is the maximum stomatal conductance of water vapor (mol H_2O m^{-2} s^{-1}) and $f(Q)$ is a function of PPFD. $f(D)$ $f(T)$ is the total stress function, where $f(D)$ is the stress function for VPD and $f(T)$ is the stress function for T. The total stress function consists of those environmental factors that reduce the stomatal conductance below the value of the potential stomatal conductance at the current PPFD, g_{swmax} $f(Q)$. The values of the stress functions are between 0 and 1. If there are no limits on stomatal conductance, the stress function has a value of 1. When the value approaches 0, it means that the stress condition for stomatal conductance is increasing. With no stress factors, g_{sw} is represented by an original function of stomatal conductance as

$$g_{sw} = g_{sw\,max}\, f(Q). \tag{8}$$

An empirical model of Eq. 8 is a hyperbolic function of the maximum stomatal conductance at the current PPFD, which is given by

$$g_{sw} = \frac{g_{sw\,max}\, Q}{Q + (g_{sw\,max}/a)} \tag{9}$$

where g_{swmax} and a are fitted parameters representing the maximum of stomatal conductance and a curvature constant, respectively. Q is the incident photon flux density of PAR or PPFD (μmol photon m^{-2} s^{-1}).

There are several stress functions for $f(D)$, which have been derived by different scientists and in different years (Jarvis 1976; Farquhar 1978; Lohammer et al. 1980). We

used the following equation originally derived from Kosugi (1996) because it can represent both S-shaped and declining curves:

$$f(D) = \frac{1}{1 + (D/b)^c}. \quad (10)$$

Here, D is the vapor pressure deficit (kPa), and b and c are fitted parameters.

The stress function $f(T)$ is represented by

$$f(T) = \left(\frac{T - T_n}{T_o - T_n}\right)\left(\frac{T_x - T}{T_x - T_o}\right)^{\left(\frac{T_x - T_o}{T_o - T_n}\right)}, \quad (11)$$

where T is the air temperature (°C). T_n, T_o and T_x are fitted parameters representing the minimum, optimum, and maximum air temperatures for stomatal conductance, respectively. Here, we assumed $T_n = 0$°C and $T_x = 50$°C to reduce the degrees of freedom of the model.

Parameter fitting

The parameters in Eqs. 9, 10 and 11, i.e., g_{swmax}, a, b, c, and T_0 were determined for each of the six species. The parameters for *Q. serrata* were separated for sunlit and shaded leaves, since PPFD differed considerably. Observed hourly values of Q, D, T, and g_{sw} were used to determine the parameters.

We used nonlinear optimization with the quasi-Newtonian procedure in Microsoft Excel for parameter fitting. The observed data for each species were parameterized separately using this procedure.

From the parameterization results, the fitted parameters for each species were combined with the hourly averages of the environmental data in the model to calculate the stomatal conductance at 1-h intervals. The estimated stomatal conductance for *Q. serrata* was separated into sunlit and shaded leaves.

The model was validated by comparing the model output with variables measured independently (Forrester 1961; Innis 1974) to evaluate its performance. The well-known statistical coefficient of determination (R^2) is widely used for validation, and is calculated as

$$R^2 = 1 - \frac{\sum (y_i - \hat{y}_i)^2}{\sum (y_i - \bar{y})^2}, \quad (12)$$

where y_i is the observed value, $\hat{y}_i$ is the predicted value of y for the model, and $\bar{y}$ is the average of the observed values. The model was validated using both R^2 and plots of observed values against the estimated values.

Results

Stomatal conductance

In considering light exposure, the plants were separated into sunlit and shaded plants. The sunlit plants, i.e., *Q. serrata*, had the greatest exposure to radiation, while the shaded plants were all shaded by sunlit plants, i.e., all the other species. Moreover, the *Q. serrata* leaves exposed to irradiance were regarded as sunlit leaves, whereas all the remaining leaves, including *Q. serrata* leaves that were shaded, were referred to as shaded.

Diurnal variation

The diurnal variation in stomatal conductance exhibited identical phenomena for all of the plant species and heights studied, with a rise in the morning and a fall in the afternoon. The diurnal maximum stomatal conductance was at 1200 ± 3 h each day, although most of the peaks were from 1000–1100 h for all the species except *Q. serrata*. Sunlit leaves of *Q. serrata* had the largest diurnal variation in stomatal conductance. The stomatal conductance in various species differed only slightly when they were at the same canopy level.

The diurnal variation in PPFD for the sampled leaves was similar to that for the stomatal conductance and rose in the morning and declined in the afternoon. The PPFD of sunlit leaves underwent an extremely large diurnal change, while the diurnal change of shaded leaves was small, including the shaded leaves of sunlit *Q. serrata*. The shaded lower leaves had an incident PPFD only 1/15 that of sunlit leaves on average. The measurements showed that leaf position and leaf angle also affected the PPFD differences, although the measurements were made at the same time and height. PPFD in the lower canopy underwent greater diurnal variation in winter when the upper canopy was open (no leaves), as well as in early spring when the upper-canopy leaves were still small. Occasional rays of sunlight reached the lower canopy, producing distinct high PPFD.

The middle canopy *V. bracteatum* showed large diurnal variation in stomatal conductance when the *Q. serrata* in the upper canopy had no leaves. Once the upper-canopy leaves fell, this species behaved like an upper-canopy plant. The high diurnal variation in air temperature tended to be influenced by the incident PPFD, since T is dependent on the irradiance.

VPD increased gradually in the morning and began to decrease rapidly in late afternoon after reaching a maximum. VPD at the upper-canopy plant, *Q. serrata*, reached its maximum earlier in the morning and began to decline in late afternoon. In other words, VPD in the upper canopy rose more sharply than in the lower canopy. In the understory, VPD was very small, and during periods of low temperature, the diurnal changes were stable.

Seasonal variation

The greatest stomatal conductance seen in this study (0.24 mol H_2O m^{-2} s^{-1}) was for sunlit leaves of *Q. serrata* in June, while the greatest conductance of shaded leaves was less than 0.15 mol H_2O m^{-2} s^{-1} (see Fig. 7a,

b). Sirisampan et al. (2003) found that the peak stomatal conductance occurred in August for sunlit leaves of *Q. serrata* and *V. bracteatum*, and in March for the remaining shaded leaves. They also found that shaded leaves had low stomatal conductance and less variability during the season when *Q. serrata* was foliated. Those tendencies matched those obtained here.

Sunlit leaves of *Q. serrata* had distinctly greater stomatal conductance than the shaded leaves throughout the foliated period. This matched their exposure to light. The exception was in May, when the leaves of *Q. serrata* were very new, and their conductance was small and insensitive to PPFD. Sirisampan et al. (2003) made similar observations and postulated that it was caused by insufficient growth of the stomata. Interestingly, the stomatal conductance of both sunlit and shaded *Q. serrata* observed in November and December was large, while the transpiration and photosynthesis rates were small. Sirisampan et al. (2003) measured relatively larger stomatal conductances for shaded leaves during the leaf-fall season at this site. Turner and Heichel (1977) and Abrams (1988) revealed that stomatal conductance dropped suddenly between the senescence to leaf-fall seasons after yellow spots appeared on the leaves. Our results differed from those studies. The greater stomatal conductance during the fall at this site might be owing to the "dull-leaf" phenomenon. Other possible reasons are proposed in the section "Estimating stomatal conductance using a Jarvis-type model with SPAD parameterization."

The stomatal conductance of shaded leaves of *Q. serrata* was as small as that of middle-canopy plants, although it increased gradually after the beginning of leaf fall in October (Fig. 7b) with the increased light transmission. Sirisampan et al. (2003) also observed this phenomenon. *V. bracteatum*, a middle- to upper-canopy plant, was intermediate in terms of the magnitude of the daily average stomatal conductance and the seasonal variability, particularly from summer to winter. Likewise, the other middle-canopy species (*I. pedunculosa* and *E. japonica*) had the minimum conductance in summer, when the upper canopy intercepted light transmissions, and this increased from autumn through winter. This seasonal variation was caused by the increasing light transmission owing to the decrease in the number of leaves (or LAI) of *Q. serrata*. The seasonal trend for the lower-canopy trees was similar to that of *I. pedunculosa* and *E. japonica*.

As Sirisampan et al. (2003) pointed out, PPFD affects stomatal conductance in all species. As with the other environmental factors, VPD was higher at the upper canopy than at the lower canopy. How the environmental factors affect stomatal conductance is analyzed in section "Estimating stomatal conductance using a Jarvis-type model".

Since the different patterns of leaf age affect the physiological activities of evergreen and deciduous plants differently (Mooney and Gulmon 1982), an analysis of leaf age should be considered separately. For the deciduous species *Q. serrata* studied here, the maximum stomatal conductance occurred a few months after full leaf expansion. This result agreed with those of Turner and Heichel (1977), Abrams (1988), and Sirisampan et al. (2003), who found that the maximum stomatal conductance in *Quercus* species occured 1 or 2 months after full leaf expansion.

For evergreen plants, Sirisampan et al. (2003) found little difference in the stomatal conductance of leaves from various shooting years after full leaf expansion, except in the early spring. Old leaves exposed to high light intensities in early spring had higher conductance than younger leaves. Subsequently, these leaves aged (turned yellow-brown color) and fell over the next 2 months. New light-green leaves that grew in spring had lower conductances than older leaves.

Canopy-scale fluxes of heat and CO_2

The seasonal variation in the heat balance components for 2001 is shown in Fig. 1. The daily mean net radiation (R_n) increased gradually from the beginning of January through August and decreased from September through December. The daily mean soil heat fluxes (G) were constantly low (nearly zero). The daily mean sensible heat flux was highest while the latent heat flux was still small in the middle of April [around day 100 of the year (DOY)], when the upper-canopy trees (*Q. serrata*) began to foliate. After foliation of the upper-canopy trees (110 DOY), the latent heat flux increased and was highest in July. In the beginning of September (245 DOY), the latent heat flux dipped with the decrease in the net radiation caused by continuous rainfall.

The seasonal variation in the CO_2 flux (NEE) is shown in Fig. 2. The daily mean NEE was positive (net source of CO_2) in January, February, and December, and nearly zero with day-to-day fluctuations in March and April (up to 100 DOY). After the end of April (110 DOY), NEE decreased suddenly (increased uptake) and was minimal (maximum uptake) in the middle of May. NEE diminished gradually from the middle of May through the beginning of November, and then decreased suddenly. The seasonal trend was similar to that of the canopy-scale NDVI of the upper-canopy trees (Fig. 3, described below). Therefore, the canopy-scale values of NEE were mostly dependent on the upper-canopy trees. The sudden drop in NEE might be caused by the decrease in the chlorophyll density (or SPAD; Fig. 4) or leaf nitrogen content (Fig. 5). The timing of this sudden drop in NEE was not synchronized with the decrease in LAI (i.e., leaf-fall time), which occurred a few weeks after the drop in NEE.

Canopy-scale NDVI

The seasonal variation in the canopy-scale NDVI is shown in Fig. 3. There was clear seasonal variation in

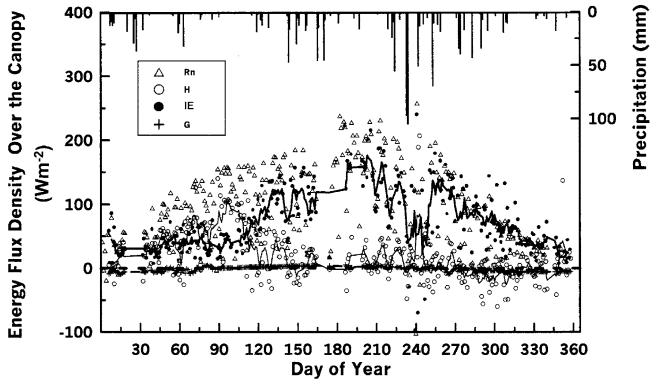

Fig. 1 Seasonal variation in the daily mean flux densities of the net radiation (R_n), sensible heat flux (H), latent heat flux (lE), and soil heat flux (G). The *points* plotted for each flux represent the daily mean values of the flux densities. *Thick* and *thin solid lines* show the 5-day running averages of the latent and sensible heat fluxes, respectively. The figure also shows the daily precipitation

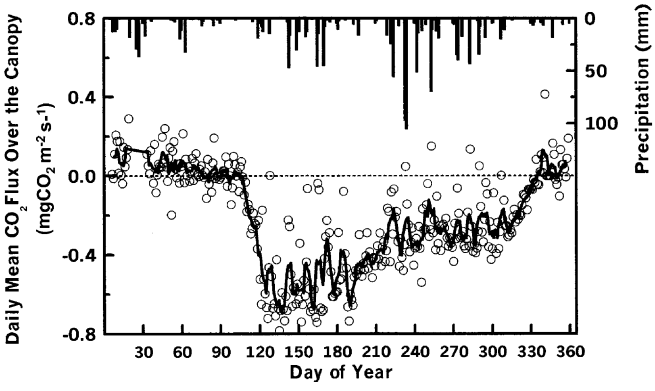

Fig. 2 Seasonal variation in the daily mean CO_2 flux (NEE) over the canopy. *Open circles* represent daily mean values and the *solid line* shows the 5-day running average of the fluxes. The figure also shows the daily precipitation

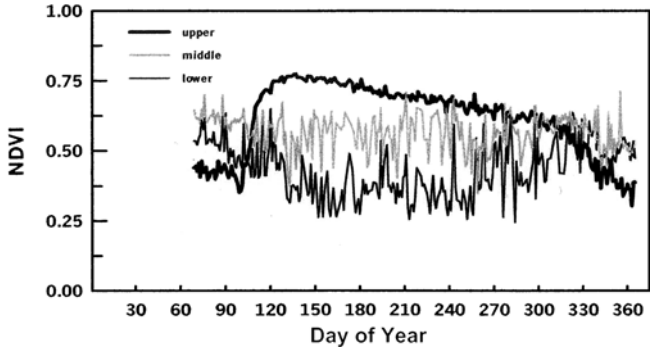

Fig. 3 Seasonal variation in the normalized difference vegetation indexes (NDVI) of the upper (*thick line*), middle (*gray line*), and lower (*thin line*) canopies

the NDVI for the upper canopy, which corresponded well with that in the latent heat flux (Fig. 1) and NEE (Fig. 2). The minimum seen at 100 DOY was due to silky soft hairs that covered the young leaves just after *Q. serrata* foliated. The presence of silky soft hairs on the *Q. serrata* leaves matched the peak in ρ_{PAR} just after foliation (not shown). Interestingly, ρ_{PAR} decreased a few days after the peak. These phenomena might be correlated with physiological tactics just after the foliation of *Q. serrata* to prevent PAR absorption (described in section "Estimating stomatal conductance using a Jarvis-type model with SPAD parameterization"). Subsequently, the NDVI of the upper canopy increased suddenly owing to leaf expansion (from 110 DOY). It then deceased gradually until the beginning of November (310 DOY), and then decreased suddenly until 340 DOY. The sudden decrease in November and December corresponded to the decreases in SPAD (Fig. 4) and leaf nitrogen content (Fig. 5).

For the middle canopy, NDVI was relatively constant. NDVI decreased from 130 to 140 DOY owing to new leaf shootings on the evergreen trees. It was difficult to observe trends in the lower canopy NDVI, because the reflectance values of ρ_{PAR} and ρ_{NIR} were on the same order of magnitude as the error.

SPAD

The seasonal variation in SPAD for the six species is shown in Fig. 4. The upper trees (*Q. serrata*) were separated into sunlit and shaded leaves. SPAD was higher for shaded leaves than sunlit leaves for the entire season. This means that shaded leaves contained much more chlorophyll than sunlit leaves. Some previous studies reported that the area-based amount of chlorophyll in sunlit leaves exceeded that of shaded leaves in most plant species (Lichtenthaler et al. 1981; Hoflacher and Bauer 1982). However, several studies indicate that shaded leaves contain more chlorophyll than sunlit leaves. There was a clear seasonal change in SPAD for *Q. serrata*: SPAD was low during leaf expansion, high when the leaves were mature, and dropped suddenly with senescence. The low SPAD during leaf expansion means that leaves contain little chlorophyll at this time, making it difficult to capture PPFD. During the senescence season, the between-leaf differences in SPAD were relatively large.

For the middle-canopy species, SPAD was highest in *E. japonica*, followed by *V. bracteatum*, and *I. pedunculosa* in turn, and showed similar seasonal changes. Note that the SPAD for all the middle-canopy species was lowest in June (around 160 DOY). This is because new leaves sprouted in this season. The standard deviations of the measurements were the largest at this time. As the new leaves changed color, the SPAD gradually increased, reaching in November the values seen in the previous January. The large SPAD in winter, i.e., when *Q. serrata* is not foliated, might be a strategy allowing middle-canopy tree species to catch PPFD.

For the lower-canopy species, SPAD was higher in *L. japonica* than in *A. japonica* year-round. There was no

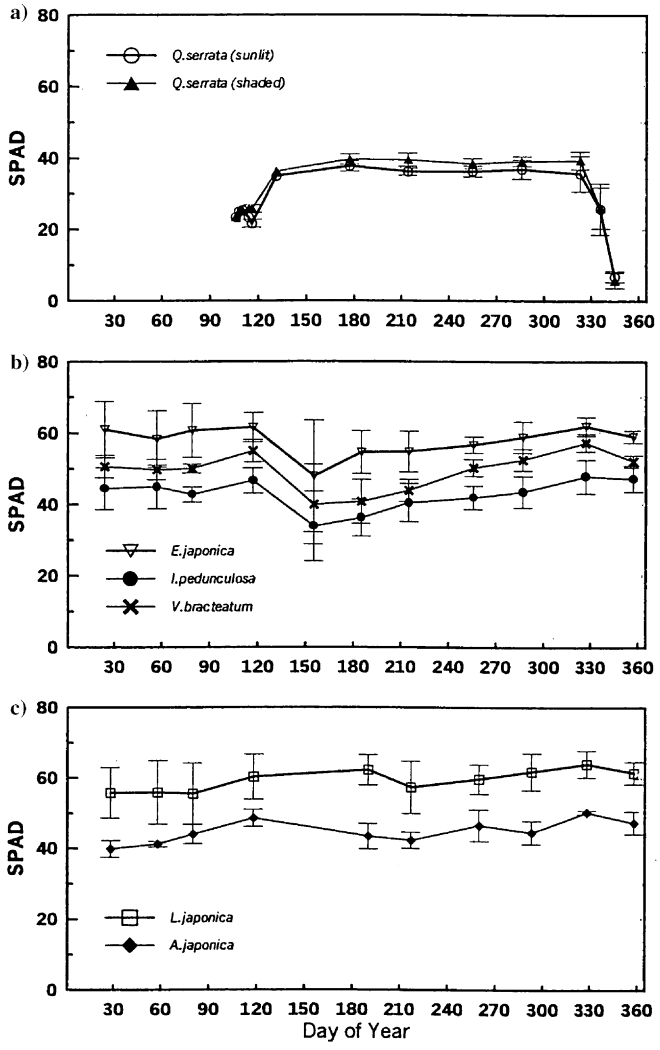

Fig. 4 Seasonal variation in SPAD for the **a** upper-, **b** middle-, and **c** lower-canopy trees. The upper-canopy trees (*Q. serrata*) were divided into sunlit and shaded leaves. The *vertical bars* represent standard deviation

significant seasonal variation in the lower-canopy trees, although the SPAD in June may have been low, as occurs in the middle canopy (there were no data for June). Note that we cannot compare the absolute amount of chlorophyll across species based on the SPAD.

Leaf nitrogen content

The seasonal variation in the area-based leaf nitrogen content (N_a) for the six species is shown in Fig. 5. The upper trees (*Q. serrata*) were separated into sunlit and shaded leaves. For *Q. serrata*, N_a differed from SPAD. After leaf foliation up to 130 DOY, N_a was typically high. As the majority of leaf nitrogen is in chlorophyll (Evans 1989), the seasonal variation in N_a and SPAD should be similar. In fact, their behaviors were opposite from leaf foliation until 130 DOY. N_a might be high in this season owing to the small leaf area of *Q. serrata* at this time. From 131 DOY (11 May) to 345 DOY (11 December), the seasonal change in N_a was similar to that of SPAD. For the period when N_a was constant, the N_a of sunlit leaves was higher than that of shaded leaves because the sunlit leaves were thicker than the shaded leaves, although the leaf area did not differ significantly (see below).

The seasonal trend in the mass-based leaf nitrogen content (N_m) was similar to that of N_a for *Q. serrata*. In particular, N_m was higher from leaf foliation until 130 DOY, after which it remained constant before dropping in the fall (figures not shown). However, N_m was higher in shaded leaves than in sunlit leaves, again because the sunlit leaves were thicker than the shaded leaves, i.e., the specific leaf area (SLA) of sunlit leaves was smaller than that of shaded leaves (Fig. 6).

The seasonal changes in N_a for the middle-canopy plants were similar in *V. bracteatum*, *I. pedunculosa*, and *E. japonica* (Fig. 5). Conversely, although N_m was similar in *I. pedunculosa* and *E. japonica*, it was higher in *V. bracteatum* year-round (figures not shown) because *V. bracteatum* leaves are thinner than those of the other two plants, i.e., the SLA of *V. bracteatum* leaves was larger than that of the leaves of *I. pedunculosa* and *E. japonica* (Fig. 6).

There were no significant seasonal trends in N_a or N_m for the lower-canopy plants. *A. japonica* had a lower N_a, but a higher N_m compared with *L. japonica* year-round because *A. japonica* had a large SLA (Fig. 6).

Discussion

Estimating stomatal conductance using a Jarvis-type model

Our Jarvis-type model used three environmental functions to predict stomatal conductance: PPFD, T, and VPD (see sections "Jarvis-type stomatal conductance model" and "Parameter fitting"). The fitted results for the five parameters with R^2 are shown in Table 1. The maximum R^2 was 0.77 (*I. pedunculosa*), and the minimum was 0.31 (shaded leaves of *Q. serrata*). To validate our Jarvis-type model of stomatal conductance, the observed and estimated stomatal conductances were compared (figures not shown). The fitted parameters for the model were substituted into the equations and the curves were drawn in order to see whether the stomatal conductance responded to each environmental factor in various plants.

The stomatal conductance–light response curves differed considerably between sunlit and shaded species [Table 1; a and g_{swmax} $f(Q)$]. With respect to the light response curves of stomatal conductance, sunlit leaves had a higher maximum stomatal conductance (g_{swmax}) than shaded leaves, perhaps because of their greater response to gas transfer. However, shaded leaves had low light saturation relative to sunlit leaves. In other

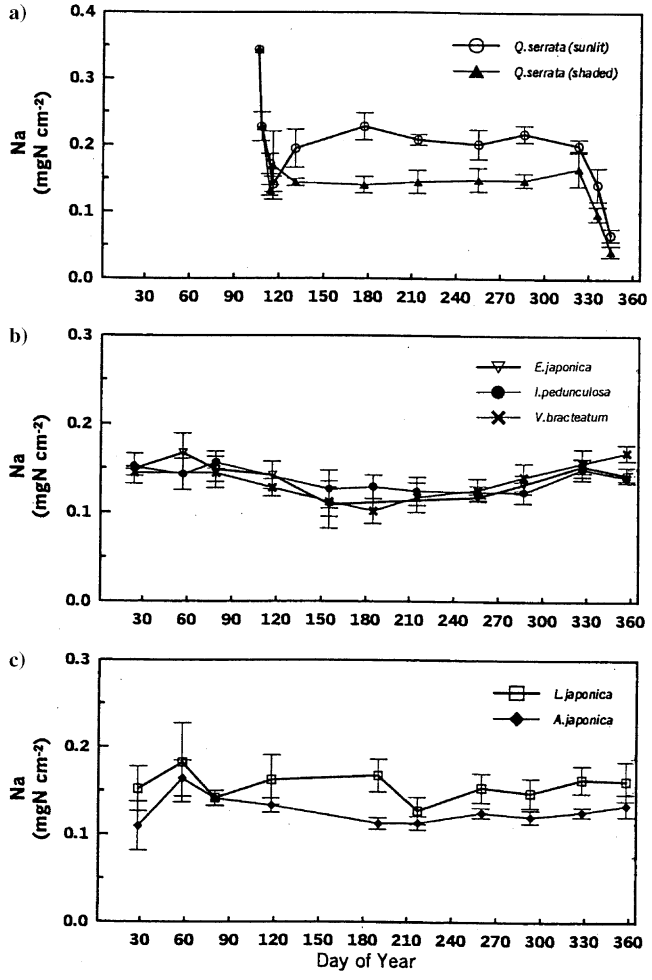

Fig. 5 Seasonal variation in the leaf nitrogen content based on leaf area (N_a) for the **a** upper-, **b** middle-, and **c** lower-canopy trees. The upper-canopy trees (*Q. serrata*) were divided into sunlit and shaded leaves. The *vertical bars* represent the standard deviation

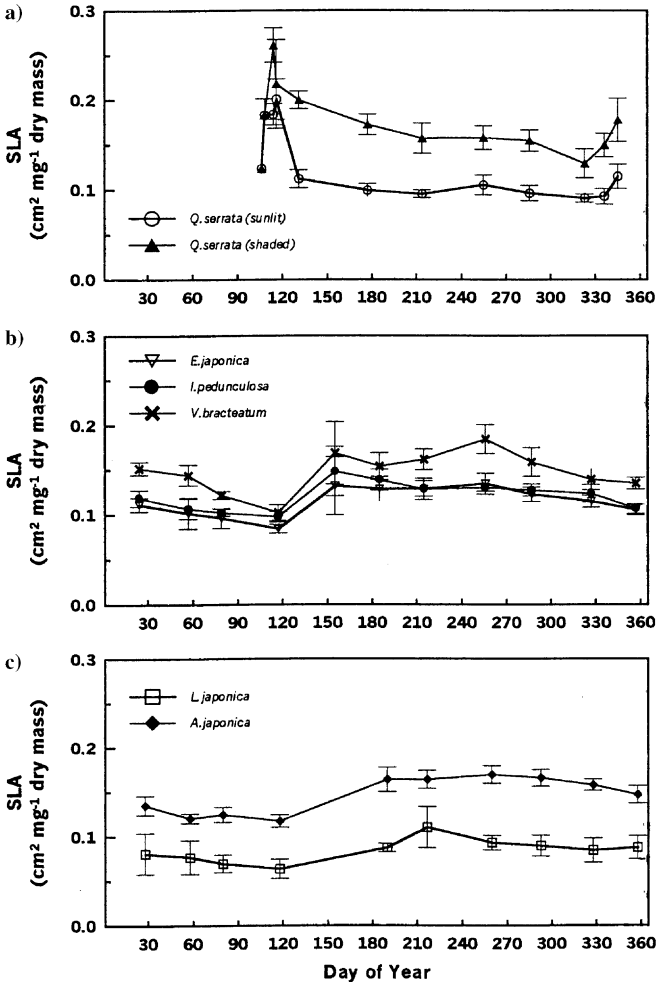

Fig. 6 Seasonal variation in the specific leaf area (SLA) for the **a** upper-, **b** middle-, and **c** lower-canopy trees. The upper-canopy trees (*Q. serrata*) were divided into sunlit and shaded leaves

words, shaded leaves could reach their maximum stomatal conductance at lower light intensities than sunlit leaves. Accordingly, the initial slopes (*a*; quantum yield) were higher for shaded leaves than for sunlit leaves. Sirisampan et al. (2003) reached similar conclusions. The nature of these differences has been studied widely for photosynthetic approaches, but not for stomatal conductance, and has been studied most thoroughly using leaves of the same plant that have been produced under either low or high light intensities. Shaded leaves do not have the capacity to use up the excess energy via the xanthophyll cycle, thus the light energy trapped by shaded leaves under intense light cannot be used fully for photosynthesis. Moving a shaded leaf directly into the sun can damage the photosynthetic system (photo-inhibition) (Demmig-Adams and Adams 1992).

These results are similar to the photosynthetic behavior of sunlit and shaded plants. Sunlit plants have a higher maximum rate of photosynthesis and light saturation than shaded plants, while the quantum yield of sunlit plants is lower than that of shaded plants (Lüttge 1985). Other studies have found that the quantum yield of photosynthesis of sunlit and shaded leaves is the same, particularly in the same species (Björkman et al. 1972; Björkman 1981).

The optimum temperature (T_o) of sunlit leaves in *Q. serrata* and of the middle-canopy plants was higher than for shaded leaves in *Q. serrata* and lower-canopy plants. T_o of the lower-canopy plants was 10°C lower than for sunlit leaves in *Q. serrata* and middle-canopy plants. The fitted parameters were reasonable for the environmental conditions.

Note that the model produces overestimates for April and underestimates for June for almost every species, probably because it does not include physiological factors, such as leaf age. Sirisampan et al. (2003) had similar results, but they found that the overestimation occurred in May. As described before, from late April to May, new leaves showed reduced stomatal conductance compared with other seasons. Larcher (1994) suggested that stomatal conductance was affected by both environmental and physiological factors, such as plant

Table 1 Parameter sets fitted for the stomatal conductance model without SPAD parameterization together with the coefficient of determination (R^2)

	R^2	g_{swmax}	a	b	c	T_o
Q. serrata (sunlit)	0.345	0.4627	0.00573	15.090	0.7876	38.82
Q. serrata (shaded)	0.309	0.2335	0.02694	11.974	1.1748	34.01
V. bracteatum	0.415	0.1978	0.01640	26.688	1.6275	39.88
I. pedunculosa	0.774	0.2117	0.01378	14.183	1.6595	38.29
E. japonica	0.530	0.2509	0.02800	14.023	1.6871	38.99
A. japonica	0.632	0.1378	0.04669	10.855	2.2304	31.49
L. japonica	0.514	0.0611	0.06048	16.261	2.4534	27.71

hormones. Although measuring hormone levels is relatively difficult, if the model included a physiological stress factor for leaf age, this overestimate might not occur.

Estimating stomatal conductance using a Jarvis-type model with SPAD parameterization

In this section, we incorporate physiological factors representing leaf age in the Jarvis-type model in order to estimate stomatal conductance better. The Jarvis-type stomatal conductance model includes various environmental factors that are insufficient to explain all the stomatal conductance behaviors. We hypothesized that stomatal conductance is also controlled by physiological factors, such as leaf age.

Based on the results shown in sections "SPAD" and "Leaf nitrogen content", N_a or N_m cannot represent chlorophyll density directly. Conversely, based on the seasonal variation in the canopy-scale NDVI (see section "Canopy-scale NDVI"), SPAD can represent the seasonal variation in chlorophyll density, because SPAD was low in the leaf-expansion season for almost all of the species and in the senescence season for the deciduous plant *Q. serrata*. Therefore, SPAD was included in the Jarvis-type model. Fortunately, measuring SPAD is relatively easy compared with measuring the leaf nitrogen content.

As SPAD is a parameter that represents the acquisition of light at the leaf surface, we incorporated it in the hyperbolic function for the maximum stomatal conductance at the current PPFD (Eq. 9). A new parameter $\mathrm{SPAD}/\mathrm{SPAD}_{max}$ was multiplied by Q in $f(Q)$ to represent the acquisition intensity of PAR. Therefore, g_{swmax} $f(Q)$ in Eq. 9 can be recast as

$$g_{sw\,max}\, f(Q) = \frac{g_{sw\,max}(\mathrm{SPAD}/\mathrm{SPAD}_{max})Q}{(\mathrm{SPAD}/\mathrm{SPAD}_{max})Q + (g_{sw\,max}/a)}, \quad (13)$$

where SPAD is the measured value and SPAD_{max} is the annual maximum value. When SPAD equaled SPAD_{max} on a given measurement day, the leaves had the maximum ability to acquire light.

All the data were again fitted in the model using the same procedures as for the normal Jarvis model, and the five parameters (g_{swmax}, a, b, c, and T_o) were again determined. Using Eq. 13, the estimated results improved somewhat for sunlit ($R^2 = 0.368$) and shaded ($R^2 = 0.329$) leaves of *Q. serrata*, *V. bracteatum* ($R^2 = 0.418$), *I. pedunculosa* ($R^2 = 0.778$), *E. japonica* ($R^2 = 0.534$), and *L. japonica* ($R^2 = 0.520$). However, *A. japonica* ($R^2 = 0.630$) produced somewhat lower results. The five fitted parameters changed slightly, but the differences were not pronounced (Table 2).

One possible reason why the estimates for *Q. serrata* did not change much is that the observed stomatal conductance in December was unexpectedly large (Fig. 7a, b). Turner and Heichel (1977) and Abrams (1988) found that stomatal conductance dropped suddenly from the senescence to the leaf-falling seasons after yellow spots appeared on the leaf surface. Our results differed from theirs. In this season, the observed rates of photosynthesis and transpiration were small, despite the large stomatal conductance. In addition, the obtained values of VPD and the difference between the atmospheric CO_2 concentration and the CO_2 concentration within the stomata were small. A small difference between the atmospheric CO_2 concentration and the CO_2 concentration within the stomata is reasonable, owing to the small rate of photosynthesis even with a large stomatal conductance. This large stomatal conductance might be owing to the dull-leaf phenomenon. Conversely, the chlorophyll density decreased based on the SPAD measurements (Fig. 4), and N_a decreased (Fig. 5). Therefore, the physiological activity was low during this season. The decrease in these physiological activities is consistent with data obtained for the canopy-scale CO_2 flux (NEE) and NDVI. Therefore, we cannot find any reasons not to include the SPAD when modeling the stomatal conductance to include a leaf-age effect.

Another possible reason why the estimates for *Q. serrata* did not change markedly is that the observed stomatal conductance in late April was unexpectedly small (Fig. 7a, b). As described in section "Canopy-scale NDVI", the ρ_{PAR} peaked just after foliation, while the upper-canopy NDVI dropped slightly at the same time (Fig. 3). This means that the ability of *Q. serrata* to absorb PAR was very small in this season. The existence of silky soft hairs on the *Q. serrata* leaves might be the reason; this postulate is supported by the peak in ρ_{PAR} just after foliation. These phenomena might be correlated with physiological tactics just after the foliation of *Q. serrata* to prevent PAR absorption. These tactics

Table 2 Parameter sets fitted for the stomatal conductance model with SPAD parameterization together with the coefficient of determination (R^2)

	R^2	g_{gwmax}	a	b	c	T_o
Q. serrata (sunlit)	0.368	0.4299	0.00667	18.956	0.9052	41.26
Q. serrata (shaded)	0.329	0.2771	0.02844	11.283	1.2908	35.87
V. bracteatum	0.418	0.2025	0.01996	26.748	1.5549	39.98
I. pedunculosa	0.778	0.2124	0.01565	14.158	1.6127	38.83
E. japonica	0.534	0.2794	0.03476	11.984	1.5309	39.02
A. japonica	0.630	0.1449	0.05206	10.624	2.2190	32.44
L. japonica	0.520	0.0614	0.06066	16.312	2.4652	27.80

might be designed to prevent exposure to excess PAR in order to protect photosynthetic pigments and thylakoid disks (membrane) (Larcher 1994). Just after foliation, the photosynthetic system might be damaged if strong PAR strikes the leaf because the cuticular layer on the leaf surface is not fully developed. This results in a

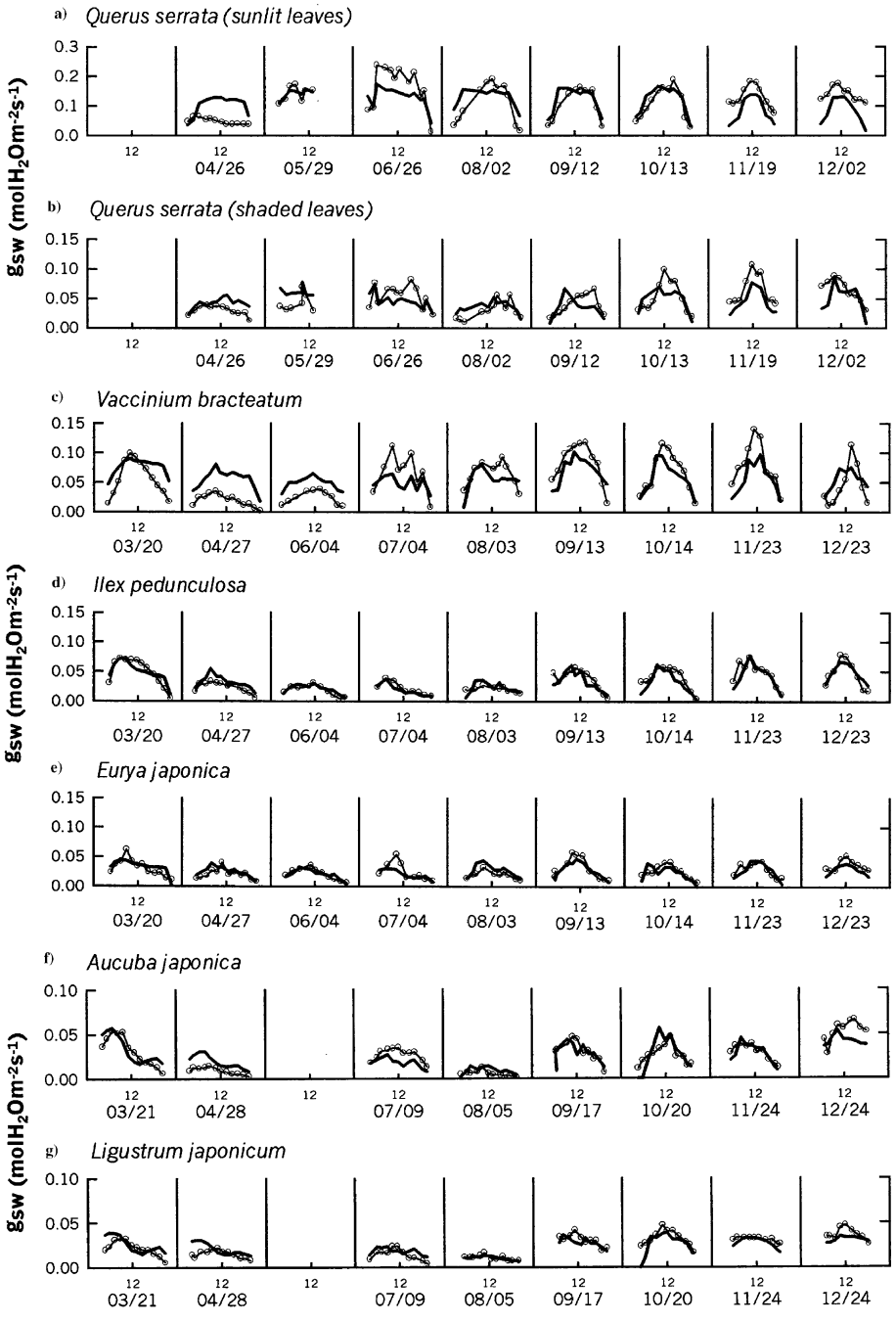

Fig. 7a–g Observed (*open circles with thin lines*) and estimated (*thick lines*) stomatal conductance using the model with SPAD parameterization. The upper-canopy trees (*Q. serrata*) were divided into **a** sunlit and **b** shaded leaves

smaller stomatal conductance. Other possible reasons for the small stomatal conductance in April might be insufficient growth of stomata or low activation of photosynthetic enzymes despite the large amount of nitrogen in the *Q. serrata* leaves. As described in the section "Leaf nitrogen content", most of the leaf nitrogen is in chlorophyll (Evans 1989). Therefore, the seasonal variations in N_a and SPAD should show similar tendencies. However, their behaviors were opposite from leaf foliation until 130 DOY. These opposite tendencies might arise if there is insufficient growth of stomata or low activation of photosynthetic enzymes. Under such conditions, there is no need to open the stomata of *Q. serrata* because the ability of CO_2 absorption is nearly zero, while the H_2O loss is large. Consequently, the stomatal conductance might be smaller. These results correspond well with the canopy-scale data for the latent heat and CO_2 fluxes and NDVI (as described in sections. "Canopy-scale fluxes of heat and CO_2" and "Canopy-scale NDVI").

Strictly speaking, it was difficult for the SPAD meter to measure the canopy-scale SPAD, including the effect of silky soft hairs on the leaf surface of *Q. serrata*, because the SPAD meter held the leaves tightly. Therefore, the actual SPAD might be significantly lower than the measured value, because the upper-canopy ρ_{PAR} was large (i.e., the upper-canopy NDVI was small) just after foliation (Fig. 3).

For the middle- and lower-canopy species, except *A. japonica*, inclusion of SPAD in the Jarvis-type model gave a better estimate of stomatal conductance (Tables 1, 2). Therefore, SPAD (or chlorophyll density) appears to be a new measure representing stomatal conductance in evergreen species.

In the future, in order to better estimate the stomatal conductance for deciduous species, such as *Q. serrata*, other physiological parameters than chlorophyll density and leaf nitrogen content should be included in the conductance model. In nature, it is very difficult to discover which factors influence plant activities because leaf age changes in parallel with environmental changes. The most appropriate age is also the most appropriate environment. At any rate, Larcher (1994) suggested that stomatal conductance was affected by both environmental and physiological factors, such as plant hormones. Physiological parameters must be included in the model in the hyperbolic function of the maximum stomatal conductance, g_{swmax}.

Conclusions

We tried to quantify stomatal conductance in a CO_2-fertilized warm-temperate forest, using a Jarvis-type model, while considering both environmental variables and physiological factors. This study considered (1) the characteristics of the diurnal and seasonal variation, (2) simultaneous measurements with the canopy-scale fluxes of heat and CO_2, and NDVI, (3) the stomatal conductance of sunlit and shaded leaves, (4) a stomatal conductance model, and (5) the effects of leaf age on stomatal conductance.

Sunlit leaves had the largest stomatal conductance in terms of both the magnitude and variability of the diurnal and seasonal variation, whereas shaded leaves had only a small variation in conductance.

No significant differences in the seasonally observed stomatal conductance or leaf-level exchange rates of H_2O and CO_2 were detected for 1998 and 2001.

The Jarvis-type model overestimated stomatal conductance while new leaves were sprouting in spring. Therefore, we incorporated SPAD in the model as an easily measured representative of chlorophyll density. As SPAD represents the acquisition of light on the leaf surface, it was used in the hyperbolic function of the maximum stomatal conductance for the current PPFD. However, the estimates for *Q. serrata* did not change much compared with estimates using only environmental factors. The negative correlation between stomatal conductance and SPAD during the senescence season was thought to be one reason. Other possible reasons were that the SPAD sensor could not detect the chlorophyll density owing to the existence of silky soft hairs covering young leaves just after the foliation of *Q. serrata*, or that enzyme activation was low during this season despite the high nitrogen content.

Canopy-scale data, such as the heat and CO_2 exchanges (fluxes) and upper-canopy NDVI, corresponded with the upper-canopy characteristics of leaves, except for the stomatal conductance in the leaf-fall season in this forest.

Although leaves of evergreen plants, which sprouted in different years have similar stomatal conductances (Sirisampan et al. 2003), the estimates for evergreen species using SPAD were slightly better than those using environmental factors only. Perhaps the model can be improved if it includes other physiological factors (e.g., hormones) as limiting factors in g_{swmax}.

Acknowledgements We thank Prof. Fukushima at the Research Institute for Humanity and Nature, and our colleagues in the Laboratory of Eco-Hydrometeorology at the Hydrospheric-Atmospheric Research Center, Nagoya University, for their useful comments and discussion. We also thank Dr. Konohira of Nagoya University and Dr. Shimoyama of the National Institute for Environmental Studies, for their help with the field measurements and discussion. In addition, we thank the anonymous reviewers for their time and patience in helping to improve this study significantly. This research was financially supported, in part, by Grants-in-Aid from the Ministry of Education, Culture, Sports, Science, and Technology of Japan (Grant Nos. 11213209, 11480130, and 14206018).

References

Abrams MD (1988) Comparative water relations of three successional hardwood species in central Wisconsin. Tree Physiol 4:263–273

Aoki H (1997) Bi-weekly variations of stable carbon isotopic composition within tree rings using the shot pinning method and their correlation with environmental factors. MS Dissertation, Graduate School of Sciences, Nagoya University

Björkman O (1981) Responses to different quantum flux densities. In: Lange OL, Nobel PS, Osmond CB, Ziegler H (eds) Encyclopedia of plant physiology, new series, vol 12A. Springer-Verlag, Berlin, pp31–45

Björkman O, Boardman NK, Anderson JM, Thorne SW, Goodchild DJ, Pyliotis NA (1972) Effect of light intensity during growth of *Atriplex patula* on the capacity of photosynthetic reactions, chloroplast components and structure. Carnegie Inst Yearbook 71:115–135

Cox PM (2001) Description of the TRIFFID dynamic global vegetation model. Hadley Centre Tech Note 24:1–16

De Pury DGG, Farquhar GD (1997) Simple scaling of photosynthesis from leaves to canopies without the errors of big-leaf models. Plant Cell Env 20:537–557

Demmig-Adams B, Adams WW III (1992) Photoprotection and other responses of plants to high light stress. Annu Rev Plant Physiol Mol Biol 43:599–626

Evans JR (1989) Photosynthesis and nitrogen relationship in leaves of C3 plants. Oecologia 78:9–19

Farquhar GD (1978) Field found response of stomata to humidity. Aust J Plant Physiol 5:787–800

Foley JA, Prentice IC, Ramankutty N, Levis S, Pollard D, Sitch S, Haxeltine A (1996) An integrated biosphere model of land surface processes, terrestrial carbon balance, and vegetation dynamics. Global Biogeochem Cycles 10:603–628

Foley JA, Levis S, Prentice IC, Pollard D, Thompson SL (1998) Coupling dynamic models of climate and vegetation. Global Change Biol 4:561–579

Forrester JW (1961) Industrial dynamics. MIT Press, Cambridge, MA

Hoflacher H, Bauer H (1982) Light acclimation in leaves of the juvenile and adult life phases of ivy (*Hedera helix*). Physiol Plant 56:177–182

Innis GS (1974) A spiral approach to ecosystem simulation, I. In: Innis GS, O'Beukk RV (eds) Systems analysis of ecosystem. International Cooperative Publishing House, Fairland, MD, pp 211–386

Jarvis PG (1976) The interpretation of the variations in leaf water potential and stomatal conductance found in canopies in the field. Phil Trans R Soc Lond B 273:593–610

Jones HG (1992) Plants and microclimate: a quantitative approach to environmental plant physiology. Cambridge University Press, Cambridge

Kaimal JC, Finnigan JJ (1994) Atmospheric boundary layer flows: their structure and measurement. Oxford University Press, New York

Kosugi Y (1996) Leaf-scale analysis of the CO_2 and H_2O exchange processes between trees and the atmosphere. PhD Thesis, Kyoto University

Larcher W (1994) Ökophysiologie der Pflanzen, 5. Auflage. Eugen Ulmer, Stuttgart, Germany

Lichtenthaler HK, Buschman C, Döll M, Fietz HJ, Bach T, Kozel U, Meier D, Rahmsdorf U (1981) Photosynthetic activity, chloroplast ultrastructure, and leaf characteristics of high-light and low-light plants and of sun and shade leaves. Photosynth Res 2:115–141

Lohammer T, Linder S, Falk O (1980) FAST-simulation models of gaseous exchange in Scots. Pine Ecol Bull (Stockholm) 32:505–523

Lüttge U (1985) Epiphyten: Evolution und Ökophysiologie. Naturwissenschaften 72:557–566

Monteith JL (1965) Evaporation and environment. In: The state and movement of water in living organisms. Proceedings of the 19th symposium of Society for Experimental Biology, Swansea, 1964. Cambridge University Press, Cambridge, pp 205–234

Mooney HA, Gulmon SL (1982) Constraints on leaf structure and function in reference to herbivory. BioScience 32:198–206

Ogink-Hendriks MJ (1995) Modelling surface conductance and transpiration of an oak forest in The Netherlands. Agr For Meteorol 74:99–18

Oguri H, Hiyama T (2002) Seasonal variations of CO_2 and heat fluxes in a secondary temperate forest. J Jpn Soc Hydrol Water Resour 15:264–278

Pearcy RW, Ehleringer JR, Mooney HA, Rundel PW (1989) Plant physiological ecology: field method and instrument. Chapman & Hall, London

Pitman AJ (2003) The evolution of, and revolution in, land surface schemes designed for climate models. Int J Climatol 23:479–510

Sellers PJ, Berry JA, Collatz GJ, Field CB, Hall FG (1992) Canopy reflectance, photosynthesis and transpiration. III: a reanalysis using improved leaf models and a new canopy integration scheme. Remote Sensing Env 42:187–216

Sellers PJ, Randall DA, Collatz GJ, Berry JA, Field CB, Dazlich DA, Zhang C, Collelo GD, Bounoua L (1996) A revised land surface parameterization (SiB2) for atmospheric GCMs. Part I: model formulation. J Clim 9:676–705

Sellers PJ, Dickinson RE, Randall DA, Betts AK, Hall FG, Berry JA, Collatz GJ, Denning AS, Mooney HA, Nobre CA, Sato N, Field CB, Henderson-Sellers A (1997) Modelling the exchanges of energy, water and carbon between continents and the atmosphere. Science 275:502–509

Sirisampan S, Hiyama T, Takahashi A, Hashimoto T, Fukushima Y (2003) Diurnal and seasonal variations of stomatal conductance in a secondary temperate forest. J Jpn Soc Hydrol Water Resour 16:113–130

Smith WK, Hollinger DY (1991) Measuring stomatal behaviour. In: Lassoie JP, Inckley TM (eds) Techniques and approaches in forest tree ecophysiology. CRC Press, Boca Raton

Stewart JB (1988) Modelling surface conductance of pine forest. Agr For Meteorol 43:19–35

Turner NC, Heichel GH (1977) Stomatal development and seasonal changes in diffusive resistance of primary and regrowth foliage of red oak (*Quercus rubra L*) and red maple (*Acen rabrum L*). New Phytol 78:71–81

Watanabe T, Yokozawa M, Emori S, Takata K, Sumida A, Hara T (2004) Developing a multilayered integrated numerical model of surface physics—growing plants interaction (MINoSGI). Global Change Biol 10:963–982

Webb EK, Pearman GI, Leuning R (1980) Correction of flux measurements for density effects due to heat and water vapour transfer. Q J R Meteorol Soc 106:85–100

Yu G-R, Nakayama K, Matsuoka N, Kon H (1998) A combination model for estimating stomatal conductance of maize (*Zea mays* L). leaves over a long term. Agr For Meteorol 92:9–28

Section 4
Forest–lake interface in watershed systems

Ecol Res (2005) 20: 347–358
DOI 10.1007/s11284-005-0050-0

ORIGINAL ARTICLE

Masatoshi Kawasaki · Nobuhito Ohte
Masanori Katsuyama

Biogeochemical and hydrological controls on carbon export from a forested catchment in central Japan

Received: 17 September 2004 / Accepted: 29 December 2004 / Published online: 9 March 2005

Abstract Here we review research on the links between hydrological processes and the biogeochemical environment controlling the dynamics of dissolved organic carbon (DOC) and dissolved inorganic carbon (DIC) in temperate forested catchments. In addition, we present the results of original experiments. The spatial and temporal changes in DIC and DOC concentrations were investigated in tandem with observations of elementary belowground hydrological processes for a forested headwater catchment in central Japan. The soil CO_2 gas concentration, which is the source of DIC, increased with depth. The hydrological characteristics of groundwater also affected the spatial variation of partial pressure of dissolved CO_2 (pCO_2) in groundwater. The temporal variations in the soil CO_2 gas concentration and the pCO_2 values of groundwater suggested that the dynamics of DIC were strongly affected by biological activity. However, the geographical differences in DIC leaching were affected not only by the link between climatological conditions and biological activity, but also by other factors such as geomorphologic conditions. The DOC concentrations decreased with selective removal of hydrophobic acid during vertical infiltration. The major DOC-removal mechanisms were retention of metal-organic complexes to soil solids in the upper mineral soil layer and decomposition of DOC in the lower mineral soil layer. The responses of the DIC and DOC concentrations to changes in discharge during storm events were explained by the spatial variation in the DIC and DOC concentrations. Seasonal variation, which represents a long-term change, in stream water DOC concentrations was affected not only by the temporal variation in DOC concentrations in the topsoil, which may be affected by biological activity, but also by water movement, which transports DOC from the topsoil to stream water. These results indicate that both a biogeochemical approach and a method for evaluating the hydrological effects on carbon dynamics are critical for clarifying the carbon accumulation-and-release processes in forested ecosystems.

Keywords Forest ecosystem · DIC · DOC · Hydrological processes · Biogeochemical processes

M. Kawasaki (✉) · N. Ohte · M. Katsuyama
Laboratory of Forest Hydrology, Division of Environmental Science and Technology, Graduate School of Agriculture, Kyoto University, Kyoto 606-8502, Japan
E-mail: kawasaki@kais.kyoto-u.ac.jp
Tel.: +81-75-7536093
Fax: +81-75-7536088

Introduction

Since the 1980s, the increasing concentration of atmospheric CO_2 caused by human activities such as fossil-fuel combustion and changes in land use has been a serious concern not only for the scientific community, but also for the general public. Therefore, more importance has been placed on understanding the changes in carbon storage in forest ecosystems, given that forest ecosystems act as large carbon reservoirs and are consequently important components of the global carbon cycle (e.g., Ciais et al. 1995; Fung 2000; Pacala et al. 2001; Schimel et al. 2001).

The CO_2 exchange between terrestrial ecosystems and the atmosphere has been quantified in various biomes and climate regions (Oakridge National Laboratory 2003). Assimilated carbon is stored not only in vegetation (aboveground) but also in roots and soil organic carbon (belowground). In humid regions, litterfall and the resulting decomposed material [particulate organic carbon (POC)] are exported to aquatic ecosystems by surface-water flow in the stream–river continuum. The movement of water exports dissolved organic carbon (DOC) and dissolved inorganic carbon (DIC) from the root zone. DIC is also released from deeper mineral soils and bedrock below the root zone. Since the 1980s, studies have shown that these carbon fluxes through rivers are an important component in the global carbon cycle (e.g., Schlesinger and Melack 1981; Meybeck 1982).

The leaching of carbon below the soil surface is one of the decomposition processes involving carbon that has been assimilated photosynthetically aboveground. To clarify the mechanisms sustaining the intrasystem cycles (Bormann and Likens 1967; Likens and Bormann 1972), an analysis of this underground decomposition process is indispensable. In addition, exported carbon from forest ecosystems is an important energy source for downstream ecosystems, such as rivers and lakes (Hynes 1975). Studies of these processes, however, remain challenging because the occurrence of decomposition and the pathways of solutes transported by water are highly heterogeneous, both spatially and temporally. Moreover, the root zone, where both plants and soil microorganisms affect carbon dynamics, is only one part of an active subsurface zone that affects carbon dynamics (Richter and Markewitz 1995). The carbon dynamics in the deep soil zone below the root zone are also affected by chemical weathering from carbonic acid produced by the dissolution and dissociation of soil CO_2 derived from decomposition and root respiration. To accurately discuss carbon cycles on a watershed scale, the carbon dynamics in soil zones deeper than those considered by previous studies must be included.

The discussion of carbon cycles at a watershed scale must also include hydrological parameters, because dissolved carbon is primarily transported by the movement of water. The processes affecting DOC quantity and quality in the soil profile have been examined in several studies (Neff and Asner 2001), but few have examined DOC dynamics in the soil–groundwater–stream continuum (e.g., McDowell and Likens 1988; Moore 1989; Moore and Jackson 1989). Studies integrating the dynamics of DOC, soil CO_2, and DIC are very limited.

The importance of carbon accumulation and carbon export processes has been reconsidered in new approaches to understanding biogeochemical cycles in forested ecosystems (Kume 2002), but the occurrence mechanisms for many phenomena are still unclear. Here we review relatively recent literature on the mechanisms of carbon export from forested ecosystems and refer to original results of a catchment-scale experiment in a forested ecosystem. The changes in DIC and DOC concentrations coupled with belowground hydrological processes in a forested headwater catchment are discussed.

Changes in DIC in relation to hydrological processes in a forested catchment

We investigated the dynamics of DIC and hydrological processes in a forested headwater catchment. The study site was a forested headwater catchment (0.68 ha, Matsuzawa catchment) in the Kiryu Experimental Watershed, south of Lake Biwa, central Japan (35°N, 136°E; Fig. 1a). A longitudinal section of the catchment is illustrated in Fig. 1b. The catchment is underlain by weathered granitic rock. The soils are predominantly Cambisols, and the average soil depth is 1.51 m (Katsuyama 2002). The Matsuzawa catchment has two different forest types: deciduous trees on the upper slopes and Japanese cypress on the intermediate and lower parts of the catchment. Groundwater was sampled from 13 wells distributed throughout the catchment, and the water chemistry was analyzed. The wells were grouped into three categories based on their hydrological behavior (Ohte et al. 1991):

1. The saturated zone (type S) is saturated by groundwater year-round and is adjacent to the stream. The groundwater flows downward into the perennial groundwater body and discharges through a spring. This groundwater is the major source of stream water during base flow.
2. The unsaturated zone (type U) is characterized by shallow soils and is located on the hillslope part of the catchment. This zone is not saturated continuously, but during rainstorms groundwater saturation may temporarily occur. The groundwater is thought to be affected by unsaturated flow (soil solution), which is the major source of temporal lateral flow.
3. The transient saturated zone (type T) is situated at the edge of the saturated zone. During the wet season, from spring to fall, the zone is continuously saturated. During the drier winter, saturation by groundwater occurs occasionally.

In addition, two plots (G1 and G34) were established to sample soil gas and soil solution.

DIC concentration was strongly affected by the pH and partial pressure of dissolved CO_2 (pCO_2). The pH ranged from 4.7 in throughfall to 5.7–5.9 for perennial groundwater (Ohte et al. 1995). The pH of the stream water exceeded 6.0, which was higher than that of the springwater and perennial groundwater. Field observations of the electrical ion balance and direct measurements of the pCO_2 indicated that these differences in pH resulted from the electrical ion balance and the spatial variation in pCO_2 in the soil and groundwater (Ohte et al. 1995).

The dissolved CO_2 in groundwater is produced by biological activity, such as root and microbial respiration, as there is little geological CO_2 in granite rocks. The dissolved CO_2 produced by biological sources is called soil respiration, and it induces chemical weathering in the soil and weathered bedrock layers and increases the alkalinity and pH.

Figure 2 shows the average pCO_2 values of rainfall, throughfall, groundwater, springwater, and stream water during the observation period (Ohte et al. 1995). The pCO_2 values of rainfall and throughfall were similar to those of atmospheric pCO_2, about 1.0×10^{-3} atm. In contrast, pCO_2 of perennial groundwater was one order of magnitude greater than that of rainfall and throughfall. The differences in the pCO_2 values of throughfall, perennial groundwater, and groundwater in the unsaturated zone indicate that water passed from a

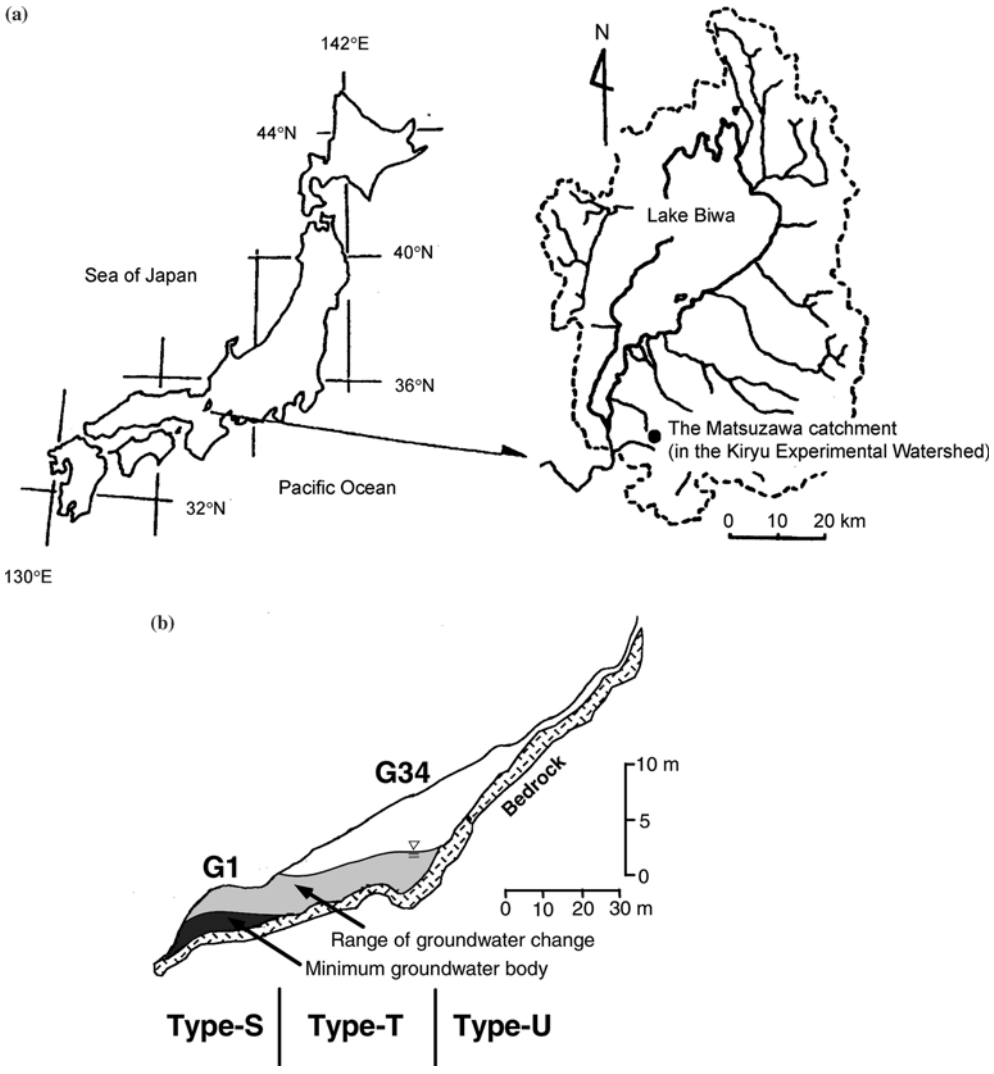

Fig. 1 **a** Location of the study site. **b** Longitudinal section of the Matsuzawa catchment and a schematic of the hydrological processes in the catchment (modified from Ohte et al. 1995). Three groundwater zones were distinguished based on hydrological characteristics (Ohte et al. 1991). *G1* and *G34* indicate the locations of observation points

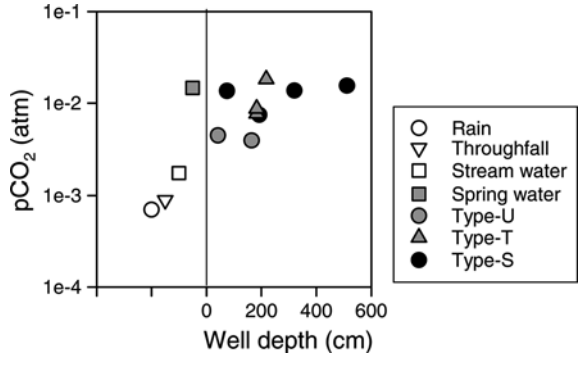

Fig. 2 Average pCO_2 values for rainfall, throughfall, springwater, stream water and U-, T-, and S-types of groundwater (modified from Ohte et al. 1995). The groundwater data are plotted with the depth of the well from which the samples were taken on the *horizontal axis*

low CO_2 zone in the unsaturated zone to a high CO_2 zone in the groundwater zone. The average pCO_2 values in the saturated zone were similar, regardless of the depth or location of the sampling wells within the perennial groundwater body. The pCO_2 value of springwater was the same as that of perennial groundwater and was about one order of magnitude greater than that of stream water. The pCO_2 value of stream water was slightly higher than the atmospheric level, indicating that CO_2 degassing occurred instantaneously.

Figure 3 shows the seasonal variation in pCO_2, pH, and the water temperatures of groundwater and springwater (Ohte et al. 1995). The pCO_2 values of groundwater and springwater varied with water temperature, while their pH varied inversely with pCO_2. This pattern is explained by the equilibrium relationship between pCO_2 and pH, i.e., a high pCO_2 reduces pH under conditions of high alkalinity (Reuss et al. 1987).

The spatial and temporal variations in the soil CO_2 concentration in the Matsuzawa catchment have been described by Hamada et al. (1996; Fig. 4). Their results suggested that temporal variation in the soil CO_2 concentration was controlled by changes in soil temperature and soil moisture. The soil CO_2 concentration reached a maximum in July, and the concentration at a depth of 150 cm was more than 10 times higher than that of the

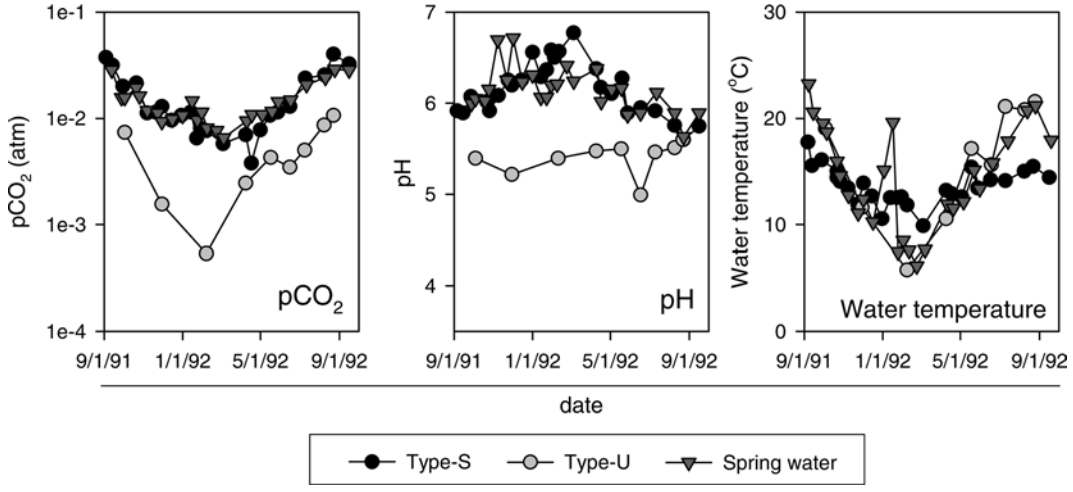

Fig. 3 Seasonal variation in pCO_2, pH and water temperature in springwater and U- and S-types of groundwater (modified from Ohte et al. 1995)

atmosphere. The pCO_2 of the perennial groundwater (about 1.0×10^{-2} atm; Fig. 2) was the same as the soil CO_2 concentration ($0.2–1.5\times10^{-2}$ atm; Fig. 4).

The dissolution and dissociation of CO_2 are promoted by chemical weathering. The CO_2 dissolution-dissociation reaction process and a chemical weathering reaction are expressed by the following equations:

$$CO_2 + H_2O \leftrightarrow H^+ + HCO_3^- \quad (1)$$

$$NaAlSi_3O_8(s) + CO_2 + (11/2)H_2O \leftrightarrow Na^+ + HCO_3^- + 2H_4SiO_4 + (1/2)Al_2Si_2O_5(OH)_4(s) \quad (2)$$

The protons supplied by the CO_2 dissolution reaction cause direct dissolution from primary minerals, such as in the above reaction, where CO_2 is consumed and HCO_3^- is produced. Moreover, the release of cations into the soil solution increases the alkalinity.

Geographical differences in bicarbonate concentration

HCO_3^- produced during chemical weathering is the major form of DIC in stream waters of pH 6–8.4, as in the Matsuzawa catchment. Chemical weathering reactions are generally controlled by bedrock mineralogy and various environmental factors (e.g., Berner and Berner 1996; Schlesinger 1996). Berner (1992) reviewed studies of global-scale long-term carbon cycles, which are influenced by chemical weathering and vegetation changes. White and Blum (1995) evaluated the climatic effects on chemical weathering using variation in the SiO_2 concentrations in 68 watersheds around the world that are underlain by granitic bedrock. Ohte and Tokuchi (1999) examined the factors determining the geographical variation in HCO_3^- leaching in 107 experimental watersheds. Figure 5 shows the relationship between the HCO_3^- concentration and the pH of

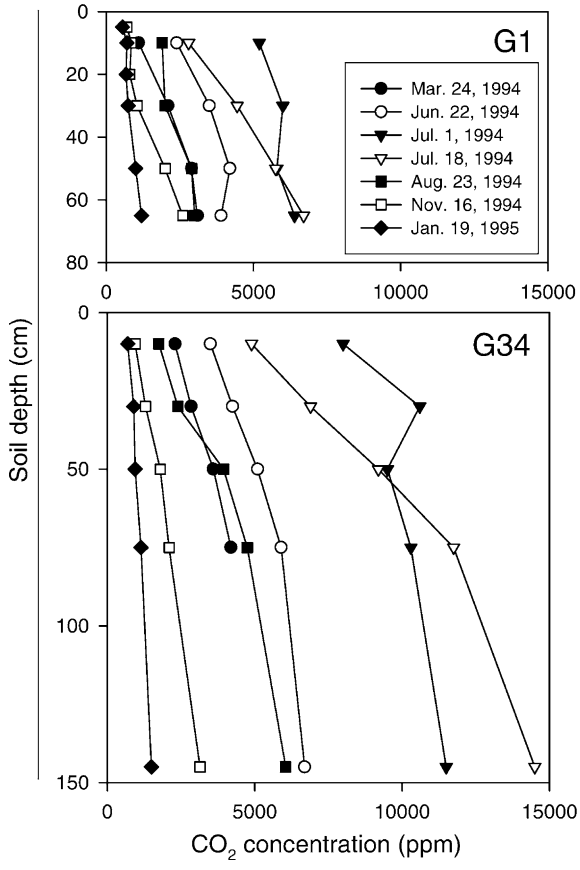

Fig. 4 Soil CO_2 profile at G1 and G34 (modified from Hamada et al. 1996). The observation period was from May 1994 to January 1995

stream water in vegetated watersheds worldwide. The HCO_3^- leaching can be considered to be the bulk expression of the acid-buffering status of watersheds.

The HCO_3^- concentration and pH of stream water in Asian forests, including those in Japan, under warm-humid temperate climates are generally higher than those in European and northeastern American forests under cool temperate to subpolar climates. Ohte and Tokuchi (1999) proposed the hypothesis that, in addition

to the effects of precipitation and temperature (White and Blum 1995), tectonic level topographical variations cannot be ignored as a controlling factor of weathering when discussing geographical variation in HCO_3^- leaching. That is, the geographical differences in DIC leaching are affected not only by the link between climatological conditions and biological activity, but also by other factors such as geomorphologic conditions.

The change in DOC in relation to hydrological processes in a forested catchment

In nature, water contains varying amounts of DOC, which originates from plant litter, soil humus, microbial biomass, or root exudates. DOC is often defined operationally as the continuum of organic molecules of different sizes and structures that can pass through a 0.45-μm filter. Most of what is collectively termed "dissolved organic carbon" in soils consists of complex molecules of high molecular weight, i.e., humic substances. As with soil organic carbon, a general chemical definition of DOC is impossible. Only small proportions of DOC, mostly low-molecular-weight substances such as organic acids, sugars, and amino acids, can be identified chemically (Kalbitz et al. 2000). Herbert and Bertsch (1995) reviewed fractionation and characterization methods for determining DOC.

Here we present a case study describing the dynamics of DOC in a forested headwater catchment. Figure 6 shows the DOC concentrations and specific UV absorbance (SUVA: absorbance at 250 nm/DOC concentration) of rainfall, throughfall, soil solutions, groundwater, and stream water. SUVA represents an average absorptivity for all molecules that comprise the DOC in a water sample, and has been used as a surrogate measurement for aromaticity. SUVA increases with humification, suggesting that it is a good indicator of the humic fraction of DOC (Yonebayashi 1989). In addition, SUVA is well correlated with the rate of the hydrophobic acid fraction (Imai et al. 1998). Both DOC concentrations and SUVA decrease with depth, suggesting that hydrophobic acids are removed selectively as they pass downwards during the infiltration process, especially in the upper mineral soil layer. Figure 7a represents the relationships between the total dissolved Al concentrations and pH, and also shows the solubility of amorphous $Al(OH)_3$. While inorganic Al dissolves in soil solutions, its actual solubility is limited by the solubility of amorphous $Al(OH)_3$ (Bolts and Bruggenwert 1980). If all dissolved Al were inorganic, then the Al concentration should be lower than the solubility of amorphous $Al(OH)_3$. This was not the case, suggesting that most of the total dissolved Al in soil solution was organic. Figure 7b shows the positive correlation between DOC concentration and total dissolved Al concentration ($r = 0.872$, $P < 0.01$, $n = 169$), a pattern probably caused by the formation of an organic complex between DOC and Al. It is generally accepted in the study of soil formation processes that organic matter and Al migrate downward from the E to the B horizon in the form of organic complexes (e.g., Dawson et al. 1978; Lundström et al. 2000). Cronan and Aiken (1985) reported that the selective removal of the hydrophobic acid fraction of DOC was related to the precipitation of metal-saturated DOC. While the mechanisms of immobilization of metal-organic complexes have not been demonstrated, hypotheses propose that metal-organic complexes increase during the infiltration process, followed by precipitation or adsorption caused by the higher molecular-weight fraction of the DOC or by neutralization of the initially negatively charged fraction of DOC (Bolts and Bruggenwert 1980). These mechanisms do not contradict the results that both DOC concentration and SUVA decreased with depth. Therefore, the DOC concentration in the upper mineral soil layer may be decreased by the retention of metal-organic complexes to soil solids (Kawasaki et al. 2002a).

After the rapid decrease in DOC concentration caused by the retention of metal-organic complexes to soil solids, the change in DOC concentrations was small at depths of 30–100 cm at G34 (30 cm: 3.93 mg C l^{-1}, 100 cm: 3.79 mg C l^{-1}; Fig. 6). However, DOC concentration of G34 groundwater (1.21 mg C l^{-1}) was lower than these concentrations. The direct adsorption

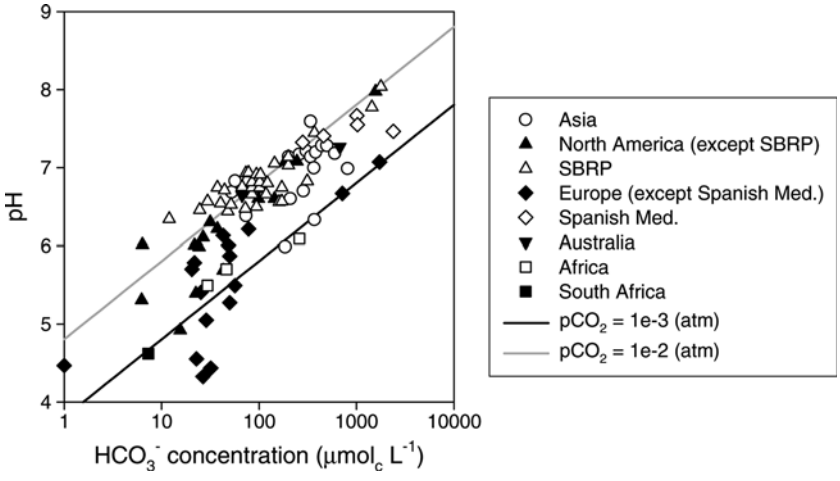

Fig. 5 Relationship between the HCO_3^- concentration and the pH of stream water at each site (modified from Ohte and Tokuchi 1999). The geographic areas are Asia, North America except the southern Blue Ridge Province (SBRP), SBRP, Europe except the Spanish Mediterranean, and the Spanish Mediterranean. The geographical characteristics of each region were detailed by Ohte and Tokuchi (1999)

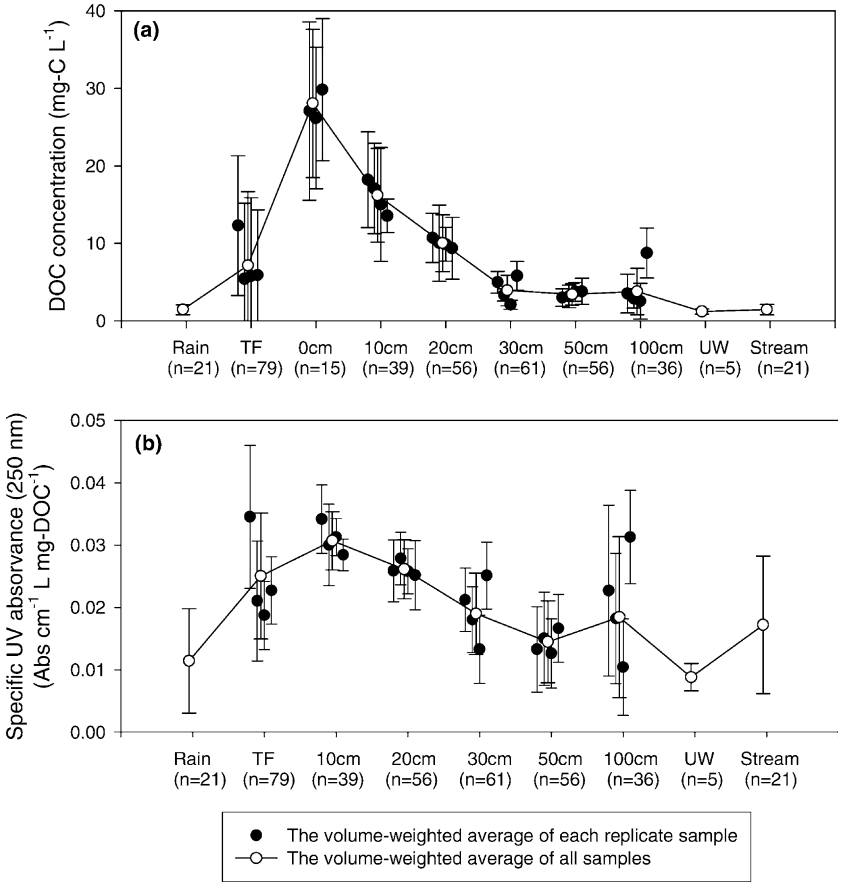

Fig. 6 **a** DOC concentrations and **b** specific UV absorbance (250 nm) of rainfall, G34 throughfall (*TF*), soil solution from G34 soils at six profile depths (*0, 10, 20, 30, 50,* and *100 cm*), G34 groundwater (*UW*), and stream water (modified from Kawasaki et al. 2002a). The concentrations and absorbances were calculated using the volume-weighted average, except for the rainfall, groundwater, and stream water concentrations, which were calculated using the arithmetic average

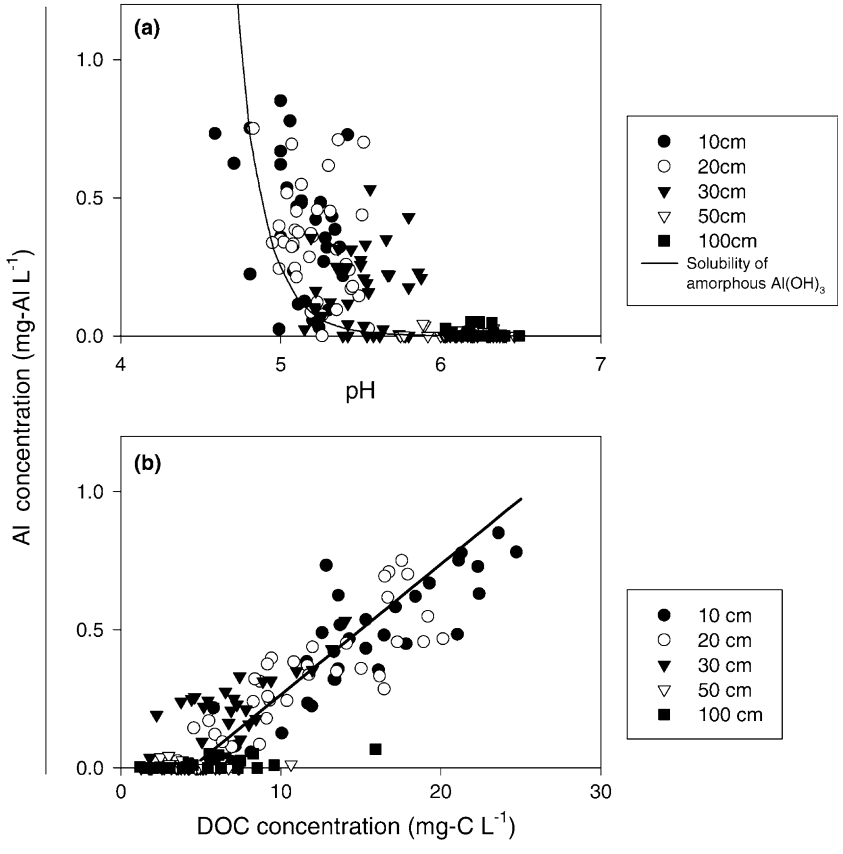

Fig. 7 **a** Relationship between pH and Al concentrations in soil solutions from G34, including the solubility of amorphous $Al(OH)_3$. **b** Relationship between DOC and Al concentrations in soil solutions from G34 (modified from Kawasaki et al. 2002a)

of DOC onto soil minerals and the decomposition of DOC are considered to be DOC-removal mechanisms, with the exception of the retention of metal-organic complexes to soil solids. The DOC adsorption efficiency appeared to be homogeneous from the upper to the lower soil layers (Fig. 8). In addition, the soil properties in the Matsuzawa catchment below the C horizon were homogeneous, suggesting that the DOC adsorption efficiency may be homogeneous below the C horizon. However, there were two patterns in the decrease of DOC concentrations, suggesting that the easily adsorbed DOC fraction had been removed in the upper mineral soil layer, and that decomposition contributed to lowering the DOC concentrations in the lower mineral soil layer. The decomposition of DOC is thought to occur in any location, but the slow rate of decomposition makes it difficult to detect changes in concentrations during infiltration from 0- to 100-cm soil depths. On the other hand, the depth of G34 groundwater exceeds 5 m, and water reaches G34 groundwater not only through vertical infiltration but also, considering the topography and soil depths of the Matsuzawa catchment, through temporal lateral flow (Kim et al. 1988). The long residence time of G34 groundwater may be sufficient for the detection of decomposition-related reduction in DOC concentration (Kawasaki et al. 2002a).

Not only the quantity but also the quality of DOC is important for evaluating the function of DOC in both terrestrial and aquatic ecosystems. Some fractionation and characterization techniques have been developed (reviewed by Herbert and Bertsch 1995). However, these methods involve processing large volumes of water and are labor intensive, making them impractical in studies involving many sampling sites or many time points (McKnight et al. 2001). Spectroscopic techniques have the potential to meet this need. In particular, three-dimensional fluorescence spectrometry has been useful for characterizing the different components of DOC (e.g., Coble et al. 1990; Mopper and Schultz 1993; McKnight et al. 2001).

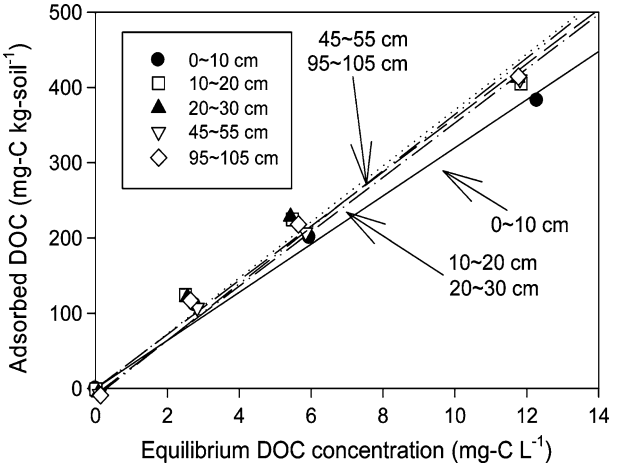

Fig. 8 Freundlich isotherms for DOC adsorption at G34 (modified from Kawasaki et al. 2002a). The Freundlich isotherm is a function of the equilibrium DOC concentration (Bolts and Bruggenwert 1980). The results of the adsorption experiment were described by fitting them to Freundlich isotherms. The experimental procedure was detailed by Kawasaki et al. (2002a)

Nakanishi et al. (1999) reported the changes in the fluorescence characteristics of DOC along the hydrological continuum in the Matsuzawa catchment. They pointed out that the relative fluorescence intensities of the soil solutions decreased, and their spectroscopic properties changed with soil depth. To clarify the mechanisms of these changes, Kawasaki (2002) compared the fluorescence characteristics of the DOC component fractionated by the molecular-weight distribution using the gel-filtration technique (Okazaki 2001) and by the hydrophobicity and acid–base properties using adsorption chromatography (DAX-8: macroreticular nonionic resin) and ion-exchange chromatography (Kawasaki 2002). Figure 9 shows the peak positions of each fraction on the excitation emission matrix (EEM). The peak emission wavelengths of hydrophobic and hydrophilic acids were within the range of 470–305 nm (Fig. 9a). In contrast, the peak emission wavelengths of hydrophobic and hydrophilic bases and neutrals were within the range of 430–395 nm (Fig. 9a). In addition, the peak wavelengths of the components fractionated by the molecular-weight distribution were also within the range of 440–405 nm (Fig. 9b). These results suggested that the peak position was affected not by the hydrophobic/hydrophilic properties and the molecular weight, but by the acid–base and neutral properties of the DOC. Therefore, the change in spectroscopic properties of soil solutions reported by Nakanishi et al. (1999) represented a change in the acid fraction of DOC. Given that the acid fraction of DOC forms the organic complex, this does not interfere with the mechanism of DOC removal which is the retention of metal-organic complexes to soil solids.

Quantification of carbon flux and accumulation rates in forest soil

The net annual rate of addition or removal of DOC along the hydrological continuum was estimated using the spatial variation in the DOC concentrations and physical observations of rainfall, soil pore water pressure, and discharge (Fig. 10; Kawasaki 2002). As precipitation moved through the vegetation and A_0 layer, the net annual addition of DOC was 61.3 and 220.3 kg C ha^{-1} year^{-1}, respectively. In the mineral soil layer, DOC was removed rapidly, especially at soil depths between 0 and 30 cm; the DOC removal rate was 262.8 kg C ha^{-1} year^{-1}, which was 87% of the inflow DOC flux to the mineral soil layer. After passing through the upper mineral soil layer, no marked change in the DOC flux was evident, and the net DOC removal rate from a soil depth of 30 cm to the upper perennial groundwater was 35.7 kg C ha^{-1} year^{-1}. During groundwater flow, the net rate of DOC addition or removal was low, while the export of DOC

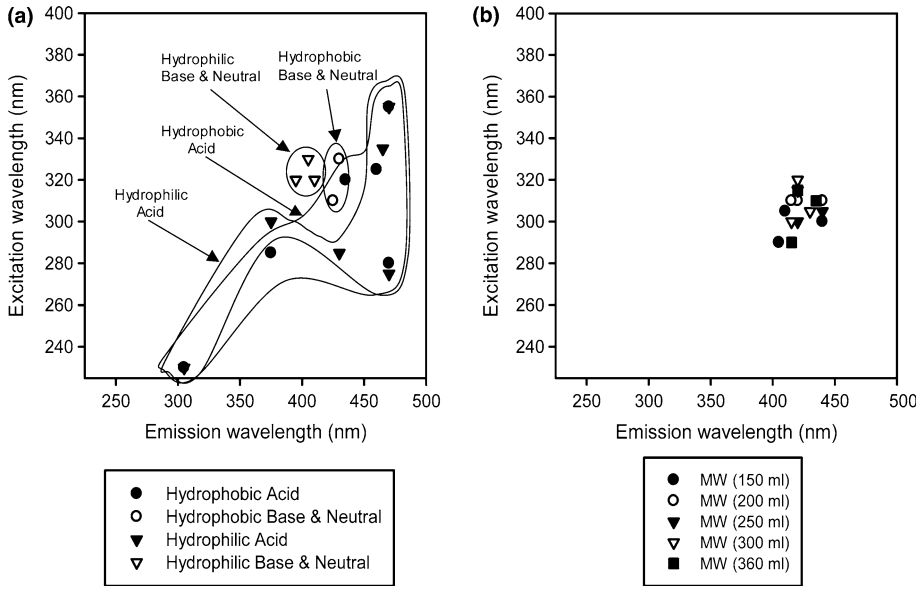

Fig. 9 **a** Fluorescence peaks of components fractionated using adsorption chromatography with a macro-reticular nonionic DAX8 resin and ion-exchange resin. The sampling and analysis procedures were detailed by Kawasaki (2002). **b** Fluorescence peaks of components fractionated using a gel-filtration technique with Sephadex G-25 [molecular weight (*MW*) detection range 1,000–5,000; MW represents the elution volume]. The void volume of this experiment was 137.5 ml. The sampling and analysis procedures were detailed by Okazaki (2001) and Kawasaki (2002)

exceeded the DOC flux during groundwater flow owing to storm events, as described in detail below.

Based on these results, Kawasaki (2002) compared the DOC removal rate to soil carbon and the total rate of inorganic carbon production (Fig. 11).

If all the removed DOC were to accumulate as soil organic carbon in the upper mineral soil layer and decompose in the lower mineral soil layer, 0.8% of the soil carbon would be retained from DOC annually and 6.7% of the total production of inorganic carbon (DIC and CO_2) would derive from DOC. While these values are small, soil organic carbon can accumulate in the mineral soil layer for a long time (Hakamata et al. 2000), making the 0.8% of soil carbon retained from DOC annually an important component of the missing carbon sink in forest ecosystems.

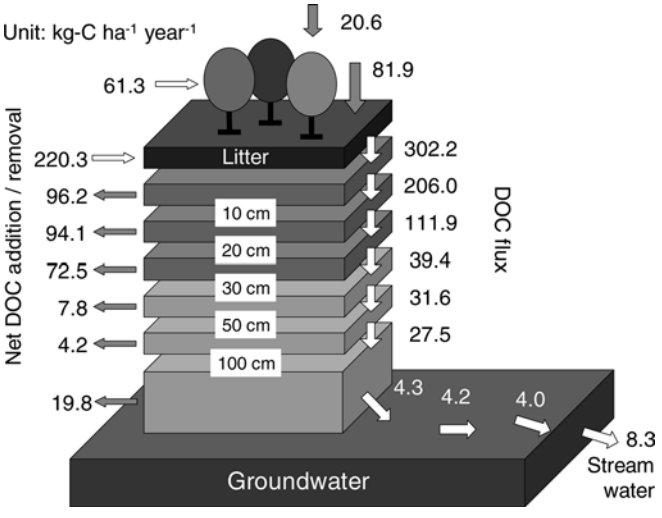

Fig. 10 DOC flux and net DOC addition or removal rates per stratum or horizon from April 2000 to March 2001 (modified from Kawasaki 2002)

Factors controlling DIC and DOC export from forested headwater catchments

The response of DIC and DOC concentrations to changes in discharge during storm events can be explained by the spatial variation in DIC and DOC concentrations, as described above (Figs. 2, 6). DIC (HCO_3) concentrations decreased with increasing discharge as a result of dilution, because DIC concentrations in groundwater are higher than in soil solutions. In contrast, DOC concentrations increased with increasing discharge, because DOC concentrations in groundwater are lower than in soil solutions (Katsuyama and Ohte 2002; Kawasaki 2002). These trends are illustrated in Fig. 12, which presents the relationships between DIC and DOC concentrations and the discharge in Matsuzawa catchment from 23–26 June 2003. These trends have

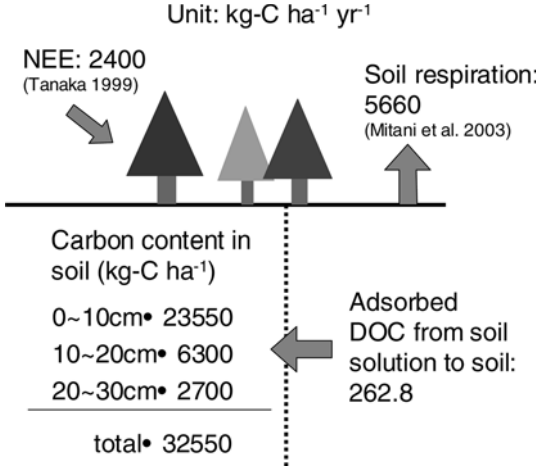

Fig. 11 Summary comparing the DOC removal rate and soil carbon in the upper mineral soil layer

also been observed in southern Hokkaido, North America, and Europe (e.g., Boyer et al. 1996; Hagedorn et al. 2000; Shibata et al. 2001).

It is difficult to generalize the response of DIC and DOC concentrations to long-term changes in the seasonal variation of discharge, because changes in both hydrological conditions and biological activity, such as root respiration and microbial activity, affect DIC and DOC concentrations. Figure 13b shows the temporal variation in DOC concentrations in G1 soil solutions, G34 and G1 groundwater, and stream water. In summer 1999, an increase in the stream water DOC concentration was found, but this was not the case in 2000; nevertheless, the DOC concentration in the topsoil increased in both years. The temporal variation in the hydraulic gradient in G1, calculated as the lower minus the upper piezometric head value divided by the distance between the two points, is shown in Fig. 13a. The positive hydraulic gradient value represents a downward water flux. The difference in summer rainfall amount between 1999 and 2000 caused the different water flux at G1 (Fig. 13a). These results suggest that the temporal variation in DOC concentration in the topsoil, which may be affected by biological activity, is important to the temporal variation in stream water DOC concentrations. However, water movement, which transports DOC from the topsoil to stream water, is also important (Kawasaki et al. 2003).

Table 1 Mean specific fluorescence intensities of amino acids or protein-like peaks and humic or fluvic acid peaks in bedrock groundwater sampled from 24 October 2000 to 17 January 2001 ($n = 5$)

	Amino acid or protein-like	Humic acid or fluvic acid
Excitation wavelength (nm)	225–270	320–360
Emission wavelength (nm)	300–350	410–450
Mean specific fluorescence intensity (QSU/mg C l^{-1})	13.4 ($n = 5$)	2.3 ($n = 5$)

The average areas of each standard material (amino acids or protein-like materials, and humic or fluvic acids) in the EEM were defined by Yoshioka et al. (1999). The sampling procedure was detailed by Kawasaki et al. (2002b), and the fluorescence analysis procedure was detailed by Nakanishi et al. (1999). *QSU* (quinine sulfate unit): a standardized unit of fluorescence intensity using quinine sulfate (Mopper and Schultz 1993)

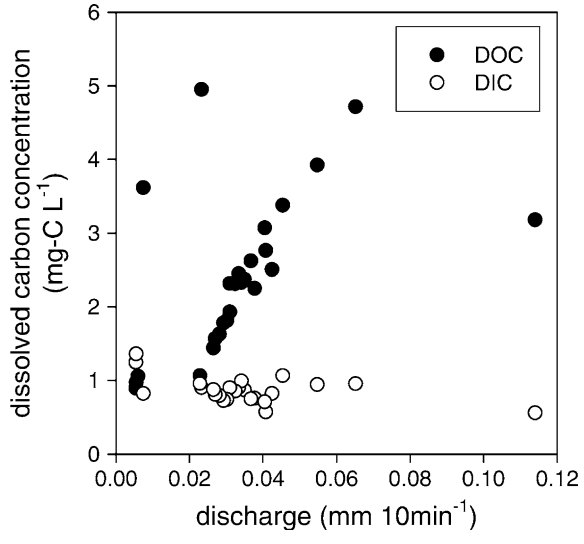

Fig. 12 Relationship between the dissolved carbon concentrations (*DIC* and *DOC*) and discharge in Matsuzawa catchment from 23–26 June 2003. During this period, the total rainfall was 128.3 mm and the maximum rainfall was 19.9 mm h^{-1}. The sampling and analysis procedures were detailed by Okazaki (2001)

Properties of DOC from forested headwater catchments

In the Fudoji catchment (8 km south of the Matsuzawa catchment), fluorescence intensity representing amino acids or proteins in bedrock groundwater was several times higher than that of fulvic or humic acid (Table 1). Recent studies have demonstrated the importance of

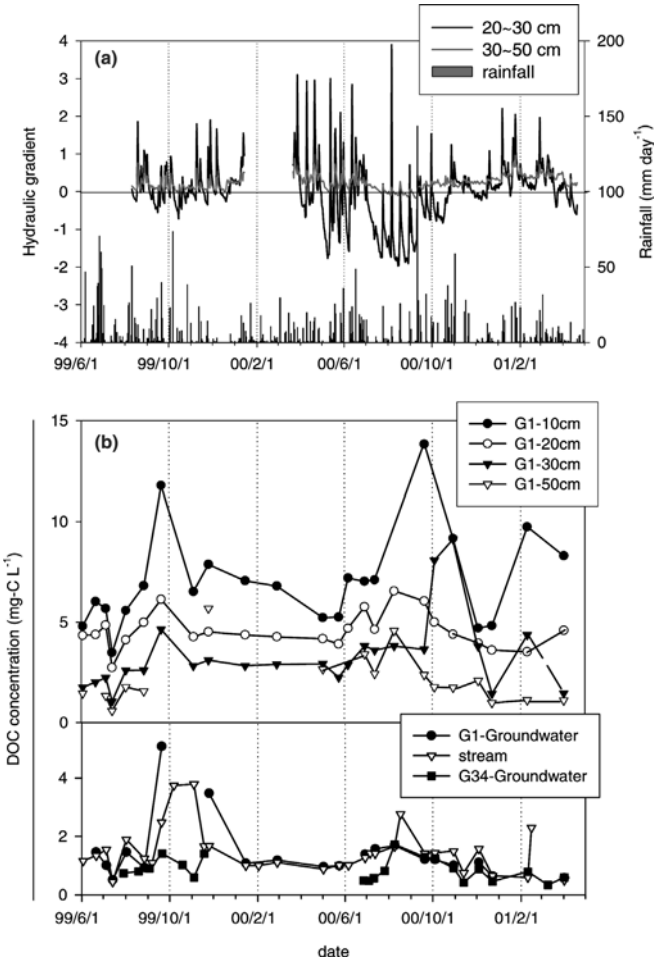

Fig. 13 a Hyetograph and temporal variations in hydraulic gradient in G1. The positive hydraulic gradient value represents a downward water flux. **b** Temporal variations in the DOC concentrations in the G1 soil solutions, G34 and G1 groundwater, and stream water (modified from Kawasaki et al. 2003)

water movement through the bedrock in the rainfall-runoff process on steep slopes (e.g., Mulholland 1993; Montgomery et al. 1997). Uchida et al. (2003) also demonstrated that the contribution of bedrock groundwater was considerable (50–95% of stream flow) in the Fudoji catchment. These results suggest that fulvic and humic acids, considered a major fraction of the allochthonous DOC in aquatic ecosystems, are not the main components of DOC from a forested headwater catchment during base flow. Conversely, Katsuyama and Ohte (2002) found that the intensity of fulvic acid fluorescence increased with increasing discharge during storm events in the Matsuzawa catchment. These results suggest that changes to the hydrological flow path control both the quantity and quality of DOC export from forested headwater catchments.

Stream fluxes of DIC, DOC and POC

Fluxes of DIC and DOC in the stream flowing in the Matsuzawa catchment have been estimated by Okazaki (2001). Based on the relationships between DIC and DOC fluxes and discharge, DIC and DOC exports from the catchment have been estimated to be 2.4–9.4 and 7.6–26.1 kg C ha^{-1} $year^{-1}$, respectively (Okazaki 2001; Kawasaki 2002).

We have not discussed the mechanisms of particulate organic carbon (POC) leaching and consider it more useful to examine the POC formation processes separately, because in-stream processes influence POC formation more strongly than the biogeochemical processes in forest soils do. However, we cannot ignore POC, because 14–19% of the total carbon export in the Matsuzawa catchment is POC (Okazaki 2001).

Shibata et al. (2001) reported that a high DIC concentration and DIC/DOC ratio were observed in the Horonai River because of the relatively high discharge during base flow. This result indicates that the hydrological characteristics of a catchment may affect the dissolved carbon flux and DIC/DOC ratios in streams. It is difficult to generalize these results because of the lack of environmental information for each catchment. In addition, we must emphasize that few such observational data sets are available for Japan. Hope et al. (1994) also pointed out the paucity of available data for POC and dissolved CO_2.

Conclusion

Based on original catchment-scale experiments for a forested ecosystem, we have discussed the changes in DIC and DOC concentrations coupled to belowground hydrological processes in a forested headwater catchment. The soil CO_2 concentration, which is the source of DIC, increased with depth. The hydrological characteristics of groundwater also affected the groundwater pCO_2 values. The temporal variation in soil CO_2 gas concentrations and groundwater pCO_2 values suggested that the dynamics of DIC were strongly affected by biological activity. However, the geographical differences in DIC leaching patterns are affected not only by the link between climatological conditions and biological activity, but also by other factors, such as geomorphological conditions.

DOC concentrations decreased with the selective removal of hydrophobic acid during vertical infiltration. The major mechanisms of DOC removal were retention of metal-organic complexes to soil solids in the upper mineral soil layer and decomposition of DOC in the lower mineral soil layer. The response of DIC and DOC concentrations to changes in discharge during storm events was explained by the spatial variation in DIC and DOC concentrations. On the other hand, seasonal variation, which represents a long-term change, in stream water DOC concentrations was affected by the temporal variation in DOC concentrations in the topsoil, which may be affected by biological activity, and also by water movement, which transports DOC from the topsoil to stream water.

Both a biogeochemical approach and methods for evaluating hydrological effects on carbon dynamics are necessary to better understand the carbon accumulation and release processes in forested ecosystems, and few such observational data sets are available for Japan. Therefore, more field experiments based on the soil–groundwater–stream continuum for DOC and DIC dynamics are required.

Acknowledgements We thank Drs. Makoto Tani, Ken'ichiro Kosugi, Naoko Tokuchi, Takahito Yoshioka, Yuko Asano, and Taro Uchida for their valuable suggestions. We also thank Mr. Ryota Okazaki and Dr. Su-Jin Kim for helping with our fieldwork and laboratory analysis. We thank Dr. Takashi Kohyama and two anonymous reviewers for helpful insights. This study was supported by grants from the Ministry of Education, Culture, Sport, Science and Technology, Japan, for scientific research (IGBP-MESSC and JSPS Research Fellow).

References

Berner RA (1992) Weathering, plants, and the long-term carbon-cycle. Geochim Cosmochim Acta 56:3225–3231

Berner EK, Berner RA (1996) Global environment: water, air, and geochemical cycles. Prentice Hall, Englewood Cliffs, NJ, pp 376

Bolts GH, Bruggenwert MGM (1980) Soil chemistry. Elsevier, Amsterdam

Bormann FH, Likens GE (1967) Nutrient cycling. Science 155:424–439

Boyer EW, Hornberger GM, Bencala KE, McKnight D (1996) Overview of a simple model describing variation of dissolved organic carbon in an upland catchment. Ecol Model 86:183–188

Ciais P, Tans PP, Trolier M, White JWC, Francey RJ (1995) A large northern hemisphere terrestrial CO_2 sink indicated by the $^{13}C/^{12}C$ ratio of atmospheric CO_2. Science 269:1098–1102

Coble PG, Green SA, Blough NV, Gagosian RB (1990) Characterization of dissolved organic matter in the Black Sea by fluorescence spectroscopy. Nature 348:432–435

Cronan CS, Aiken GR (1985) Chemistry and transport of soluble humic substances in forested watersheds of the Adirondack Park, New York. Geochim Cosmochim Acta 49:1697–1705

Dawson HJ, Ugolini FC, Hrutfiord BF, Zachara J (1978) Role of soluble organics in the soil processes of a Podozol, Central Cascades, Washington. Soil Sci 126:290–296

Fung I (2000) Climate change—variable carbon sinks. Science 290:1313–1313

Hagedorn F, Schleppi P, Waldner P, Fluhler H (2000) Export of dissolved organic carbon and nitrogen from Gleysol dominated catchments—the significance of water flow paths. Biogeochemistry 50:137–161

Hakamata T, Hatano R, Kimura M, Takahashi M, Sakamoto K (2000) Interaction between greenhouse gases and soil ecosystem 1 (in Japanese). Jpn J Soil Sci Plant Nutr 71:263–274

Hamada M, Ohte N, Kobashi S (1996) A measurement of soil CO_2 profile in a forest watershed (in Japanese with English summary). J Jpn For Soc 78:376–383

Herbert BE, Bertsch PM (1995) Characterization of dissolved and colloidal organic matter in soil solution: a review. In: McFee WW, Kelly JM (eds) Carbon forms and functions in forest soils. Soil Science Society of America, Madison, WI, pp 63–88

Hope D, Billett MF, Cresser MS (1994) A review of the export of carbon in river water—fluxes and processes. Env Pollut 84: 301–324

Hynes HBN (1975) Edgardo Baldi memorial lecture. The stream and its valley. Verh Int Ver Theor Angew Limnol 19:1–15

Imai A, Fukushima T, Matsushige K, Inoue T, Ishibashi T (1998) Fractionation of dissolved organic carbon from the waters of Lake Biwa and its inflowing rivers (in Japanese with English summary). Jpn J Limnol 59:53–68

Kalbitz K, Solinger S, Park JH, Michalzik B, Matzner E (2000) Controls on the dynamics of dissolved organic matter in soils: a review. Soil Sci 165:277–304

Katsuyama M (2002) Study on hydrochemical dynamics of groundwater and streamwater in forested headwater catchments. PhD Thesis, Kyoto University, Kyoto

Katsuyama M, Ohte N (2002) Determining the sources of stormflow from the fluorescence properties of dissolved organic carbon in a forested headwater catchment. J Hydrol 268:192–202

Kawasaki M (2002) Study on the dissolved organic carbon dynamics in the forested catchments (in Japanese). MS Thesis, Kyoto University, Kyoto

Kawasaki M, Ohte N, Nambu K, Hobara S, Okazaki R, Katsuyama M, Kim SJ (2002a) The dynamics of DOC in the hydrological process in a forested watershed (in Japanese with English summary). Jpn J Limnol 63:31–45

Kawasaki M, Ohte N, Asano Y, Uchida T (2002b) Dynamics of DOC through vadose-saturated zones at a forested headwater catchment (in Japanese). Jpn J Ecol 52:119–123

Kawasaki M, Ohte N, Okazaki R, Katsuyama M (2003) Seasonal variation of DOC export from a forested headwater catchment, pp 69–70. In: Yoh M, Yoshioka T (eds) Biogeochemistry in watersheds—importance and outlook (in Japanese). Jpn J Limnol 64:49–79

Kim J, Kubota J, Suzuki M, Fukushima Y (1988) Variations of soil moisture and groundwater table at a gentle hillslope in the Kiryu watershed (in Japanese with English summary). Bull Kyoto Univ For 60:174–189

Kume A (2002) Importance of below ground parts on the matter flow process: comparisons of physical and biological process between above and below ground (in Japanese). Jpn J Ecol 52:101–106

Likens GE, Bormann FH (1972) Nutrient cycling in ecosystems. In: Wiens J (ed) Ecosystem structure and function. Oregon State University Press, Corvallis, OR, pp 25–67

Lundström US, van Breemen N, Bain D (2000) The podzolization process. A review. Geoderma 94:91–107

McDowell WH, Likens GE (1988) Origin, composition, and flux of dissolved organic carbon in the Hubbard Brook valley. Ecol Monogr 58:177–195

McKnight DM, Boyer EW, Westerhoff PK, Doran PT, Kulbe T, Andersen DT (2001) Spectrofluorometric characterization of dissolved organic matter for indication of precursor organic material and aromaticity. Limnol Oceanogr 46:38–48

Meybeck M (1982) Carbon, nitrogen, and phosphorus transport by world rivers. Am J Sci 282:401–450

Mitani T, Kosugi Y, Tani M, Takanashi S, Katayama T, Wada T (2003) Spatial and temporal variation of soil respiration rate in an artificial forest of Hinoki (*Chamaecyparis obtusa*) (in Japanese with English summary). J Jpn Soc Reveget Tech 29:153–158

Montgomery DR, Dietrich WE, Torres R, Anderson SP, Heffner JT, Loague K (1997) Hydrologic response of a steep, unchanneled valley to natural and applied rainfall. Water Resour Res 33:91–109

Moore TR (1989) Dynamics of dissolved organic carbon in forested and disturbed catchments, Westland, New Zealand.1. Maimai. Water Resour Res 25:1321–1330

Moore TR, Jackson RJ (1989) Dynamics of dissolved organic carbon in forested and disturbed catchments, Westland, New Zealand. 2. Larry River. Water Resour Res 25:1331–1339

Mopper K, Schultz CA (1993) Fluorescence as a possible tool for studying the nature and water column distribution of DOC components. Mar Chem 41:229–238

Mulholland PJ (1993) Hydrometric and stream chemistry evidence of three storm flowpaths in Walker Branch watershed. J Hydrol 151:291–316

Nakanishi A, Tokuchi N, Katsuyama M (1999) Change of fluorescence characteristics of dissolved organic carbon down through the forest soil (in Japanese with English summary). Appl For Sci 8:95–102

Neff JC, Asner GP (2001) Dissolved organic carbon in terrestrial ecosystems: synthesis and a model. Ecosystems 4:29–48

Oakridge National Laboratory (2003) FLUXNET. Integrating worldwide CO_2 flux measurements. http://www-eos-dis.ornl.gov/FLUXNET/

Ohte N, Tokuchi N (1999) Geographical variation of the acid buffering of vegetated catchments: factors determining the bicarbonate leaching. Global Biogeochem Cycles 13:969–996

Ohte N, Tokuchi N, Suzuki M (1991) Variations in qualities of groundwater and streamwater corresponding to hydrological cycle in a forested watershed (in Japanese with English summary). Bull Kyoto Univ For 63:69–81

Ohte N, Tokuchi N, Suzuki M (1995) Biogeochemical influences on the determination of water chemistry in a temperate forest basin—factors determining the pH value. Water Resour Res 31:2823–2834

Okazaki R (2001) Study on the export of organic carbon from a forested catchment (in Japanese). MS Thesis, Kyoto University, Kyoto

Pacala SW, Hurtt GC, Baker D, Peylin P, Houghton RA, Birdsey RA, Heath L, Sundquist ET, Stallard RF, Ciais P, Moorcroft P, Caspersen JP, Shevliakova E, Moore B, Kohlmaier G, Holland E, Gloor M, Harmon ME, Fan SM, Sarmiento JL, Goodale CL, Schimel D, Field CB (2001) Consistent land-based and atmosphere-based US carbon sink estimates. Science 292:2316–2320

Reuss JO, Cosby BJ, Wright RF (1987) Chemical processes governing soil and water acidification. Nature 329:27–32

Richter DD, Markewitz D (1995) How deep is soil? Bioscience 45:600–609

Schimel DS, House JI, Hibbard KA, Bousquet P, Ciais P, Peylin P, Braswell BH, Apps MJ, Baker D, Bondeau A, Canadell J, Churkina G, Cramer W, Denning AS, Field CB, Friedlingstein P, Goodale C, Heimann M, Houghton RA, Melillo JM, Moore B, Murdiyarso D, Noble I, Pacala SW, Prentice IC, Raupach MR, Rayner PJ, Scholes RJ, Steffen WL, Wirth C (2001) Recent patterns and mechanisms of carbon exchange by terrestrial ecosystems. Nature 414:169–172

Schlesinger WH (1996) Biogeochemistry: an analysis of global change. Academic Press, San Diego, pp 588

Schlesinger WH, Melack JM (1981) Transport of organic carbon in the world's rivers. Tellus 33:172–181

Shibata H, Mitsuhashi H, Miyake Y, Nakano S (2001) Dissolved and particulate carbon dynamics in a cool-temperate forested basin in northern Japan. Hydrol Process 15:1817–1828

Tanaka H (1999) Study on CO_2 and H_2O transfer processes in forest (in Japanese). PhD Thesis, Kyoto University, Kyoto

Uchida T, Asano Y, Ohte N, Mizuyama T (2003) Seepage area and rate of bedrock groundwater discharge at a granitic unchanneled hillslope. Water Resour Res 39:1018 DOI 10.1029/2002WR001298

White AF, Blum AE (1995) Effects of climate on chemical weathering in watersheds. Geochim Cosmochim Acta 59:1729–1747

Yonebayashi K (1989) Research procedure for humic substances 2 (in Japanese). Pedologist 33:37–48

Yoshioka T, Tanoue E, Ohta K, Konohira E, Nakanishi A (1999) Comprehension of fluorescence characteristics of dissolved organic carbon as an index of matter cycle in forest ecosystems (in Japanese). In: Wada E (ed) Report of the research project on response of terrestrial watershed ecosystems to global change in the fiscal year 1999, pp 96–111

Ecol Res (2005) 20: 359–365
DOI 10.1007/s11284-005-0051-z

ORIGINAL ARTICLE

Eiichi Konohira · Takahito Yoshioka

Dissolved organic carbon and nitrate concentrations in streams: a useful index indicating carbon and nitrogen availability in catchments

Received: 15 September 2004 / Accepted: 12 November 2004 / Published online: 9 March 2005

Abstract Dissolved organic carbon (DOC) and NO_3^- are important forms of C and N in stream water. Hypotheses concerning relationships between DOC and NO_3^- concentrations have been proposed, but there are no reports demonstrating a relationship between them in stream water. We observed 35 natural streams in the Lake Biwa watershed, central Japan, and found an inverse relationship between DOC and NO_3^- concentrations. This relationship was also found in observations of their seasonal variations in the Lake Biwa watershed. Moreover, this relationship was also found to apply to watersheds in other regions in Japan. These results suggest that forest biogeochemical processes which control DOC and NO_3^- concentrations in Japanese streams are closely related. Excess N availability together with a C (energy) deficit in a soil environment may explain this relationship. DOC and NO_3^- concentrations in streams will thus be a useful index indicating C and N availability in catchments.

Keywords Dissolved organic carbon · Nitrate · Stream · Forest · Lake Biwa watershed

Introduction

Dissolved organic carbon (DOC) and NO_3^- are important forms of C and N in streams. Stream DOC and NO_3^- both originate from soil organic matter in forested ecosystems, and a hypothesis has been proposed regarding their relationship (Aber 1992). Recently, Aitkenhead and McDowell (2000) showed that an increase in riverine DOC flux occurs with increased soil C/N ratio on a global scale. This result suggests that DOC in rivers is controlled by both C and N biogeochemical cycling in the catchment, implying that riverine DOC concentrations are related to the NO_3^- levels. However, there has been no report demonstrating a clear relationship between DOC and NO_3^- concentrations in stream water.

Although observations on DOC concentrations in Japanese stream water are scarce, an annual mean DOC concentration of 127 μM was reported for a Japanese stream (Shibata et al. 2001). This is a lower DOC level than in North American streams (Sedell and Dahm 1990). A large regional variation of stream NO_3^- concentration has been observed in Japan, and some streams showed levels exceeding 100 μM (Yoh et al. 2001). High NO_3^- concentrations in Japanese streams are a result of excess N availability caused by high atmospheric N deposition (Ohrui and Mitchell 1997; Yoh et al. 2001).

We carried out intensive observations of stream DOC and NO_3^- concentrations in the Lake Biwa watershed in central Japan. Lake Biwa is the biggest lake in Japan, and an important water resource for the Kansai region including the cities of Kyoto and Osaka. We discuss the relationship between DOC and NO_3^- concentrations in these streams and the potential mechanisms responsible for the observed relationship.

Materials and methods

Stream water samples were collected in the Lake Biwa watershed located in central Japan (35°10′N, 136°10′E). Annual precipitation ranged from $<1{,}600$ mm in the southern region to $>2{,}400$ mm in the northern region of the watershed (Lake Biwa Research Institute, 1986). It snows in the winter, but the southern part of the watershed is usually free from snow cover. The annual average temperature is 14.1°C in the city of Hikone near

E. Konohira (✉)
Graduate School of Environmental Studies,
Nagoya University, Nagoya 464-8601, Japan
E-mail: ekonohira@nagoya-u.jp
Tel.: +81-52-7895469
Fax: +81-52-7893436

T. Yoshioka
Research Institute for Humanity and Nature,
Kamigyo, Kyoto 602-0878, Japan

Lake Biwa. Elevation ranges from 86 m a.s.l. at the lake surface to >1,000 m in the mountainous area. Sampling sites are located in the steep mountainous area (slopes range from 0.10 to 0.53; average 0.22). The catchment areas of the sampling sites are covered by forest and free from human dwellings or activity such as cultivation of paddy fields and croplands. Vegetation type varies among sites, but the coniferous plantation tree species, *Cryptomeria japonica* and *Chamaecyparis obtusa* are usually predominant.

Samples from 35 streams were collected in the summer of 1998 (26–30 July and 3–5 September) to study the regional variation. Thirteen of the 35 streams were also sampled in November 1998, and in February, April and June 1999 to monitor the seasonal variations. All samples were collected during the base flow period.

Collected samples were filtered (Whatman GF/F filters, pore size 0.7 μm) in the field. Samples for DOC analysis were placed in brown glass bottles and 25 μl of purified 6 M HCl was added per 15 ml of sample. These bottles were sealed with a rubber cap coated inside with Teflon. Glass bottles and filters had been pre-burned at 450°C for 2 h to prevent contamination. Samples for NO_3^- analysis were collected in clean polyethylene bottles. These samples were cooled by ice during transport to the laboratory, and stored at −40°C until analysis.

DOC concentration was measured using the high-temperature catalytic oxidation method (TOC5000A; Shimadzu., Kyoto). The injection volume was 200 μl, and a high-sensitivity catalyst was used. NO_3^- concentration was measured by ion chromatography (QIC analyser; Dionex Japan., Osaka).

To examine the regional variability of DOC and NO_3^- concentrations on a larger scale in Japan, we collected stream water samples in two other regions: Okutama (35°50′N, 139°00′E) near Tokyo, where high NO_3^- concentrations in streams have been reported by Yoh et al. (2001); and Uryu (44°20′N, 142°10′E) in Hokkaido located in the northern part of Japan. This latter region receives a great deal of snow in winter and has a much cooler climate than the Lake Biwa watershed and Okutama. The streams in Okutama and Uryu are also free from human activity. Detailed information about these areas can be found in Yoh et al. (2001) for the Okutama region and in Ozawa et al. (2001) for the Uryu region. Collected samples were treated and measured in the same way as described above.

We also sampled soil and the soil organic layer at four catchments in the Lake Biwa watershed (Azusa, Itanago, Kakagawa, Shigaraki) in order to consider mechanisms responsible for differences in DOC and NO_3^- concentrations in streams. Soil organic layer and surface soil (0–10 cm depth) were collected on 23–24 October 2001. These soil sampling sites (from four to eight for each catchment) were located in the valley area near the streams (within 100 m of streams) (Table 1).

Soil organic layers were dried (60°C, 2 days) and milled, and the C/N ratio was measured by elemental analyser (NA2500; Thermo Quest, Italy). Fifty milliliters of pure water was added to the 10-g soil samples and shaken for 30 min to extract soil solutions. These extracts were centrifuged and filtered (Whatman GF/F filters). DOC and NO_3^- concentrations in soil extracts were measured in the same way as for stream waters.

Results

Regional distribution of NO_3^- and DOC concentrations in stream water in the Lake Biwa watershed

NO_3^- concentrations in stream water ranged from 4.7 μM to 60 μM (Fig. 1), and the average concentration of the 35 streams was 22 μM. NO_3^- concentrations were high in the eastern part of the watershed (>30 μM) and low in the southern part (<10 μM). The DOC concentration ranged from 12 μM to 280 μM, and the average concentration was 57 μM (Fig. 1), with considerable regional variations; high in the southern part of the watershed (>80 μM) and low in the eastern part (<40 μM). As a result, an inverse relationship was found between NO_3^- and DOC concentrations in stream waters (Fig. 2).

Seasonal variations of NO_3^- and DOC concentrations in stream water in the Lake Biwa watershed

To monitor the seasonal variation of DOC and NO_3^-, we chose four streams where the DOC concentrations in the summer of 1998 were >80 μM (C-type streams), five where NO_3^- concentrations were >30 μM (N-type streams) and four streams where the DOC concentrations were <80 μM, and NO_3^- concentrations were also <30 μM (M-type streams).

NO_3^- concentrations in C-type streams were always low (usually <10 μM) and showed little seasonal vari-

Table 1 Soil sampling sites[a]

	Site no.	Latitude, longitude	Altitude (m)	Vegetation	Soil type
Azusa	35	N35°18′56″, E136°22′34″	270	*Cryptomeria japonica*, plantation	Brown forest soil
Itanago	22	N35°26′5″, E136°23′52″	320	*C. japonica*, plantation	Brown forest soil
Kakagawa	10	N34°54′21″, E135°59′3″	370	*C. japonica*, plantation	Brown forest soil
Shigaraki	12	N34°55′10″, E136°6′22″	350	*C. japonica* and broadleaf forest	Brown forest soil

[a]The location of each soil sampling site (*site no.*) is shown in Fig. 1

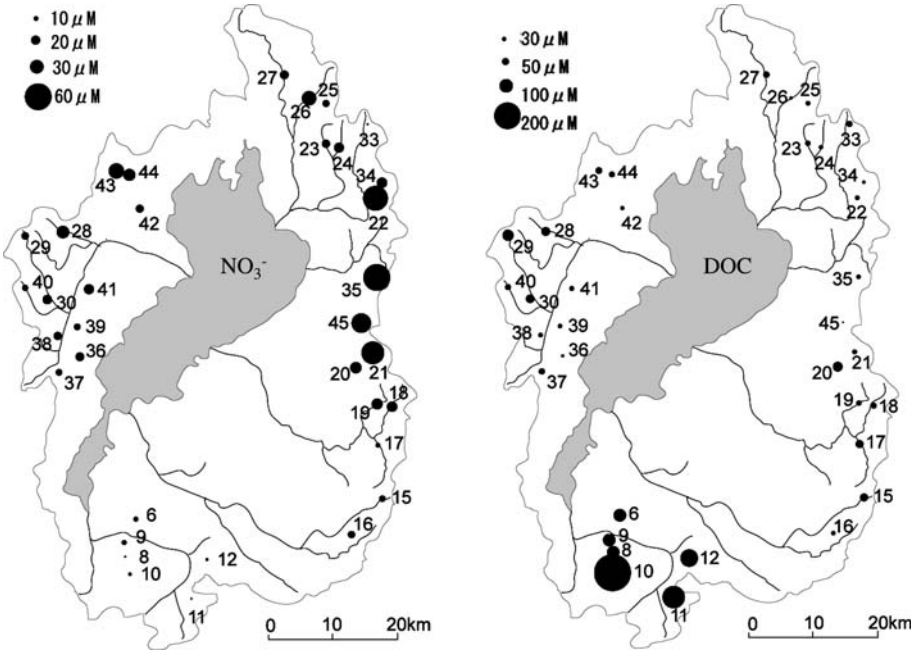

Fig. 1 Regional distribution of NO_3^- and dissolved organic C (*DOC*) concentrations of stream water in the Lake Biwa watershed (summer 1998). The *circles* show the sampling site, and the *size of circles* shows the concentration. The *numbers* next to the circles are the site number

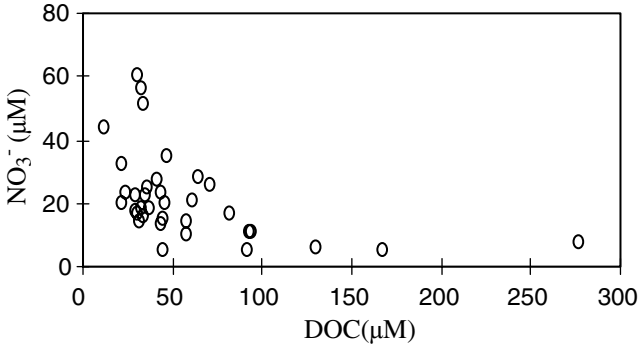

Fig. 2 Relationship between DOC and NO_3^- concentrations in stream water in the Lake Biwa watershed (summer 1998)

ation (Fig. 3). On the other hand, DOC concentrations in C-type streams were considerably higher in summer and lower in winter. However, DOC levels in C-type streams were higher than in other types of streams throughout the year. N-type streams maintained a low DOC concentration (usually <30 μM), while NO_3^- concentrations fluctuated (Fig. 3). Although a clear seasonal trend in NO_3^- concentration was not found, the concentrations were higher than in the other types of stream. M-type streams showed minimal seasonal variations in both DOC and NO_3^- . The inverse relationship between DOC and NO_3^- concentrations found in the regional distribution (Fig. 2) was conserved when seasonal variation data were included.

NO_3^- and DOC relationship in stream water in other regions in Japan

Stream water in the Okutama region showed a large variation in NO_3^- concentration, ranging from 2.8 μM to 262 μM (Fig. 4). The maximum concentration in the Okutama region greatly exceeded that of the Lake Biwa watershed. The high NO_3^- levels in the Okutama region are mainly due to the high atmospheric N deposition from the Tokyo metropolitan area (Yoh et al. 2001). However, DOC concentrations in the Okutama region were low and showed small variation, ranging from 14 μM to 62 μM. These concentrations were in the low end of the range of DOC found in the Lake Biwa watershed. Stream water in the Uryu region showed higher and variable DOC concentrations ranging from 80 μM to 230 μM and showed a low NO_3^- concentration (<10 μM). Even though the range of NO_3^- concentrations was much higher in the Okutama region, the inverse relationship between DOC and NO_3^- concentration in streams persisted when the streams from all regions were analysed.

C/N ratio of soil organic layers and DOC and NO_3^- concentrations in soil extracts in the Lake Biwa watershed

We selected two C-type streams and two N-type streams. The C/N ratio in soil organic layers and DOC and NO_3^- concentrations in soil extracts of these catchments were measured (Fig. 5).

C/N ratios in soil organic layers ranged from 43 to 53. Since the variation within a catchment is quite large, we could not detect differences in C/N ratios between C-type and N-type catchments. Gundersen et al. (1998) showed that N leaching was mainly controlled by C/N ratios of soil organic layers, but no relationship was found between C/N ratios in soil organic layers and stream NO_3^- in the Lake Biwa watershed.

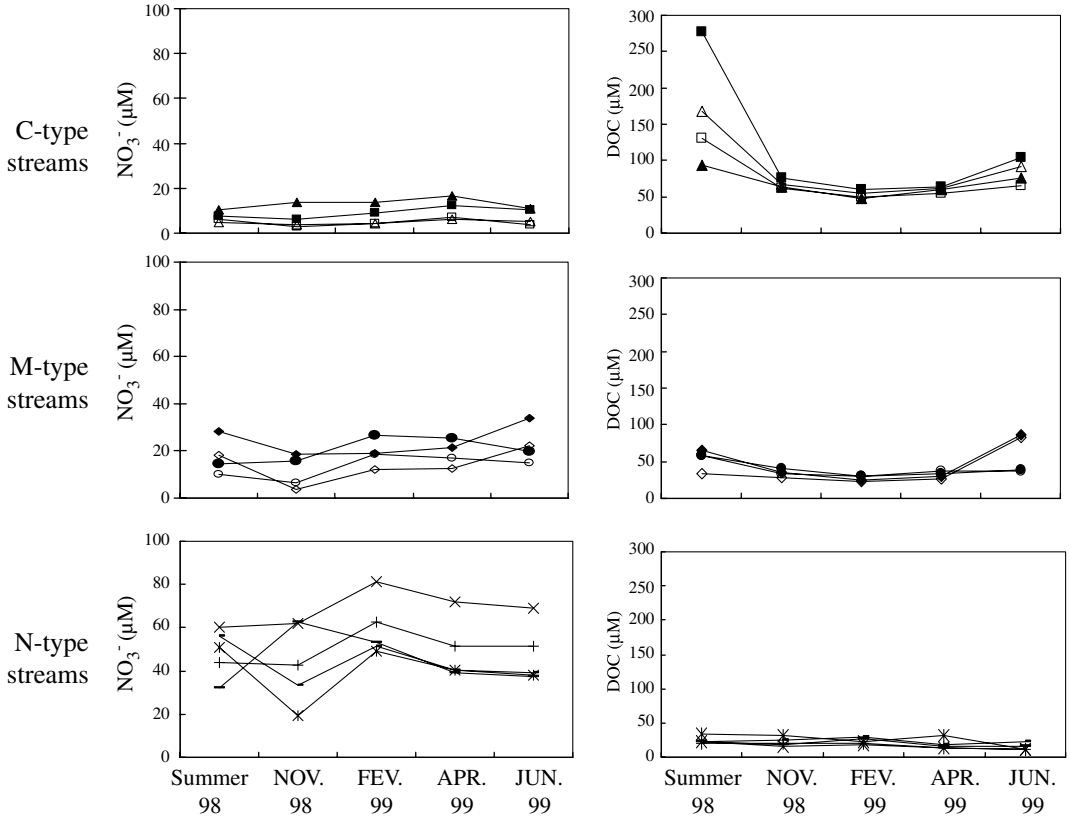

Fig. 3 Seasonal variation of DOC and NO_3^- concentrations in stream water in the Lake Biwa watershed. *C-type streams* DOC concentrations >80 μM; *N-type streams* NO_3^- concentrations >30 μM; *M-type streams* DOC concentrations <80 μM, NO_3^- concentrations <30 μM; *NOV*. November, *FEV*. February, *APR*. April, *JUN*. June, *98* 1998, *99* 1999

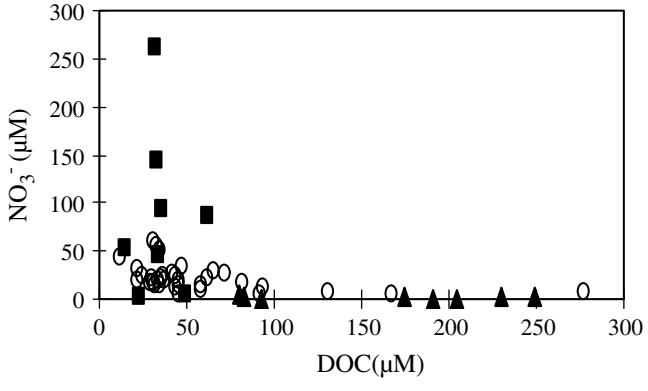

Fig. 4 Relationship between DOC and NO_3^- concentrations of stream water in Okutama, Uryu and the Lake Biwa watershed. *Filled squares* Streams in the Okutama region, *filled triangles* streams in the Uryu region, *circles* streams in the Lake Biwa watershed (the same data are presented in Fig. 2). Stream water in the Okutama and Uryu regions was collected within a month after sampling in the Lake Biwa watershed

DOC concentrations in soil extracts were higher in the C-type than N-type catchments (Fig. 5). Although the variation within a catchment was also large, we detected differences in DOC concentrations between C-type and N-type catchments ($P < 0.01$, *t*-test). NO_3^- concentrations in soil extracts were higher in N-type catchments, and NO_3^- was not detected in Shigaraki (C-type catchment). A clear difference in NO_3^- concentrations was also observed between C-type and N-type catchments ($P < 0.01$, *t*-test).

Discussion

An inverse relationship between DOC and NO_3^- concentrations was found and persisted throughout the seasons in the Lake Biwa watershed. Moreover, this inverse relationship was found for watersheds in other regions of Japan. These results suggest that forest biogeochemical processes which control DOC and NO_3^- concentrations in Japanese streams are closely related.

Biogeochemical processes that control NO_3^- leaching from forests have been intensively studied recently in association with N saturation in forest ecosystems (Aber et al. 1989). Gundersen et al. (1998) showed that N concentrations and transformation rates in forest ecosystems were closely related to N leaching below the rooting zone and subsequently into streams. An increased N concentration and N transformation rate in forests (increased N availability) were thought to be responsible for N leaching to streams. On the other hand, several factors in stream and riparian processes have been discussed as the main factors controlling DOC in streams (Meyer 1990; Dillon and Molot 1997;

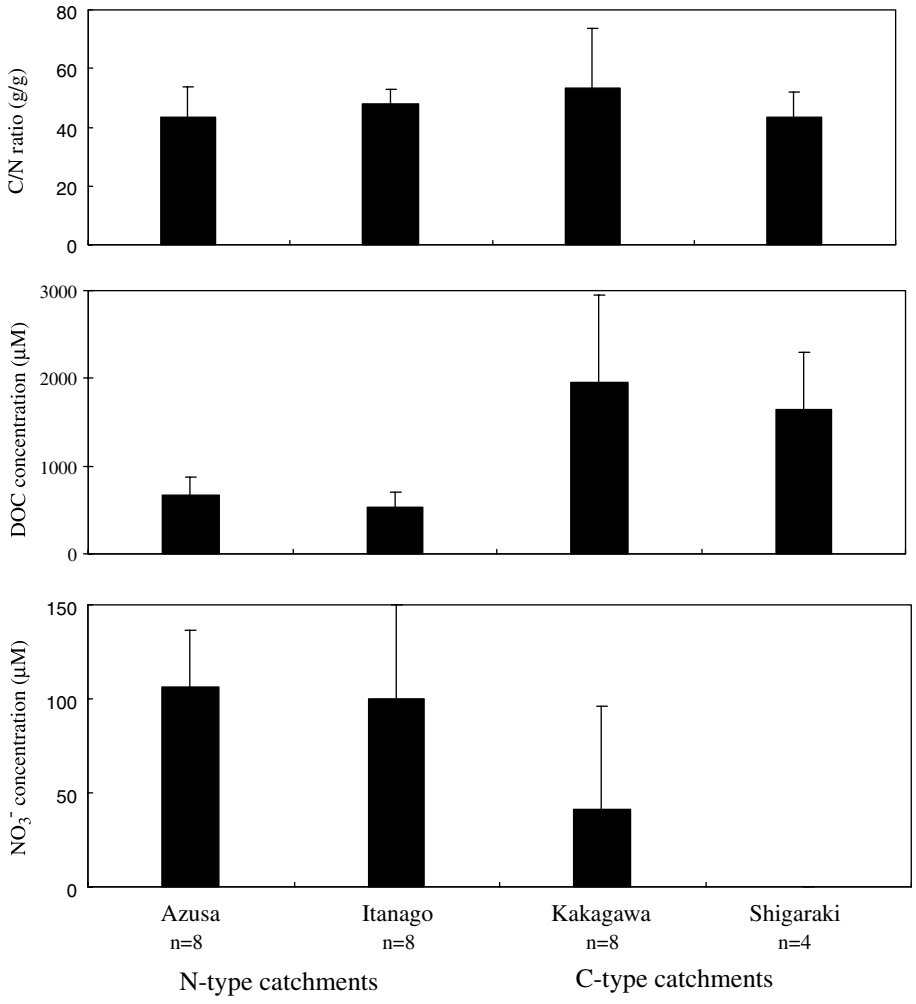

Fig. 5 C/N ratio of soil organic layers and DOC and NO_3^- concentrations in soil extracts in the Lake Biwa watershed. For an explanation of terms, see Fig. 3

Ekhardt and Moore 1990). The biogeochemical processes controlling stream DOC are not as clear as those for NO_3^-, and DOC concentrations in streams may be controlled by different factors depending on the site.

In-stream and riparian processes determining DOC

In-stream processes are important factors for the regulation of DOC concentrations in streams (Meyer 1990). These processes include leaching of stored organic matter from the stream bed into the water and autochthonous production of DOC by algae and macrophytes. However, these in-stream processes are probably not important for DOC in the Lake Biwa watershed. The effects of autochthonous production would be minimum in the Lake Biwa watershed because most of the streams are shaded by dense forests surrounding the streams. We found a great deal of leaf litter in and around the streams especially in the litterfall season in autumn, but an increase in DOC was not detected in this season (Fig. 3; November samples). The very steep slope of each catchment (high flow velocity) and very small catchment area (short stream length to the sampling site) reduces the contact of water with potential DOC sources in the streams.

Riparian wetlands contribute considerably to stream DOC (Dillon and Molot 1997; Eckhardt and Moore 1990). Eckhardt and Moore (1990) observed that the DOC concentration in 42 streams in Canada ranged from 3.5 mgC/l to 40 mgC/l (290–3,300 μM), and showed that these concentrations were related to the wetland area in each catchment. However, these DOC concentrations were much higher than those in the Lake Biwa watershed (Fig. 2; 12–280 μM). The steep slopes resulted in a lack of wetland area and explain the low DOC concentrations in the Lake Biwa watershed.

The steep slopes and small catchment area in the Lake Biwa watershed minimize in-stream and riparian effects on DOC concentrations in streams. These topography of the Lake Biwa watershed also minimizes in-stream and riparian effects on NO_3^- concentrations in the streams.

Upland processes for DOC and NO_3^-

Whereas in-stream and riparian effects on stream DOC and NO_3^- are minimal in the Lake Biwa watershed,

upland processes are likely to be important both for DOC and NO_3^- in the streams.

Nitrification produces NO_3^- that is leached into streams and also produces protons that can acidify the soil environment. This potential change in soil pH may affect the DOC concentration through biotic or abiotic processes. However, the pH of the stream water was close to neutral, ranging from 6.3 to 8.5 in the Lake Biwa watershed (data not shown). Thus acidification by nitrification probably does not affect the DOC concentration in the streams.

Soil inorganic N is produced by the decomposition of organic N and consumed by N-immobilization processes. A decrease in N immobilization generated from a deficit in available C could explain the increase in NO_3^- in the soil environment (Hart et al. 1994). C (energy) deficit in a soil environment causes an increase in the NO_3^- concentration, and will cause DOC consumption. DOC and NO_3^- concentrations in soil extracts corresponded to those in streams (Fig. 5). The soil environment is spatially and temporally variable, and our measurements are not sufficient to detect differences between catchments, but qualitative differences detected in soil extracts suggested that the inverse relationship in DOC and NO_3^- in streams could be attributed to the decomposition of organic matter in the surface soil layer. Thus, the C (energy) deficit in the soil environment may be the best explanation for the observed inverse relationship between DOC and NO_3^- concentrations in-stream.

Denitrification is another possible mechanism that affects both DOC and NO_3^- concentrations because denitrification reduces NO_3^- to other N forms using DOC as the energy source (Hedin et al. 1998). The importance of riparian denitrification was reported in some Japanese catchments (Konohira et al. 2001; Koba et al. 1997). However, the denitrification processes cannot explain the depletion of DOC with the increase in NO_3^- concentration, because it consumes both DOC and NO_3^- . Moreover, decomposition processes of organic matter generate different levels of DOC and NO_3^- in surface soil, and denitrification in riparian areas reduces DOC and NO_3^- until DOC or NO_3^- are completely consumed. This combined mechanism can explain the DOC and NO_3^- relationship in streams, but minor effects of riparian processes due to the steep slopes of Lake Biwa watershed suggest that denitrification does not contribute to stream DOC and NO_3^- concentrations.

Stream DOC and NO_3^- as an index of forest C and N cycling

The inverse relationship between DOC and NO_3^- concentrations in the Lake Biwa watershed suggests an excess N availability and C (energy) deficit in the soil environment. Our results support Aber's (1992) hypothesis that there would be DOC depletion in an excess N environment. This also implies that the stream DOC and NO_3^- concentrations could be an index indicating C and N availability in the catchment. This index may be applicable to other steep-slope catchments where in-stream and riparian processes did not contribute to stream DOC and NO_3^- concentrations.

Effects of N addition on DOC concentration were tested by plot-scale observations (Gundersen et al. 1998; McDowell et al. 1998) and catchment-scale observations (David et al. 1999). However, no change in DOC concentration was detected in these studies. DOC depletion following an increase in N availability may be too slow to be detected in short-term experiments. Alternately, since the change in DOC concentration will be very small, it may be detected only in the lower range of the DOC concentration (e.g. < 80 μM).

Furthermore, DOC in streams and soil percolates is mainly composed of refractory C (Yano et al. 2000; Buffam et al. 2001). In any case, information about the bioavailability of DOC in forest soils and streams is limited, and the biological production and utilization of DOC must be studied in detail.

Acknowledgements We thank Dr H. Shibata of Hokkaido University, Dr N. Ohte of Kyoto University, Dr M. Yoh of Tokyo University of Agriculture and Technology, and Dr E. Tanoue of Nagoya University for their kind arrangements for the field sampling and analysis. We also thank Miss Y. Ito, Nagoya University for her assistance with the DOC analysis. This work was supported and financed by the Asahi Breweries Foundation, and Grant-in-Aids for Scientific Research (no. 09041159), for the Scientific Research of Priority Area B (no.11213101), and for the International Geosphere–Biosphere Programme awarded to Nagoya University by the Ministry of Education, Culture, Sports, Science and Technology, Japan.

References

Aber JD (1992) Nitrogen cycling and nitrogen saturation in temperate forest ecosystems. Trees 7:220–224

Aber JD, Nadelhoffer KJ, Steudler P, Melillo JM (1989) Nitrogen saturation in northern forest ecosystems. BioScience 39:378–386

Aitkenhead JA, McDowell WH (2000) Soil C: N ratio as a predictor of annual riverine DOC flux at local and global scale. Global Biogeochem Cycles 14:127–138

Buffam I, Galloway JN, Blum LK, McGlathery KJ (2001) A stormflow/baseflow comparison of dissolved organic matter concentrations and bioavailability in an Appalachian stream. Biogeochemistry 53:269–306

David M, Vance G, Kahl J (1999) Chemistry of dissolved organic carbon at Bear Brook watershed, Maine: stream water response to $(NH_4)_2SO_4$ additions. Environ Monitor Assess 55:149–163

Dillon PJ, Molot LA (1997) Effect of landscape form on export of dissolved organic carbon, iron, and phosphorus from forested stream catchments. Water Resour Res 33:2591–2600

Eckhardt BW, Moore TR (1990) Controls on dissolved organic carbon in streams, Southern Quebec. Can J Fish Aquat Sci 47:1537–1544

Gundersen P, Emmett BA, Kjonaas OJ, Koopmans CJ, Tietema (1998) Impact of nitrogen deposition on nitrogen cycling in forests: a synthesis of NITREX data. For Ecol Manage 101:37–55

Hart SC, Nason GE, Myrold DD, Perry DA (1994) Dynamics of gross nitrogen transformation in an old-growth forest: the carbon connection. Ecology 75:880–891

Hedin LO, Fischer JC, Ostrom NE, Kennedy BP, Brown MG, Robertson GP (1998) Thermodynamic constraints on nitrogen transformations and other biogeochemical processes at soil-stream interfaces. Ecology 79:684–703

Koba K, Tokuchi N, Wada E, Nakajima T, Iwatsubo G (1997) Intermittent denitrification:the application of a ^{15}N natural abundance method to a forested ecosystem. Geochim Cosmochim Acta 61:5043–5050

Konohira E, Yoh M, Kubota J, Yagi K, Akiyama H (2001) Effects of riparian denitrification on stream nitrate—evidence from isotope analysis and extream nitrate leaching during rainfall. Water Air Soil Pollut 130:667–672

Lake Biwa Research Institute (1986) Shiga prefecture regional environmental atlas (in Japanese). Lake Biwa Research Institute, Ohtsu, Shiga, Japan

McDowell WH, Currie WS, Aber JD, Yano Y (1998) Effects of chronic nitrogen amendments on production of dissolved organic carbon and nitrogen in forest soil. Water Air Soil Pollut 105:175–182

Meyer JL (1990) Production and utilization of dissolved organic carbon in riverine ecosystems. In: Perdue EM, Gjessing ET (eds) Organic acids in aquatic ecosystems. Wiley, New York, pp 281–299

Ohrui K, and Mitchell MJ (1997) Nitrogen saturation in Japanese forested watershed. Ecol Appl 7:391–401

Ozawa M, Shibata H, Satoh F, and Sasa K (2001) Annual element budget of soil in snow-dominated forested ecosystem. Water Air Soil Pollut 130:703–708

Sedell JR, Dahm CN (1990) Spatial and temporal scale of dissolved organic carbon in streams and rivers. In Perdue EM, Gjessing ET (eds) Organic acids in aquatic ecosystems. Wiley, New York pp 261–279

Shibata H, Mitsuhashi H, Miyake Y, Nakano S (2001) Dissolved and particulate carbon dynamics in a cool-temperate forested basin in northern Japan. Hydrol Process 15:1817–1828

Yano Y, McDowell WH, Aber JD (2000) Biodegradable dissolved organic carbon in forest soil solution and effects of chronic nitrogen deposition. Soil Biol Biochem 32:1743–1751

Yoh M, Konohira E, Yagi K (2001) Regional distribution of natural stream nitrate in central Japan. Water Air Soil Pollut 130:655–660

Ecol Res (2005) 20: 367–375
DOI 10.1007/s11284-005-0052-y

ORIGINAL ARTICLE

**Jotaro Urabe · Takehito Yoshida · Tek Bahadur Gurung
Tatsuki Sekino · Narumi Tsugeki · Kentaro Nozaki
Masahiro Maruo · Eiichioro Nakayama
Masami Nakanishi**

The production-to-respiration ratio and its implication in Lake Biwa, Japan

Received: 5 October 2004 / Accepted: 30 November 2004 / Published online: 1 March 2005

Abstract Production-to-respiration (P:R) ratio was estimated at an offshore site of Lake Biwa in order to examine whether the plankton and benthic community is subsidized with allochthonous organic carbon, and to clarify the role of this lake as potential source or sink of carbon dioxide. The respiration rate of protozoan and metazoan plankton was calculated from their biomass and empirical equations of oxygen consumption rates, and that of bacterioplankton was derived from their production rate and growth efficiency. In addition, the carbon mineralization rate in the lake sediments was estimated from the accumulation rate of organic carbon, which was determined using a ^{210}Pb dating technique. On an annual basis, the sum of respiration rates of heterotrophic plankton was comparable to net primary production rate measured by the ^{13}C method. However, when the mineralization rate in the lake sediments was included, the areal P:R ratio was 0.89, suggesting that Lake Biwa is net heterotrophic at the offshore site with the community being subsidized with allochthonous organic carbon. Such a view was supported by the surface water pCO_2 that was on average higher than that of the atmosphere. However, the estimate of net CO_2 release rate was close to that of carbon burial rate in the sediments. The result suggests that the role of Lake Biwa in relation to atmospheric carbon is almost null at the offshore site, although the community is supported partially by organic carbon released from the surrounding areas.

Keywords Carbon budget · Heterotrophs · Lake metabolism · pCO_2 · P:R ratio

J. Urabe · T. Yoshida · T. B. Gurung · T. Sekino
N. Tsugeki · K. Nozaki · M. Nakanishi
Center for Ecological Research,
Kyoto University, Otsu, Japan

M. Maruo · E. Nakayama
School of Environmental Science,
University of Shiga Prefecture, Hikone, Japan

Present address: J. Urabe (✉)
Division of Ecology and Evolutionary Biology,
School of Life Sciences, Tohoku University,
Biological Buildings, Aoba, Sendai 980-8578, Japan
E-mail: urabe@mail.tains.tohoku.ac.jp
Tel.: +81-22-2176681
Fax: +81-22-2176686

Present address: T. Yoshida
Department of Ecology and Evolutionary Biology,
Cornell University, Ithaca, NY, USA

Present address: T. B. Gurung
Fisheries Research Division,
Nepal Agricultural Research Council, Katmandu, Nepal

Present address: T. Sekino
Research Institute for Humanity and Nature,
Kyoto, Japan

Present address: K. Nozaki
School of Human Science,
Sugiyama Jogakuen University, Nagoya, Japan

Present address: M. Nakanishi
Shiga-cho, Japan

Introduction

Recently, growing evidence shows that many ecosystems or habitats are subsidized with often heavy amounts of organic carbon derived from surrounding ecosystems or habitats (Nakano and Murakami 2001; Polis et al. 2004). The fact suggests that a community in a given ecosystem processes and respires more organic carbon than is fixed within that ecosystem. However, it is often difficult to track material flows in all conduits across ecosystems, and more specifically, to quantify to what degree a community in a given ecosystem relies on other ecosystems with regard to its energetic base.

One way to quantify the degree is to measure the balance between production and community respiration rates, expressed by the production-to-respiration (P:R) ratio. It is defined as

$$P:R = \frac{GPP}{CRR}$$

where GPP and CRR are gross primary production and community respiration rates, respectively. This ratio can be rewritten as

$$P:R = \frac{NPP}{HRR}$$

where NPP is the net primary production rate or the fraction of GPP not respired by the autotrophs themselves, and HRR is respiration or mineralization rates by heterotrophic organisms. P:R > 1 implies that a given ecosystem is net autotrophic—communities are producing an amount of organic carbon sufficient to sustain themselves. P:R < 1 implies that a given ecosystem is net heterotrophic and organic carbon derived from other ecosystems supports, at least in some part, communities in that ecosystem. In addition, P:R < 1 implies that a given ecosystem vents carbon brought in from other ecosystems into the atmosphere. As such, the P:R ratio can provide useful insights into the material bases sustaining communities and the roles of ecosystems in the production of atmospheric carbon.

In lake ecosystems, a number of studies have examined the P:R ratio (Schindler et al. 1972; del Giorgio and Peters 1994; Cole et al. 2000). Some studies have shown that P:R < 1 is common, especially in unproductive oligotrophic lakes (del Giorgio and Peters 1994; Hanson et al. 2003), while others have failed to observe a P:R ratio < 1, even in such lakes (Carignan et al. 2000). It is suggested that this discrepancy stems from differences in the geographical area where the lakes were located (Prairie et al. 2002) as well as from methods for measuring primary production and community respiration rates (Cole et al. 2000; Hanson et al. 2003). More importantly, most previous studies have examined the P:R ratio in limited seasons at the surface layer or epilimnion, focusing on activities of plankton alone. In aquatic ecosystems, phytoplankton fix organic carbon at the surface layer where light is available for photosynthesis, but consumption of organic carbon takes place not only through the water column but also in the lake sediments. In addition, time-lag is common in ecological processes: organic carbon fixed by autotrophs in one season may be processed by heterotrophs in different seasons. Thus, to examine whether a lake is subsidized with organic carbon derived from the drainage basin, it is essential to measure the P:R ratio per unit of area over an ecologically relevant time scale, such as a year (Cole et al. 2000).

Lake Biwa is the largest lake in Japan, with a surface area of 674 km^2, a mean depth of 41 m, a drainage basin of 3,848 km^2 and water residence time of ca. 6 years. In the present study, P:R ratio was estimated at an offshore site of Lake Biwa, in order to examine whether or not the community (plankton + benthic organisms) is subsidized with allochthonous organic carbon. Since the details of the primary production rate in this lake have been previously reported (Urabe et al. 1999;Yoshimizu 2001), we mainly estimated the respiration rate of planktonic heterotrophs and carbon mineralization rate in the lake sediments. The respiration rates were calculated based on weekly data of plankton biomass using production-to-biomass ratio and growth efficiencies (in the case of bacterioplankton), and empirical equations of size-specific oxygen consumption rates (in the case of protozoan and metazoan plankton). In these procedures, we chose to underestimate the respiration rates. This is because, if P:R < 1 in spite of the underestimated values of the respiration rates, we can safely conclude that the Lake Biwa ecosystem is net heterotrophic. To verify such a conclusion, partial pressure of carbon dioxide (pCO_2) in the lake surface water was also measured in different seasons as in del Giorgio et al. (1999) and Kelly et al. (2001).

Note that "net heterotrophic" does not mean that the lake is a net source of atmospheric carbon (Hanson et al. 2004). Even if P:R < 1, the lake functions as a net sink of atmospheric carbon if net CO_2 release rate (R−P) is smaller than the burial rate of carbon in the sediment. Therefore, we also examined the burial rate of organic carbon in the Lake Biwa sediments to determine the role of this lake in relation to atmospheric carbon. The carbon mineralization rate and burial rate in the lake sediments were calculated from a decadal time profile of the organic carbon accumulation rate, measured using a ^{210}Pb dating technique.

Materials and methods

Sampling, enumeration and biomass estimation of heterotrophic plankton

Sampling was performed during the period from April 1997 to June 1998 at a pelagic site 3-km off Wani (50-m deep). Plankton was collected at weekly intervals, except from December 1997 to March 1998 when sampling was performed biweekly. For each sampling date, thermal profiles were obtained with a multiple vertical profiler (SBE 25, Sea-Bird Electronics) at 1-m intervals, and lake water was collected using a 10-l modified Van Dorn sampler at eight fixed depths (0, 2.5, 5, 10, 15, 20, 30 and 45 m). For each depth, metazoans (rotifers and crustaceans) and protozoans (mainly ciliates) in 10-l lake water were concentrated using a 20-μm mesh net, killed by 0.4% Lugol's solution, and fixed with 2% sugar-buffered formalin. At the same time water samples from each depth were fixed with 2% cold glutaraldehyde for enumeration of protozoans [mainly heterotrophic nanoflagellates (HNF)] and bacteria.

Since details of the methods for enumeration and biomass estimation are shown elsewhere (Yoshida et al. 2001; Gurung et al. 2001, 2002), we describe them here briefly. For crustacean species, individual counts were made according to developmental stages (copepods) or

size classes (cladocerans) under a dissecting microscope. The individual dry weights were estimated using length–mass equations from Kawabata and Urabe (1998) and McCauley (1984) and converted to carbon mass using a carbon-to-dry weight ratio of 0.45 (Urabe and Watanabe 1990). Rotifers and large ciliates were enumerated under a compound microscope at 100–400×. Their species- or size-specific biovolumes were measured according to Ruttner-Kolisko (1977) for rotifers and Foissner and Berger (1996) for ciliates. Carbon biomass of rotifers and ciliates was then calculated assuming a carbon-to-volume ratio of 0.05 (Latja and Salonen 1978) and 0.14 (Putt and Stoecker 1989), respectively. HNF and small ciliates were enumerated with epifluorescence microscopy by the method described in Sherr and Sherr (1983). The carbon biomass of HNF was calculated assuming an average cell volume of 33 μm and a carbon-to-volume ratio of 0.15 as in Nagata et al. (1996). Note that cell volumes of protozoans applied in the present study were not corrected for any potential shrinkage due to preservation. Thus, the present estimates of the biomass and subsequent metabolic rates of HNF may have been underestimated (see below). Bacteria were enumerated according to Hobbie et al. (1977) and their cell sizes were measured by the method in Lee (1993). The carbon biomass of the bacteria was then calculated using a conversion factor of 106 fg C μm^{-3}, an average value measured during various seasons in Lake Biwa (Nagata 1986).

Respiration rate of heterotrophic plankton

For estimating the respiration rate of metazoan plankton (crustacean and rotifers), we applied the equation of oxygen consumption rate to body weight described by Lampert (1984). This equation was established by compiling oxygen consumption rates of various freshwater metazoan plankton without food at 20°C. The effect of water temperature was corrected using Krogh's normal curve, which represents metabolic activities of various aquatic invertebrates at different water temperatures (Winberg 1971; Lampert 1984). Oxygen consumption rate was converted to CO_2 production rate assuming that RQ was 0.9. Note that the equation used here likely underestimated the in-situ respiration rate because, in general, weight-specific respiration rates of metazoan plankton individuals were 20–50% lower in the absence of food than in the presence of food (Lampert 1986; Urabe and Watanabe 1990).

Respiration rates of protozoan plankton were derived from an equation describing the relationship between oxygen consumption rates and biovolumes of various planktonic protozoan species (Caron et al. 1990). This equation was established for protozoans that are well fed, and that are therefore growing well. In nature, however, protozoans are not necessarily in prime growing conditions (Fenchel 1987; Caron et al. 1990). Indeed, the growth rate of HNF populations in Lake Biwa has been found to be food limited at times (Gurung et al. 2000). According to Caron et al. (1990), oxygen consumption rates under starved conditions are, on average, 75% lower for heterotrophic flagellates and 50% lower for ciliates than under well-fed conditions. Therefore, assuming half of the protozoan cells were under starved conditions, we used 65% lower values than those derived from the equation by Caron et al. (1990). Conversion from oxygen consumption to CO_2 production with the correction for water temperature was made as for metazoans. Since we did not correct for any shrinkage of protozoan cells due to preservation, the estimated respiration rate would again likely be an underestimated value.

To our knowledge, there is no reliable empirical equation for respiration rate that can be applied to natural bacteria under a wide range of environmental conditions. Therefore, we estimated bacterial respiration (R_B) from the biomass (B_B), production (P_B) and growth efficiency (GE_B). The GE_B in terms of carbon is expressed as

$$GE_B = \frac{P_B}{P_B + R_B}$$

Thus, R_B can be calculated as

$$R_B = \frac{1 - GE_B}{GE_B} \times P_B$$

Gurung et al. (2000) have already measured the bacterial growth rate at different depths and seasons in the north basin of Lake Biwa. According to their data, μ_B is highly related to water temperature (Fig. 1). Using this relationship, we estimated bacterial production rate (P_B) as

$$P_B = \mu_B \times B_B$$

This rate is an underestimated value of the finite daily production rate calculated as $B_B \exp(\mu_B - 1)/\mu_B$. In nat-

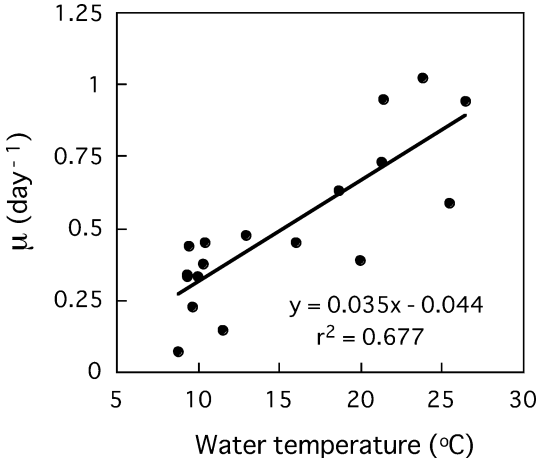

Fig. 1 The relationship between water temperature and growth rate (μ) of bacterioplankton in Lake Biwa (data presented in Gurung et al. 2000)

ure, the GE_B of bacteria varies widely from 0.01–0.6 but tends to approach 0.5–0.6 when bacterial production is higher than 10 mg C m^{-3} d^{-1} (del Giorgio and Cole 1998). Therefore, we fixed the GE_B value at 0.5 in the present study. In the north basin of Lake Biwa, however, the P_B did not necessarily exceed 10 mg C m^{-3} d^{-1} (Nagata 1987; Nakano 1992; Gurung et al. 2002). In addition, we did not quantify bacteria attached to large suspended particles, which are known to contribute 2–15% of bacterial production in the water column of Lake Biwa (Nagata 1987). Thus, the present calculations of bacterial respiration rates are underestimations at least for some seasons.

Zooplankton such as crustaceans and rotifers change their vertical position more or less within a day. In the present study, therefore, we divided the water column into three layers, surface (< 12.5 m), middle (12.5–25 m), and deep (> 25 m). The respiration rate was then calculated using average abundance of heterotrophic plankton and water temperature within each layer. Areal respiration rate through the water column was estimated by vertically integrating the data.

Carbon mineralization and accumulation rates in the lake sediments

Annual carbon mineralization rate in the lake sediment was estimated from the accumulation rate of organic carbon (g C m^{-2} $year^{-1}$) in the lake sediment. The accumulation rate was calculated as organic carbon content per unit volume of sediment (g C m^{-3} $year^{-3}$) multiplied by sedimentation rate (m $year^{-1}$). In contrast to some preserved components in the sediment such as metals and minerals, a fraction of organic carbon is subjected to aerobic and anaerobic decomposition within the sediment. If deposition rate of organic carbon onto the surface of a lake bottom is constant for an extended period, the accumulation rate of organic carbon calculated as above must decrease with increasing age of sediments (those buried at deeper sediment depths) due to decomposition, and would reach a certain value at sediment depths where there is no longer any biologically available organic carbon. Under an equilibrium where vertical profiles of the accumulation rate within sediments remain unchanged for a long period, the amount of organic carbon that is mineralized within the sediment would correspond to the difference in the accumulation rate of organic carbon at the surface and in the deep sediments. We applied this assumption to estimate carbon mineralization rate in the sediment.

To estimate accumulation rate of organic carbon at various sediment depths, a 26-cm-long sediment core was collected at a pelagic site in the north basin of Lake Biwa with a gravity corer (inside diameter 10 cm) on 16 April 2001. The site was 17 km away from where plankton samples were collected. We chose this site because the sediment was not disturbed vertically (Tsugeki et al. 2003). The sediment core was sliced into 1-cm intervals, and several subsamples were collected from each slice. One series of subsamples was used to measure ^{210}Pb for determining the age of the lake sediments. Then, sedimentation rate was calculated from the estimated calendar year and the thickness of the sediment samples. Another series of subsamples was used to determine organic carbon using a CN analyzer (PE2400II, Perkin Elmer). More details on the radiolead dating method and results of the sediment dating with the validity check with the peak of ^{137}Cs impulse are provided elsewhere (Tsugeki et al. 2003).

Primary production rate and pCO_2

Primary production rate and pCO_2 at the lake surface were examined 13 times during the period from June 1996 to October 1997 at the same pelagic site where the heterotrophic plankton were collected. Although the examined period was not exactly the same, it largely overlapped the period of plankton collection. Details on the method and results of primary production rates are presented elsewhere (Urabe et al. 1999; Yoshimizu et al. 2001; Gurung et al. 2002). In short, they were measured using the ^{13}C method by incubating lake water for 4 h starting at 10:00 a.m. at the same depth at which the water had been collected. We used the measured rate as the net primary production rate. Strictly, however, the measured rate is not the net rate but somewhere between net and gross production rates, because a fraction of ^{13}C which had been fixed by algae and had entered into the metabolic pool is respired after the incubation. Thus, the primary production rates used here were apparently overestimations of the net rates.

The pCO_2 at the lake surface was calculated from temperature, pH and dissolved inorganic carbon (DIC) with corrections for known ionic strength according to Zeebe and Wolf-Gladrow (2001). Temperature and pH were measured by the multiple vertical profiler. DIC was determined by a Shimazu TOC-500. Major anions and cations were measured by a DIONEX AQ-1110 suppression ion chromatography system and a Tehermo Jarrel Ash IRIS-AP ICP-AES spectrometer system. Data on these anions and cations at each sampling date are available upon request.

Results

Total biomass of heterotrophic plankton ranged from 1.8–6.5 g C m^{-2} and showed three distinct peaks, early spring, midsummer and late fall (Fig. 2). In most cases, these peaks were due to an increase in abundance of crustacean plankton, especially *Daphnia galeata*. However, *Eodiatomus japonicus* was the most dominant crustacean species because they were abundant regardless of season (Yoshida et al. 2001). A number of rotifer species were present but their biomass was limited, ex-

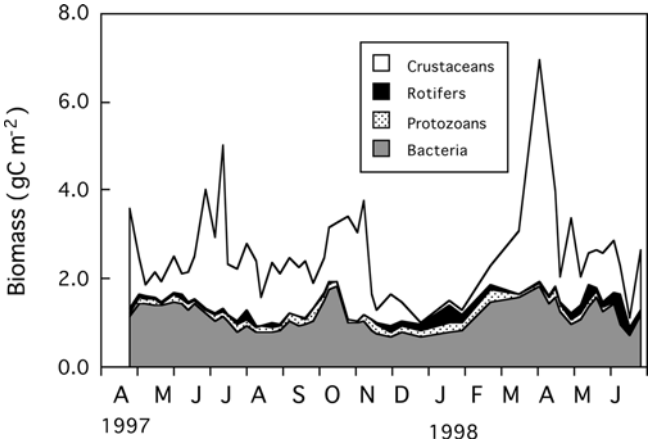

Fig. 2 Seasonal changes in biomass of heterotrophic plankton in the north basin of Lake Biwa

cept in winter and spring when their abundance increased somewhat. Similarly, contribution of protozoans to the total biomass was consistently low except in winter when ciliate occurrence was widespread (Yoshida et al. 2001). In contrast to these heterotrophs, bacterial biomass did not largely change and was seasonally stable. On average, crustaceans and bacteria comprised 47 and 45% of the total biomass, respectively, while rotifers and protozoans composed only 3 and 5% of the biomass, respectively.

Due to the temperature dependency of metabolic rates, community respiration rate of the heterotrophic plankton showed a clear seasonal pattern and ranged from 0.45 g C m^{-2} day^{-1} in winter to 1.6 g C m^{-2} day^{-1} in fall (Fig. 3d). During the period from May to September when the thermocline developed at 10–15 m deep (Gurung et al. 2002), the amount of respired organic carbon reached 0.7–1.0 g C m^{-2} day^{-1} within the surface layer (0–12.5 m) (Fig. 3a) because the heterotrophs were abundant and the water temperature was high. In the middle layer (12.5–25 m), the respiration rate increased to a level equal to the surface layer only in mid-October when vertical mixing of the warm surface water extended into this layer (Fig. 3b). As a result, the highest areal community respiration rate occurred in mid-October. Compared to these layers, the respiration rate in the deep layer was consistently low, although it tended to increase somewhat in winter when the lake water was vertically isothermal due to holomixing (Fig. 3c). Among heterotrophic plankton, bacteria were the most important contributors to the total respiration rate, followed by protozoans. Although the biomass of metazoan plankton was comparable to that of bacteria and higher than that of protozoans, the metazoans contributed much less to the community respiration rate because of a lower weight-specific oxygen consumption rate. In summary, the annual respiration rate of the heterotrophic plankton estimated using data from May 1997 to April 1998 was 339 g C m^{-2} $year^{-1}$ (Table 1).

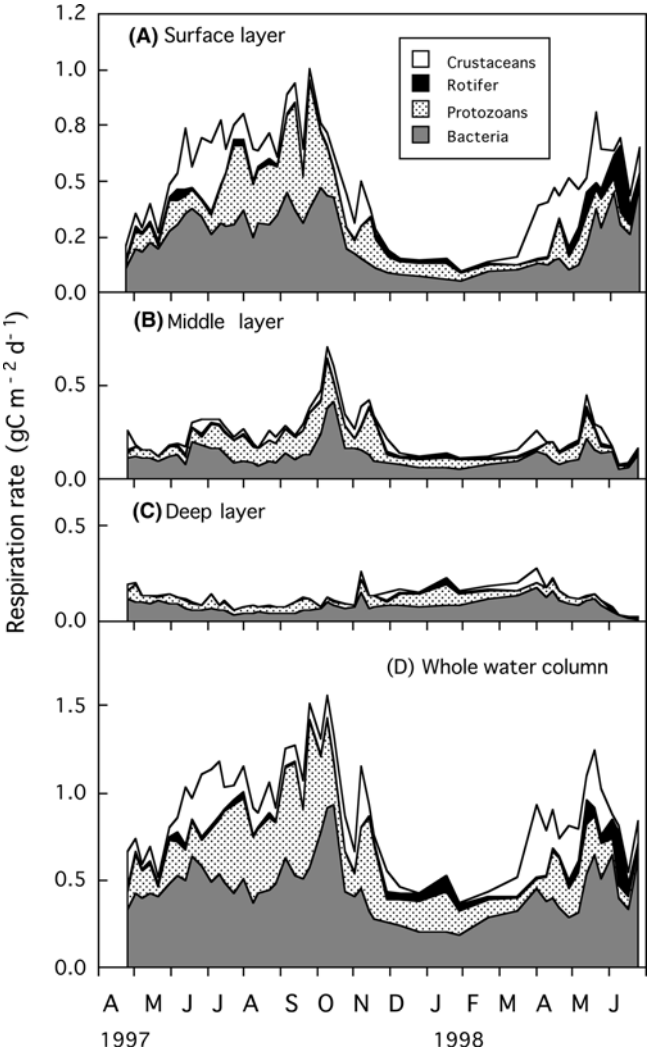

Fig. 3A–D Seasonal changes in the areal respiration rate of heterotrophic plankton in **A** the surface, **B** middle and **C** deep layers and **D** the whole water column in the north basin of Lake Biwa

Sedimentation rate estimated from calendar years based on ^{210}Pb activity and the thickness of the lake sediment varied between 1.1 and 0.18 cm $year^{-1}$. The accumulation rate of organic carbon in the sediment was 52 g C m^{-2} $year^{-1}$ in the upper most layer but, as expected, decreased gradually with the sediment depth (Fig. 4). According to Ogawa et al. (2001) and Tsugeki et al. (2003), Lake Biwa was eutrophicated rapidly in the 1960s, but the trophic condition seems to have stabilized since 1980. Indeed, the accumulation rate did not change substantially among the sediments dated from 1980–1985. The accumulation rate in the sediment dated 1980 was 28 g C m^{-2} $year^{-1}$. If organic carbon was no longer mineralized in sediments deeper than 10 cm (dated at 1980), organic carbon was buried at this rate. Furthermore, if the vertical profiles of the accumulation rate in the sediment have not changed significantly for the past 25 years, the annual rate of carbon mineralization in the sediments can be estimated as the difference between the

Table 1 Summary of respiration rates of heterotrophs in water column and sediments, net primary production rate and P:R ratio at an offshore site (50-m deep) in the north basin of Lake Biwa

	This study	Yoshimizu et al. (2002)
Respiration rate of heterotrophs (g C m^{-2} $year^{-1}$)		
Water column		
0–12.5 m layer	183	
12.5–25 m layer	94	
25–50 m layer	62	
Total	339	262
Sediments	24	
Total	363	
Net primary production rate (g C m^{-2} $year^{-1}$)	323	
P:R ratio		
Water column	0.95	
Water column + sediments	0.89	

accumulation rates in the sediments dated between 2000 and 1980. This was 24 g C m^{-2} $year^{-1}$. Thus, heterotrophs in the lake water and sediment respired organic matter corresponding to 363 g C m^{-2} $year^{-1}$.

The primary production rate varied seasonally, and was low in winter but exceeded 1 g C m^{-2} d^{-1} in summer (Fig. 5a). In contrast, pCO_2 at the lake surface was high in winter but decreased to < 360 ppmv in summer (Fig. 5b), indicating net efflux of CO_2 from the lake in winter and net influx into the lake in summer. To estimate annual net primary production, we divided a year into four periods according to the state of thermal stratification; April to May (thermocline was developed), June to August (stable thermocline was established), September to November (thermocline moved to deep depths) and December to March (holomixing). We then calculated average values for each period and integrated the data for a year. Similarly, annual average pCO_2 at the lake surface was calculated from the averaged values and durations of each period. The estimated annual net primary production rate was 323 g C m^{-2} $year^{-1}$ and average pCO_2 was 424 ppmv.

From these values, the P:R ratio at the offshore site in the north basin was calculated as 0.95 when plankton alone was considered and 0.89 when carbon mineralization at the lake sediments was included (Table 1).

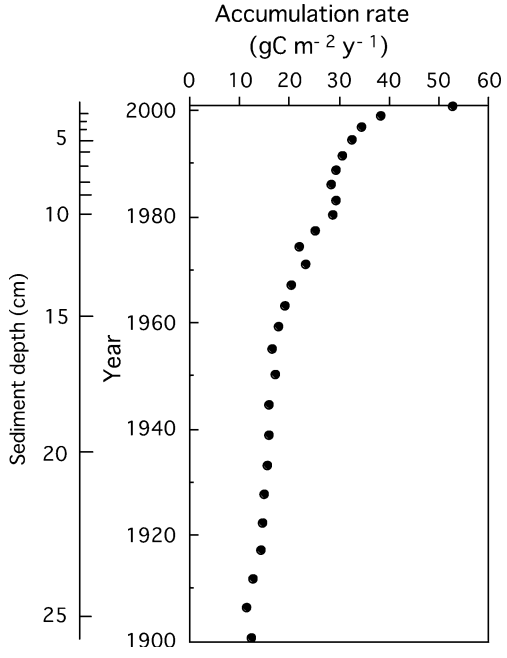

Fig. 4 Depth and time profiles of accumulation rate of organic carbon in the sediments at an offshore site in the north basin of Lake Biwa

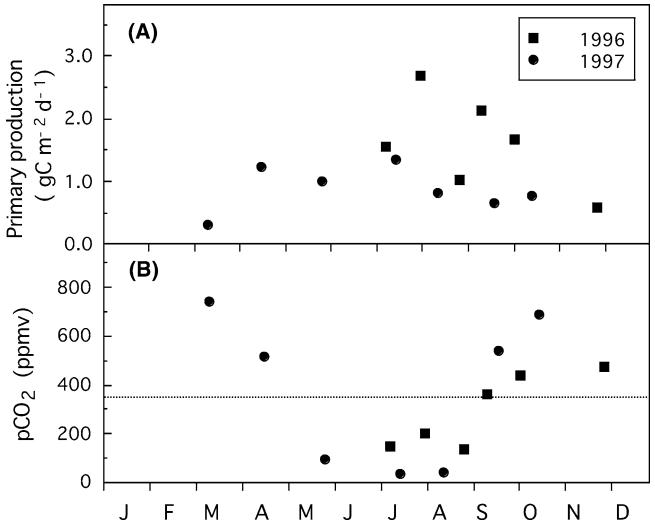

Fig. 5A, B Seasonal changes in **A** net primary production rate and **B** pCO_2 in the surface water in the north basin of Lake Biwa

Discussion

The present study suggests that the Lake Biwa ecosystem is, if anything, net heterotrophic at the offshore area. To estimate bacterial respiration rate, which was 48% of the areal respiration rate of heterotrophs (both in the water column and sediments), we set the growth efficiency to 0.5 in the equation. However, this number is almost at the upper limit of the bacterial growth efficiency found in nature (del Giorgio and Cole 1998). If, for example, the efficiency is 0.25, which is a mean value found in various lakes (del Giorgio and Cole 1998), the bacterial respiration rate becomes three times higher than that estimated at an efficiency of 0.5. In addition, we set a number of assumptions or conditions that resulted in underestimates of the respiration rate of heterotrophic plankton (see Methods and materials). Moreover, we utilized the primary production rate estimated by the ^{13}C method as net production rate. It is likely, therefore, that the areal P:R ratio would be lower than the present estimation.

Nonetheless, the present estimate of community respiration rate in the lake water is higher than that estimated by Yoshimizu et al. (2002), who examined the

carbon budget in the north basin of Lake Biwa using water mass balance, primary production rate and sinking flux of organic carbon (Table 1). Since the respiration rate in Yoshimizu et al. (2002) was also estimated indirectly, it probably includes varying degrees of errors associated with assumptions. Considering such potential artifacts, the estimates of community respiration rate by Yoshimizu et al. (2002) seem not to differ largely from the corresponding estimate in the present study.

To confirm that the Lake Biwa ecosystem is indeed net heterotrophic, we examined CO_2 concentration at the lake surface, as in del Giorgio et al. (1999). The exchange of CO_2 in lakes occurs across the air–water interface. The direction of this exchange is determined by the CO_2 concentration gradient between the air and the surface water. Thus, it is most likely that the pCO_2 is higher in the surface water than in the air for net heterotrophic lakes (Schindler et al. 1972; Cole et al. 2000; Hanson et al. 2003). In Lake Biwa, the surface water pCO_2 showed clear seasonal changes as found in other lakes (Cole and Caraco 1998; Kelly et al. 2001): it decreased to a low level when the lake was thermally stratified. Although the pCO_2 was < 360 ppmv in summer, the annual average was higher than the atmospheric pCO_2, suggesting net release of CO_2 from the lake water in agreement with the areal $P:R < 1$.

Strictly, to judge whether a given lake ecosystem vents CO_2 to the atmosphere, estimation of CO_2 flux is needed. Other than the concentration gradient, the magnitude of CO_2 exchange across the air–water interface depends on the gas exchange coefficient. We have no data on this coefficient that would be applicable to various seasons in Lake Biwa. However, it is well known that the gas exchange coefficient is mainly affected by wind velocity (Cole and Caraco 1998). In Lake Biwa, summer is less windy than other seasons. For example, according to the meteorological records at the Minamikomatsu Station of Japan Meteorological Agency, located 15 km from our sampling station, a daily average wind speed above 1.5 m s^{-1} occurred only 4–5 days per month from May to August, but 9–15 days in other months during the period from 1997 to 1998. In addition, solubility of CO_2 is higher at lower temperatures. Thus, total CO_2 influx into the lake during the period from May to August seems to be lower than total CO_2 efflux to the atmosphere during the remaining period in the year.

Other than respiration, there are two CO_2 sources in lake ecosystems: CO_2 carried by the inflowing groundwater and CO_2 generated by the difference in alkalinity between the inflow and lake waters. Since water residence time of Lake Biwa is $\sim$6 years, the role of these sources in CO_2 flux would be probably minor. Indeed, although pCO_2 in the groundwater in the Lake Biwa watershed is 100 times higher than that in the atmosphere (Ohte et al. 1995), annual inflow of groundwater to Lake Biwa corresponds to only 1.4% of the lake water volume (Endo, unpublished data). This implies that CO_2 brought by groundwater is, at most, 11 g C m^{-2} in a 50-m-thick water column, which is $\sim$3% of the present estimate of the community respiration rate. In addition, alkalinity in the water of major rivers flowing into Lake Biwa was on average 629 μeq l^{-1} (A. Konohira, unpublished data), which did not differ largely from the seasonal average of alkalinity in the lake surface water (611 μe l^{-1}; J. Urabe, unpublished data). These data suggest that heterotrophic metabolisms are a major source of CO_2 in Lake Biwa.

Moreover, it is hard to imagine that direct inputs of inorganic carbon create the clear seasonal patterns of the lake surface pCO_2 found here. In Lake Biwa, CO_2 fixation by photosynthesis took place at the top 10–15 m (Urabe et al. 1999) and exceeded 1 g C m^2 day^{-1} in summer (Fig. 5). However, the respiration rate of heterotrophic plankton at a depth of 0–12.5 m was less than 1 g C m^{-2} day^{-1} (Fig. 3). During summer, the lake water body is physically separated into shallow and deep layers by the thermocline, typically at 10–15 m depths. Thus, the surface water pCO_2 in summer seems to reflect well the carbon balance above the thermocline where the production of organic carbon exceeded the consumption of organic carbon. Leftover production from the organic carbon produced in the shallow layer sinks to the deep layer (hypolimnion) and is utilized in heterotrophic metabolism. The respired CO_2, however, must be accumulated within the deep layer during summer because the thermal stratification creates an obstacle to CO_2 diffusion toward the upper layer. Together with the higher community respiration rate relative to the primary production rate, the accumulated CO_2 would cause high pCO_2 in the lake water in successive seasons when the thermal stratification is weakened or disappears.

The present study showed that the mineralization rate in the lake sediments contributed less than 10% of the areal respiration rate of heterotrophs. According to Murase (personal communication), oxygen consumption rate in the lake sediments was as high as 70 g O_2 m^{-2} $year^{-1}$. The rate corresponds to 27 g C m^{-2} $year^{-1}$ under aerobic respiration with $RQ = 1$. Thus the present estimate is in surprisingly strong agreement with the measured mineralization rate. Note that, in the lake sediments, organic carbon is mineralized not only through aerobic microbial metabolism but also through anaerobic metabolism. Murase and Sugimoto (2002) showed that at a deep offshore site in Lake Biwa, methane corresponding to 2.2–8 g C m^{-2} was produced annually in sediments deeper than a few centimeters from the lake bottom. This amount corresponds to 8–30% of the mineralization rate in the lake sediments. However, the majority of methane is oxidized when it diffuses into the lake water, although the biological or chemical processes are unclear (Murase et al. 2005). Therefore, we regarded the breakdown of organic carbon in the sediments to result in production of CO_2.

As mentioned above, CO_2 released in the deep layer and the lake sediments is accumulated in that layer during the period from May to September due to the

thermal stratification. From the daily respiration rate in the deep layer of the water column and the mineralization rate in the lake sediments, it is expected that CO_2 corresponding to ~42 g C m^{-2} will accumulate below the thermocline during this period. This value means that ~4.5 g O_2 m^{-3} was consumed in the deep layer with 25 m of thickness if RQ = 1. In agreement with this estimate, ~4–6 g O_2 m^{-3} has been consumed every year during the thermally stratified period at deep depths in Lake Biwa since 1970 (i.e., Ishikawa et al. 2004). Thus, although the carbon mineralization rate is much lower in the deep layer compared with the surface layer, further increases in the rate would result in serious impacts on the chemical environments at deep depths in Lake Biwa (see also Murase et al. 2005).

Murase and Sakamoto (2000) showed that allochthonous organic carbon is preferentially preserved in the Lake Biwa sediments. Assuming that organic carbon is not mineralized in sediments deeper than 10 cm, we estimated that the lake has permanently buried organic carbon into the lake bottom at a rate of 28 g C m^{-2} $year^{-1}$ for the past 20 years (Fig. 4). This burial rate is smaller than rates in lakes with a surface area < 500 km^2 but larger than those in larger lakes such as Lake Michigan and Lake Baikal (e.g., Dean and Gorham 1998; Einsele et al. 2001). From our estimates of the respiration and net primary production rates, net CO_2 release (R−P) from the lake is calculated to be 40 g C m^{-2} $year^{-1}$. This value falls well within the expected range of CO_2 efflux in various lakes (Hanson et al. 2004) and is close to the burial rate above. Thus, although the Lake Biwa ecosystem vents carbon to the atmosphere, it buries similar amount of carbon. This implies that the role of this lake in the production of atmospheric carbon is almost null. Note, however, that the present estimate of the burial rate is uncertain because it is not clear to what sediment depth organic carbon is mineralized. Apparently, further study is needed to determine whether the Lake Biwa ecosystem acts as a net source or sink of atmospheric carbon.

In summary, the present study indicates that the Lake Biwa ecosystem is, if anything, net heterotrophic at the offshore area. Such a view is supported by the annual mean of the surface water pCO_2. The result suggests that at the offshore area Lake Biwa receives a substantial amount of organic carbon from the littoral area drainage basin and vents CO_2 to the atmosphere through decomposition. However, the role of the lake as a net source of atmospheric carbon should be discounted because similar amount of carbon is buried in the lake sediments. According to del Giorgio and Peters (1994), P:R varies from < 0.5 in oligotrophic lakes to > 1.5 in eutrophic lakes. Given this wide range, the P:R ratio in Lake Biwa does not deviate largely from 1, suggesting that this lake is situated on the edge between net heterotrophic and net autotrophic. Recently, Konohira and Yoshioka (2005) found an inverse relationship between organic carbon and nutrient concentrations in the river water inflowing to Lake Biwa. Considering the nutrient limitation on primary production (Urabe et al. 1999), an increase in nutrient loading may push Lake Biwa toward net autotrophy and a role as a C sink through an increase in autochthonous production (Hanson et al. 2004). In contrast, an increase in the discharge rate of biologically available organic carbon from the surrounding area would likely push this lake toward net heterotrophy and a role as a C source through an increase in the community respiration rate. In either case, the Lake Biwa ecosystem would be subjected to serious impacts through an increase in oxygen consumption rate in the deep layer and the lake sediment that may result in accelerating eutrophication (Carpenter et al. 1999).

Acknowledgments We thank T. Koitabashi, T. Miyano, and T. Ueda for their assistance in the field and E. Wada for his invaluable suggestions. M. Kyle improved the manuscript. This study was supported by Grants-in-aid for scientific research (A) No. 10308025, (B) No. 10440234 and (B) No. 12440218 from the Ministry of Education, Culture, Sports, Science and Technology (MEXT), Japan, and was conducted as part of IGBP-MEXT-in-Japan (Second Term).

References

Carignan R, Planas D, Vis C (2000) Planktonic production and respiration in oligotrophic Shield lakes. Limnol Oceanogr 45:189–199

Caron DA, Goldman JC, Fenchel T (1990) Protozoan respiration and metabolism. In: Capriulo GM (ed) Ecology of marine protozoa. Oxford University Press, New York, pp 307–322

Carpenter RS, Ludwig D, Brock WA (1999) Management of eutrophication for lakes subject to potentially irreversible change. Ecol Appl 9:751–771

Cole JJ, Caraco NF (1998) Atmospheric exchange of carbon dioxide in a low-wind oligotrophic lake measured by the addition of SF_6. Limnol Oceanogr 43:647–656

Cole JJ, Pace ML, Carpenter SR, Kitchell JF (2000) Persistence of net heterotrophy in lakes during nutrient addition and food web manipulations. Limnol Oceanogr 45:1718–1730

Dean WE, Gorham E (1998) Magnitude and significance of carbon burial in lakes, reservoirs, and peatlands. Geology 26:535–538

del Giorgio PA, Cole JJ (1998) Bacterial growth efficiency in natural aquatic systems. Annu Rev Ecol Syst 29:503–541

del Giorgio PA, Peters RH (1994) Patterns in planktonic P:R ratios in lakes: influence of lake trophy and dissolved organic C. Limnol Oceanogr 39:772–787

del Giorgio PA, Cole JJ, Caraco NF, Peters RH (1999) Linking planktonic biomass and metabolism to net gas fluxes in northern temperate lakes. Ecology 80:1422–1431

Einsele G, Yan J, Hindere M (2001) Atmospheric carbon burial in modern lake basins and its significance for the global carbon budget. Global Planet Change 30:167–195

Fenchel T (1987) Ecology of protozoa. Springer, Berlin Heidelberg New York

Foissner W, Berger H (1996) A user-friendly guide to the ciliates (protozoa, ciliophora) commonly used by hydrobiologists as bioindicators in rivers, lakes, and waste waters, with note on their ecology. Freshw Biol 35:375–482

Gurung TB, Nakanishi M, Urabe J (2000) Seasonal and vertical difference in negative and positive effects of grazers on heterotrophic bacteria in Lake Biwa. Limnol Oceanogr 45:1689–1696

Gurung TB, Kagami M, Yoshida T, Urabe J (2001) Relative importance among biotic and abiotic factors affecting bacterial abundance in Lake Biwa: an empirical analysis. Limnology 2:19–28

Gurung TB, Urabe J, Nozaki K, Yoshimizu C, Nakanishi M (2002) Bacterioplankton production in a water column of Lake Biwa. Lakes Reserv 7:317–323

Hanson PC, Bade DL, Carpenter SR, Kratz TK (2003) Lake metabolism: relationships with dissolved organic carbon and phosphorus. Limnol Oceanogr 48:1112–1119

Hanson PC, Pollard AI, Bade DL, Predick K, Carpenter SR, Foley JA (2004) A model of carbon evasion and sedimentation in temperate lakes. Global Change Biol 10:1285–1298

Hobbie JER, Daley J, Jasper S (1977) Use of Nuclepore filters for counting bacteria by fluorescent microscopy. Appl Env Microbiol 33:1225–1228

Ishikawa T, Narita T, Urabe J (2004) Long-term changes in the abundance of *Jesogammarus annandalei* (Tattersall) in Lake Biwa. Limnol Oceanogr 49:1840–1847

Kawabata K, Urabe J (1998) Length-weight relationships of eight freshwater planktonic crustacean species in Japan. Freshw Biol 39:199

Kelly CA, Everett F, Ramla PS, Rudd JW, Hesslein RH, Anema C, Shindler EU (2001) Natural variability of carbon dioxide and net epilimnetic production in the surface waters of boreal lakes of different sizes. Limnol Oceanogr 46:1054–1064

Konohira A, Yoshioka T (2005) Dissolved organic carbon and nitrate concentrations in stream—a useful index indicating carbon and nitrogen availability in catchments. Ecol Res (in press)

Lampert W (1984) The measurement of respiration. In: Downing JA, Rigler FH (eds) A manual on methods for the assessment of secondary productivity in fresh waters, 2nd edn. Blackwell, Oxford, pp 413–468

Lampert W (1986) Response of the respiratory rate of *Daphnia magna* to changing food conditions. Oecologia 70:495–501

Latja R, Salonen K (1978) Carbon analysis for the determination of individual biomass of planktonic animals. Verh Int Verein Limnol 20:2556–2560

Lee S (1993) Measurement of carbon and nitrogen biomass and biovolume from naturally derived marine bacterioplankton. In: Kemp FP, Sherr FB, Sherr EB, Cole JJ (eds) Handbook of methods in aquatic microbial ecology. Lewis, Boca Raton, pp 319–325

McCauley E (1984) The estimation of the abundance and biomass of zooplankton in samples. In: Downing JA, Rigler FH (eds) A manual on methods for the assessment of secondary productivity in fresh waters, 2nd edn. Blackwell, Oxford, pp 228–265

Murase J, Sakamoto A (2000) Horizontal distribution of carbon and nitrogen and their isotopic compositions in the surface sediment of Lake Biwa. Limnology 1:177–184

Murase J, Sugimoto A (2002) Seasonal and spatial variations of methane production in mesotrophic lake sediments (Lake Biwa, Japan). Verh Int Verein Limnol 28:971–974

Murase J, Sakai Y, Kametani, A, Sugimoto A (2005) Dynamics of methane in a mesotrophic Lake Biwa, Japan. Ecol Res (in press)

Nagata T (1986) Carbon and nitrogen content of natural planktonic bacteria. Appl Environ Microbiol 52:28–32

Nagata T (1987) Production rate of planktonic bacteria in the north basin of Lake Biwa, Japan. Appl Environ Microbiol 53:2872–2882

Nagata T, Takai K, Kawabata K, Nakanishi M, Urabe J (1996) The trophic transfer via a picoplankton-flagellate-copepod food chain during a picocyanobacterial bloom in Lake Biwa. Arch Hydrobiol 137:145–160

Nakano S (1992) Changes in bacterioplankton production and dominant algal species in the north basin of Lake Biwa. Jpn J Limnol 53:145–149

Nakano S, Murakami M (2001) Reciprocal subsidies: dynamic interdependence between terrestrial and aquatic food webs. Proc Natl Acad Sci USA 98:166–170

Ogawa NO, Koitabashi T, Oda H, Nakamura T, Wada E (2001) Fluctuations of nitrogen isotope ratio of gobiid fish (Isaza) specimens and sediments in Lake Biwa, Japan, during the 20th century. Limnol Oceanogr 46:1228–1236

Ohte N, Tokuchi N, Suzuki M (1995) Biogeochemical influences on the determination of water chemistry in a temperate forest basin: factors determining the pH value. Wat Resource Res 31:2823–2834

Polis GA, Power ME, Huxel GR (2004) Food webs at the landscape level. Chicago University Press, Chicago

Prairie YT, Bird DF, Cole JJ (2002) The summer metabolic balance in the epilimnion of southeastern Quebec lakes. Limnol Oceanogr 47:316–321

Putt M, Stoecker DK (1989) An experimentally determined carbon:volume ratio for marine 'oligotrichous' ciliates from estuarine and coastal waters. Limnol Oceanogr 34:1097–1103

Ruttner-Kolisko A (1977) Suggestions for biomass calculations of planktonic rotifers. Arch Hydrobiol Beih 21:71–76

Schindler DW, Brunskill GJ, Emerson S, Broekcer WS, Peng T-H (1972) Atmospheric carbon dioxide: its role in maintaining phytoplankton standing stocks. Science 177:1192–1194

Sherr EB, Sherr BF (1983) Double-staining epifluorescence technique to assess frequency of dividing cells and bacterivory in natural populations of heterotrophic microprotozoa. Appl Env Microbiol 46:1388–1393

Tsugeki N, Oda H, Urabe J (2003) Fluctuation of the zooplankton community in Lake Biwa during the 20th century: a paleolimnological analysis. Limnology 4:101–107

Urabe J, Watanabe Y (1990) Influence of food density on respiration rate of two crustacean plankters, *Daphnia galeata* and *Bosimina longirostris*. Oecologia 82:362–368

Urabe J, Sekino T, Nozaki K, Tsuji A, Yoshimizu C, Kagami M, Koitabashi T, Miyazaki T, Nakanishi M (1999) Light, nutrients and primary productivity in Lake Biwa: an evaluation of the current ecosystem situation. Ecol Res 14:233–242

Winberg GG (1971) Methods for the estimation of production of aquatic animals. Academic, London

Yoshida T, Kagami M, Gurung TB, Urabe J (2001) Seasonal succession of zooplankton in the north basin of Lake Biwa. Aquat Ecol 35:19–21

Yoshimizu C, Yoshida T, Nakanishi M, Urabe J (2001) Effects of zooplankton on the sinking flux of organic carbon in Lake Biwa. Limnology 2:37–43

Yoshimizu C, Urabe J, Sugiyama M, Maruo M. Nakayama E, Nakanishi M (2002) Carbon and phosphorus budgets in the pelagic area of Lake Biwa, the largest lake in Japan. Verh Int Verein Limnol 28:1409–1414

Zeebe RE, Wolf-Gladrow D (2001) CO_2 in seawater: equilibrium, kinetics, isotopes. Elsevier, Amsterdam

Ecol Res (2005) 20: 377–385
DOI 10.1007/s11284-005-0053-x

ORIGINAL ARTICLE

Jun Murase · Yuji Sakai · Aya Kametani
Atsuko Sugimoto

Dynamics of methane in mesotrophic Lake Biwa, Japan

Received: 16 September 2004 / Accepted: 29 December 2004 / Published online: 17 March 2005

Abstract As a part of a core project of IGBP (International Geosphere-Biosphere Programme), distribution, production, oxidation and transport processes of methane in bottom sediments and lake water in a mesotrophic lake (Lake Biwa) have been studied with special reference to the spatial heterogeneity of each process. In this study, we attempted to synthesize previously reported results with newly obtained ones to depict the methane dynamics in the entire lake. The pelagic water column exhibited subsurface maxima of dissolved methane during a stratified period. Transect observation at the littoral zone suggested that horizontal transportation may be a reason for the high methane concentration in epilimnion and thermocline at the offshore area. Tributary rivers and littoral sediments were suggested to be the source. Observations also showed that the internal wave caused resuspension of the bottom sediment and release of methane from the sediment into the lake water. The impact of the internal waves was pronounced in the late stage of a stratified period. The littoral sediment showed much higher methanogenic activity than the profundal sediments, and the bottom water of the littoral sediments had little methanotrophic activity. In the profundal sediment, most of the methane that diffused up from the deeper part was oxidized when it passed through the oxic layer. Active methane oxidation was also observed in the hypolimnetic water, while the lake water in the epilimnion and thermocline showed very low methane oxidation, probably due to the inhibitory effect of light. These results mean a longer residence time for methane in the epilimnion than in the hypolimnion. Horizontal inflow of dissolved methane from the river and/or littoral sediment, together with the longer residence time in the surface water, may cause the subsurface maxima, which have also been observed in other lakes and in the ocean.

Keywords Methane · Mesotrophic lake · Resuspension · Seiche · Subsurface maximum

J. Murase · Y. Sakai · A. Kametani
School of Environmental Science,
University of Shiga Prefecture, Hikone,
Shiga 522-8533, Japan

A. Sugimoto
Center for Ecological Research, Kyoto University,
Otsu, Shiga 520-2113, Japan

Present address: J. Murase (✉)
Graduate School of Bioagricultural Sciences,
Nagoya University, Furocho, Chikusa,
Nagoya 464-8601, Japan
E-mail: murase@agr.nagoya-u.ac.jp
Tel.: +81-52-7895323
Fax: +81-52-7894136

Present address: A. Sugimoto
Graduate School of Environmental Earth Science,
Hokkaido University, Sapporo 060-0810, Japan

Introduction

Methane is a terminal product of anaerobic carbon metabolism, and methanogenesis is a dominant biogeochemical process in anaerobic freshwater environments (Zehnder and Stumm 1988). Methane production and emission from various anaerobic ecosystems have been studied since methane is the most important greenhouse gas after CO_2 and adsorption of infrared radiation by methane is more effective than by CO_2 on a per-mol basis (e.g., Cicerone and Oremland 1988; Mitchell 1989).

Methane release from a lake depends on the balance between methane production and oxidation (e.g., Reeburgh et al. 1991). A decrease in oxygen supply and an increase in supply of organic matter on the surface of the bottom sediment in a lake both stimulate methane production, and both also diminish the oxic layer at the surface of the lake sediment. Methane produced in the sediment also contributes to oxygen

consumption through its oxidation (Gelda et al. 1995). Methane release from a lake is, therefore, sensitive to the redox condition at the surface of the sediment. Eutrophication of the lake also accelerates methane release from lake sediment by increasing the supply of organic matter on the surface of the lake sediment. It can be said that methane release from the lake-bottom sediment is also an indicator of the trophic condition of the lake.

Research on carbon flow in the watershed of Lake Biwa, the largest freshwater lake in Japan, has been carried out as a part of the core project TEMA (Terrestrial Ecosystem in Monsoon Asia) under IGBP (International Geosphere-Biosphere Programme). Various studies on methane dynamics in this lake have also been carried out. The spatial distribution of methane concentration and its carbon isotope ratio (Murase and Sugimoto 2001), the temporal variations in concentration and isotopic composition of dissolved methane in the lake and tributaries (Murase et al. 2003), and the rate of production of methane in the bottom sediment (Murase and Sugimoto 2002) have been previously reported. Many interesting results, such as photoinhibition of methane oxidation in the water column of the lake (J. Murase and A. Sugimoto, submitted), methane release from the sediment by an internal seiche (Sakai et al. 2002), and storage of methane on the surface of the sediment particles by adsorption (Sugimoto et al. 2003), have also been reported.

In order to discuss methane dynamics in the entire lake, mechanisms of methane production, oxidation, and release at each part of the lake should be taken into consideration. We have already reported most of them except for the oxidation process at the surface of the sediment and the release mechanism of methane from the sediment by the internal wave. In this article, we show the observational and experimental results for these remaining problems, and discuss the methane dynamics in the entire lake together with the previously reported results.

There are many studies on methane dynamics in eutrophic lakes (Kiene 1991), while oligotrophic and mesotrophic lakes have been studied much less so far. Limited studies (Schmidt and Conrad 1993; Miyajima et al. 1997; Schulz et al. 2001) showed that, in a mesotrophic lake, methane concentration is higher in the upper layer of the water column than in the lower layer. This is in contrast to the eutrophic lake, where the bottom sediment is the most important source of methane in water, and the highest methane concentration is generally observed in the bottom water (Kiene 1991). The subsurface maxima of methane have also been observed in the sea and open ocean (Dafner et al. 1998; Seifert et al. 1999), but the mechanism is poorly understood. A diagnostic synthesis of our work on methane in mesotrophic Lake Biwa will be attempted in this study to elucidate the mechanism for subsurface maxima of dissolved methane in the lake.

Materials and methods

The series of studies on methane dynamics was conducted in Lake Biwa, in Japan. The sampling and observation sites are indicated in Fig. 1.

To determine the oxidation rate of methane diffused from sediment at the surface, sediment core samples were collected from the profundal zone (Station A) using a gravity corer (i.d. 5 cm). The surface part (0–10 cm) of the sediment was transferred to an acrylic tube (length 15 cm; i.d. 5 cm) keeping the structure of the sediment. Overlying water was removed with a syringe until 5 mm of water film was left on the sediment. The top of the tube was capped with a rubber stopper with a port for gas sampling. The headspace of the core was exchanged with N_2 for anaerobic incubation by flushing through the port. The core samples were incubated at the in situ temperature (8°C), and methane concentration in the headspace was monitored. Rate of methane oxidation at the surface layer of the sediment was estimated by comparing the rate of methane release from the sediment under oxic and anoxic conditions.

A microcosm experiment was done to estimate the impact of water current through the bottom water on release of methane from the sediments. Core samples were collected from Station A using a gravity corer (i.d. 5 cm), and the surface part (0–6 cm) of the core samples were transferred together with overlying water (5 cm deep) to an acrylic tube (i.d. 5 cm; length 20 cm) that

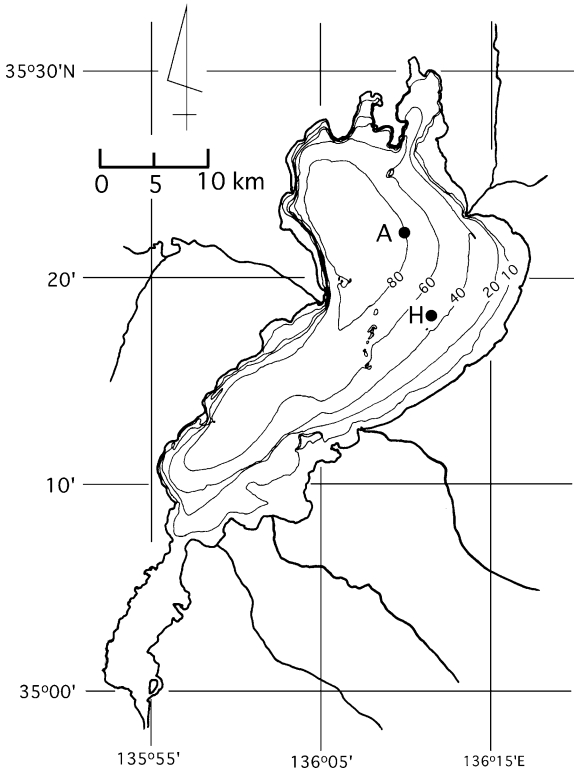

Fig. 1 Map of Lake Biwa

had holes on the side. The overlying water was removed with a syringe and the filtered (< 95 μm) surface water (10-m depth) collected in Station A was gently added above the sediment. The top of the tube was capped with a rubber stopper excluding bubbles inside the tube. Different rates (5.7 and 30 cm s^{-1}) of horizontal water flow were applied to the bottom part of the overlying water for 10 s from the side of the tube by a water pump. Concentration in the water was immediately determined by the headspace method (Kimura et al. 1992).

The temporal change in the depth profiles of the water temperature was observed to determine the amplitude and frequency of internal waves in the lake. Measurement of water temperature was conducted in the late stage of a stratified period (from 29 November to 20 December in 2000) offshore of Hikone (Station H, water depth of 50 m; Fig. 1). A thermistor chain that had 22 thermistors at intervals of 3.5–4.5 m for epilimnion and 1.5 m for the deeper layer was set, and water temperature was measured at intervals of 30 min.

Observations which have been already published elsewhere are used for the discussion on the dynamics of methane in the entire lake. Spatial distribution of methane concentration and its stable carbon isotope ratio in the bottom sediment were obtained from the top-10-cm layer (Murase and Sugimoto 2001). Methane production rates of sediments were measured from the surface to 23 cm deep for the profundal area and from 2–8 cm for the littoral area (Murase and Sugimoto 2002). The amount of methane retained in the sediment (surface to 10 cm) were analyzed by Sugimoto et al. (2003) and Dan et al. (2004). Methane concentrations in the lake and tributary rivers were observed by Murase et al. (2003). Oxidation of the in situ methane in the lake water was determined by an incubation experiment, and the effect of light on methane oxidation was also examined (J. Murase and A. Sugimoto, submitted). Briefly, lake water samples, which were collected from the different depths of the pelagic area and from the bottom of the littoral area, were incubated in serum bottles at 15°C under dark and light conditions (57 μmol m^{-2} s^{-1} for 12 h day^{-1}), and temporal change in methane concentration was monitored.

Results

Methane oxidation in the surface layer of the sediment

Methane concentration in the headspace of the sediment core linearly increased with time when the headspace was exchanged with nitrogen (Fig. 2). The cores that were incubated with air in the headspace released much less methane into the headspace. The carbon isotopic composition of methane in the headspace was −70‰ under anaerobic conditions and −48‰ under aerobic conditions, suggesting that methane was oxidized in the oxic layer of the sediment under aerobic conditions.

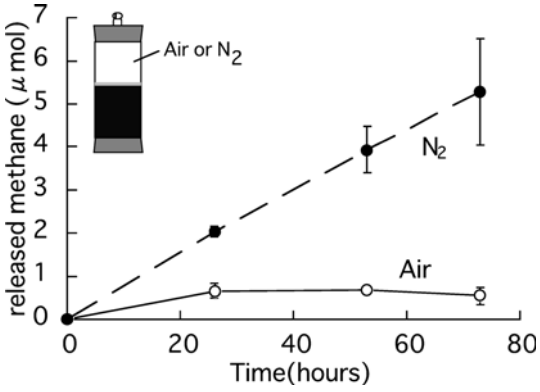

Fig. 2 Release of methane from profundal (Station A) sediment cores under oxic and anoxic atmospheres. *Bars* represent the error in duplicate

Based on the difference in release rate of methane from the sediment under oxic and anoxic conditions, approximately 90% of methane diffused from the deeper part of the sediment was considered to be oxidized when passing through the oxic layer of the surface sediment. High methane oxidation rates in the surface sediment of a mesotrophic lake have also been reported by Frenzel et al. (1990).

The effect of water current on release of methane from the sediment

Water current applied to the overlying water of the sediment core at 30 cm s^{-1} for 10 s resulted in a remarkable increase in methane concentration in the overlying water (Fig. 3). A water current of 30 cm s^{-1} is as high as the field data, and water currents higher than 200 cm s^{-1} have been observed in the lake (Endo, personal communication). Thus, our results reflect the impact of water current on release of methane from sediment. In the field, a rapid downward shift of the thermocline (5 m in depth in 3 h), probably due to an internal wave, was observed (Sakai et al. 2002). Turbidity and methane concentration synchronistically increased in the thermocline after the downward movement, suggesting that the water current of the internal wave caused resuspension of bottom sediment and release of dissolved methane (Sakai et al. 2002).

It is recognized that internal wave causes resuspension of bottom sediments of the lake (Shteinman et al. 1997). However, little attention has been given to the fact that considerable amounts of methane are released by an internal wave. Our observation is the first showing methane release caused by an internal wave.

Frequency and amplitude of internal waves

The amplitude and frequency of internal waves in the lake were studied by monitoring the temporal change in the depth profiles of water temperature. Water temper-

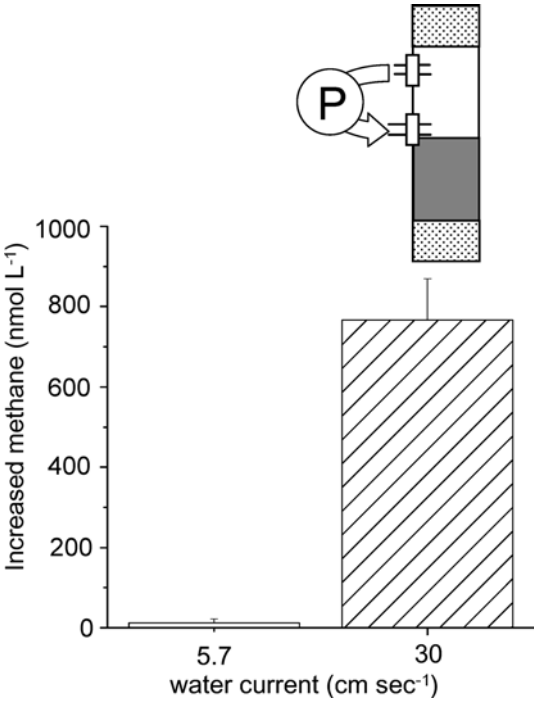

Fig. 3 The effect of water current on methane concentration in bottom water. The bottom water of the sediment core sample was circulated using a pump to provide water currents at the indicated speeds (see the illustration). *Bars* indicate the error of duplicate measurements

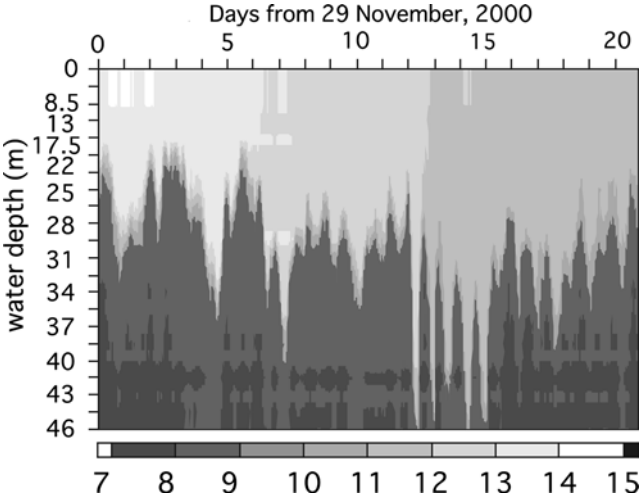

Fig. 4 Temporal change in depth profile of water temperature (°C) at the late stage of a stratified period offshore of Hikone at a water depth of 50 m (Station H)

ature in the epilimnion decreased from 14.0 to 11.4°C during the observation period (Fig. 4). Internal waves with amplitudes higher than 5 m were observed more than once a day on average, with a higher frequency in the late period. Internal waves with high amplitude (> 20 m) occurred in a short time especially at the late stage, when the water temperature in the epilimnion decreased.

The amplitude of the internal waves was large. It is highly possible that considerable methane is released when the internal wave hits the bottom sediment. Actually, in the late stage of a stratified period (in December and January 2000), a high concentration of dissolved methane (100–140 nM) was observed in the bottom water of the site (Station B) where the thermocline was situated around the lake bottom (Murase et al. 2003).

Discussion

There are few studies on methane dynamics in oligo- to mesotrophic lakes, and little attention has been paid to the spatial heterogeneity of methane dynamics in an entire lake ecosystem. Our series of studies demonstrates that transport, production, and oxidation processes of methane differ among the subsystems of the lake; water versus sediment, littoral area versus pelagic area, and epilimnion versus hypolimnion, and the spatial heterogeneities characterize the methane dynamics of the entire lake. Methane dynamics in the subsystems of Lake Biwa are discussed below.

Methane production and release from the lake sediments

Methane content in the surface (0–10 cm) sediments of the north basin of the lake ranged from 0.06–2.4 mmol l^{-1} (Table 1). The carbon isotopic ratio of methane ranged from −71 to −80‰, and the apparent carbon fractionations between methane and inorganic carbon ranged from 1.064–1.084 (Murase and Sugimoto 2001), suggesting that CO_2 reduction is the major pathway of methanogenesis (Whiticar et al. 1986; Sugimoto and Wada 1993).

The littoral sediments showed much higher methane production rates than the profundal sediments (Table 2). One of the main reasons for the high activity of methanognesis in the littoral sediments was the high summer temperatures. Other factors such as quality of organic matter deposited may be also responsible, since the littoral sediment in winter showed a higher methanogenic activity than the profundal sediments (Murase and Sugimoto 2002).

The profundal sediments showed apparent methane production even in the deeper layers (23 cm depth) upon anaerobic incubation (Murase and Sugimoto 2002). However, part of the methane released by incubation may have been produced earlier by methanogenic bacteria and stored in adsorbed form in the sediment particles (Sugimoto et al. 2003). Dan et al. (2004) investigated the methane release and found that methane is released biotically and abiotically as well from the sediment slurry. Methane stored on the sediment particles can be desorped by release of hydrostatic pressure or decrease in the concentration of dissolved methane in

Table 1 Methane content and its carbon stable isotopic ratio in lake water, sediment, and tributary rivers of Lake Biwa

Site	Methane content (μmol l^{-1})	$\delta^{13}C$ (‰)	Remarks	Reference
Lake water				
Pelagic	0.004–0.17	−62.6 to −21.8	Station A	Murase et al. (2003)
Littoral	0.49–3.04	−57.3 to −47.6	Stations Y5 and Y10 (22 July 2000)	Murase et al. (2003)
Sediments				
North basin	60–2,400	−78.8 to −70.9	12–100 m	Murase and Sugimoto (2001)
South basin	40–710	−79.7 to −60.7	in water depth	Murase and Sugimoto (2001)
Tributary rivers			Distance from the river mouth (km)	
Echi	0.33–2.03	−54.4 to −46.8	1.2	Murase et al. (2003)
Hino	0.24–2.17	−59.5 to −47.6	1.8	Murase et al. (2003)
Yasu	0.24–3.43	−64.0 to −49.3	1.2	Murase et al. (2003)
Ado	0.014–2.29	ND	1.2	Murase et al. (2003)
Ane	0.015–0.26	ND	1.2	Murase et al. (2003)

ND no data

Table 2 Production rates of methane in the bottom sediments of Lake Biwa (Murase and Sugimoto 2002)

Site	Production rate (μmol l^{-1} day^{-1})	$\delta^{13}C$ (‰)
Profundal sediment		
Station A	0.02–12.3	−72.3 to −69.3
Station B	0.04–9.82	−78.0 to −73.3
Littoral sediments		
In situ temperature	11.4–88.0	−68.7 to −60.1
10°C	9.87–14.3	−69.8 to −67.4

the pore water. The amount of methane stored on the clay minerals in the Lake Biwa sediment was small compared to the total amount of methane in the sediment (Sugimoto et al. 2003). However, we should pay attention to the adsorption of methane on the surface of the sediment particles because clay minerals are universally observed in lake and ocean sediments, and high adsorption ability may be expected in some cases.

Methane in the sediment is the potential source of dissolved methane in the lake water, since the methane contents in the sediment were higher than those in lake water by 2–5 orders of magnitude (Table 1). However, the surface of the sediment is oxic in the mesotrophic lake, and active oxidation at the surface layer is a strong sink for methane produced in the deeper layer of the sediment. Consequently, only a small amount of methane is released to the lake water (Fig. 2). Rate of oxygen consumption by methane oxidation at the sediment surface was comparable to that by decomposition of organic matter in the surface layer of the sediment (0–5 mm) (A. Kametani, unpublished data). The active methane oxidation at the surface layer of the sediments implies that methane-oxidizing bacteria may significantly contribute to carbon flow in the sediment. Extremely low values of carbon isotope ratio observed in chironomid larvae suggest ingestion of microbial biomass of methanotrophs and flow of methane-derived carbon in the bottom sediment in Lake Biwa (Kiyashko et al. 2001).

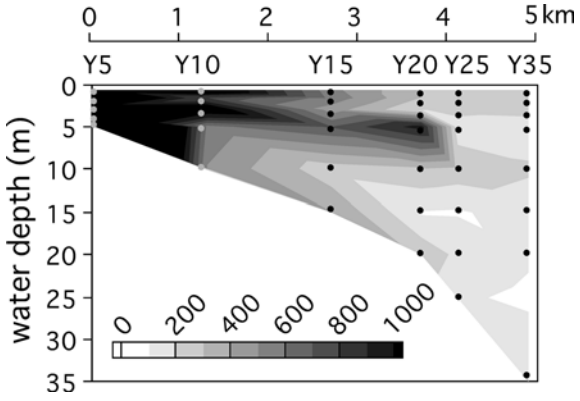

Fig. 5 Transect observation of distribution of dissolved methane (nmol l^{-1}) in the offshore of Yasu River (redrawn from Murase et al. 2003)

Methane dynamics in the littoral zone

The lake water in the near-shore area contained much higher amounts of methane than the pelagic water (Table 1) (Murase et al. 2003). The transect observation indicated that high concentrations of dissolved methane in the littoral zone were horizontally transported offshore (Fig. 5).

All the river waters examined were replete with dissolved oxygen, but were oversaturated with dissolved methane to the atmospheric concentration of methane (Murase et al. 2003). The water samples of the rivers located on the eastern side of the lake (Echi, Hino, and Yasu Rivers) contained much higher amounts of dissolved methane than the pelagic water column of the lake (Table 1). Thus, transportation from the tributary rivers may be a source of the dissolved methane in the lake water as reported in the coastal area (de Angelis and Lilley 1987; Jones and Mulholland 1998). River water can transport high concentrations of methane into the different depths of the water column in the lake according to seasonal changes in density current. That

is, in the early stage of the thermal stratification period, when the water temperature of the river water is higher than that of the surface water of the lake, the river water is discharged onto the surface of the lake water and may contribute to the high methane concentration in the surface water. This was observed offshore of the Yasu River in July 1999 (Fig. 5). In the late stage of a stratified period, the temperature of the river water becomes lower than that of the surface water and the river water intrudes into the water column of the lake, probably onto the thermocline.

The high levels of microbial activities due to the high temperature in the littoral sediments and the diurnal thermal stratification of the lake water may cause depleted oxygen concentration in the bottom water in the littoral zone. Although methanotrophs may oxidize methane even at low O_2 concentrations (Rudd et al. 1974), some part of the methane diffused from the deeper sediment can diffuse into the lake water, passing through the less oxic surface layer of sediments without being oxidized. Decreased oxygen and increased methane concentrations were observed in the bottom water of the littoral zone of Lake Biwa in summer (Murase et al. 2003). The transect observations demonstrated that methane diffused from the littoral sediments was horizontally transported to the offshore of the lake like river water. This suggests that methane diffused from the littoral sediment is another potential source of methane in the epilimnion and thermocline of the pelagic water column.

Because the bottom sediments contain high amounts of methane compared to the lake water as described above, resuspension of the surface sediment causes release of methane from the sediment, which may be a source of methane in the lake water. Resuspension of the littoral sediments is induced by a surface wave, while an internal wave induces resuspension of the deeper sediments (Bloesch 1995). Our results demonstrate the potential importance of internal waves in release of methane from the "sub-littoral" sediments. The water depth of the thermocline seasonally shifts according to the change in the structure of water temperature. In the early to middle stage of a stratified period, the thermocline is situated at a depth of around 15–20 m in Lake Biwa. In the late stage, the thermocline moves down to 30–40 m accompanied by a decrease in the water temperature of the epilimnion until the lake water is overturned. The internal waves can cause resuspension of the bottom sediments over broad depths due to the vertical shift of the thermocline. Especially in the late stage of a stratified period, differences in the water temperature between the epilimnion and hypolimnion become smaller, and the amplitude of the internal wave consequently becomes larger (Fig. 4). The strong seasonal winds in winter may induce frequent occurrence of internal waves, which may also cause the resuspension of the sediment and release of methane from the sediment.

Dynamics of dissolved methane in the water column in the pelagic zone

Methane concentration in the pelagic water column ranged from 4.3–166 nmol l^{-1} (Table 1). During the stratified period, methane concentration was higher in the epilimnion and thermocline than in the hypolimnion (Murase et al. 2003). The peaks in methane concentration were observed in the thermocline in the middle of a stratified period. The transportation of dissolved methane from the littoral and sub-littoral zones described above may be the most important source of dissolved methane. The highest methane concentration in the pelagic water column was recorded during the late stage of a stratified period (Murase et al. 2003). The river inflows may not explain this maximum methane content because no significant increase in methane concentration in the major river waters was observed in this period (Murase et al. 2003), nor in the amount of water discharge (data not shown). The littoral sediment had a lower methane production activity in winter than in summer (Murase and Sugimoto 2002). Therefore, release of methane from sediment resuspended by internal waves is the possible source of the increased methane. This conclusion is supported by the observational result that the maximum methane content in the pelagic water column was observed just before the overturn of the lake water in the late stage of the stratified period, when the bottom water of the sub-littoral zone (30-m depth) showed the highest methane concentration probably due to the internal waves (Murase et al. 2003).

Active oxidation of dissolved methane was observed in the hypolimnion of the pelagic area (Fig. 6). This is in agreement with the stable carbon isotope data of methane which showed a seasonal increase in the

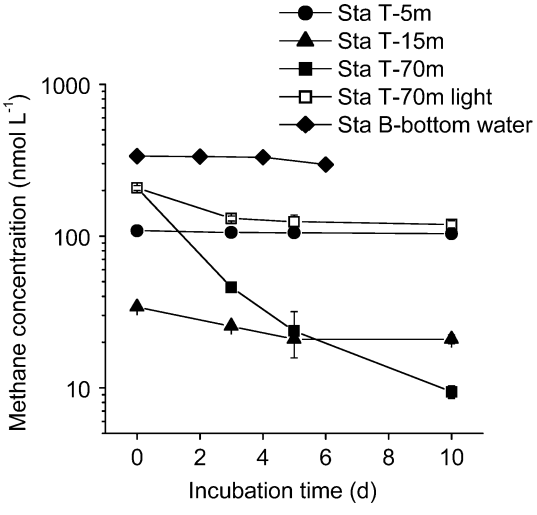

Fig. 6 Methane oxidation in lake water collected from different depths of the pelagic water column [Station T (*Sta T*)] and bottom water in the littoral zone [Station B (*Sta B*), 10 m depth]. Water depths of 5, 15, and 70 m in the pelagic water column correspond to epilimnion, thermocline, and hypolimnion, respectively

hypolimnion during a stratified period (Murase et al. 2003). Methane in the water column has been reported to be a carbon source for the lake pelagic food webs (Bastviken et al. 2003). Methane oxidation in the water samples from the epilimnion and thermocline (Station T, 5 and 15 m depth) was insignificant. Methane oxidation in the hypolimnetic water was insignificant when the water was incubated under light. Epilimnion water incubated under dark conditions showed methane oxidation after a long-term incubation period (> 1 month). These results indicate the inhibitory effect of light on methane oxidation in the lake water (J. Murase and A. Sugimoto, submitted).

The bottom water of the littoral area (Station B) also showed little methane oxidation (Fig. 6) (J. Murase, unpublished data). Because of the low methane oxidation and the high methane production rate in the sediment, the concentration of dissolved methane may be high in the littoral zone. This may be one of the strong sources of dissolved methane in the pelagic water column.

Methane dynamics in the entire lake

Based on data obtained, the dynamics of methane in the lake are summarized in Fig. 7. The horizontal inflow of dissolved methane from the river and littoral sediment is an important source of dissolved methane in the epilimnion and thermocline. Release of methane from the sub-littoral sediment caused by internal waves is another important source, especially at the end of a stratified period. Profundal sediment may be a minor source of methane in the hypolimnion because of the active oxidation of diffused methane in the sediment surface.

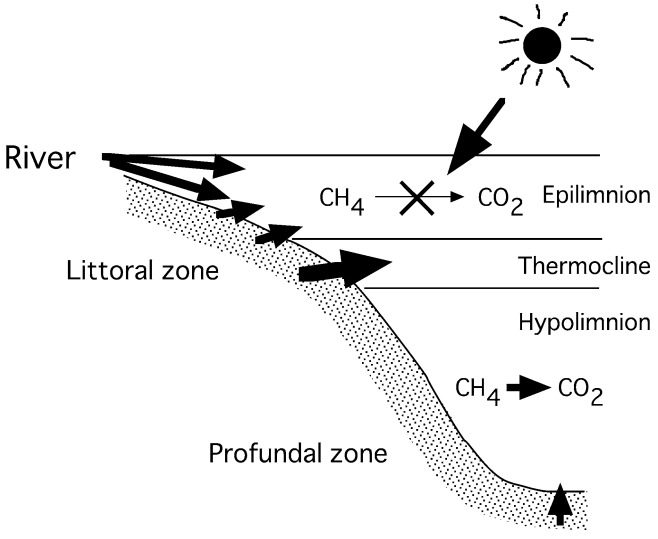

Fig. 7 A schematic model of the dynamics of methane in Lake Biwa. Methane in the lake water is supplied from the subsystems of the lake (rivers, littoral and profundal sediments) at different strengths (indicated with *arrows*). Dissolved methane is oxidized in the hypolimnion but not in the epilimnion because of the inhibitory effect of light

Methane oxidation is very low in the epilimnion and thermocline due to the inhibitory effect of light. Methane in the surface water is oversaturated to the atmospheric methane level and released to the atmosphere without oxidation in water. In contrast, methane is actively oxidized in the hypolimnion. The high loading and inactive oxidation of methane cause higher methane concentration in the epilimnion and thermocline than in the hypolimnion with the low loading and active oxidation of methane. This may be a mechanism for subsurface maxima of dissolved methane in the lake water, which have been observed in other lakes and in the ocean.

Other possible sources of dissolved methane in the lake water

A correlation between biomass of zooplankton and methane concentration has been observed in the near surface of marine environments (Traganza et al. 1979; Brooks et al. 1981; Conrad and Seiler 1988), and methane production by zooplankton (copepods) during grazing on marine phytoplankton has been reported (de Angelis and Lee 1994). However, methane production by zooplankton in freshwater environments has still not been clarified. Miyajima et al. (1997) detected no methane production by copepods in Lake Biwa. We also found no correlation between methane concentration and abundance of zooplankton (J. Murase, unpublished data). de Angelis and Lee (1994) reported methane production by zooplankton was species specific.

The presence of methane in the oxic open ocean is often explained by methanogensis in the anaerobic microsites inside particulate organic matter such as fecal pellets of copepods or marine snow. Karl and Tilbrook (1994) reported that the sinking particles released methane to seawater, explaining in part the in situ production of methane in the oxic seawater. Evidence of methanogenic archaea was revealed by analyses of lipid (King et al. 1998) and 16S rRNA genes (van der Maarel et al. 1999). The significance of methanogenesis from particulate matter in the methane budget of lakes remains to be studied.

Submarine groundwater discharge is often reported as a significant source of dissolved methane in the coastal oceans (e.g., Bugna et al. 1996; Bussmann and Suess 1998; Corbett et al. 2000). There is no study on the effect of groundwater discharge on methane budget in a lake. However, groundwater may be a possible source of dissolved methane in the lake water, because Taniguchi (2001) reported that the internal seiche enhanced the groundwater seepage in Lake Biwa.

Concluding remarks

Oxygen uptake by microbial metabolisms including methane oxidation in the profundal sediments may be

accelerated by an increase in temperature at the lake bottom due to global warming (Hayami and Fujiwara 1999). Excessive depletion of benthic oxygen may release much more methane from the sediment to the lake water. Phosphorus can be also released from the sediment to the lake water due to oxygen depletion. Accelerated eutrophication of the lake by release of phosphorus may cause a catastrophic change in the methane dynamics in the lake.

The fact that methane is produced/released from the deeper layer (> 20 cm from the surface) of the profundal sediments suggests that the methane originated from organic matter deposited in the past (more than 100 years ago if the sedimentation rate is assumed to be 2 mm $year^{-1}$), and that this "old" methane contributes to the present carbon flow and oxygen budget of the sediments. The organic matter in the deeper layer of the profundal sediments as well as the littoral sediments is suggested to be relatively dominated by the allochthonous (terrestrial) origin in comparison to the surface layer of the profundal sediments (Murase and Sakamoto 2000). Further study is needed to elucidate the link between terrestrial organic matter and methane dynamics in lake sediments.

Acknowledgements We are grateful to the leader of our project, E. Wada (Frontier Research Center for Global Warming). We thank Captain B. Kaigai of the R/V *Hassaka* of University of Shiga Prefecture for his help and cooperation. We are also grateful to K. Okubo, Okayama University, for his valuable comments on internal waves in a lake. This research was financially supported by a Grant in Aid (No.11213208) from the Ministry of Education, Sports, Science, Culture, and Technology, Japan.

References

de Angelis MA, Lee C (1994) Methane production during zooplankton grazing on marine phytoplankton. Limnol Oceanogr 39:1298–1308

de Angelis MA, Lilley MD (1987) Methane in surface waters of Oregon estuaries and rivers. Limnol Oceanogr 32:716–722

Bastviken D, Ejlertsson J, Sundh I, Tranvik L (2003) Methane as a source of carbon and energy for lake pelagic food webs. Ecology 84:969–981

Bloesch J (1995) Mechanisms, measurement and importance of sediment resuspension in lakes. Mar Freshw Res 46:295–304

Brooks JM, Reid DF, Bernard BB (1981) Methane in the upper water column of the northwestern Gulf of Mexico. J Geophys Res 86:1029–1040

Bugna GC, Chanton JP, Cable JE, Burnett WC, Cable PH (1996) The importance of groundwater discharge to the methane budgets of nearshore and continental shelf waters of the northeastern Gulf of Mexico. Geochim Cosmochim Acta 60:4735–4746

Bussmann I, Suess E (1998) Groundwater seepage in Eckernforde Bay (Western Baltic Sea): effect on methane and salinity distribution of the water column. Cont Shelf Res 18:1795–1806

Cicerone RJ, Oremland RS (1988) Biogeochemical aspects of atmospheric methane. Global Biogeochem Cycles 2:299–327

Conrad R, Seiler W (1988) Methane and hydrogen in seawater (Atlantic Ocean). Deep Sea Res 35:1903–1917

Corbett DR, Dillon K, Burnett W, Chanton J (2000) Estimating the groundwater contribution into Florida Bay via natural tracers, ^{222}Rn and CH_4. Limnol Oceanogr 45:1546–1557

Dafner E, Obzhirov A, Vereshzhagina O (1998) Distribution of methane in waters of the Okhotsk and western Bering Seas, and the area of the Kuril Islands. Hydrobiology 362:93–101

Dan J, Kumai T, Sugimoto A, Murase J (2004) Biotic and abiotic methane releases from Lake Biwa sediment slurry. Limnology 5:149–154

Frenzel P, Thebrath B, Conrad R (1990) Oxidation of methane in the oxic surface layer of a deep lake sediment (Lake Constance). FEMS Microbiol Ecol 73:149–158

Gelda RK, Auer MT, Effler SW (1995) Determination of sediment oxygen demand by direct measurement and by inference from reduced species accumulation. Mar Freshw Res 46:81–88

Hayami Y, Fujiwara T (1999) Warming of hypolimnetic water in Lake Biwa (in Japanese). Oceanogr Jpn 8:197–202

Jones JB, Mulholland PJ (1998) Influence of drainage basin topography and elevation on carbon dioxide and methane supersaturation of stream water. Biogeochemistry 40:57–72

Karl DM, Tilbrook BD (1994) Production and transport of methane in oceanic particulate organic matter. Nature 368:732–734

Kiene RP (1991) Production and cunsumption of methane in aquatic systems. In: Rogers JE, Whitman WB (eds) Microbial production and cunsumption of greenhouse gases: methane, nitrogen oxides, and halomethanes. American Society of Microbiology, Washington, pp 111–146

Kimura M, Miura Y, Watanabe A, Murase J, Kuwatsuka S (1992) Methane production and its fate in paddy fields.1. Effects of rice straw application and percolation rate on the leaching of methane and other soil components into the subsoil. Soil Sci Plant Nutr 38:665–672

King LL, Pease TK, Wakeham SG (1998) Archaea in Black Sea water column particulate matter and sediments—evidence from ether lipid derivatives. Org Geochem 28:677–688

Kiyashko SI, Narita T, Wada E (2001) Contribution of methanotrophs to freshwater macroinvertebrates: evidence from stable isotope ratios. Aquat Microb Ecol 24:203–207

van der Maarel MJEC, Sprenger W, Haanstra R, Forney LJ (1999) Detection of methanogenic archaea in seawater particles and the digestive tract of a marine fish species. FEMS Microbiol Lett 173:189–194

Mitchell JFB (1989) The greenhouse-effect and climate change. Rev Geophys 27:115–139

Miyajima T, Yamada Y, Wada E, Nakajima T, Koitabashi T, Hanba YT, Yoshii K (1997) Distribution of greenhouse gases, nitrite, and δ^{13} C of dissolved inorganic carbon in Lake Biwa: implications for hypolimnetic metabolism. Biogeochemistry 36:205–221

Murase J, Sakamoto M (2000) Horizontal distribution of carbon and nitrogen and their isotopic compositions in the surface sediment of Lake Biwa. Limnology 1:177–184

Murase J, Sugimoto A (2001) Spatial distribution of methane in the Lake Biwa sediments and its carbon isotopic compositions. Geochem J 35:257–263

Murase J, Sugimoto A (2002) Seasonal and spatial variations of methane production in mesotrophic lake sediments (Lake Biwa, Japan). Verh Int Verein Limnol 28:971–974

Murase J, Sakai Y, Sugimoto A, Okubo K, Sakamoto M (2003) Sources of dissolved methane in Lake Biwa. Limnology 4: 91–99

Reeburgh WS, Ward BB, Whalen SC, Sandbeck KA, Kilpatrick KA, Kerkhof LJ (1991) Black Sea methane geochemistry. Deep Sea Res 38:S1189–S1210

Rudd JWM, Hamilton RD, Campbell NER (1974) Measurement of microbial oxidation of methane in lake water. Limnol Oceanogr 19:519–524

Sakai Y, Murase J, Sugimoto A, Okubo K, Nakayama E (2002) Resuspension of bottom sediments by an internal wave in lake. Lakes Reserv 7:339–344

Schmidt U, Conrad R (1993) Hydrogen, carbon monoixde, and methane dynamics in Lake Constance. Limnol Oceanogr 38:1214–1226

Schulz M, Faber E, Hollerbach A, Schroder HG, Gude H (2001) The methane cycle in the epilimnion of Lake Constance. Arch Hydrobiol 151:157–176

Seifert R, Delling N, Richnow HH, Kempe S, Hefter J, Michaelis W (1999) Ethylene and methane in the upper water column of the subtropical Atlantic. Biogeochemistry 44:73–91

Shteinman B, Eckert W, Kaganowsky S, Zohary T (1997) Seiche-induced resuspension in lake kinneret: a fluoresent tracer experiment. Water Air Soil Pollut 99:123–131

Sugimoto A, Wada E (1993) Carbon isotopic composition of bacterial methane in a soil incubation experiment: contributions of acetate and CO_2/H_2. Geochim Cosmochim Acta 57:4015–4027

Sugimoto A, Dan J, Kumai T, Murase J (2003) Adsorption as a methane storage process in natural lake sediment. Geophys Res Lett 30 doi:10.1029/2003GL018162

Taniguchi M (2001) Evaluation of the groundwater capture zone for modelling of nutrient discharge. Hydrol Processes 15:1939–1949

Traganza ED, Swinnerton JW, Cheek CH (1979) Methane supersaturation and ATP-zooplankton blooms in near-surface waters of the western Mediterranean and the subtropical North Atlantic Ocean. Deep Sea Res 26A:1237–1245

Whiticar MJ, Faber E, Schoell M (1986) Biogenic methane formation in marine and freshwater environments: CO_2 reduction vs. acetate fermentation—isotope evidence. Geochim Cosmochim Acta 50:693–709

Zehnder AJB, Stumm W (1988) Geochemistry and biogeochemistry of anaerobic habitats. In: Zehnder AJB (ed) Biology of anaerobic microorganisms. Wiley, New York, pp 1–38

SUBJECT INDEX